TYPE-2 DIABETES AND INNATE IMMUNITY:

NEW CONNECTIONS REVEALED BY MULTI-DIMENSIONAL

FRACTIONATION OF BLOOD PLASMA PRIOR

TO PROTEOMIC ANALYSIS

by

Scott Bradley Laffoon

A dissertation submitted in partial fulfillment
of the requirements for the degree

of

Doctor of Philosophy

in

Biochemistry

MONTANA STATE UNIVERSITY
Bozeman, Montana

November, 2010

APPROVAL

of a dissertation submitted by

Scott Bradley Laffoon

This dissertation has been read by each member of the dissertation committee and has been found to be satisfactory regarding content, English usage, format, citation, bibliographic style, and consistency, and is ready for submission to the Division of Graduate Education.

Dr. Edward A. Dratz

Approved for the Department of Chemistry and Biochemistry

Dr. David Singel

Approved for the Division of Graduate Education

Dr. Carl A. Fox

STATEMENT OF PERMISSION TO USE

In presenting this dissertation in partial fulfillment of the requirements for a doctoral degree at Montana State University, I agree that the Library shall make it available to borrowers under rules of the Library. I further agree that copying of this dissertation is allowable only for scholarly purposes, consistent with "fair use" as prescribed in the U.S. Copyright Law. Requests for extensive copying or reproduction of this dissertation should be referred to ProQuest Information and Learning, 300 North Zeeb Road, Ann Arbor, Michigan 48106, to whom I have granted "the exclusive right to reproduce and distribute my dissertation in and from microform along with the non-exclusive right to reproduce and distribute my abstract in any format in whole or in part."

Scott Bradley Laffoon

November, 2010

DEDICATION

To my mother, Edna Laffoon, for her encouragement and support as I tried to do science: Thank you. Your love is felt from far away.

To my darling daughter, Rosie, for inspiring me to be the best father ever: Thank you.

To MSU, the Department of Chemistry and Biochemistry and Professor Edward A. Dratz: Thank you for this opportunity.

TABLE OF CONTENTS

TABLE OF CONTENTS-CONTINUED

LIST OF TABLES

LIST OF FIGURES

Figure Page

LIST OF FIGURES-CONTINUED

Figure Page

LIST OF FIGURES-CONTINUED

Figure Page

LIST OF FIGURES-CONTINUED

Figure Page

LIST OF FIGURES-CONTINUED

LIST OF FIGURES-CONTINUED

Figure Page

LIST OF FIGURES-CONTINUED

LIST OF FIGURES-CONTINUED

Figure Page

GLOSSARY

AA	Amyloid A
A1BG	Alpha-1 beta glycoprotein
ACHA	α-cyano-4-hydroxycinammic acid
ACC	Acetyl-CoA carboxylase
ACN	Acetonitrile
ADP	Adenosine diphosphate
AGE	Advanced glycation end-product
AR	Aldose reductase
ATP	Adenosine triphosphate
Apo A-I	Apolipoprotein A-I
APS	Ammonium persulfate
BCG	Bromocresol green
BEPHE	BCG error from polyclonal HSA ELISA
BME	B-mercaptoethanol
BMI	Body mass index
CAP	CRISP, antigen-5 and pathogenesis related protein superfamily
CAD	Coronary artery disease
CFH	Complement factor H
CFHR	Complement factor H related
CHAPS	3-[(3-Cholamidopropyl)dimethylammonio]-1-propanesulfonate detergent
CHD	Coronary heart disease
CID	Collision induced dissociation
CPT	Carnitine palmitoyl transferase
CRP	C-reactive protein
CRISP-3	Cysteine-rich secreted protein 3
DAG	Diacylglycerol
dF	Degrees of freedom
dI	Deionized
DIGE	Difference gel electrophoresis
DM	Diabetes mellitus
DMF	Dimethylformamide
ELISA	Enzyme-linked immunosorbent assay
ESI	Electrospray ionization
ETD	Electron transfer dissociation
F(#)	Fraction (as F2 is fraction 2)
FALP	CFHR associated lipoprotein particle
FATP	Fatty-acid transport protein
FFA	Free fatty-acids
FPG	Fasting plasma glucose (concentration)
FPI	Fasting plasma insulin (concentration)
F6P	Fructose-6-phosphate

GLOSSARY-CONTINUED

GAPDH	Glyceraldehyde-3-phosphate dehydrogenase
GH	Garry Handelman (donor of plasma used as standard)
G6P	Glucose-6-phosphate
GSH	Reduced glutathione
HB	Hydrazide-biotin
Ha1c	Glycated hemoglobin
HGP	Hepatic glucose production
HMA	Human mercaptoalbumin
HSA	Human serum albumin
HDL	High density lipoprotein
HMA	Human mercaptoalbumin (reduced Cys-34)
HMW	High molecular weight
HNA	Human non-mercaptoalbumin
HOMA-IR	Homeostasis-model assessment of insulin resistance
HPLC	High performance liquid chromatography
Hpt	Haptoglobin
HRG	Histidine-rich glycoprotein
HRP	Horseradish peroxidase
IDDM	Insulin dependent diabetes mellitus (archaic-replaced with T1DM)
IEF	Isoelectric focusing
IGF	Insulin-like growth factor
IGT	Impaired glucose tolerance
IL	Interleukin
IPG	Immobilized pH gradient
IR	Insulin resistance
IRS	Insulin receptor substrate
K_{ATP}	ATP dependent potassium channel
kDa	kilodaltons
KO	Knock-out
LC	Liquid chromatography
LCCoA	Long chain acylcoenzyme A
LDL	Low density lipoprotein
LMW	Low molecular weight
LOOH	Lipid peroxides
MALDI	Matrix assisted laser desorption ionization
MARS	Multiple affinity removal system
MC	Macrophage conditioned
MeOH	Methanol
MHC-I	Major histocompatibility complex class I protein
MODY	Maturity onset diabetes in the young
M_r	Relative mobility

GLOSSARY-CONTINUED

MS	Mass spectrometry
MS/MS	Tandem mass spectrometry
MW	Molecular weight
NC	Non-chromagenic
NCBI	National Center for Biotechnology Information
NDU	Newly-diagnosed untreated
NEFA	Non-esterified fatty acid
NGT	Normal glucose tolerance
NHS	N-hydroxysuccinimidyl
NHRP	NeutrAvidin horseradish peroxidase
NIDDK	National Institute of Diabetes and Digestive and Kidney Diseases
NIDDM	Non-insulin dependent diabetes mellitus (archaic-replaced with T2DM)
NIH	National Institutes of Health
NMR	Nuclear magnetic resonance
NS	Non-significant
OGTT	Oral glucose tolerance test
PAGE	Polyacrylamide gel electrophoresis
PEG	Polyethylene glycol
PI3K	Phosphatidylinositol 3-kinase
PIP_3	Phosphatidylinositol triphosphate
PKC	Protein kinase C
PMT	Photo multiplier tube
POI	Protein-of-interest
PPAR	Peroxisome-proliferator-activated receptor
polyAb	Polyclonal antibody
RCA	Regulator of complement activation (gene cluster)
RDS	Rate determining step
ROS	Reactive oxygen species
RP	Reversed-phase
RT	Room temperature
SAA	Serum amyloid A
SCR	Short consensus repeat
SDS	Sodium dodecyl sulphate
SEC	Size exclusion chromatography
SGP28	28 kDa secreted glycoprotein
SM	Spectrum Mill
SNP	Single nucleotide polymorphism
SPI	Scored peak intensity
SUV	Small unilaminar vesicles
TCA	Tricarboxylic acid
TEMED	N,N,N’,N’,-tetra-methyl-ethylenediamine

GLOSSARY-CONTINUED

TFA	Trifluoroacetic acid
TNF	Tumor necrosis factor
TOF	Time-of-flight
TZD	Thiazolidinedione
2DGE	Two-dimensional gel electrophoresis
T1DM	Type 1 diabetes mellitus
T2DM	Type 2 diabetes mellitus
UV	Ultraviolet
WHO	World Health Organization
WT	Wild type
ZAG	Zinc alpha-2 glycoprotein

ABSTRACT

We compared levels of protein isoforms in human blood plasma from patients with newly diagnosed and untreated type-2 diabetes (T2DM) with non-diabetic controls in samples obtained from US NIH. We immunodepleted fourteen of the most abundant proteins from pooled plasma samples and separated the depleted samples into six fractions by reverse-phase liquid chromatography at 80°C. Proteins from these fractions were labeled with new high quantum yield, hydrophilic and spectrally resolved fluorescent detection dyes developed at MSU and resolved on large-format (24cm x 20cm) two-dimensional gels.

By fluorescence analysis of 2D gels, using >1.4 fold change and $p<0.05$ acceptance criteria, we have identified five T2DM associated proteins and isoforms, including: two isoforms of zinc-alpha glycoprotein (ZAG), one isoform of serum amyloid A-1 (SAA-1) preprotein, one isoform of cysteine-rich secreted protein-3 (CRISP-3), one isoform of haptoglobin, and an A1-apolipoprotein fragment. Complement factor H related-5 (CFHR-5) is the likely identification of a sixth protein found significantly down in T2DM. Changes in the plasma levels of CRISP-3 and CFHR-5 strengthen the hypothesis that T2DM is a disease involving innate immunity. Three of these proteins are known to specifically bind to the transport protein, human serum albumin (HSA). Also, CRISP-3 is a specific and high-affinity ligand of $\alpha 1\beta$ glycoprotein, which is an HSA binder.

To investigate HSA binding properties, we quantitatively measured the binding of a dye probe by HSA at neutral pH. These measurements revealed that HSA binding of the probe correlates with several metabolic parameters of central importance to the diagnosis of T2DM, including fasting plasma glucose (FPG). Therefore, this assay may reveal altered properties of HSA that could be developed for the clinical assessment of individuals' metabolic status.

We sought modifications of HSA or altered cargo of HSA that may cause the difference in binding. 1D gels of plasma proteins reacted with maleimide dye showed no changed levels of the oxidation state of HSA's lone thiol, Cys-34. However, 1D blots of plasma proteins reacted with the oxidative carbonyl probe, hydrazide-biotin conjugate, and probed with luminol reactive HRP-neutravidin showed a surprising anti-correlation of HSA oxidation with hemoglobin A1c, an indicator of glycemic control.

INTRODUCTION TO TYPE II DIABETES

Introductory Statement

Type II diabetes mellitus (T2DM) is characterized by persistent, high circulatory glucose concentration (hyperglycemia) that appears to be causal for serious secondary complications, including: peripheral nerve damage (neuropathy), kidney disease, (nephropathy), retinal degeneration (retinopathy) and cardiovascular disease [2]. The primary causal defect, if there is only one, which leads to T2DM's diverse metabolic imbalances, including hyperglycemia, is still unknown. Whatever the underlying cause of T2DM, hyperglycemia is a symptom of the primary cause, and there is considerable evidence that hyperglycemia is the causal agent of the late complications [3]. Although profoundly systemic, T2DM is often asymptomatic and the complications typically don't emerge until years after the afflicted individual has crossed the diagnostic cutpoint for diabetes. According to the U.S. Centers for Disease Control and Prevention, 24% of U.S. citizens afflicted with T2DM in the year 2007 were undiagnosed [4]. Thus, it is not infrequent for people with T2DM to go undiagnosed and not realize that they are afflicted until they experience complications [5]. This situation is compounded by a diagnostic test, the oral glucose tolerance test (OGTT), which although considered the "gold standard" is also regarded as inconvenient, requiring an 8 hour fast, a 2 hour office visit, and is not highly reproducible [6]. Our motivation for the investigation presented here was to seek protein markers of T2DM in the blood plasma of humans with the hope that

the discovered markers may be developed into a sensitive and less burdensome diagnostic assay, while also adding to the understanding of T2DM and its associated complications.

This dissertation ends with novel evidence that the *ex vivo* binding character of the major soluble blood protein, serum albumin (HSA), is correlated to the individual's fasting plasma glucose concentration (FPG), throughout the range encompassed by the non-diabetic control subjects and the newly-diagnosed, untreated T2 diabetics of this study. This appears to put the functional state of HSA at the interface between its known roles in lipid metabolism, and as we will show, glycemic control. HSA is also known to bind several acute-phase or inflammation sensitive proteins (ISPs), which are part of the innate immune response. The modern understanding of T2DM has deep roots in each of these 3 areas: lipid metabolism, glycemic control and innate immunity. Thus, after a brief historical introduction, I thought it important to provide a relatively thorough exegesis on the etiology of T2DM, considering lipid metabolism, glycemic control and innate immunity.

Medical History of Diabetes to the Discovery of T1DM and T2DM

The name "diabetes" (from δια, through, and Βαιϖεν, to pass [7]) reflects the fact that ancient medical practitioners, and their patients, faced pitiably advanced cases of some type of diabetes. The Greek physician, Aretaeus (2nd to 3rd century A.D.), stated that the name "diabetes", also interpreted as "siphon", referred to the dual symptoms of patients who were unable to quench their thirst by drinking any amount of water (polydipsia), and who passed copious urine (polyuria), "as if from the opening of

aqueducts". He described their inexorable emaciation as "melting down of the flesh and limbs into urine" [8].

For millennia, diabetics had little positive prognosis to hope for, as almost no progress in the treatment, or even the understanding of the disorder, was made until nearly the beginning of the twentieth century. At this time, an important discrimination was made of diabetes as either "mellitus" (honey sweet) or, referring to the dysregulation of urine production resulting from a pituitary or hypothalamic disorder, "insipidus" (bland), according to the taste-testing of urine by physicians in Elizabethan England.

As late as 1878 [9], the Encyclopedia Britannica's entry for diabetes made no mention of the pancreas, although the essay seems a strikingly modern treatment in several other ways. Britannica noted that although diabetes had often been classified as a disease of the kidneys, it should be regarded as a constitutional disorder including roles for the liver, blood, glucose, oxidation, glycogen, environmental triggers, diet, heredity, and even regulation of liver secretions by the brain. The Britannica also included a statement that implicitly presaged the division of diabetes into the modern "type 2" and "type 1" designations, observing that the disease, "as a rule advances comparatively slowly (type 2- *SBL*)[1] except in the case of young persons (type 1- *SBL*)".

As for the medical care options for people with diabetes mellitus (DM), in the same 1878 encyclopedia entry it was recognized, from measurements of the amount of glucose crystallized from the urine, that foods of "saccharine and starchy matter" aggravated the disease. So, diets had been developed, which attained moderate success at improving the patient's overall health and life expectancy, by eliminating what are now

[1] SBL The author's initials, signifies the author's parenthetical insertion within a quotation.

known as carbohydrates. The Encyclopedia Britannica essay also noted, "(t)he plan of treatment once proposed, of administering sugar in large quantity in diabetes, proved to be highly injurious, and is now abandoned." At this time, according to the encyclopedia, no medicinal substance had been shown to possess any efficacy except, reportedly, opium which had been found of great service, and its administration was followed "according to some high authorities, with cure of the disease."

Actually, in 1878, a discovery of unrecognized importance had already been made. The pancreas (from παν, all, and κρεασ, flesh [7]), shown in Figure 1, is a jelly-

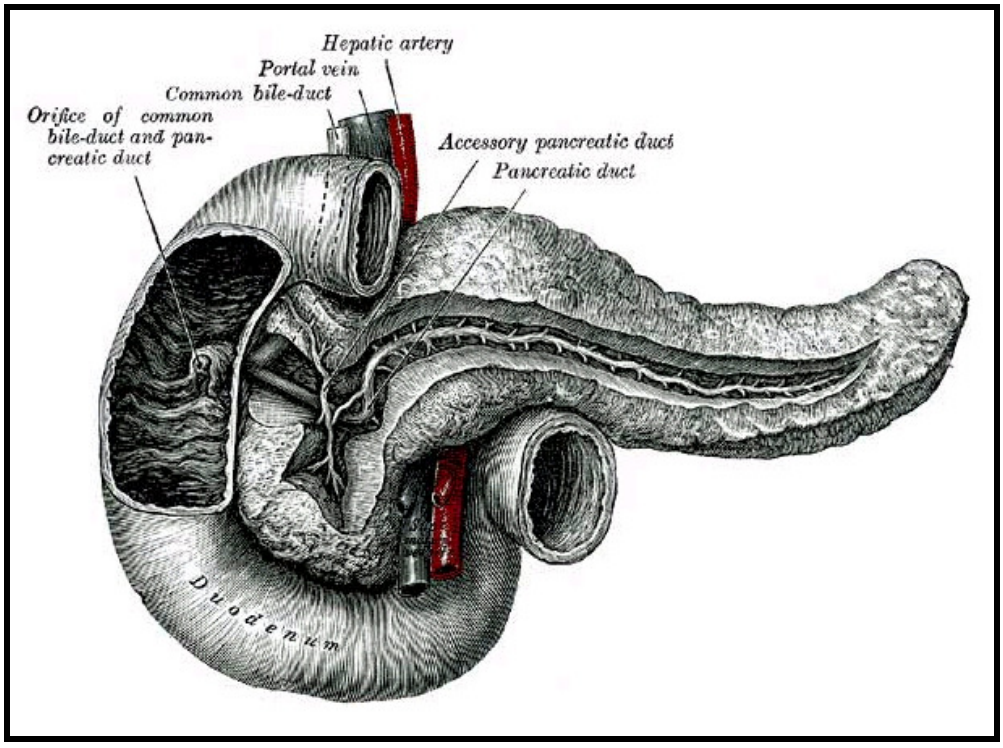

Figure 1 "Historic drawing of the pancreas" from University of New South Wales, from the Australia Embryology Department Website [10].

like gland situated below the stomach and was known since Eudemos, 300 B.C., to secrete "a fluid similar to saliva…into the intestine, intended for the improvement of digestion" [11]. From the middle of the 19th century, the accumulating evidence from autopsies showed increased prevalence of damage to the pancreas in diabetics. In 1869, Paul Langerhans, a German graduate student, demonstrated in his dissertation [12] the presence of a previously unnoticed histological detail of the human pancreas. Among the clusters of known cells (acini) which secrete digestive "pancreatic juice" into the small intestine, Langerhans found round groups of polygonal cells which appeared to be unconnected to the acini and seemed to be floating in a sea of the acinar cells. He called these "Häufchen" (little lumps), and stated that he was completely ignorant of their function [13]. These cells would be named the "islets of Langerhans" by the French histologist Edouard Laguesse in 1893, who was the first to suggest that the islets were the site of an "internal secretion" that was a function of the pancreas additional to the external digestive secretion [13].

The evidence of a connection between the pancreas (but not yet the islets) and diabetes was discovered, four years prior to Laguesse's publication, by researchers Oskar Minkowski and Joseph von Mering in 1889 at the University of Strasbourg, Germany. They showed dramatic increases in the level of glucose, indistinguishable from that in DM, in the urine (glycosuria) of dogs after total surgical pancreatectomies, which, they stated, "starts sometime after the operation and will persist for weeks continuously until their death" [14]. Further, they showed that dogs that had their pancreatic ducts merely

ligated or cut, which prevented the external secretions from entering the small intestine, did not develop diabetic symptoms.

The first formal, systematic association of damage to the islets of Langerhans with DM came from the American pathologist Eugene Opie at John Hopkins Hospital. Opie cited contemporaneous work by Leonid Ssobelew (*Centralbl. f. algem Path. U. path. Anat*., 1900 xi, p. 202) in St. Petersburg, Russia whom, he said, had shown "the only evidence in support" of Laguesse's proposed internal secretion, by showing that "after feeding animals on carbohydrates the cells of the islands become more granular." Secondly, (and more importantly to the coming clinical research on insulin) Opie noted Ssobolew's conclusion that, "(a)fter ligating the duct of Wirsung (the pancreatic duct which secretes into the intestine, *S.B.L.*) in dogs the islands of Langerhans…are not implicated in the sclerotic process which ensues," and "this fact, he thinks, explains why they are spared glycosuria." [15]. The sites of the internal secretion had been inferred by Ssobelew by feeding animals "carbohydrates in considerable quantity" and observing the resulting morphological changes in the islets. The islets were also implicated by being unaffected during the physiological ablation of the sites of the external secretion, which resulted from the ligation of the pancreatic duct.

As inspiration to his own investigation, Opie stated that, "(in) the pancreas of two diabetics, Ssobolew was unable to discover islands of Langerhans." Opie introduced his investigation as follows,

> "Embedded as are these bodies in the substance of the organ, they cannot readily be subjected to experimental conditions which do not equally affect the secreting structures. It is particularly desirable, therefore, to observe what changes they undergo under pathological conditions and, if possible, to

> bring such alterations into correlation with concomitant pathological phenomena. From such a study, heretofore little pursued, we may hope for suggestions of the function or anatomical relationship of these obscure structures" [16].

Opie was able to discriminate several types of pancreatitis and report the histological effect on the islets of Langerhans. In congenital syphilitic pancreatitis, several changes in the gross anatomical structure of the pancreas were observed including islets that were encircled by fibrous tissue, but were not invaded by it and were intact (Figure 2A). Chronic pancreatitis cases in which there were obstructions to the duct, either calculi or carcinoma, were also investigated. In these cases, Opie found that "though the secreting acini have undergone marked degenerative changes, the islands of Langerhans may be unaltered" (Figure 2B). Only in the case where the obstruction was associated with extreme inflammation were the islets found to be distorted or involved in general sclerosis. This pancreatitis was accompanied by glycosuria that could be remedied by diet. In a case of apparently undiagnosed diabetes, a patient with excessive

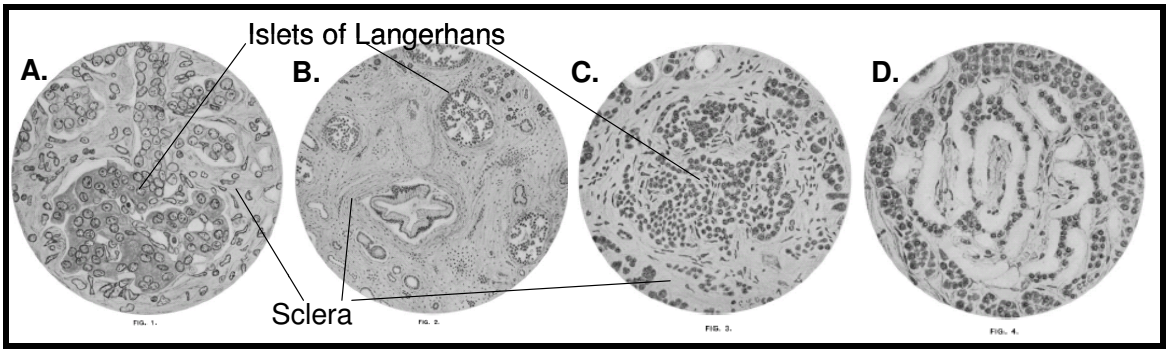

Figure 2 Changes in the human islets and surrounding acinar cells with pathology. A) Syphilitic pancreatitis-sclerotic, B) Chronic obstructive pancreatitis-sclerotic, C) Glycosuria and ketoacidosis-sclerotic with fibrous ingrowths, D) Frank diabetes-islets of Langerhans not found, "tortuous hyaline columns".

thirst, polyuria, glycosuria and noted to have “acetone present”, a symptom now known as keto-acidosis, the islets were found to be surrounded and infiltrated with sclera (Figure 2C). And in the final example, a case of a patient who had been diagnosed with frank diabetes for two years, Opie was unable to find any islets but found “very remarkable lesions of…tortuous hyaline (glassy) columns” (Figure 2D).

Opie’s work is believed to be the first reported observation of the association of diabetes with destruction of the islets, including the B-cells that were later found to produce insulin and are of central importance to the metabolism of glucose and the etiology of both type 1 and type 2 diabetes mellitus. Opie’s “hyaline degeneration of the islets of Langerhans” is now known to be an amyloid deposition, believed to be caused by protein misfolding [17], not the connective tissue hyalin. The amyloid identity of the deposits was established in 1943 [18] and confirmed in 1961 [19]. How the amyloid deposition occurs and whether it is the cause, a contributor or the result of islet destruction are among the lingering mysteries in DM research [20, 21].

In 1922, Frederick G. Banting and Charles H. Best published landmark results on the effectiveness of an extract from the pancreases of dogs and cows in treating the glycosuria and ketonuria (presence of ketones in the urine) of depancreatinized dogs [22, 23] and in people with diabetes [24]. Banting’s original idea for the work was directly related to a phenomenon shown in Opie’s work, and more explicitly in the work of Mary Kirkbride (Figure 3) in 1912 [25]; specifically, that the degeneration of only the pancreatic acinar cells, surrounding the islets, occurs after ligating the duct of Wirsung. The islets remain viable and productive. The figure shows blue stained guinea pig islets

of Langherhans before, Figure 3A, and 21 days after, Figure 3B, the ligation of the duct to the duodenum. The brown stained cells in Figure 3A that selectively atrophy after ligation (Figure 3B) are the acinar cells. The selective atrophy of the acinar cells, in dogs with ligated ducts of Wirsung, was the process that was central to Banting's idea for

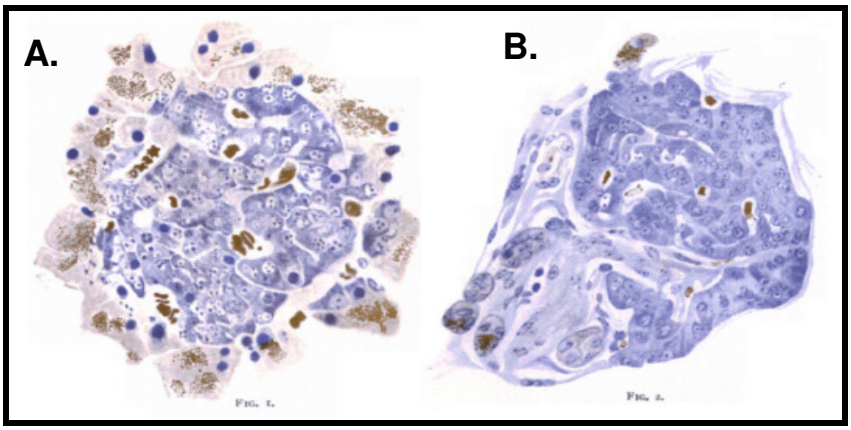

Figure 3 Blue stained guinea pig islets of Langerhans, from [25].

extracting insulin in 1921. It had become widely suspected that there was an internal secretion in the pancreas which was controlling the metabolism of glucose, but no one had been able to prove its presence or to purify it. Simple extracts of the pancreas didn't consistently work, because the active principle was destroyed in the process of maceration of the tissue when the internal secretion mixed with the external secretion. It was known that the external secretion of the pancreas contained trypsinogen which, when mixed with the internal secretion, became activated to a digestive enzyme that destroyed the activity of the internal secretion [26]. This was the first evidence that the active agent was proteinaceous.

So the advancement required was the extraction of the unknown agent, without allowing it to be destroyed in the process. Several researchers had tried various extractions that showed promise. E.L. Scott, Israel Kleiner, and Nicolas Paulesco had each shown significant decreases in the urine glucose of depancreatinized dogs upon the injection of their variously prepared pancreatic extracts, but they had each discontinued or been delayed in their research by World War I [27]. Banting wanted to use the phenomenon of acinar degeneration, which occurred subsequently to the ligature of the pancreatic duct, in his process of isolating the internal secretion. In this way, he reasoned that after ligature and a period of time during which the pancreas became depleted of the digestive enzyme, he could surgically remove the pancreas from an animal, and then extract the active internal secretion [28].

Banting's extract worked reasonably well in depancreatinized dogs to lower the blood glucose (part of his group's quick success was because of advancements in measuring blood glucose [26]) and was the initial success that propelled the research of his group. However, it was his co-worker, James B. Collip, who discovered that alcohol, and later acetone, extraction of whole macerated pancreases produced more and purer active principle, without the need for duct ligature. Collip found that the relatively pure, active agent precipitated out of solution with a small change in concentration of alcohol, at around 90%, and could then be recovered in relatively pure, active form [26]. Initially, the purified, active extract was called "isletin" but was changed to "insulin" for obscure reasons. "Insulæ" was a term used by Lydia Dewitt in a 1906 review article [29] of islet research.

The human effect of the discovery of insulin on world health is one of the most famous and dramatic success stories in medicine. Initially hailed as a "miracle of medicine" it soon became clear that DM had not gone away. From a physiological perspective, artificially administered insulin is a "Band-Aid" that doesn't perfectly compensate for lost pancreatic function and obscures DM's chronic, subtle and profound nature. The underlying cause of the disease had not been affected by insulin administration. But because of the clinical use of insulin, "early-onset" or "type-1" diabetics, who before the clinical administration of insulin would have likely died in a coma at a young age, are able to live much longer and relatively normally.

Injections of extracted insulin had the disadvantage of having a very fast action; its activity onset is within 0.5-1 hour, it peaks in 2-3 hours and it has an effective duration of only 3-6 hours. This meant that many early patients were required to have four injections per day. Early beneficial innovations came from researchers who complexed insulin with other substances that delayed and prolonged its activity.

In 1936, Hagedorn, at the Danish company Novo, discovered that bovine or porcine insulin that was complexed with the arginine–rich protamine polypeptide from the sperm of a river trout, had prolonged blood glucose lowering (hypoglycemic) activity (Figure 4) [30, 31]. This preparation is still used today and is called NPH (Neutral Protamine Hagedorn) or Isophane, although it now uses a recombinant human insulin analogue. Isophane has an onset time of 2-4 hours, a peak activity in 4-10 hours and has an effective duration of 10-16 hours. Hagedorn's contemporaries, Scott and Fisher in Toronto, Canada found that insulin which was complexed with zinc also had delayed

activity [32]. This prolonged effect was a result of the time required for the insulin, complexed in the bio-unavailable zinc-insulin hexamers to equilibrate to the bio-available monomeric form [33]. Later, in the 1950's, further refinements of the zinc and protamine

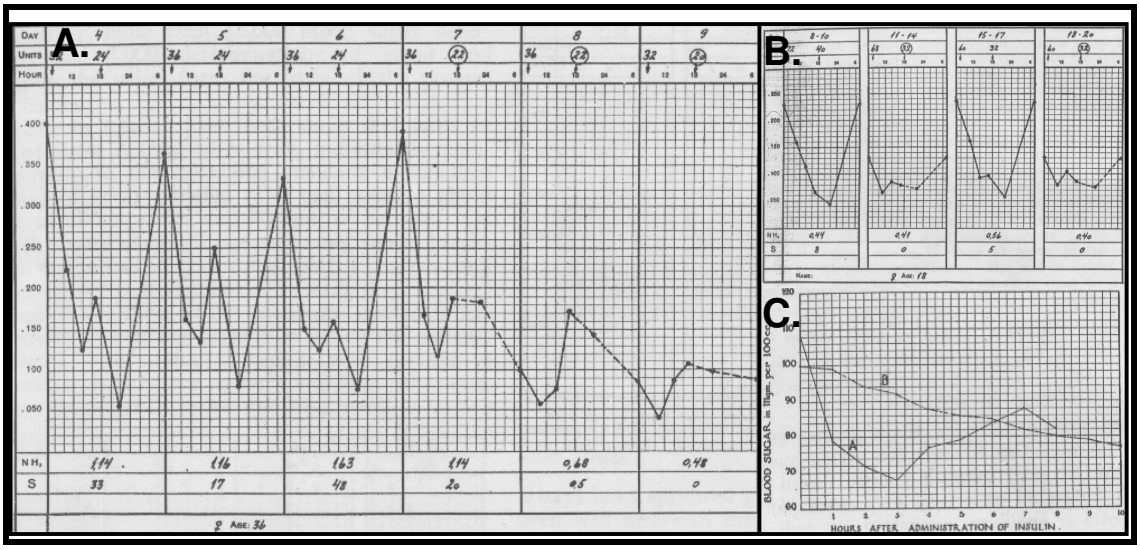

Figure 4 The first protamine-insulin experiments-1936 A) Hagedorn et al. [30]-6 days of treatment of diabetic patient. The first 3 days with a morning and 6 pm injection of just regular insulin, the last 3 days with the 6 pm injection replaced by protamine-insulin. Above the chart is shown the day of the month, insulin dosage in international units, circled when insulin-protamine and written at the hour coordinate of injection. The Y-axis is blood glucose as a percentage. Below the chart is given the daily averaged: "NH_3" ammonia excretion (indicator of acidosis) and "S" glucose excretion. Note the abolition of the nighttime "sugar excursions", the lower required dosages, and the lower glycemic indices on days of protamine-insulin injections. B) Hagedorn et al. [30]-Daily averages of alternating periods of just insulin (period 1 and 3) and of protamine insulin (periods 2 and 4). Note the relatively "blunted" features of blood glucose during periods 2 and 4. C) Root et al. [31]-Blood glucose in a non-diabetic after injection of: curve A, 8 units of regular insulin and curve B, 10 units of protamine-insulin. Note the slow and extended activity of the protamine-insulin.

complexes, including their combination with "regular" un-complexed insulin, made possible a multiplicity of rapid-acting, intermediate and long-lasting activities for improved clinical application. This line of research on time-release preparations

continues to this day, in combination with improved recombinant protein production technology, and has yielded many insulin analogues of varying potency and activity times. One long-lasting recombinant insulin analogue, insulin Detemir, contains a covalently bound fatty acid [34]. Detemir has an onset time of 0.8-2 hours and has a relatively flat pharmacological activity with an effective duration of 20-24 hours because this form binds to HSA via its fatty acid component [34].

In 1936, a formal distinction of different types of human DM was made for the first time when Himsworth published clinical observations (Figure 5) of "insulin sensitive" and "insulin insensitive" types of diabetes [35]. To do this, Himsworth developed a test in which insulin was injected simultaneously with orally administered glucose followed by monitoring the blood glucose over two hours (Figure 5). Figure 5A shows blood glucose vs time after an insulin injection simultaneously with an oral glucose dosage of an "insulin-insensitive" patient (I), compared to an insulin-sensitive patient (II). In Figure 5B the insulin-insensitive person's blood glucose (capillary and venous) is compared with insulin-sensitive person's blood glucose in Figure 5C. These figures include traces with (right side) and without (left side) simultaneous injections of insulin. In the insulin-insensitive case, some recovery is seen at 40 minutes where none is seen in the insulin-sensitive case. As will be discussed, this is due to the high secretion of insulin to overcome the loss of insulin sensitivity.

The preceding type of analysis showed that diabetic patients fell into one of two major types. The "insulin sensitive" and "insulin insensitive" cases were the precursors,

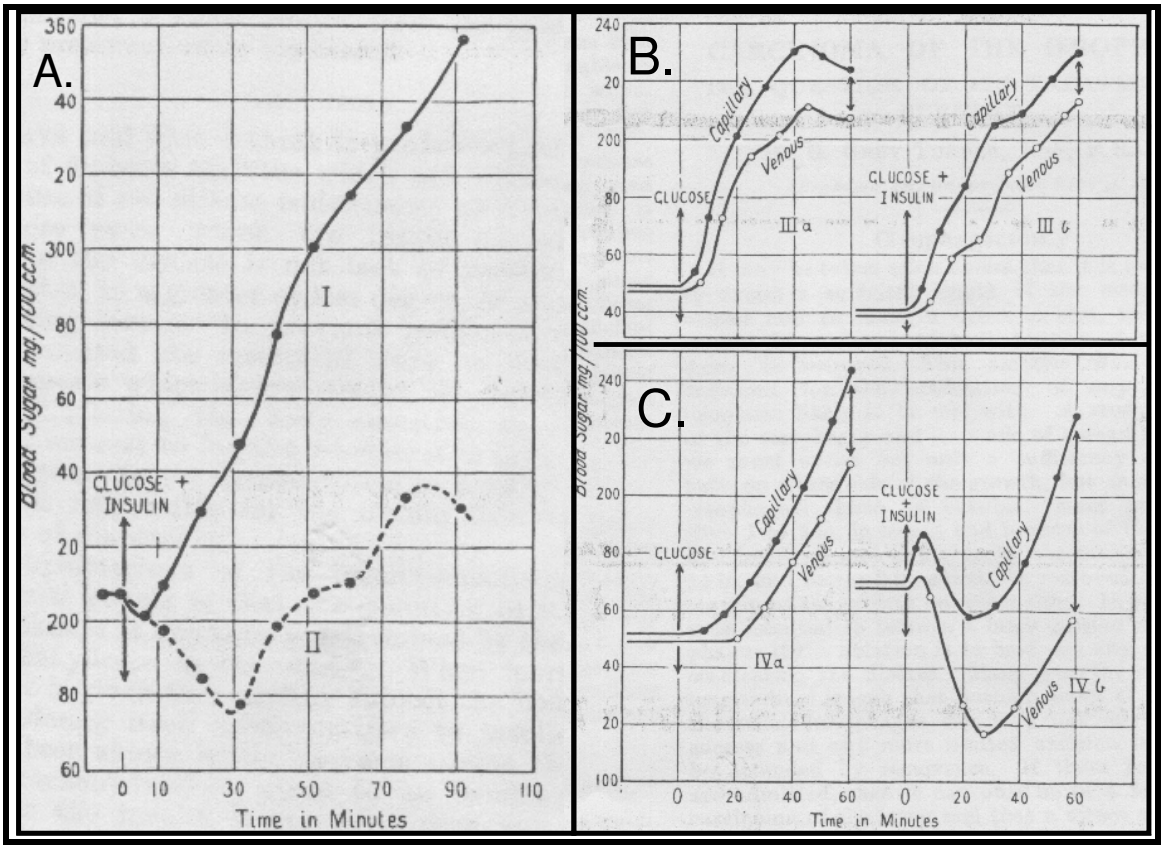

Figure 5 Himsworth discriminating two types of diabetics in 1936 [35]. Blood glucose vs time after insulin injection simultaneously with an oral glucose dosage. A) Comparison of "insulin-insensitive" patient (I) with insulin-sensitive patient (II). B) Insulin-insensitive patient's capillary and venous blood glucose is compared with C) insulin-sensitive patient's capillary and venous blood glucose. The traces on the left are after simple glucose dosage with no insulin injection. The traces on the right are with insulin injection. In the insulin-insensitive case, some recovery is seen at 40 minutes without insulin injection (left) where no recovery is seen in the insulin-sensitive case. Insulin-insensitive is the present-day insulin resistant "type 2". Insulin-sensitive is "type 1".

respectively, of what are known today as the "type 1" (T1DM) and "type 2" (T2DM) classifications of diabetics. It is now known that the insulin sensitive or T1DM person is hyperglycemic because their ability to produce insulin has been lost. They are sensitive to insulin precisely because the exogenous administration of insulin recovers their ability to metabolize glucose. On the other hand, the insulin insensitive or T2DM person has

generally been on a long, pathogenic path of progressively blunted insulin effectiveness that eventually involves the loss of β-cell function, the mechanics of which are only dimly understood to this day. These issues will be treated in more detail in the sections on the etiology of T2DM.

Himsworth observed that,

> "(a) general relationship appears to exist between the type of onset of the disease and the type of diabetes. The onset in insulin-sensitive patients is as a rule acute; the onset in insulin-insensitive patients is insidious…The insulin-insensitive type is more common in but not confined to the elderly, whilst the insulin-sensitive type is commoner in the young. As diabetes mellitus becomes more frequent with increasing age it would appear probable…that the commonest type of diabetes mellitus will eventually prove to be that which is not essentially due to insulin deficiency" [35].

Putting aside the importance of Himsworth's closing prediction until the epidemiology chapter; these clinical observations have been repeatedly upheld. The term "insulin-insensitive" has fallen from favor, however, and has been replaced by "insulin resistant".

This early discernment of the two major types of diabetes has been supported with discernment of different etiologies and differing treatment strategies. T1DM's acute onset has been found to be concurrent with the presence of diagnostic circulatory auto-antibodies against cytosolic components of the B-cells of the islets. This diagnostic marker is believed to result from an acute autoimmune "loss of self-tolerance", indicating T cell aggression against, and destruction of the insulin secreting B-cells [36, 37]. Because of relatively rapid, and ultimately absolute, destruction of the pancreatic insulin secreting capability in T1DM, the lack of insulin plays the predominant early role in the

disease, thus the observed relative “insulin-sensitivity” and inability to control blood glucose without exogenous insulin.

Although insulin resistance is frequently observed in T1DM, it is rarely associated with the period of onset [38]. In the pathogenesis of T2DM, skeletal muscle insulin resistance is the earliest detectable lesion and typically precedes the loss of insulin secreting function of the pancreas by 10 to 20 years [39]. The classical physiological progression to T2DM is marked by elevated levels of circulatory insulin, concurrent with elevated blood glucose, as the pancreas increasingly fails to compensate for the insulin resistance of the body, occurring primarily in hepatic, adipose and skeletal tissues [40].

Because of the awareness of differences between the types of DM that began to emerge in the 1930’s, different pharmaceutical management strategies have been developed. The administration of insulin and its analogues are well suited for T1DM, because insulin is a critical missing factor. But because T2DM is not usually marked by the complete destruction of the B-cells until a relatively advanced stage of the disease, several dietary and pharmaceutical approaches have succeeded in reducing blood glucose and delaying the onset of complications without the use of insulin [41]. The natural history of T2DM is to be treated in detail in the following chapter, but was introduced here to make a comparison of the two diseases, as we now leave the discussion of T1DM and henceforth pursue T2DM in depth.

The Etiology of T2DM

Several large and loosely connected bodies of understanding have grown within T2DM research. At least 20 gene polymorphisms that are associated with T2DM have been discovered since the year 2000, but each polymorphism explains only a small percentage of the risk for the disease [42]. For most of the genes, understanding of how their polymorphisms manifest as insulin resistance or diabetes is not at all clear [43]. Also, how insulin resistance culminates in β-cell degeneration is not known. And finally, despite progress in the clinical management of diabetes-associated complications, how the complications develop as a consequence of the phenotype of T2DM is not well understood. The portrayal of the current understanding of T2DM that follows will seek to bring disparate bodies of research into view, with the intention of rationalizing how our research fits within that framework.

Genetics of T2DM

As will be shown in more detail in the chapter on its epidemiology, T2DM has dramatically increased in prevalence, particularly in developing regions of the world where lifestyles are becoming more "westernized" [42] . This is due, in part, to the longer life spans of the inhabitants of these regions, but the prevalence is also increasing in younger people [44]. The increased prevalence is hypothesized to be caused by the relatively modern and culturally driven phenomena of "over-nourishment" and "under-activity" coincident with our genetic heritage of "thrifty genes". According to the "thrifty gene hypothesis" [45], genetic alleles, which during eons of seasonally unstable food

sources, gave humans the phenotypic ability to efficiently carry excess food energy as body fat are now, in an era of regionally plentiful food and less motivation for exercise, increasing the predisposition for the disease. But clearly this is not the entire explanation for the occurrence of T2DM because even among very obese people (BMI > 40), in one large[2] study [46] only ~26% had T2DM, and not every person who has T2DM is obese [42].

There are several rare forms of diabetes, such as "Maturity Onset Diabetes in the Young" (MODY) that share much of the phenotype of T2DM and are known to be monogenic disorders. For example, MODY-2 can be caused by one several known missense or nonsense mutations of glucokinase (hexokinase IV) gene 7p13-15 [47]. The different mutations affect the affinity of the glucokinase protein for its substrate, glucose, and this affects the efficiency of catalyzing the critical glucose phosphorylation when it enters the cell. Glucokinase is expressed in both the liver and in the B-cells, and the glucokinase mutation affects a negative feedback loop linking blood glucose level to insulin secretion. In MODY-2 the clinical manifestation is usually a mild form of glucose intolerance.

The evidence for a genetic component of T2DM is well established. For example, the concordance of T2DM between monozygotic twins is about 70% while that between dizygotic twins is only 20-30% [48]. Also, the lifetime risk for offspring is 40% if one parent has T2DM. If both parents have T2DM then the risk to offspring is 70% [42].

---

[2] The authors of this 2003 telephone survey of 195005 U.S. adults stated that their results likely underestimated the association of obesity with diabetes because of the tendency of the participants to underestimate their own weight, overestimate height and because the telephone survey misses those of low socioeconomic status which is associated with both obesity and T2 diabetes. The risk factor of BMI > 40 was 7.37 that of normal weight adults.

However, the relationship of phenotype to the genotype is not as simple as the MODY cases. The evidence linking T2DM to specific genes suggests that it is a polygenic disease, involving several genetic variants and combinations of variants [42]. Because it is polygenic and also clearly has an environmental component, which makes it appear to be an acquired condition, it is "complex". This is strikingly evident in studies of identical twins, showing that the concordance of T2DM is less than 100% [49]. Additionally, it is

Table 1 T2DM associated genes-PPARG, peroxisome proliferator-activated receptor gamma; CAPN10, calpain 10; KCNJ11, potassium inwardly rectifying channel, subfamily J, member 11; TCF7L2, transcription factor 7-like 2; CDKAL1, CDK5 regulatory subunit associated protein 1-like 1; CDKN2A/B, cyclin-dependent kinase inhibitor 2A/B; HHEX, haematopoietically expressed homeobox; IDE, insulin-degrading enzyme; SLC3OA8, solute carrier family 30 member 8; IGF2BP2, insulin-like growth factor 2 mRNA binding protein 2; FTO, fat mass and obesity associated; MC4R, melanocortin 4 receptor; NOTCH2, Notch homolog 2 Drosophila; ADAMTS9, ADAM metallopeptidase with thormbospondin type 1 motif, 9; THADA, thyroid adenoma associated; TSPAN8, tetra spanin 8; LGR5, leucine-rich repeat-containing G protein-coupled receptor 5; CDC123, cell division cycle 123 homolog; CAMK1D, calcium/calmodulin-dependent protein kinase ID; JAZF1, juxtaposed with another zinc finger gene 1; KCNQ1, potassium voltage-gated channel, KQT-like subfamily, member 1.

Year (major publication)	Gene (suggested)	Disease mechanism
2000	*PPARG*	Insulin sensitivity
2003	*CAPN10*	Glucose transport
2003	*KCNJ11*	Beta-cell dysfunction
2006	*TCF7L2*	Beta-cell dysfunction
2007	*CDKAL1*	Beta-cell dysfunction
2007	*CDKN2A/2B*	Beta-cell dysfunction
2007	*HHEX/IDE*	Beta-cell dysfunction
2007	*SLC30A8*	Beta-cell dysfunction
2007	*IGF2BP2*	Beta-cell dysfunction
2007	*WFS1*	Unknown
2007	*TCF2*	Unknown
2007	*FTO*	Obesity
2008	*MC4R*	Obesity
2008	*NOTCH2*	Unknown
2008	*ADAMTS9*	Unknown
2008	*THADA*	Unknown
2008	*TSPAN8/LGR5*	Unknown
2008	*CDC123/CAMK1D*	Unknown
2008	*JAZF1*	Unknown
2008	*KCNQ1*	Beta-cell dysfunction

a “heterogeneous” disease because within a given population of type-2 diabetics, few of the members will have the same genetic factors [47]. Nevertheless, a growing number of genes (Table 1) are associated with the risk of T2DM, some very strongly. For example, a single nucleotide polymorphism (SNP) of the gene transcription factor 7-like 2 (TCF7L2), the strongest associated T2DM SNP to date, has a joint p-value $< 10^{-50}$ correlation with T2DM from 3 independent genome-wide association scans [42]. TCF7L2 is involved in Wnt signaling and may be involved in proliferation of β-cells in response to increased demands. The Wnt signaling pathway is most well known for its roles in embryogenesis and cancer, but is also involved in normal physiological processes such as polarity signaling in epithelial cells [50]. At the onset of T2DM, subjects have a 5-fold increased expression of *TCF7L2* in their islets and the more copies of the risk allele the higher the expression [42]. However, is estimated that the list of genes discovered so far (2009) that are associated with T2DM explain only about 30% of the individual risk of developing T2DM [42].

Glucose Homeostasis

To understand the mechanisms, both cellular and molecular, that are important in T2DM, it will be helpful to first present the currently understood conceptual framework within which glycemic conditions are controlled. In normal individuals, the plasma glucose level is tightly regulated by hormones (eg. Insulin and glucagon), enzymes (eg. hexokinase, pyruvate dehydrogenase) and substrates (eg. glucose, ADP). Despite cycles of sudden influxes of glucose after meals and potentially long periods of fasting,

circulatory glucose concentration is normally maintained between 70 mg/dL and 120 mg/dL (4-7 mM) [41]. If circulatory glucose concentration gets too low (hypoglycemia), then brain function can be impaired to the point of coma, permanent damage and death. If the concentration is too high, over ~180 mg/dL (10.5 mM), the immediate evolutionary disadvantage is energy loss through glycosuria. Over a period of years of high glucose, serious progressive and debilitating diabetes-associated complications are likely to develop, even at elevated concentrations as low as 120 mg/dL. The ability of the body to maintain the normal range of blood glucose concentration (euglycemia) is referred to as "normal glucose tolerance" (NGT). When this ability becomes compromised, it is known as "impaired glucose tolerance" (IGT).

The complex organization of hormones, enzymes and substrates is physiologically successful if the net flux of blood glucose maintains the normal range of concentration. As represented schematically in Figure 6, glucose is initially input from the

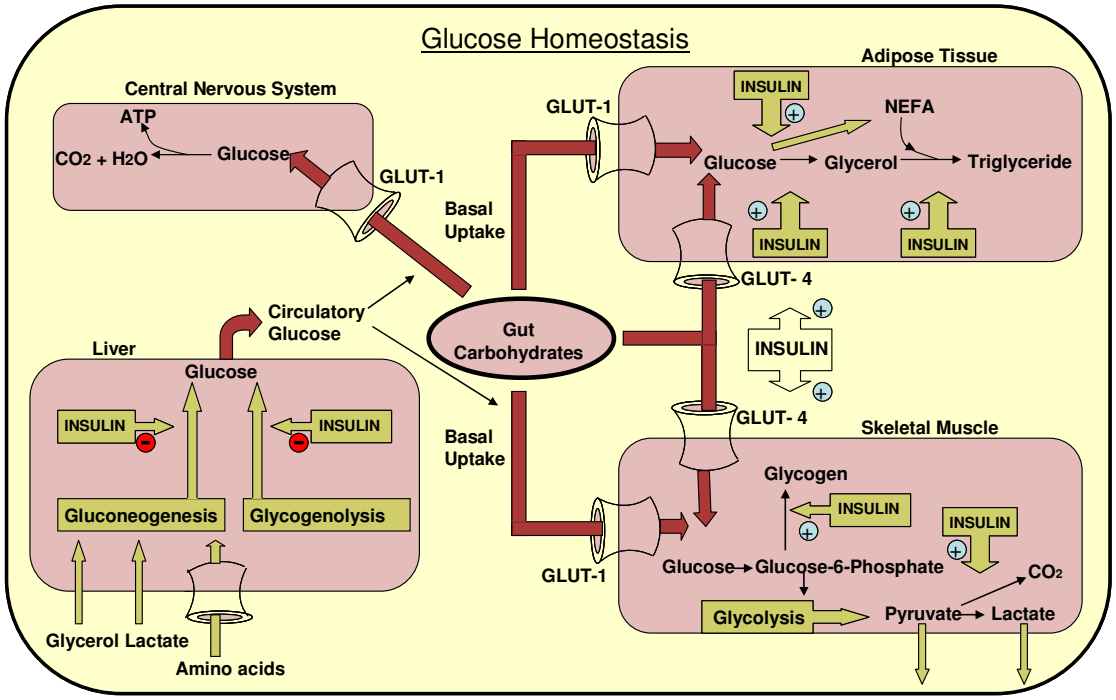

Figure 6 Glucose Homeostasis-The dark red lanes represents circulatory glucose. The two sources of plasma are from digested carbohydrates in the gut and, under fasting conditions, hepatic production. ATP-Adenosine triphosphate; GLUT-1, GLUT-4, glucose transporters 1 and 4; NEFA-non-esterified fatty acids. Insulin action is at the cell surface insulin receptor. Yellow boxes labeled "insulin" show regulatory sites within the cell that are regulated by downstream intracellular components within the insulin response pathway. GLUT-1 carries out insulin-independent basal glucose uptake, whereas the GLUT-4 in the muscle and adipose membrane is controlled by insulin stimulation. Figure designed after figure in [41].

gastrointestinal tract as dietary glucose is absorbed and ingested carbohydrates are broken down into glucose after meals. Insulin is the key hormone for the regulation of blood glucose. Secreted insulin stimulates the uptake of glucose primarily into skeletal muscle and adipose tissue. In skeletal muscle glucose is either stored as glycogen or undergoes glycolysis, by which it is metabolized into three-carbon substrates, pyruvate or lactate. In adipose cells glucose is converted to glycerol for the production of triglycerides.

Normally insulin is quickly secreted by the pancreas in response to increased glucose from a meal. After the postabsorptive phase, in normal individuals blood glucose and insulin levels decrease to basal levels. Under low glucose conditions, an increased secretion of glucagon, a pancreatic hormone with many actions opposite to those of insulin, signals the liver to increasingly respond by producing glucose from hepatic glycogen catabolism (glycogenolysis) and/or by gluconeogenesis from lactate, pyruvate glycerol and alanine. During the early times of a fast (Figure 7), during the "post-

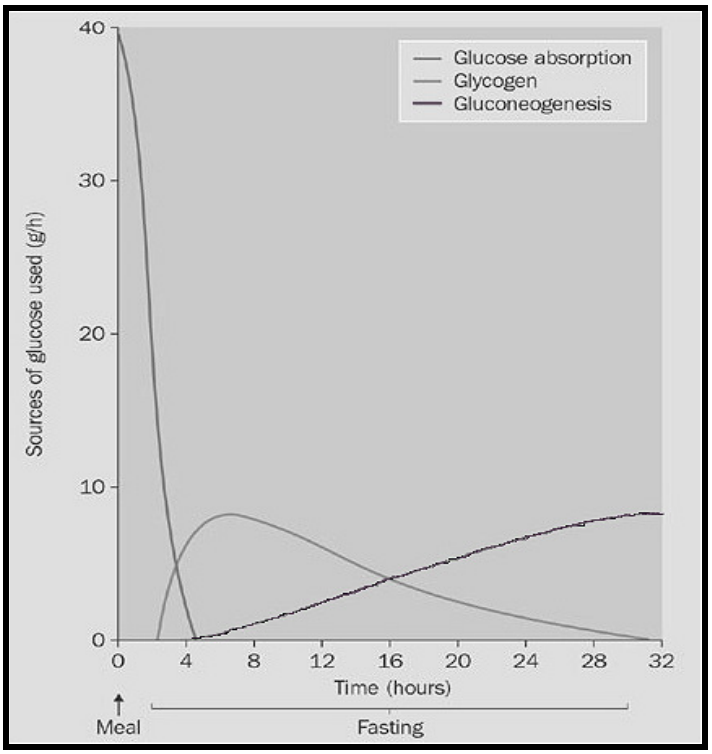

Figure 7 The sources of circulatory glucose after a meal, from [41].

absorptive phase", the needed glucose comes from glycogenolysis. Under more severe fasting conditions, 12-48 hours after a meal, when the glycogen stores are depleted,

gluconeogenesis surpasses glycogenolysis as the primary contributor to hepatic glucose production [41].

Under starving conditions and low insulin levels, mitochondrial pyruvate dehydrogenase activity ("A." in Figure 8) is decreased. This is the committing step of

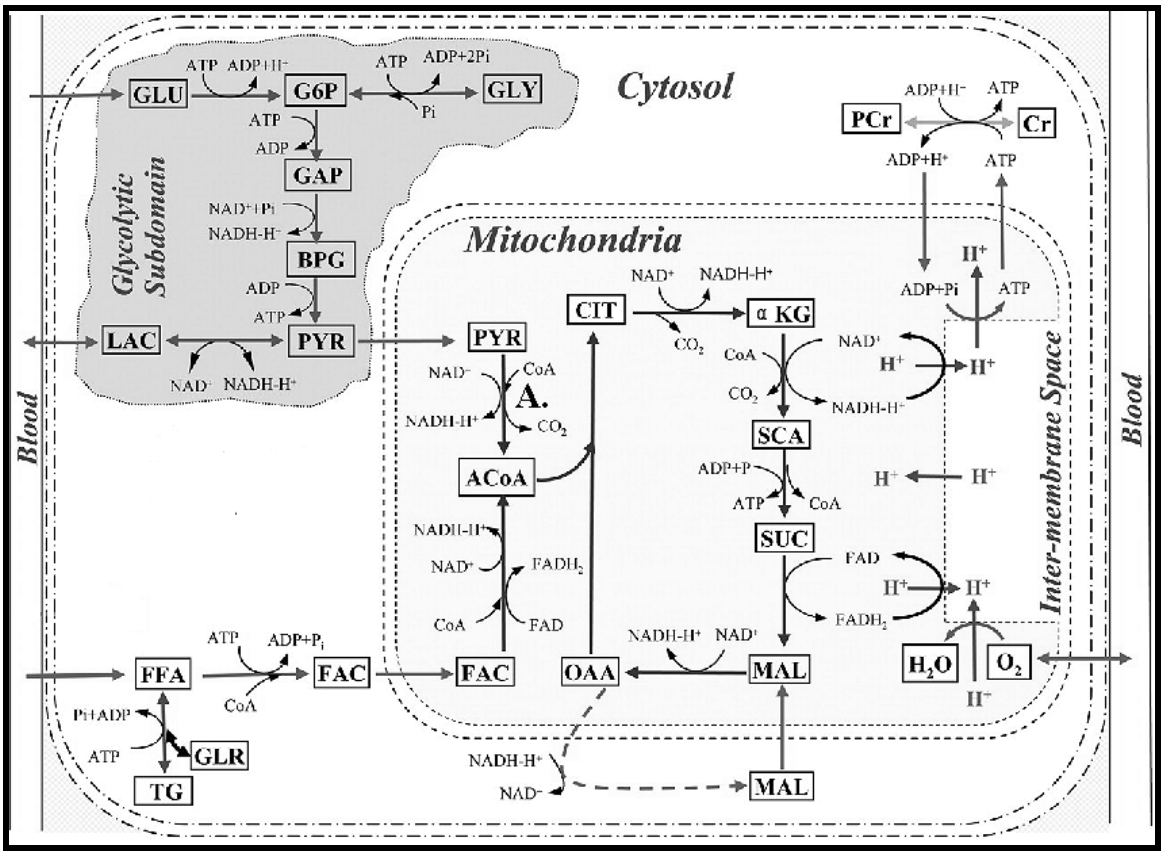

Figure 8 Overview of glycolysis and the TCA cycle, modified from [51].

pyruvate, the 3 carbon product of glycolysis, to the TCA cycle. This promotes the export of pyruvate and lactate that can be used as substrates for gluconeogenesis in the liver. The flow of pyruvate and lactate from muscle and other tissues into gluconeogenesis in the liver is known as the Cori cycle. 12-48 hours after a meal, 80% of glucose utilization

is non-insulin mediated and the primary consumer of glucose is the central nervous system [41].

As we will see, insulin's action on lipid metabolism may be as important to T2DM etiology as its action on glucose metabolism. Importantly, in healthy individuals, insulin effectively suppresses lipolysis in adipocytes and the mobilization of FFAs into the circulation. In concert with its induction of glycolysis, insulin suppresses the oxidation of fatty acids in the muscle. Insulin also promotes the synthesis of fatty acids and triglycerides in the adipose tissue and liver.

An overview of insulin's important roles in carbohydrate, lipid and protein metabolism is shown in Table 2 [41].

Table 2 The wide-ranging metabolic actions of insulin, from [41].

Metabolic Actions of Insulin		
	Action	**Tissue**
Carbohydrate Metabolism		
Glucose transport	Increases	Skeletal muscle, adipose tissue
Glycolysis	Increases	Skeletal muscle, adipose tissue
Glycogen synthesis	Increases	Liver, adipose tissue, skeletal muscle
Glycogen degradation	Decreases	Liver, adipose tissue, skeletal muscle
Gluconeogenesis	Decreases	Liver
Lipid Metabolism		
Lypolisis	Decreases	Adipose tissue
Tryglyceride and fatty acid synthesis	Increases	Liver, adipose tissue
Very low density lipoprotein synthesis	Increases	Liver
Lipoprotein lipase activity	Increases	Adipose tissue
Fatty acid oxidation	Decreases	Skeletal muscle, liver
Cholesterol formation	Increases	Liver
Protein Metabolism		
Amino acid transport	Increases	Skeletal muscle, liver, adipose tissue
Protein synthesis	Increases	Skeletal muscle, liver, adipose tissue
Protein degradation	Decreases	Skeletal muscle, liver, adipose tissue
Urea synthesis	Decreases	skeletal muscle

Three processes need to occur in a coordinated manner, each of them involving insulin, for normal glucose homeostasis in the blood, they are: 1) the secretion of insulin by pancreatic β-cells, 2) the suppression of glucose production by the liver and 3) the insulin stimulated activation of glucose uptake from the blood, especially in skeletal muscle which accounts for more than 80% of the glucose uptake during the normal period of high insulin secretion after a meal [41].

Glucose enters cells through the "GLUT" family of integral membrane facilitative transporter proteins, not all of which transport glucose. Of the 13 currently known structurally related members, GLUT-6, 9, 10, and 12 have unknown functions and GLUT-5, 7, and 11 transport fructose but not glucose [52]. The sequences among the GLUT family member are between 14-63% identical [52].

GLUT-1 is the most ubiquitously distributed glucose transporter and is not insulin mediated, but does act in a cooperative manner with other GLUT forms [52]. As such it mediates basal levels of glucose uptake throughout the body, including transport across the blood-brain barrier and clears glucose, even in insulin resistant individuals. Mutations in GLUT-1 in humans are known to cause intractable seizures as a result of a reduction in glucose transported across the blood-brain barrier [53].

GLUT-2, although a relatively minor form quantitatively, is present primarily in the plasma membranes of pancreatic β-cells, hepatocytes, and kidney epithelial cells [54]. GLUT-2 may have importance in the development of T2DM, as it has been shown to be an important glucose sensor of the pancreatic β-cells, providing feedback on the blood glucose concentration necessary to the regulation of insulin secretion by the pancreas

[54]. In homozygous GLUT-2 knockout mice, the GLUT-2 deficiency caused impaired glucose-stimulated insulin secretion, hyperglycemia and increased levels of circulatory FFA [54]. The GLUT-2 amino-acid sequence has 81% identity between human, mouse and rat [52].

The levels of GLUT-4 on cell membranes are dramatically insulin mediated. GLUT-4 is found primarily in adipose and muscle tissues, including heart and skeletal muscle. During basal levels of blood insulin, corresponding to a time when only 20% of whole-body glucose disposal is by skeletal muscle, 90% of GLUT-4 is stored in vesicles in a cytoplasmic pool. In response to an insulin signal at the cell surface insulin-receptor, these GLUT-4 containing vesicles quickly translocate to and fuse with the plasma membrane, resulting in an increased number of active (facilitative) transporters and increased glucose uptake, 75-95% by skeletal muscle [55]. After the period of insulin response, GLUT-4 transporters are recycled to the cytoplasm by membrane endocytosis and they rejoin the intracellular vescicle pool. Mice in which one allele for GLUT-4 was disrupted had only 50% of the intracellular concentrations of the transporter and, with age, developed severe unresponsiveness to insulin, followed by frank diabetes in over half of the males [56].

Insulin Resistance

Resistance to the insulin-stimulated glucose uptake from the blood has a central role in the pathogenesis and progression of several important diseases including: T2DM, hypertension and coronary artery disease (CAD) [57]. In insulin resistance (IR), insulin loses its potency at accomplishing the second and third of its functions mentioned above;

the suppression of hepatic glucose production and the activation of glucose uptake from the blood. There are many studies showing that insulin resistance plays an important role in the development of T2DM. Examples are: 1) cross-sectional studies showing the presence of insulin resistance in virtually all people with T2DM [58], 2) increased prevalence of insulin resistance in the normo-glycemic offspring of people with T2DM [59] and 3) prospective studies showing that the occurrence of insulin resistance is highly predicative for the development of T2DM [60]. As testament to the complexity of diabetes as a syndrome, although longitudinal and cross-sectional studies have shown that the earliest detectable lesion in the natural history of T2DM is insulin resistance, in some unusual lean type-2 diabetics, β-cell dysfunction is the primary defect and insulin resistance develops concomitantly or subsequently to impaired insulin secretion. But whichever defect, insulin resistance or B-cell dysfunction, initiates the development of T2DM, the second defect eventually emerges [61].

Until the β-cells begin to lose function (gross decompensation), they compensate for insulin's loss of potency by secreting higher levels of insulin (hyperinsulinemia) to keep the blood glucose in the normal range [41, 62]. Figure 9 shows representative data from an experiment called a "euglycemic-hyperinsulinemic clamp" that is often used to illustrate clinical insulin resistance. In this experiment, several initial basal measurements of blood insulin concentration (yellow trace-pmole/L) are taken and then, at t=0 minutes, an insulin infusion is begun, the rate of which is based upon the known kinetics of insulin clearance from the blood. Normally, soon after the infusion was

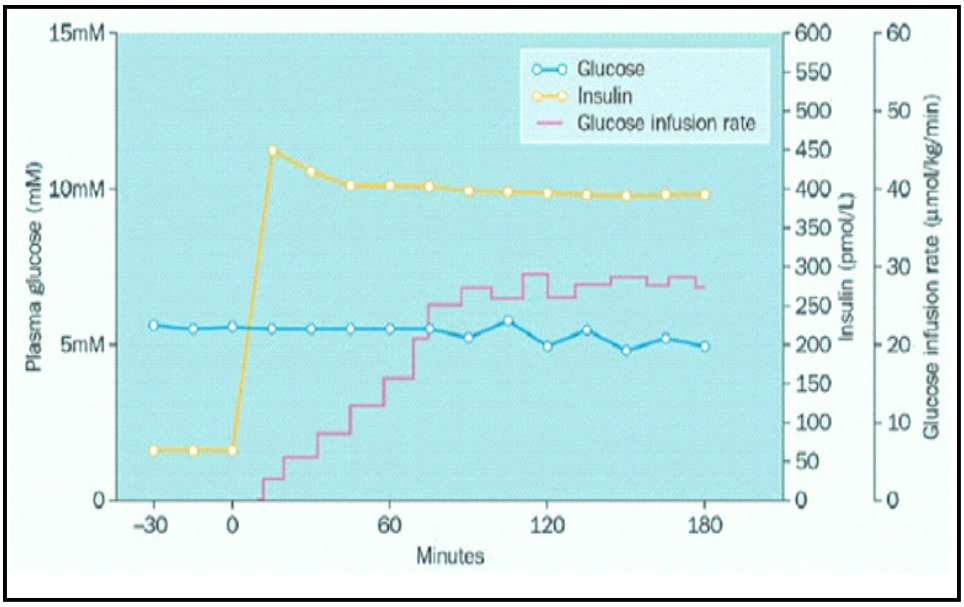

Figure 9 Representative euglycemic hyperinsulinemic clamp showing plasma glucose level, insulin level and glucose infusion rate before and after an insulin infusion that starts at 0 minutes, from [41].

started, the glucose concentration (blue trace-mM) would drop, as the insulin signals for the blood glucose uptake, primarily into cells of skeletal muscle. But during the clamp, a second infusion, of glucose, (pink trace-µmol/kg/min) is simultaneously administered to keep the blood glucose concentration at the basal level (euglycemia). Therefore, at steady state, the amount of glucose required to maintain a basal level for a given concentration of insulin can be determined. Since the blood glucose concentration is constant, the rate of glucose infusion is equal to the rate at which blood glucose is being cleared by tissue. This rate has been found to be significantly lower than controls in T2 diabetics and in normal glucose tolerant (NGT) offspring of T2 diabetics [63], demonstrating the important impairment in glucose utilization that underlies T2DM.

Similarly, insulin resistance manifests in the liver when hepatic glucose production (HGP) is no longer suppressible under hyperglycemic conditions. This manifestation of insulin resistance is believed to be generally secondary to β-cell failure and increased circulatory free fatty acids (FFA) [41], which as we will see, are also associated with T2DM. Circulatory FFA levels increase when adipocytes become resistant to the normal insulin-induced suppression of lipolysis of stored triglycerides [41].

Since skeletal muscle has the predominant role in insulin mediated glucose disposal, it has received most of the experimental focus and it will be emphasized here, followed by overviews of insulin resistance in hepatic and adipose tissue.

Human Studies on Skeletal Muscle Insulin Resistance

In the last twenty years, powerful experiments have been conducted, seeking to understand insulin resistance by attempting to experimentally isolate the molecular defects in the insulin response pathway of T2 diabetics. Non-invasive, in vivo, carbon-13 and phosphorus-31 nuclear magnetic resonance (NMR) experiments have been used to quantitatively study the metabolism of glucose and fatty acids in humans to elucidate, and eliminate, theories as to the site of the pathway defect. In the experiments to be described, [1-^{13}C]glucose was infused to study the rates of glycogen synthesis by [1-^{13}C]-[^{12}C] pulse-chase NMR experiments and [^{31}P] NMR was used to follow both ATP and glucose-6-phosphate (G6P) formation [64].

A 1990 study by Shulman et al., utilized a combination of *in vivo* ^{13}C NMR with a hyperinsulinemic hyperglycemic clamp, to compare the fates of infused [1-^{13}C]-

enriched glucose in the skeletal muscle of human T2 diabetics with the same in control subjects to investigate insulin resistance [65]. Figure 11A shows an example of the ^{13}C NMR spectra in a time course of muscle glycogen synthesis of a normal subject in the glucose-insulin clamp. In the normal subjects, this study confirmed *in vivo* what had been shown previously in biopsies, that glycogen synthesis in human muscle is the primary fate of glucose metabolism. Importantly, it was also found that, despite almost identical concentrations of plasma insulin and glucose in the two study groups under the clamp, the rate of glycogen synthesis in the skeletal muscle of the diabetic group was impaired, being 60% lower ($p<0.005$). Shulman concluded that impaired glycogen synthesis was the major intracellular metabolic defect responsible for the decrease in non-oxidative and whole-body glucose metabolism in T2 diabetics. The experiment also showed that there was a no significant difference in the whole-body oxidative glucose metabolism between the two study groups. Under these conditions, where glycogenesis accounts for the entire non-oxidative glucose metabolism, the oxidative metabolism can be calculated as the difference of the infused amount of glucose subtracted from the indirect calorimetry calculation, after unit conversion and extrapolation to the whole body.

To explain this result, three metabolic steps in the pathway to glycogen synthesis (Figure 10) were considered as candidates for the primary impaired

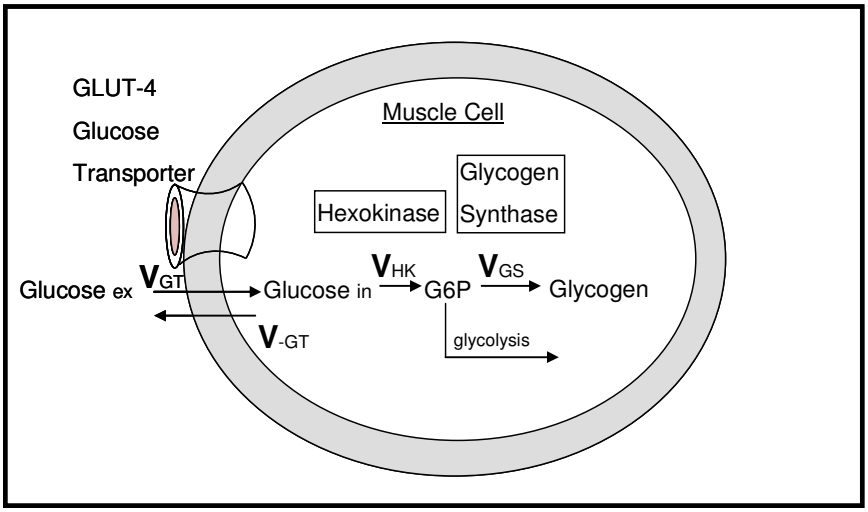

Figure 10 The 3 candidate impaired catalyzing proteins in glycogenesis: GLUT-4, hexokinase, and glycogen synthase.

rate-determining step (RDS) responsible for the decrease in muscle glycogen synthesis in T2 diabetics. The proteins catalyzing these steps were GLUT-4, hexokinase and glycogen synthase. The investigators reasoned that if the defect was at glycogen synthase, then the RDS would be the production of glycogen from G6P, and G6P would accumulate to measurably higher intracellular concentrations in the T2 diabetics. Conversely, if GLUT-4 or hexokinase were the RDS, then the concentration of G6P would be lower in the T2 diabetic group.

To address this question, Shulman's group used *in vivo* ^{31}P NMR (Figure 11B) to monitor G6P concentration in muscle [66]. Again, whole-body oxidative and non-oxidative glucose metabolism was determined by an insulin-glucose clamp in conjunction

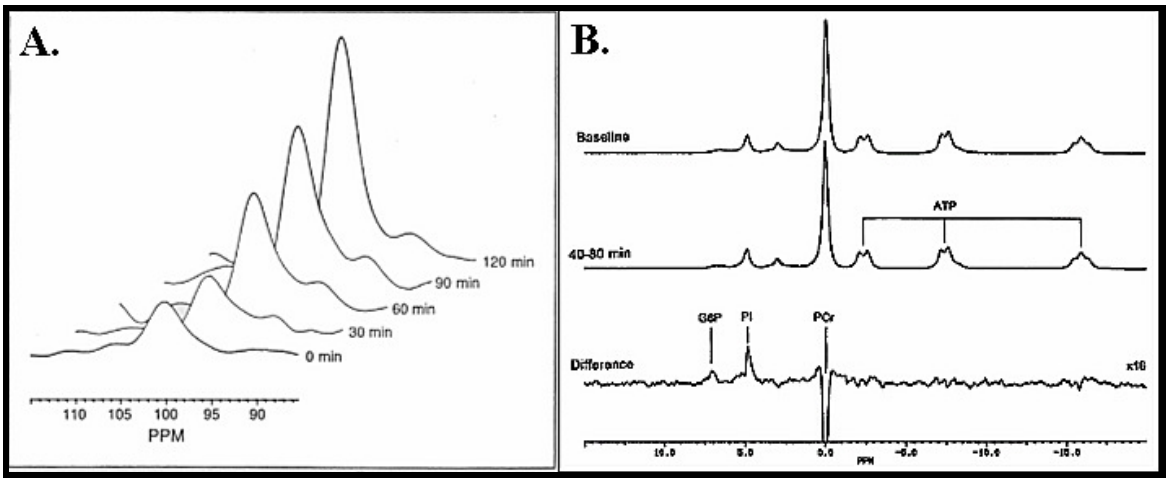

Figure 11 Examples of in vivo NMR. A) ^{13}C NMR time course of ^{13}C glycogen synthesis from infused ^{13}C-1 glucose. The 13C-1 peak of glycogen is at 100.4 ppm, from [65]. B) Difference ^{31}P NMR subtracts the spectrum of the experimental period (40-80 min) from the baseline to show changes as quantifiable peaks from G6P, intracellular phosphate (Pi), and phosphocreatine in muscle, from Rothman et al [66].

with indirect calorimetry. As expected from the previous experiment, it was found that the average glycogen synthesis in T2 diabetics was significantly lower, 13 μmol/kg body wt. vs. 31 μmol/kg ($p<0.05$) for age-matched non-diabetic controls [66]. These results were consistent with the 60% reduction in glycogen synthesis in T2 diabetics vs. control that was previously observed [65]. Moreover, it was found that the concentration of G6P in diabetics was 0.17 μmol/kg muscle wt. vs. 0.24 μmol/kg ($p<0.01$) for controls. The significantly lower level of G6P in T2 diabetics suggested that there is a defect in the glycogen synthesis pathway of insulin resistant muscle which is upstream from the glycogen synthase enzyme.

To discern if the metabolic defect that results in lower glycogen synthesis in T2DM resides at GLUT-4 or hexokinase, a hyperinsulinemic-hyperglycemic experiment

was performed by Shulman's group in 1999 which used a combination of ^{13}C and ^{31}P NMR [67] to simultaneously compare intracellular glucose, G6P and glycogen concentration between controls and T2DM patients. To control for possible differences in the flow of interstitial glucose and insulin to the muscle cells of the experimental groups, the gradient of glucose concentrations between the plasma and the interstitial fluid was measured by in vivo microdialysis. Also the interstitial insulin levels were measured by open-flow microperfusion. No difference between the study groups in either the interstitial glucose or insulin or was observed. However, an 80% decrease in the glucose infusion rate and in both glycogen synthesis and concentration of G6P in T2 diabetics was observed in an initial low rate of insulin infusion. Reasoning that intracellular glucose is the intermediary between transport and hexokinase activity, the amount of intracellular glucose in the T2 diabetics was calculated to be $1/25^{th}$ the expected amount if the impairment in glucose metabolism was at hexokinase. Upon a subsequent infusion of a higher insulin concentration, increased by a factor of 10, the changes in the concentrations of intracellular glucose and G6P showed that the rates of glucose transport were matched by increases in the rates of glucose phosphorylation and glycogen synthesis in the T2 diabetic subjects. This supported the hypothesis that the observed impairment of glycogen synthesis was largely due to an impairment of glucose transport at GLUT-4 in skeletal muscle and not in the rate of hexokinase activity, but it did not rule out the possibility of additional impairments along the glycogen synthesis pathway that may not have had a strong rate determining effect under the experimental conditions.

The researchers concluded from this series of experiments that a defect in the GLUT-4 response pathway was the likely site for the limiting step that contributed to abnormally decreased glucose metabolism in T2DM. A direct genetic cause was not likely because mutations in *GLUT-4* are very rare and have the same incidence in non-diabetics as in diabetics [68]. But insulin resistance is not only associated with impaired glucose tolerance. It frequently presents along with central obesity, high levels of circulatory FFAs and hypertension. This group of metabolic abnormalities is found together in individuals more often than should be expected by chance alone, and has variably taken the names "syndrome X", "insulin resistance syndrome" and "metabolic syndrome" among others [69]. We will now turn our attention to a line of research that focused on the mechanistic connections of insulin resistance with other components of the metabolic syndrome, specifically high levels of circulatory FFAs, which has added interesting insights into the etiology of insulin resistance.

The etiological studies of diabetes had begun to loosen from a "glucose-centric" perspective as far back as the 1960s. A cellular mechanism had been proposed by Randle in 1963 [70] that attempted to connect abnormal metabolism of FFAs to the pathogenesis of T2DM, what today is known as "lipotoxicity". Randle proposed that the oxidation of excessive FFA levels from uninhibited lipolysis of triglycerides in diabetes could create high levels of mitochondrial acetyl-CoA (see Figure 8). Acetyl-coA is a powerful allosteric inhibitor of pyruvate dehydrogenase [71] and excessive acetyl-CoA impairs glucose metabolism by inhibiting pyruvate dehydrogenase [72], which catalyses the committing reaction of the product of glycolysis, pyruvate, to the TCA cycle. Also, high

intracellular levels of FFA would be expected to lead to a rise in intracellular citrate, which regulates glycolysis by inhibiting phosphofructokinase, leading to the subsequent accumulation of G6P [70]. In Randle's model the elevated G6P levels would inhibit hexokinase activity leading to decreased glucose uptake. However, as shown in Shulman's result, G6P was found in lower levels in T2 diabetics, so a different mechanism of FFA metabolism induced insulin resistance has been sought.

Impairments of FFA metabolism in T2DM have long been acknowledged, if not as the cause of insulin resistance, at least associated with it. A clear demonstration of the defect was published in 1989 [71]. Figure 12, from that publication, shows the relationship of pre-infused plasma [^{14}C] palmitate concentration (Figure 12A) and plasma [^{14}C]palmitate turnover (Figure 12B) with the level of infused insulin at six different quantities of infused insulin, in 8 human non-diabetics (solid line) and 9 age- and weight-matched type-2 diabetics (dashed line). While the control group showed nearly maximally suppressed FFA turnover at the lowest insulin dose, the T2 diabetic group shows a marked impairment in the ability of insulin to inhibit FFA turnover during each insulin step ($P < 0.05$). Normally, the plasma FFA concentration is determined by the rate of entry from adipose tissue (lipolysis) and the rate of exit from the plasma. Exit from the plasma occurs by two metabolic pathways, entry into cells for oxidation or re-esterification to triglycerides. Using the ^{14}C isotope to measure $^{14}CO_2$ activity, it was shown that approximately 30% of basal plasma [^{14}C]palmitate turnover (Figure 12B) was accounted for by FFA oxidation (Figure 12C) in both groups. At all higher plasma

insulin concentrations, FFA oxidation was at least twice as great in the T2DM group compared to controls ($P < 0.05 – 0.01$). In the basal state both groups showed ~70% of

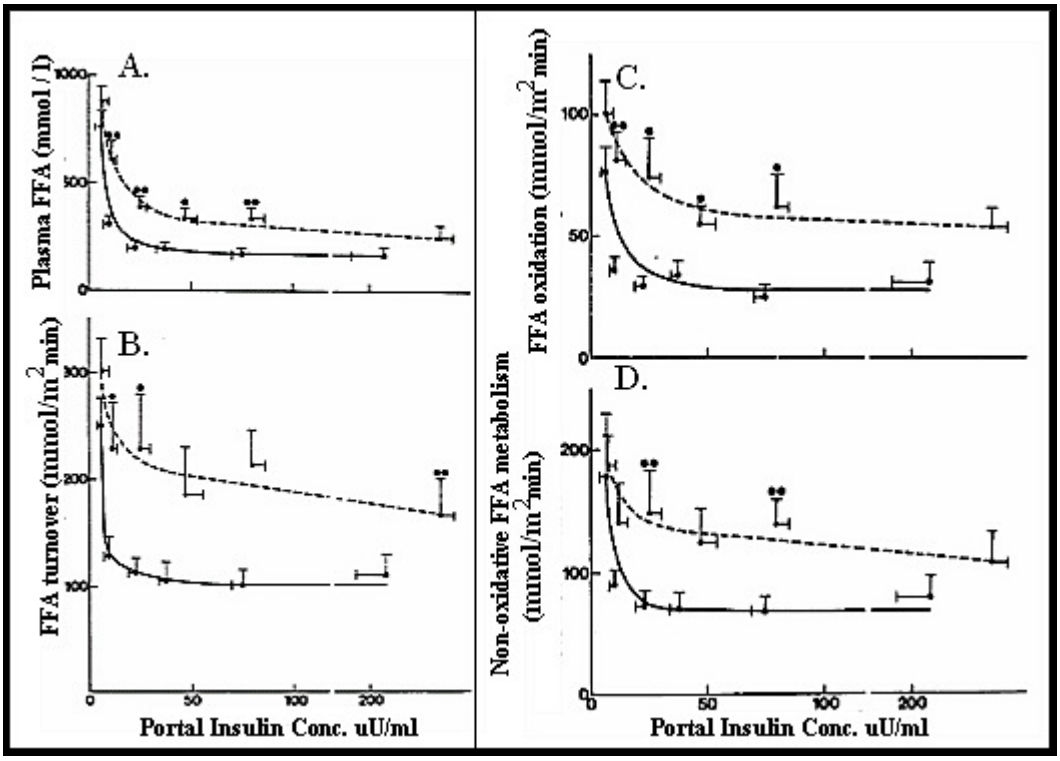

Figure 12 Impaired disposal of infused circulating [^{14}C] palmitate in T2DM as a function of infused insulin concentration. A) FFA concentration, B) FFA turnover. Dashed lines are T2 diabetics (n = 9) and solid lines are NGT subject (n = 8), (*$p < 0.05$, **$p < 0.001$), from [71].

the FFA was channeled into re-esterification to triglycerides, i.e. non-oxidative metabolism. Non-oxidative FFA metabolism in the T2 diabetic group was ~40% higher compared with the controls at each insulin dose (Figure 12D).

The authors concluded, because of the positive correlation between HGP and FFA oxidation, that insulin resistance is a ubiquitous feature of normal weight T2 diabetics as it involves both glucose and FFA metabolism. Further, they suggested that the

disturbances in FFA metabolism may be linked with the decrement in glucose utilization in skeletal muscle.

A 1997 study [73] compared the circulatory lipid compositions of 49 normoglycemic subjects (4.99 $\pm$ 0.51 vs. 4.95 $\pm$ 0.41 mmol/L) who had one parent with T2DM with 29 well-matched controls, whose parents were not diabetic. The groups were matched according to age, FPG, hemoglobin A1c, body-mass index, weight/height ratio, body fat on limbs, body fat on trunk and physical activity. With the exception of their fasting plasma FFA levels, there were no significant differences between the groups in their lipid composition profiles, which included blood concentrations of total cholesterol, high density lipoproteins (HDL), low density lipoproteins (LDL), and triglycerides. The average concentration of fasting plasma FFA in the T2DM offspring group was 582 μM vs. 470 μM for controls (p=0.007). The groups were also distinguishable by their average fasting levels of insulin concentrations (T2DM offspring=40.6 $\pm$ 15.8 vs. controls=30.9 $\pm$ 13.6 pM, P=0.005) and their insulin sensitivity in a hyperinsulinemic-euglycemic clamp (T2DM offspring=4.86 $\pm$ 1.65 vs. controls=6.17 $\pm$ 1.56 mg/kg·min glucose, P =0.001). This measurement, indicative of insulin sensitivity, is labeled "M" in Figure 13. Figure 13 shows a simple regression analysis of the individual subjects' fasting plasma FFA and insulin sensitivity M, separated into the two study groups. The figure shows that for the T2 diabetic offspring group, a moderately strong trend (dark spots, $R^2 = 0.21$ equivalent to p= 0.0005), correlating high FFA with low insulin sensitivity is produced. But for the controls, no trend (hollow spots, $R^2 = 0.03$ equivalent to p = 0.368) is produced.

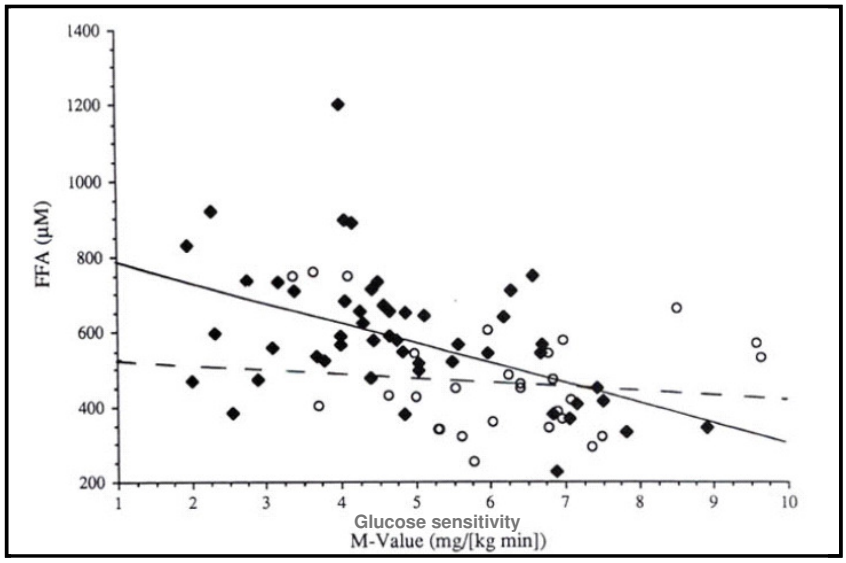

Figure 13 Plasma FFA level predicts insulin resistance. Regression analysis of plasma FFA vs glucose sensitivity (M-value). The solid line represents the adjusted $R^2 = 0.21$, equivalent to P =0.0005 for 49 offspring with one diabetic parent. The dashed line represents $R^2 = 0.03$ equivalent to P = 0.37 of 29 well-matched control subjects, from Perseghin et al 1997 [73].

This inverse relationship between insulin sensitivity and FFA concentration suggested that impaired metabolism of FFA may have an important causal role in insulin resistance, as had been suggested by Randle [70], since it appeared to occur prior to the development of elevated FPG, in these normoglycemic offspring of T2 diabetics.

The earlier findings implicating a defect in the GLUT-4 pathway inspired research along similar line of reasoning that incorporated FFA infusion. Euglycemic hyperinsulinemic clamp experiments, similar to previous ones using *in vivo* ^{31}P and ^{13}C NMR, were conducted on 9 healthy humans with the addition of an infused triglyceride/glycerol emulsion to examine the relationship of FFA to the induction of insulin resistance [74]. As seen in Figure 14, for three hours after the start of the infusion, the levels of glucose uptake were similar between the two groups. This was

matched by similar level of glycogen synthesis (not shown). But, by six hours the lipid-infused subjects' glucose uptake had decreased to 46% ($p < 0.00001$) of control values (glycerol infusion), making them as insulin resistant as T2 diabetics [74]. Glycogen synthesis was similarly, ~50% ($p < 0.05$), reduced, as measured by *in vivo* ^{13}C NMR. Importantly, and supporting the earlier findings, the earliest detection of impaired

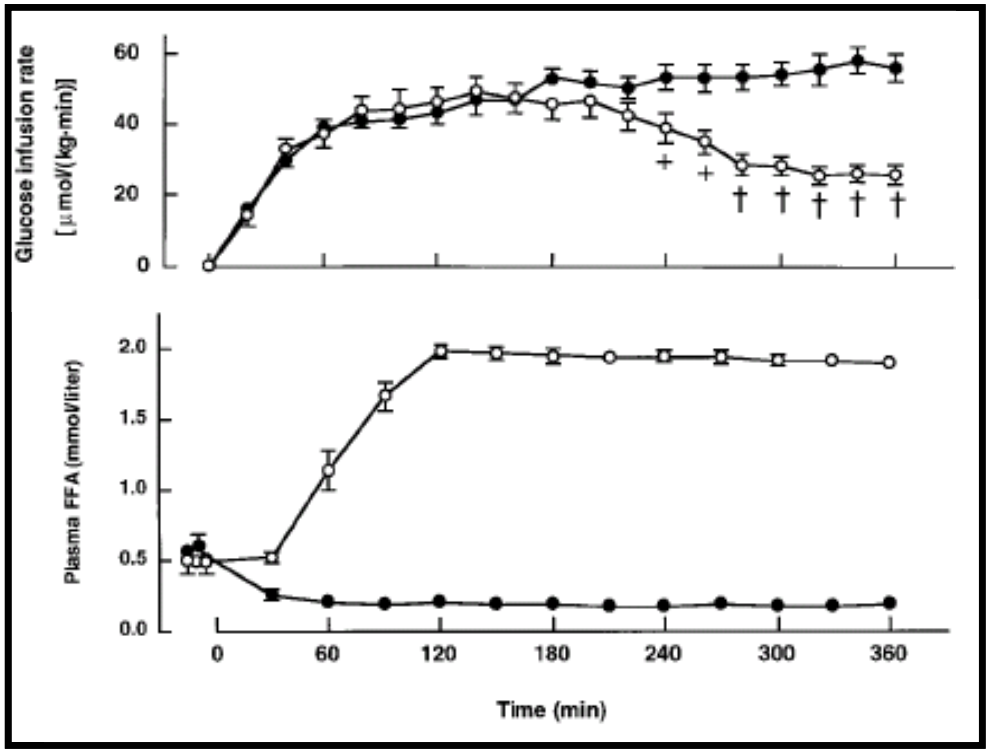

Figure 14 Acute FFA induced insulin resistance in healthy human subjects- Closed circles indicate infusion with low concentration of fatty acids. Open circles indicate infusion of high FFA concentration. By six hours from start the (previously) healthy individuals are as insulin resistant as many type-2 diabetics. All units expressed as means $\pm$ SEM of nine paired studies. + = $p < 0.01$, † = $p < 0.001$, from [74].

glycogen synthesis was preceded, by about 1.5 hours, by an 18% decrease ($p < 0.01$) in G6P, as measured by *in vivo* ^{31}P NMR (not shown) which continued to decrease to 57% of controls at the end of the 6 hour test. Again the data suggested that the mechanism, by

which elevated plasma levels of FFA had induced insulin resistance, was upstream of glycogen synthase. But because the intracellular glucose was not measured it was impossible to discern if the FFA induced impairment was at the glucose transport or the hexokinase activity [74].

A 1999 follow-up study, by Dresner et al. [75], was conducted that also used a lipid infusion in conjunction with a euglycemic-hyperinsulinemic clamp, but which measured intracellular glucose, glycogen synthesis and G6P concentration. Each of 7 healthy subjects, were tested twice, first during a basal vehicle infusion (glycerol/heparin) and then during an FFA plasma infusion (lipid/heparin). G6P concentration found to be decreased by 90% in the lipid infused protocol ($p < 0.02$). This was consistent with what had been observed in patients with T2DM [66] and another strong contradiction to the mechanism of Randle [70] who had posited that G6P would be elevated in T2DM. Importantly, this experiment also showed that there was a significant reduction in the amount of intracellular glucose in the skeletal muscle cells of the subjects under the lipid/glycerol infusion (0.04 ± 0.06 mM) compared to the glycerol infusion (0.25 ± 0.07 mM, $p = 0.04$), a result that discerned a defect in glucose transport. Dresner also attempted to trace the defect in insulin stimulated glucose transport to an intracellular event prior to glucose transport. To clarify Dresner's result it is now helpful to introduce the known intracellular insulin response transduction pathway, and return to Dresner's result afterward.

The previous discussion of facilitative glucose transporters described the intracellular pool of GLUT-4 transporters that translocate to the plasma membrane in the

human skeletal muscle cell in response to the insulin signal at the insulin receptor on the cell surface. Figure 15 shows intracellular signal transduction pathways that are initiated at the insulin receptor and that affect GLUT-4 translocation. Briefly, the insulin signaling cascade is initiated by circulating insulin binding to the extracellular domain of its receptor, which is a receptor tyrosine kinase. Homologs of the human insulin receptor

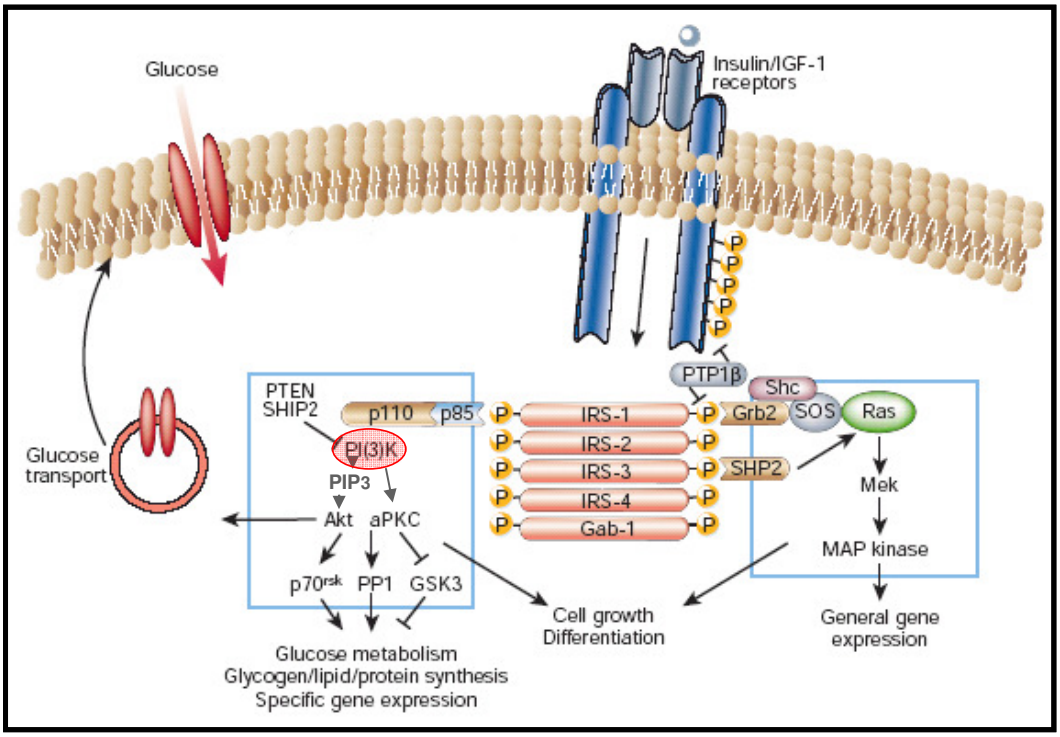

Figure 15 Skeletal muscle insulin transduction pathways. Adapted from Saltiel and Kahn, [76].

exist in *Drosophila, C. elegans* and metazoan sponges, which utilize several of the same downstream signals that are critical to regulation of mammalian cells [76]. On binding insulin, the cytoplasmic domain of the activated receptor undergoes a conformational change, resulting in autophosphorylation of tyrosine residues located in its cytoplasmic domain. Several studies have demonstrated that impairments of the insulin receptor

activity in T2 diabetics are mild to non-existent [77]. The activated receptor then recruits and phosphorylates several substrates [77]. Among these are 4 highly homologous proteins known as the insulin receptor substrate (IRS) proteins 1-4 that appear to play complementary, rather than redundant roles. Mouse knockouts of IRS-1 display insulin resistance in peripheral tissues and impaired glucose tolerance. Knockouts of IRS-2 have insulin resistance in peripheral tissues and the liver. Homozygous IRS-2 knockouts experience insulin resistance with decreased β-cell mass and development of T2DM [78]. This is contrasted with IRS-3 and IRS-4 knockouts which appear to have no loss of normal metabolic functions [76]. IRS-1/2 are adaptor proteins that play crucial roles in coupling the insulin signal to both the phosphatidylinositol 3-kinase (PI3K, orange oval in left blue box of Figure 15) pathway and the MAPK pathway (right blue box in Figure 15). Central to the regulation of IRS proteins, and indicative of their complexity, is the presence of multiple serine/threonine phosphorylation sites identified on their structure which modulate their function, positively or negatively, as a result of different phosphorylation patterns [77]. In Figure 16 is a map of human IRS-1 with some of its

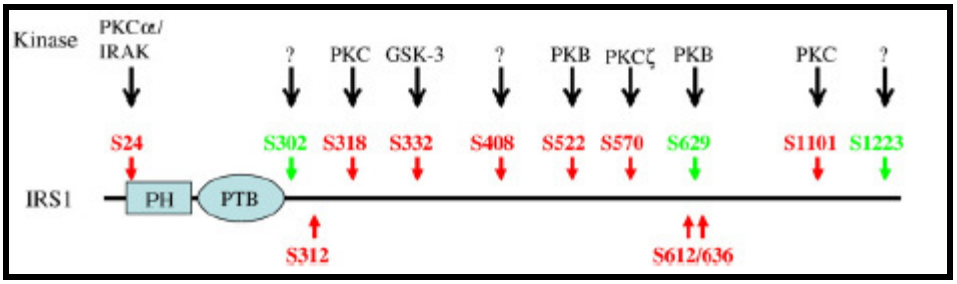

Figure 16 Phosphorylation sites of human IRS-1. Phosphorylation at the red sites inhibit IRS-1 and phosphorylation at the green sites activate IRS-1. PH, pleckstrin homology domain: PTB, phosphotyrosine binding domain, from [77].

identified phosphorylation sites and identified kinases. The PI3K pathway is believed to determine GLUT-4 translocation. As a result of insulin receptor activation, the tyrosine phosphorylated IRS-1/2s recruit heterodimeric p85/p110 and phosphoinositide 3-kinase (PI3K) at the plasma membrane, forming the lipid second messenger phosphatidylinositol triphosphate (PIP_3) (Figure 15). PIP_3 targets the serine/threonine kinase Akt, also known as protein kinase B (PKB in Figure 17). Figure 17 summarizes the human *ex vivo* tissue

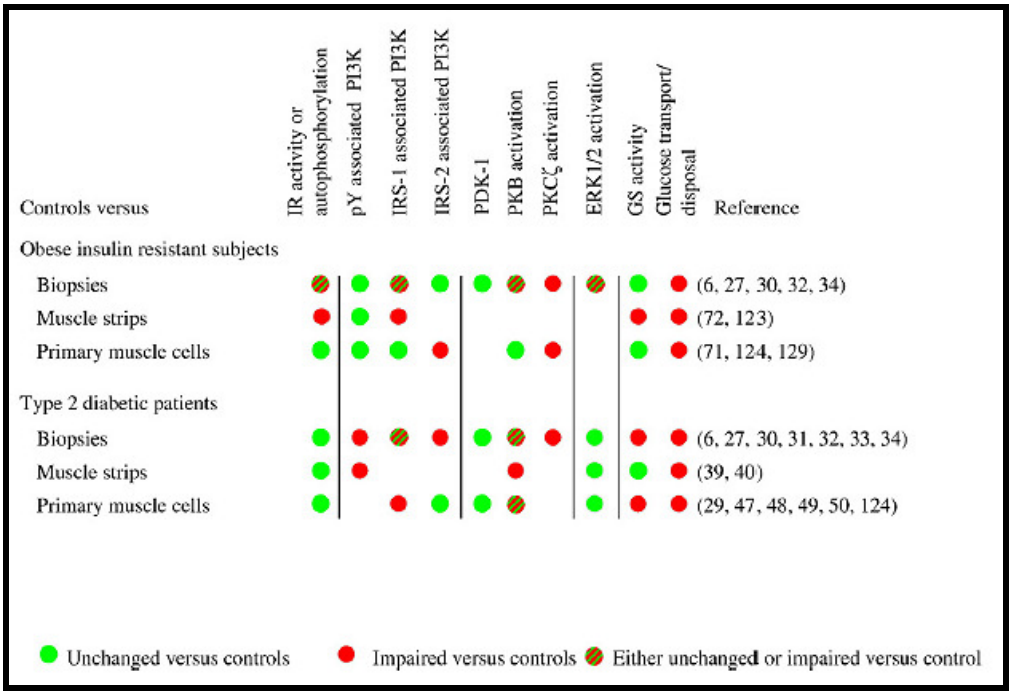

Figure 17 Points of consensus on the contributions of particular components of the insulin signaling pathway to insulin resistance, from [77].

studies and the conclusions from many independent experiments as to the contribution to insulin resistance made by the particular components of the insulin signaling pathway that were investigated. In T2DM patients, there is unanimous agreement that there is no impairment of the insulin receptor activity and that there are impairments in glucose

transport and tyrosine phosphorylation associated with signal transduction to PI3K.

We will now return to the previous discussion of Dresner's clinical lipid infusion experiment [75]. Biopsies were taken from the skeletal muscle of 7 healthy subjects (different subjects than the NMR experiment), before and after the lipid infusion. Assays were then conducted for PI3K activity in anti-IRS-1 immunoprecipitations. It was found that after 5 hours of glycerol infusion (control) and 30 minutes after starting the hyperinsulinemic-euglycemic clamp, that the IRS-1-associated PI3K activity was increased by 400 $\pm$ 120% ($p < 0.01$) over the basal level. The same test conducted concurrently with a lipid infusion yielded no significant increase, 112 $\pm$ 13%, in activity over the basal level in the same time frame. Together, these results showed that elevated plasma FFA levels caused insulin resistance in skeletal muscle by reducing insulin stimulated glucose transport, and this insulin resistance was a consequence of an effect on IRS-1-associated PI3K.

The overall importance of this line of research was to show that acutely induced insulin resistance by FFA infusion resembled insulin resistance in T2DM in that it was associated with a loss of insulin mediated glucose transport, specifically at GLUT-4. It was previously unknown whether the FFA effects were on GLUT-4 directly (eg. vesicle trafficking, budding, membrane fusion) or upstream signaling of GLUT-4. It was found that infused lipid induced an early intracellular impairment in the insulin signaling pathway of skeletal muscle, existing after receptor initiation and, at least in part, involving IRS-1 associated PI3K activity.

Animal Studies on Skeletal Muscle Insulin Resistance

It was shown in 1991 that high fat diets (59% fat) could induce insulin resistance in Zucker rats, [79] but that the effect was very dependent upon the carbon chain length of the FFA. Diets that were high in saturated FFA (19%), monounsaturated FFA (45%) or polyunsaturated FFA (46%) significantly induced insulin resistance. Diets that were high in saturated FFA (33%) but included 6% fish oil, with long-chain ω-3 FFA (eicosapentaenoic acid, 20:5 and docosahexaenoic acid 22:6), were found not to cause insulin resistance. Diets that were high in polyunsaturated long-chain FFA (41%) but included 6% fish oil were also found to not cause insulin resistance. The authors noted that studies on human T2 diabetics had shown little or no efficacy of fish oil supplementation on glucose tolerance [80].

Mouse and rat studies were conducted that further investigated the lipotoxicity model. It was shown in 1999 by Griffin et al. [81] that WT rats infused with lipid emulsions under hyperinsulinemic euglycemic conditions had the expected insulin resistance, decreased glycogen synthesis and decreased glucose transport within 5 hours. In addition it was shown that there was a 50% reduction in IRS-1 associated PI3K activity (Figure 18-1, $p<0.05$) in lipid-infused compared to glycerol-infused controls. Using anti-phosphotyrosine antibodies for immunoprecipitations, followed by anti-IRS-1

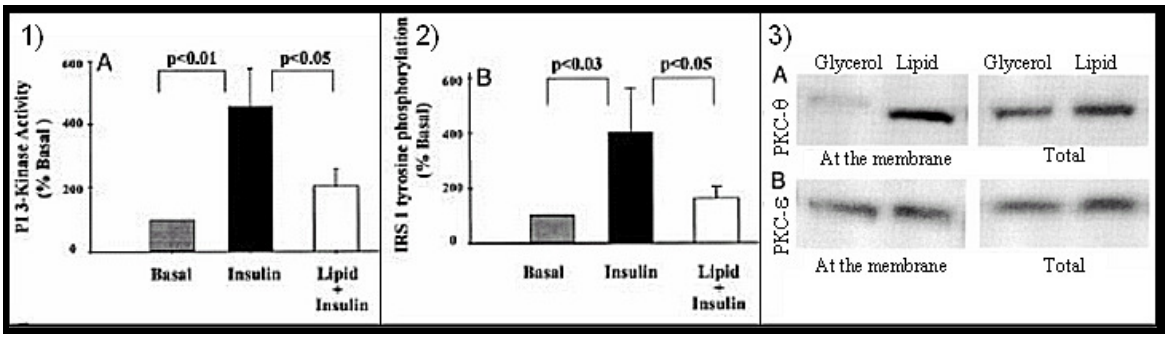

Figure 18 Changes in mouse insulin signal transduction with FFA infusion, 1) PI3K activity, 2) IRS-1 tyrosine phosphorylation, 3A) PKC-θ translocation assay and 3B) PKC-ε translocation assay, from Griffin et al. [81].

antibodies in western blots, it was also shown that there was a 58% decrease in IRS-1 tyrosine phosphorylation in the lipid infused rats relative to control (Figure 18-2, $p < 0.05$). This level with lipid and insulin was insignificantly different from basal without insulin ($p = 0.51$).

Two isozymes of a protein in the lipid metabolism pathway, PKC-θ and PKC-ε were also measured using anti-peptide antibodies specific for the θ and ε protein forms. The PKC superfamily consists of 12 known proteins that have many cellular substrates which are involved in a vast array of biological processes. The specificity within the family is a result of the PKC isotypes responding to different activation and localization signals [82]. PKC-θ and PKC-ε belong to the 4 member "novel" subgroup defined by its members' sensitivity to diacylglycerol (DAG), insensitivity to Ca^{2+} and their translocation from cytosol to membrane upon activation. It had previously been shown [83] that 5 hour lipid infusions increased skeletal muscle concentrations of triglycerides and long chain acetyl CoA (LCCoA), which could, it was speculated, have led to

increases of DAG in rats. Activation of PKC-θ was demonstrated (Figure 18-3A), as seen by its increased association with the membrane fraction in the lipid infused mice vs. controls, (2.2 ± 0.6 vs. 0.5 ± 0.1 OD, $p < 0.03$) [81]. The authors of this study concluded by hypothesizing that the increases in plasma FFA concentrations, caused by infusion, lead to the increase in muscle diacylglycerol (DAG) levels, thereby "activating PKC-θ, a serine kinase that causes increased serine phosphorylation of IRS-1. Such serine phosphorylation would reduce the ability of IRS-1 to activate PI3K" [81].

A unifying model for FFA induced insulin resistance, which incorporated the evidence outlined above is shown in Figure 19 [72]. The model proposed that elevated intracellular lipid metabolites, such as DAG and LCCoA, activate a serine/threonine phosphorylation cascade, initiated by PKC-θ, leading to phosphorylation of serine and/or threonine sites on insulin receptor substrates, such as IRS-1. These serine phosphorylated insulin receptor substrates fail to efficiently activate PI3K.

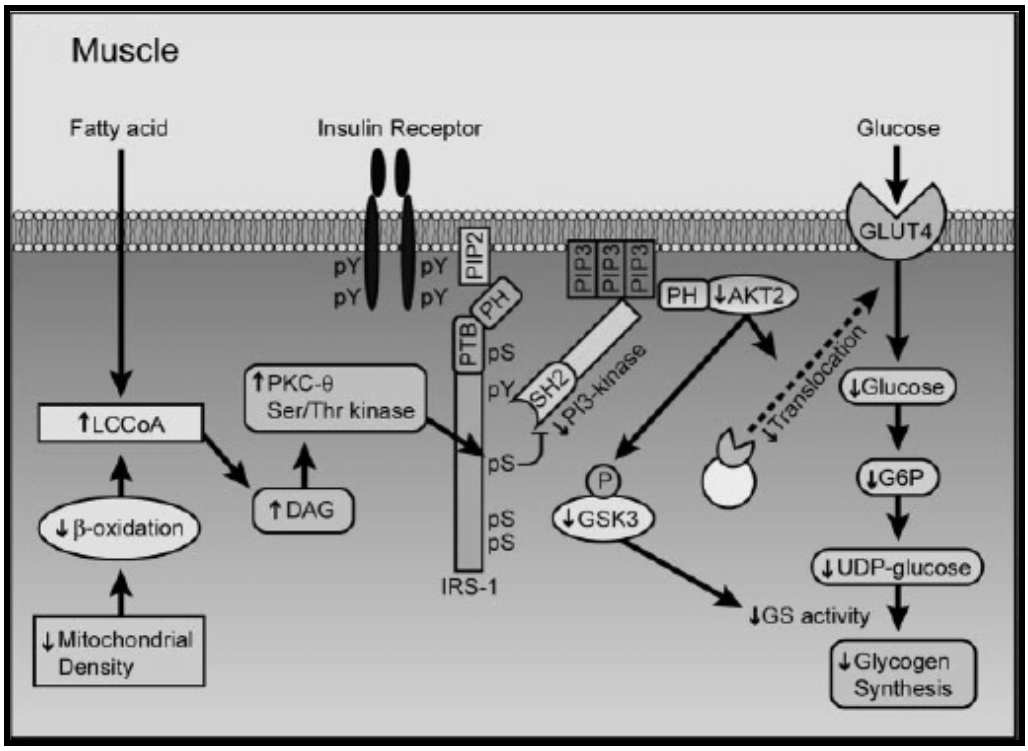

Figure 19 Model for the mechanism of FFA induced insulin resistance in skeletal muscle, from [72].

Low activation of PI3K is believed to be at the crux of the cell's blunted physiological response to insulin, specifically, the reduction of GLUT-4 translocation to the plasma membrane via AKT2 activation and thus, reduced glucose uptake. The mechanism shown in Figure 19 is proposed to lead to the clinical consequences of insulin resistance and T2DM.

In 2002, this hypothesis was tested in a study on rats by Yu et al. [84]. Quantitative liquid chromatography-tandem mass spectrometry (LC/MS/MS) was used to measure lipid metabolites in skeletal muscle tissues after infusing triglyceride emulsion. It was found that: 1) intracellular levels of LCCoA and DAG were elevated as predicted

and were associated with PKC-θ membrane translocation to the membrane from the cytosol, 2) IRS-1 tyrosine phosphorylation was reduced, 3) PI3K activity was reduced, and 4) insulin receptor tyrosine phosphorylation was unaffected, as had previously been shown. And more importantly, it was shown, using anti-phospho-ser-307 antibodies, that IRS-1 serine phosphorylation was significantly increased in lipid infused rats vs. control (1.6 fold, $p < 0.003$), as had been hypothesized [81] (although the hypothesis was not specifically increased ser-307 phosphorylation, but increased serine phosphorylation).

In 2004, PKC-θ knockout (KO) mice were developed and underwent hyperinsulinemic euglycemic tests and tissue biopsies to measure several of the important metabolites and proteins implicated above [85]. PKC-θ KO mice developed normally and had body weights, basal plasma glucose, basal plasma insulin and basal plasma lipid levels that were indistinguishable from their wild-type (WT) counterparts. Under clamp conditions, (Figure 20) however, it was found that the lipid infused PKC-θ KO mice were protected from FFA induced insulin resistance (Figure 20A and B). They also exhibited no disruptions of IRS-associated PI3K activity (Figure 20C), or reduced IRS-1 tyrosine phosphorylation (Figure 20D), and insulin receptor phosphorylation was not significantly changed from WT control (Figure 20E), within the relatively short, 90-120 minutes, time-frame of this test. However, it seems fair to ask why IRS-1 Ser-307 phosphorylation was not measured and why these tests were run for only for 90-120 minutes when most of the previously cited publications reported 5 hour experiments, particularly since this is the same laboratory that had previously measured Ser-307 phosphorylation and consistently run tests for 5 hours [84].

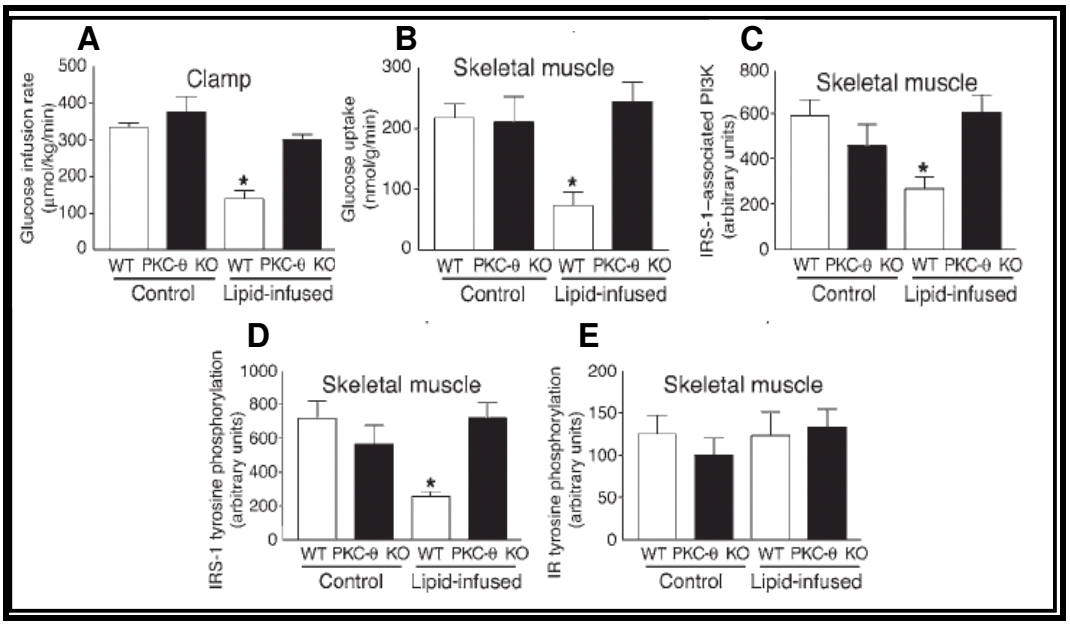

Figure 20 PKC-θ is implicated in the pathway to FFA induced IR, from Kim et al. 2004.

Nevertheless, abnormalities in the metabolism of FFAs and their effects on carbohydrate metabolism have developed into the present day "lipocentric" view of the mechanism of insulin resistance fundamental to T2DM. This disease model provides a mechanism for how FFAs cause insulin resistance in skeletal muscle and clarifies the connection between the observed high co-incidence of visceral or central obesity (lipodystrophy) and insulin resistance. It is believed that in obese states the energy storage capacity of adipose tissue can be exceeded and that there is an "overflow" or misplacement into "ectopic" sites, such as the liver and skeletal muscle [72]. In genetically predisposed individuals, this may be "lipotoxic" enough to cause insulin resistance and T2DM. This important topic will be discussed in greater detail and from the perspective of obesity-associated chronic inflammation in the last section on insulin resistance.

Gavrilova et al. [86] developed a transgenic mouse in 2000, named A-ZIP/F-1, which have almost no white adipose tissue. The A-ZIP/F-1 phenotype closely resembles that of human "lipoatrophic diabetes", including a lack of adipocytes, insulin resistance, hyperglycemia, hyperlipidemia and ectopic liver fat. This model is consistent with the hypothesis that insulin resistance in skeletal muscle is caused by "overflow" of FFA when adipose capacity is exceeded.

At 5 weeks of age, A-ZIP/F-1 mice were given several small transplants of WT fat amounting to less than 4% of their total weights. Interestingly, at this time it was found that A-ZIP/F-1 mice already had histological evidence of β-cell derangement and enlarged pancreatic islets, a sign of β-cell compensation for the reduced insulin sensitivity by attempting to produce more insulin.

Just two weeks after the WT fat was transplanted into the A-ZIP/F-1 mice, the diabetes was corrected, including restoration of normal blood glycemia and insulin concentrations and improvement of the histological appearance of the β-cells. However, after 6 weeks there was a steady diminishment in the improvement of the diabetic phenotype in the A-ZIP/F-1 mice that continued until the time of their sacrifice at 13 weeks. This was explained by the authors to be a result of limited functional capacity of the transplants or the intrinsic insulin resistance of the recipient mice, as they were already diabetic at the time of transplantation. This study also investigated whether injections of leptin, an endocrine hormone secreted by adipose cells that had been shown to improve insulin sensitivity [87], would improve the insulin sensitivity in non-transplanted mice and found that it did not.

These results show that a paucity of fat, in accord with the FFA overflow hypothesis, can cause diabetes in mice, supporting the hypothesis that an “overflow” of lipids to ectopic sites may be important to the development of insulin resistance and T2DM in humans.

Figure 21 shows an overview of the glucose and FFA metabolism

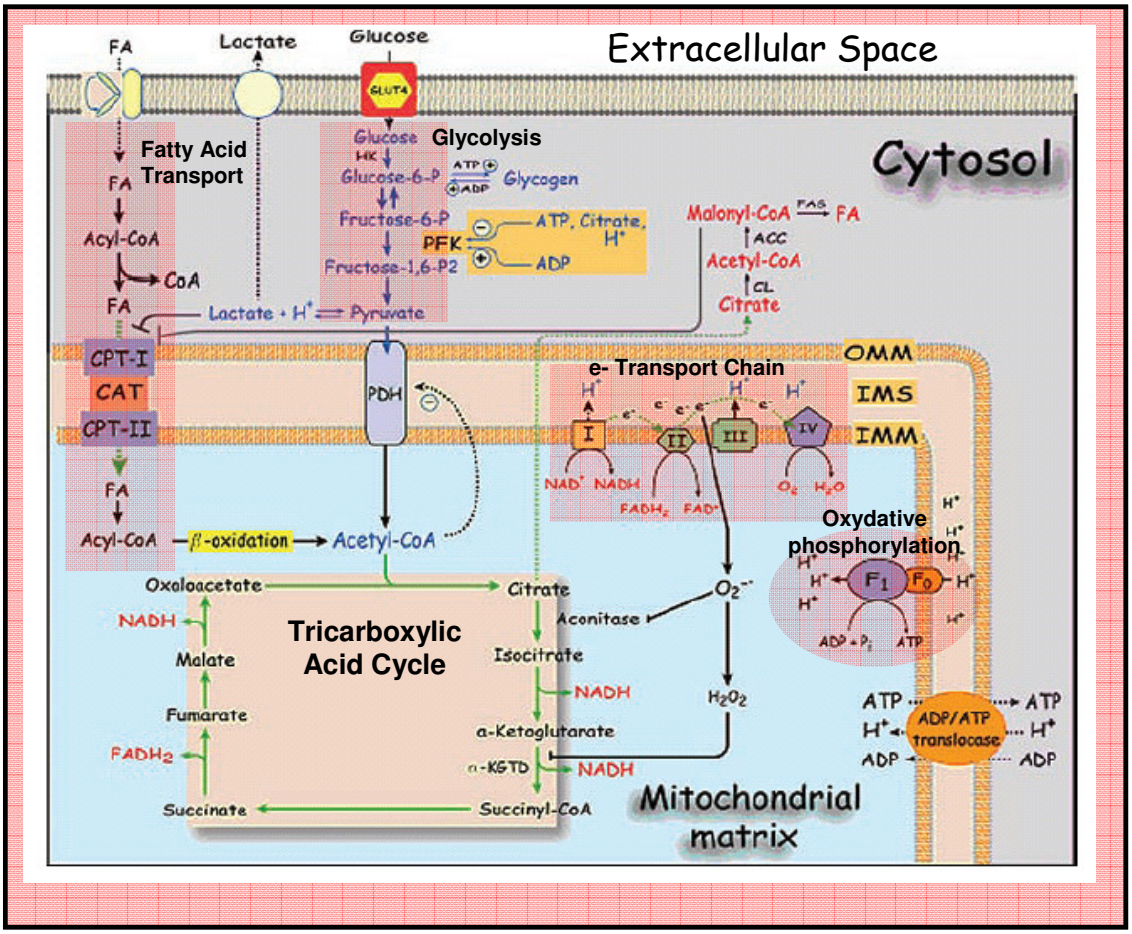

Figure 21 Fatty acid (FA) and glucose metabolism in skeletal muscle. HK, hexokinase; PK, phosphofructokinase; CPT, carnitine palmitoyl transferase; CAT, carnitine; ACC, acetyl-CoA carboxylase; PDH, pyruvate dehydrogenase; CL, citrate lyase; FAS, fatty acid synthase; a-KGTD, a-ketoglutarate dehydrogenase; OMM, outer mitochondrial membrane; IMS, intermembrane space; IMM, inner mitochondrial membrane. Adapted from Silviera et al [88].

pathways and their regulatory interrelationships. This overview is of value for understanding several recent experiments that support the mechanism of FFA induced T2DM disease model. The cytosolic enzyme, acetyl-CoA carboxylase (ACC), catalyzes the first step of FFA synthesis by catalyzing the synthesis of malonyl-CoA from acetyl-CoA. Malonyl-CoA suppresses lipid oxidation by allosterically inhibiting the transport of lipids into the mitochondria by the lipid transporter, carnitine palmitoyl transferase (CPT-1) [88].

In 2004, Kim et al. [89] showed that skeletal muscle fatty-acid transport 1 protein knockout (FATP1 KO) mice were protected from insulin resistance caused by large

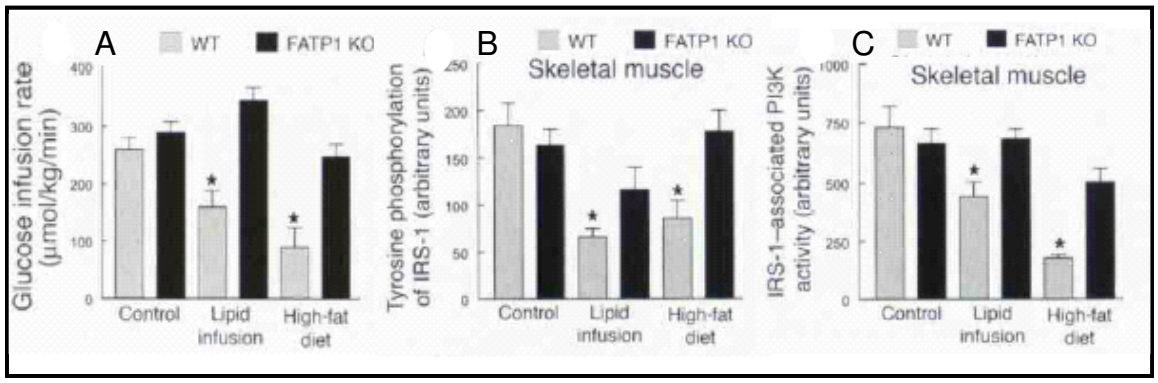

Figure 22 Response of FATP1 (fatty acid transport protein 1) KO mice to lipid infusion or three week oral administration of high fat diet. FATP1 KO mice are protected from insulin resistance, from [89].

administrations off FFA. These mice were not different from their WT counterparts in body adiposity, skeletal muscle intracellular fatty acid metabolites or insulin sensitivity (Figure 22A) when fed a regular diet. In high fat conditions, either acutely as a lipid infusion or chronically as a high fat diet, the FATP KO mice were found to not be insulin resistant in a hyperinsulinemic-euglycemic clamp (Figure 22A). They also did not have

significant alterations in the insulin signaling pathway markers, IRS-1 tyrosine phosphorylation (Figure 22B) or IRS-1 associated PI3K activity (Figure 22C) that were found in the WT mice. This study also showed that impairments of several factors associated with lipid-induced insulin resistance were just as impaired with chronic (3 week) oral administration of fat as with the 5 hour intravenous lipid infusion in mice [89].

In 2007, Choi et al. [90] found that mouse knockouts of acetyl CoA carboxylase-2 (ACC2, see Figure 21 "ACC") the isoform found mainly in skeletal muscle, were leaner and were protected from fat induced insulin resistance in high fat diets compared to WT mice. This is shown in Figure 23A as a higher glucose infusion rate in the $ACC2^{-/-}$

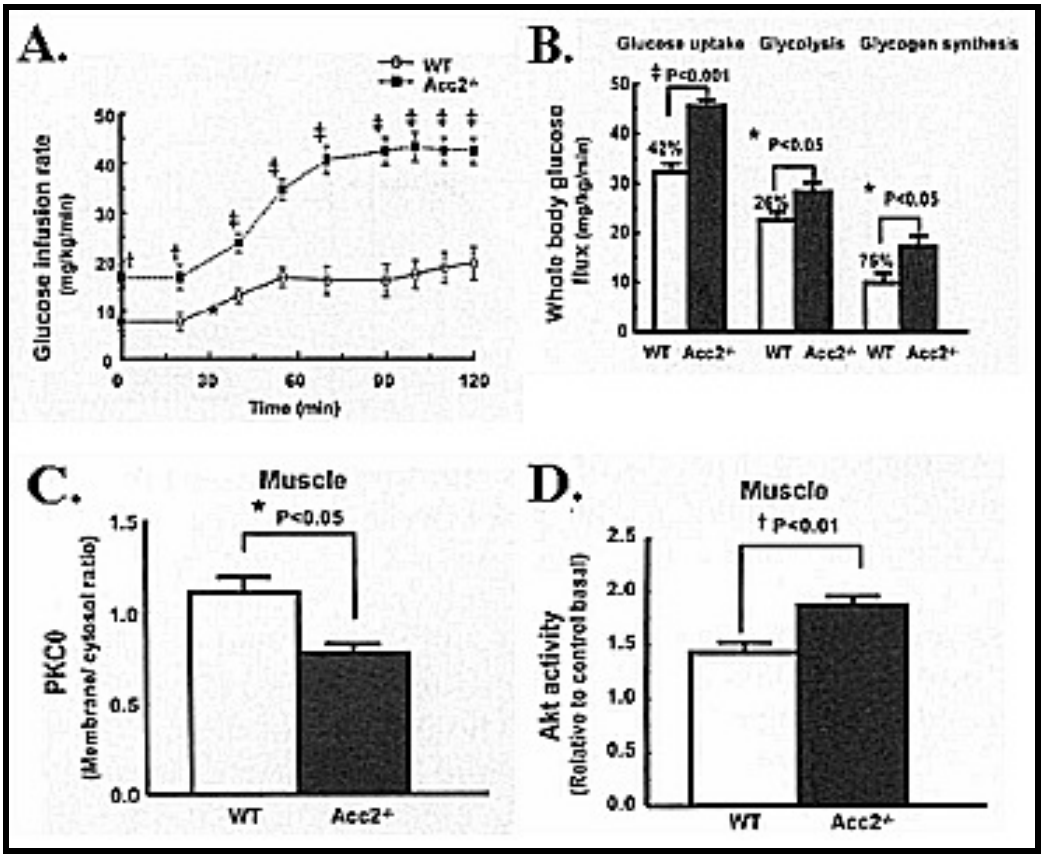

Figure 23 Improved insulin sensitivity in $ACC2^{-/-}$ mice. * $p < 0.05$, † $p < 0.01$, ‡ $p < 0.001$. Data are expressed as mean ± SEM for 9 mice per group, from Choi et al [90].

mice during a hyperinsulinemic-euglycemic insulin clamp. Figure 23B shows 3 significantly improved measures of glucose metabolism in the $ACC2^{-/-}$ mice. Importantly to the proposed model, PKC-θ membrane translocation was significantly reduced (Figure 23C) and Akt activity was increased (Figure 23D). Also, intracellular DAG was 50% decreased in $ACC2^{-/-}$ mice ($p < 0.05$).

The modern model of insulin resistance validates Randle's 1963 hypothesis that there is a substrate competition between intracellular FFA and glucose in the skeletal muscle which tends to favor FFA in T2DM. To a large degree this appears to be the result of excess FFA entering the cells due to unrestrained lipolysis at the adipocytes. Lipid metabolites appear to result in spurious serine/threonine phosphorylation on IRS proteins that are disruptive of the normal insulin stimulus-response, which results in glucose transport into the cell. The lipid metabolite which causes the disruption is not proven but DAG is a strong candidate [72]. While increased entry of FFA into skeletal muscle cells appears to be an important contributor to insulin resistance, research has shown that this may be exacerbated by an impairment of the mitochondria to oxidize FFA.

Mitochondrial Function in Skeletal Muscle Insulin Resistance

Emerging evidence suggests that while circulating FFA levels and FFA transport into muscle cells is upregulated in obesity, the lipotoxic effect of this may be exacerbated by a decrement in the ability of the mitochondria to oxidize the increased intracellular levels of lipid [91]. The mitochondrion is the site of oxidative catabolism (B-oxidation) of lipids, producing acetyl-CoA (Figure 21). Also, pyruvate, the product of glycolysis in

the cytoplasm, is transported into the mitochondria where it is transformed to acetyl-CoA by a series of reactions catalyzed by the pyruvate dehydrogenase complex (PDH). Mitochondrial acetyl-CoA enters the tricarboxylic acid cycle where the energetic molecules NADH and $FADH_2$ are produced. The reductive potential of these molecules is used to drive the electron transport chain, creating an electrochemical gradient of protons between the intermembrane space (IMS) and the matrix of the mitochondria. This stored electrochemical energy is then used to drive oxidative phosphorylation at ATP synthase, producing ATP and water from ADP and inorganic phosphate, P_i. ATP is the main "energy currency" used by the body and is transported from the mitochondria by ADP/ATP translocase to drive many biological processes.

Recent investigations have found that aberrant serine-kinase activation the that results from the accumulation of lipids in skeletal muscle may be compounded by serious inherited metabolic deficiencies in the mitochondria in insulin resistant persons, as described below.

A 2004 study by Petersen et al. [92] found that mitochondrial function in insulin resistant humans is impaired and is associated with high levels of skeletal muscle intracellular lipid content. The study compared 12 young, healthy insulin sensitive subjects with 14 age, weight, height and physical activity matched insulin resistant subjects, having at least one parent or grandparent with T2DM. Under hyperinsulinemic-euglycemic control conditions, they used a technique called "saturation transfer" ^{31}P NMR to monitor the rates of mitochondrial oxidative phosphorylation and ^{1}H NMR to measure skeletal muscle intracellular (intramyocellular) lipid and liver triglyceride

content. Rates of whole body and subcutaneous lipolysis were monitored by [$^{2}H_5$]glycerol turnover and microdialysis measurements of glycerol secreted from subcutaneous fat.

In the insulin resistant group, there was an observed 80% increase of intramyocellular lipid content ($p = 0.005$) [92]. Whole body and subcutaneous lipolysis were similar in the two groups in both the basal state and during the clamp, showing that neither increased rates of peripheral lipolysis nor defects in insulin-induced suppression of hepatic lipolysis significantly contribute to the increased intramyocellular lipid content. This suggested that under these conditions, insulin resistance, as it pertains to lipids, is largely a matter of an impaired catabolism of lipids in skeletal muscle. Importantly, the insulin resistant group also had a 30% decrease ($p = 0.01$) in the rate of skeletal muscle mitochondrial ATP synthesis, as measured by ^{31}P NMR [92]. The authors stated that this result implicated an inherited malfunction in the mitochondria as a contributor to the cellular lipid accumulation. The study also addressed questions of experimental control, suggested from previous studies, which had shown that several adipocyte secreted factors; resistin, tumor necrosis factor a, interleukin-6 and adiponectin mediate insulin resistance in obese people [93-97]. Plasma concentrations of these adipocyte-generated factors were measured and no significant differences were found between the healthy and T2DM groups, suggesting that for these BMI matched groups, differences in adipocyte metabolism was not a significant contributor.

In addition, a 2005 microscopy study by Morino et al. [98], showed that density of mitochondria in the skeletal muscle tissue of the insulin resistant offspring of parents with T2DM (Figure 24A) is reduced. Also, several proteins markers of mitochondrial

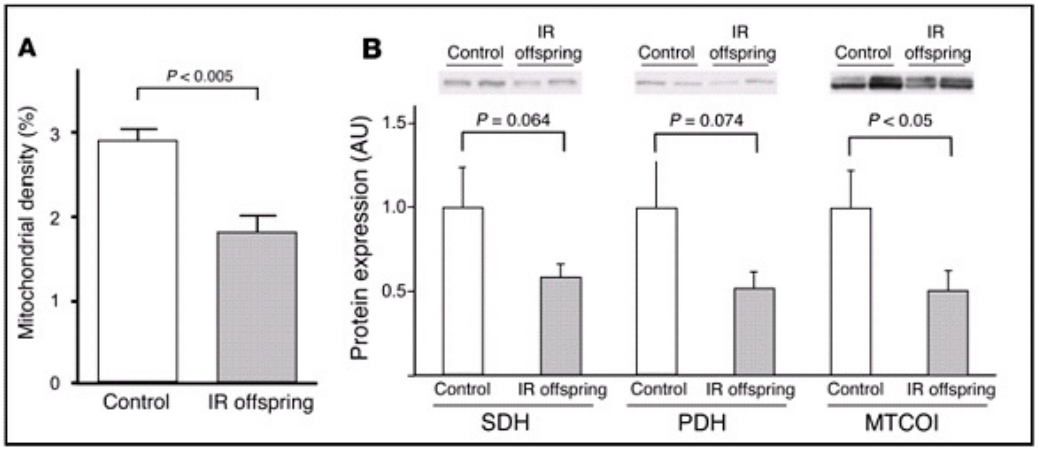

Figure 24 Indicators of diminished mitochondrial function in insulin resistant offspring of humans with T2DM.

function, succinate dehydrogenase (SDH), pyruvate dehydrogenase (PDH), and mitochondrial cytochrome c oxidase I (MTCOI) either tended to be diminished ($p \sim 0.05$) or were significantly diminished ($p < 0.05$) (Figure 24).

Studies reporting impairments in mitochondrial function in T2DM offer a hypothesis that a subtle defect, possibly arising from inherited or age-accumulated mutations in mitochondrial DNA [99], contributes to high concentrations of intracellular lipids. A recent (2010) review of mitochondrial studies in T2DM highlighted questions about the primacy of mitochondrial alterations in the pathogenesis of insulin resistance [100]. The mitochondrial defects, whether they are inherited or acquired, may be a cause or may be secondary to insulin resistance [72].

Hepatic Insulin Resistance

The preceding discussion was limited to skeletal muscle insulin resistance or whole body insulin resistance as measured in a hyperinsulinemic clamp, therefore predominantly as a function of skeletal muscle, which disposes of more than 80% of the glucose from the blood during the normal period of high insulin secretion after a meal [41]. However, the tissues responsible for insulin resistance in the basal state are different from those responsible for insulin resistance in the insulin-stimulated state. Skeletal muscle glucose uptake was given as the 3rd obligatory function of insulin for normal blood glucose homeostasis (see page 26). The 2nd necessary function of insulin for glucose homeostasis is the suppression of hepatic glucose production (HGP), which will be our focus.

The portal vein provides a close and direct route for the insulin secreted from the pancreas to reach the liver. Therefore, hepatic response to insulin is the most immediate in the body after food ingestion. The liver has a pivotal role in maintaining blood glucose homeostasis during transitions between feeding and fasting. While insulin stimulated glucose disposal after a meal is primarily the function of skeletal muscle, the liver also buffers ingested carbohydrate levels by suppressing hepatic glucose production and stimulating glucose deposition as liver glycogen [61]. Like insulin resistance in skeletal muscle, the function of insulin on the action of hepatocytes has been found to be faulty in persons with T2DM and their normoglycemic offspring .

Under high insulinemic conditions, such as after a meal, insulin resistance in the skeletal muscle accounts for >90% of the impairment of glucose uptake in T2DM [101].

In these conditions, the splanchnic tissue[3], (the liver and surrounding gastrointestinal tissues) also becomes a net consumer of glucose, although a relatively minor one. In hyperinsulinemic euglycemic insulin clamp studies by Defronzo et al. [61], the rate of glucose uptake by the splanchnic region was 0.5 mg· kg^{-1}(body weight) · min^{-1}, only about 7% of the whole body glucose uptake in healthy persons. There was no significant difference found in the splanchnic rate of uptake between healthy persons and persons with T2DM [101] under the high insulinemic conditions of the clamp. However, in the postabsorptive state, when the gastrointestinal tract has been cleared of food, the maintenance of minimal blood glucose increasingly becomes the result of hepatic glucose production (HGP) as the blood insulin concentration decreases. It is during this time that the hepatic manifestation of insulin resistance is found to play the most important role in the impaired whole-body glucose economy of T2DM. Because the glucose production by the liver increasing becomes the predominant contributor to blood glucose, the association of basal HGP is closely correlated ($r = 0.92$, $p < 0.001$) [101] with FPG (the concentration of glucose in blood plasma after 8 hours of no caloric intake). Therefore, FPG is one of the important diagnostic measurements of T2DM.

The obligatory glucose usage by the central nervous system is 1.0 – 1.2 mg · kg^{-1}(body weight) · min^{-1}, and the basal postabsorptive glucose production by the liver in a healthy person is 1.8 – 2.2 mg · kg^{-1} · min^{-1} [61]. Of this postabsorptive production, the

[3] Ideally the portal vein of the liver would be used to directly measure glucose uptake by the liver. However, it is difficult to catheterize the portal vein in humans, so the hepatic vein was used, measuring glucose uptake by the liver and surrounding tissue 101. Defronzo, R.A., *The Triumvirate: B-Cell, Muscle, Liver A Collusion Responsible for NIDDM.* Diabetes, 1988. **37**: p. 667-693.

skeletal muscle and the splanchnic tissue approximately equally split the remaining glucose that is not used by the central nervous system.

It has been shown [102, 103] that nearly 90% ($P = 0.0001$, $P < 0.05$) of the increased HGP attributable to T2DM is the result of gluconeogenesis and that the fasting glucose production rate from hepatic glycogenolysis is actually higher in controls than in T2DM (2.8 ± 0.7 umol $\cdot$ kg^{-1} body wt. $\cdot$ min^{-1} vs. 1.3 ± 0.2 umol $\cdot$ kg^{-1} body wt. $\cdot$ min^{-1}, $P < 0.05$) because of diminished stores of glycogen in T2DM [103].

In Figure 25 [61], some important metabolic indices demonstrating hepatic

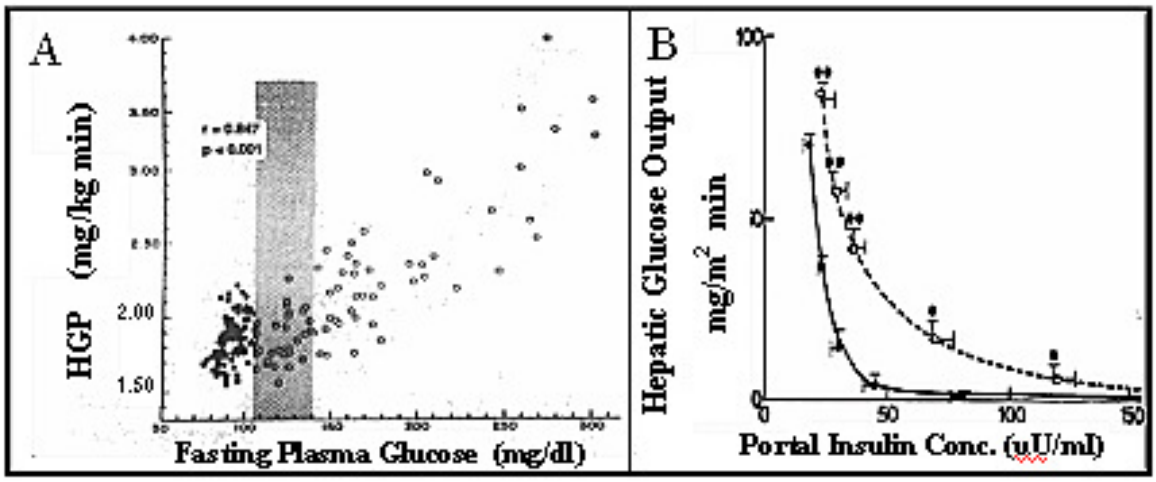

Figure 25 Metabolic parameters of hepatic insulin resistance in postabsorptive state. HGP is rate of hepatic glucose production per unit subject mass. HGO is rate of glucose production per unit subject surface area. For the purpose of demonstration they can be considered the same parameter. In A) the closed circles (●) are non-diabetic controls and the open circles (○) are normal weight T2DM subjects. In B) the solid line represents NGT controls, the dashed line represents T2DM subjects, * $p < 0.05$, ** $p < 0.001$, from [61].

insulin resistance in T2DM are shown. Figure 25A is a plot showing the relationship between FPG and fasting hepatic glucose production (HPG). The dark enclosed circles to the left of shaded region are NGT controls. The open circles within the shaded region are

T2 diabetics with FPGs (x axis) which are below the T2DM cutpoint (140 mg/dl) for overt fasting hyperglycemia. These people are considered to be early diabetics who still have fairly high functioning β-cells and are hyperinsulinemic (20 ± 2 vs. 11 ± 1 uU/mL, $p < 0.001$) and mildly hyperglycemic. As can be seen, the average rate of HGP for this T2DM group, within the shaded area, is the same as control subjects. Higher FPG should properly induce suppression of HGP, but in the shaded area group of T2 patients, it does not. Therefore, while there is no abnormal increase in HGP to account for the fasting hyperglycemia seen in this group, a normal rate of HGP in the presence of fasting hyperglycemia indicates that hepatic insulin resistance is already occurring at this early course of T2DM. The T2 diabetics with a FPG greater than 140 mg/dl had a highly correlated rise ($r = 0.847$, $P < 0.001$) of hepatic glucose production with the increase of FPG. This indicates the importance of the contribution of insulin resistance to HGP and the importance of HGP to T2DM, when it is diagnosed by FPG.

The average HGP in the T2 diabetics of the previous experiment was increased 0.5 mg · kg^{-1} · min^{-1} during the postabsorptive state [101][4]. While seemingly a relatively small amount, normal postabsorptive HGP is only 1.8-2.2 mg · kg^{-1} · min^{-1}, and this additional rate will add an additional 50 grams of glucose to the circulation of a 70 kg diabetic person in a 24 hour period. Addressing the relative contributions of impaired tissue glucose uptake and impaired suppression of HGP to the diabetic glucose economy, it was found by Ferrannini et al. [104] that hepatic insulin resistance to the suppression of

[4] The previous page stated that the glycogenolysis of the control subjects was 2.8 umol · kg^{-1} body wt. · min^{-1}. This is ~0.5 mg · kg^{-1} · min^{-1}, equal to the total defect in T2DM HGP stated directly above. But the glycogenolysis of the T2DM subjects was 1.3 umol · kg^{-1} body wt. · min^{-1}, about half that of the controls. So a net defect ~ 0.25 mg · kg^{-1} · min^{-1} excess glucose still resides with the T2DM subjects.

HGP is about half of the impairment of skeletal tissue insulin resistance during a 3.5 hour post-ingestion glucose tracer study. Tissue glucose uptake was significantly reduced in T2DM compared with controls (44 vs. 60 g, $P < 0.05$) and HGP remained higher in the diabetic group (17 vs 10 g over 3.5 hours, $P < 0.05$).

In Figure 25B is a dose-response curve of the hepatic glucose output (a similar measure to HGP but with different units, rate per unit surface area, $mg/m^2 \cdot min$) plotted as a function of the portal vein plasma insulin concentration for non-diabetic controls (solid circles) and moderate-to-severely hyperglycemic persons with T2DM (open circles). In controls, the hepatic glucose output is highly sensitive to portal vein insulin concentration, dropping 50% as the result of a 5 μU/mL (from 19 μU/mL to 24 μU/mL) change in the portal vein insulin concentration. In the diabetic group, the response to insulin is blunted. Note that as the insulin levels decrease, hepatic glucose output becomes an increasingly significant discriminator of the T2DM persons from controls (*$p < 0.05$, **$p < 0.001$) [71] .

A model, analogous to that for insulin resistance in skeletal muscle (Figure 19), has emerged from studies of insulin resistance in hepatocytes (Figure 26 from [72]). The

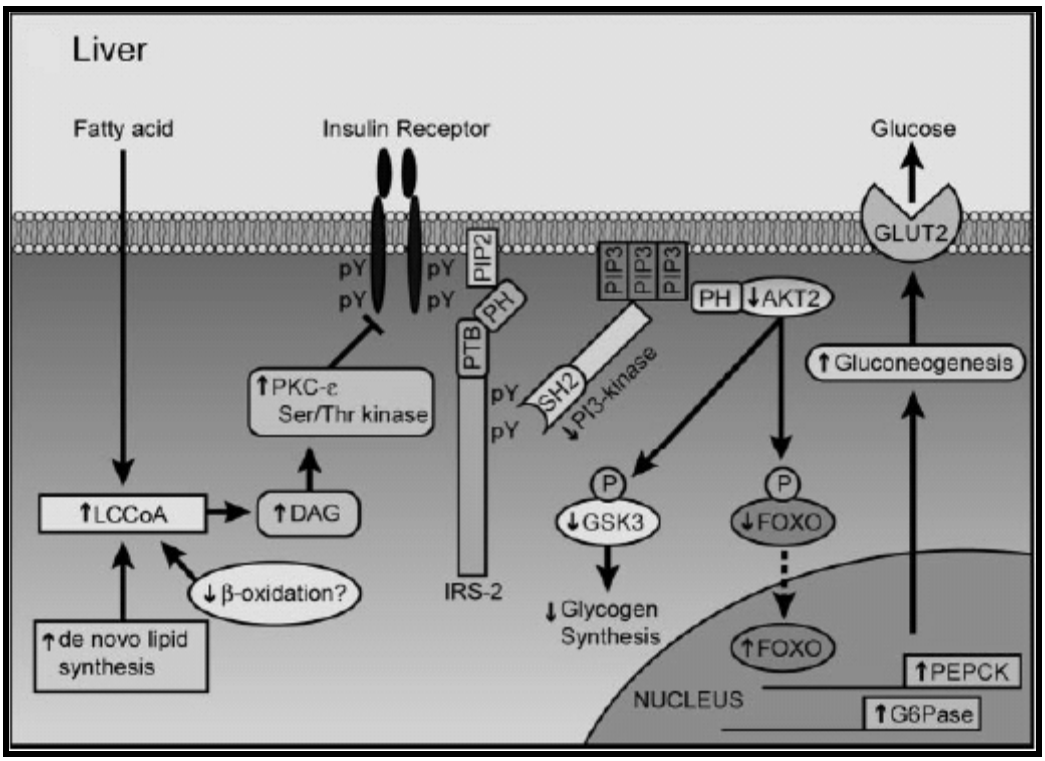

Figure 26 Pathway of hepatic FFA induced insulin resistance. From Savage et al [72].

hepatic model is more reliant upon animal studies than the muscle model, as there are few studies using organ biopsies from live humans and the mechanisms by which FFA induce gluconeogenesis are relatively poorly understood. As in the muscle model, increased levels of intracellular DAG result from ectopic FFA deposition and/or decreased mitochondrial FFA oxidation. As seen in the skeletal tissue, several hepatic isoforms of activated (membrane translocated) PKC, particularly PKC-ε, have been shown to be increased 2 or 3 fold in the livers of obese and diabetic humans and rats [105] relative to

just obese controls. PKC-ε, is also activated in the livers of rats with dietary fat-induced insulin resistance, 2-fold over rats fed normal diets ($p \leq 0.001$) [106]. PKC-ε binds and inactivates the insulin receptor kinase activity, leading to reduced insulin-stimulated IRS-1 and IRS-2 tyrosine phosphorylation. This results in lower insulin-stimulated hepatic glycogen synthesis through lower GSK-3 phosphorylation, as in skeletal muscle, but also decreased suppression of gluconeogenesis apparently through decreased FOXO phosphorylation, although this pathway is poorly understood [72].

Paradoxically, whereas insulin resistant hepatocytes have impaired suppression of HGP, they appear to have an enhanced rate of lipogenesis in the insulin stimulated state [72]. Lipid accumulation in the liver may be a result of increased delivery and synthesis of FFA when energy intake exceeds adipose tissue storage capacity, as seen in obesity and lipodystrophy. Acquired or inherited mitochondrial dysfunction may also contribute to the intracellular accumulation of lipids. Studies in the lean offspring of T2 diabetics suggest that the intramyocellular lipid accumulation and skeletal muscle insulin resistance precede the development of hepatic insulin resistance [92]. It has been proposed that skeletal muscle insulin resistance is the earliest detectable event in the pathogenesis of T2DM in most patients and that the associated hyperinsulinemia promotes accumulation of lipids in the liver, hepatic insulin resistance and T2DM [72]. Adipocyte dysfunction in T2DM is believed to cause excessive delivery of FFA to muscle and liver and probably contributes to the insulin resistance in both organs [72]. We will now turn our attention to the topic of the role of the adipocyte in the pathogenesis of T2DM.

Inflammation and Insulin Resistance in Adipocytes

T2DM has been described as a "Gordian Knot" of etiological factors, referring to the large list of contributing determinants to the disease, from which no primary cause has yet been found. These etiological determinants and risk factors include 1) genetic factors: genetic markers, family history and "thrifty genes", 2) Demographic characteristics: sex, age and ethnicity, 3) Behavioral and lifestyle related factors: obesity (including bodily fat distribution and duration of obesity), physical inactivity, diet (particularly the amount and type of carbohydrates), stress, "westernization, urbanization, modernization", and 4) Metabolic determinants: IGT, insulin resistance (related to circulating and hepatic fat deposition), pregnancy-related determinant (gestational diabetes) [107] . Among these, long known to be associated with T2DM, is obesity and more recently recognized, visceral or central obesity in particular. Insulin resistance has been called a "universal" [108] and "ubiquitous" [109] correlate" to obesity. Illustrative of this relationship is Figure 27, which shows the correlation ($P < 0.0001$) of body mass index (BMI=weight/ height squared) with the FPG for 10 of the normal glucose tolerant (NGT), 13 impaired glucose tolerant (IGT) and 8 T2DM subjects whose plasma was used in the experiments of this dissertation.

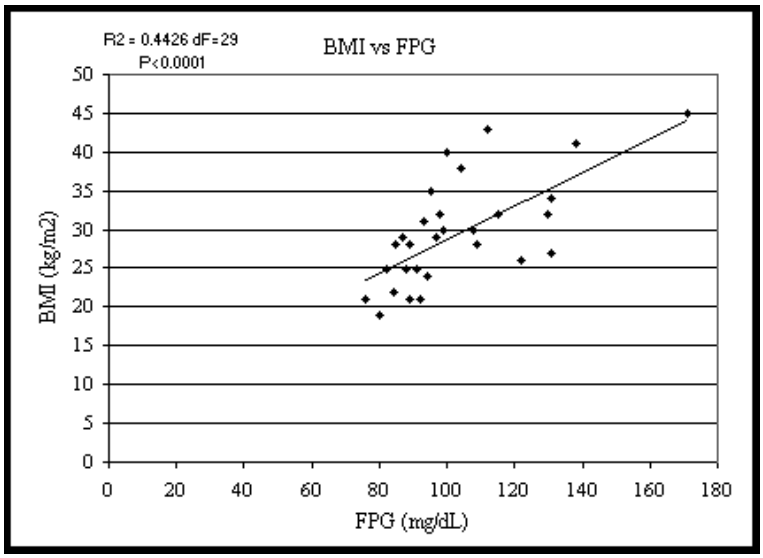

Figure 27 The correlation of BMI with FPG for 31 experimental subjects (10 NGT, 13 IGT and 8 T2DM) studied in the present project. These measurement values were provided by the NIH who also provided the plasma samples.

Obesity has received a lot of recent research interest because of modern biochemical studies on adipocytes, the isolation of factors secreted by adipocytes and strong correlations of the circulating concentrations of adipocyte factors in animal models and humans, to insulin resistance [110]. Also, large studies such as the three year Diabetes Prevention Program conducted in the United States showed that lifestyle intervention that targeted 7% weight loss and 150 minutes of moderate exercise per week reduced the risk of progressing from the IGT state to T2DM by 58% from matched controls in a 2.8 year experiment [111]. Figure 28 shows data from two separate 10 year studies that measured the relative risks of developing several conditions, including T2DM, to women and men within the time of the study. In both studies the relative risk of developing T2DM was the most highly correlated with BMI.

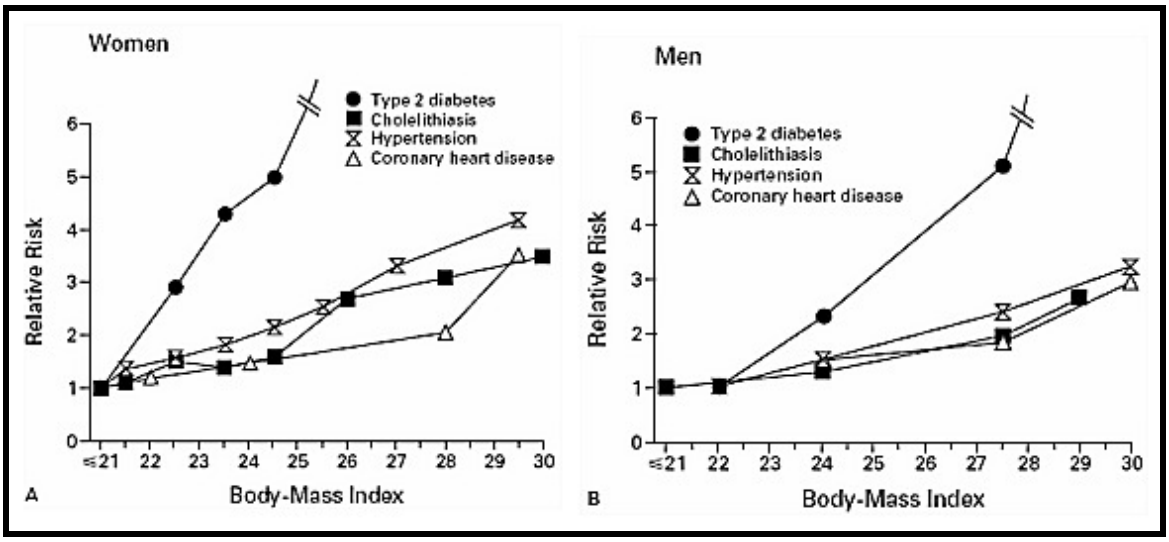

Figure 28 Two separate studies of 10 years relative risk of T2DM with body mass index for A) the Nurses Health Study of women initially 30-55 years old and B) the Health Professionals Study of men initially 40-65 years old [112].

Research has led to the recognition of a set of risk factors for developing T2DM and cardiovascular disease (CVD) that are collectively associated with "metabolic syndrome". The metabolic syndrome was first formally proposed by Reaven in 1988 [113]. The "syndrome" name indicates that the collection comprises individual risk factors that occur as a group more often than would be expected by chance alone, but that historically the mechanistic reasons for their concurrence were not understood. Although insulin resistance and accelerated atherosclerosis are not routinely measured, they are sometimes included in this group of risk factors [114]. According to the NIH, the five metabolic risk factors are: central or abdominal obesity (lipodystrophy), high blood pressure, IGT, high triglycerides, and low levels of HDL. The last of these two risk factors, along with decreased LDL particle size and postprandial triglyceride-rich lipoproteins are collectively known as insulin resistance associated "dyslipidemia" [115].

According to the NIH website [116], the concurrence of 3 of these risk factors is sufficient for the diagnosis of metabolic syndrome.

The recognition and study of the chronic inflammation that appears to accompany obesity has provided a framework through which understanding of the mechanistic connections between the five individual metabolic risk factors has begun to emerge. Although the traditional features of inflammation; swelling, redness, pain and fever are not associated with metabolic syndrome, several of the same molecular mediators, which evoke an acute inflammatory response (innate immunity) in the case of injury, are present in relatively low, but chronically elevated levels [117]. In metabolic syndrome, chronic inflammation appears to be principally triggered by nutrient imbalance and metabolic surplus, resulting in negative clinical consequences [117, 118] including insulin resistance and T2DM.

A 1997 study by Pickup et al. investigated the hypothesis that T2DM and metabolic syndrome (syndrome X) are partly a manifestation of an ongoing acute-phase inflammatory response, showed a relationship between markers of inflammation and T2DM diagnostic classifications in Caucasians [119]. Figure 29 shows six markers of acute phase response and the correlations of their serum concentrations with three metabolic classifications: 1) Non-diabetic (n=25), 2) T2DM without metabolic syndrome (n=25) and 3) T2DM with metabolic syndrome (n=19). The six acute phase markers are: a) serum sialic acid concentration, b) serum alpha-1 acid glycoprotein concentration, c) serum C-reactive protein (CRP), d) serum amyloid A (SAA) protein, d) serum cortisol,

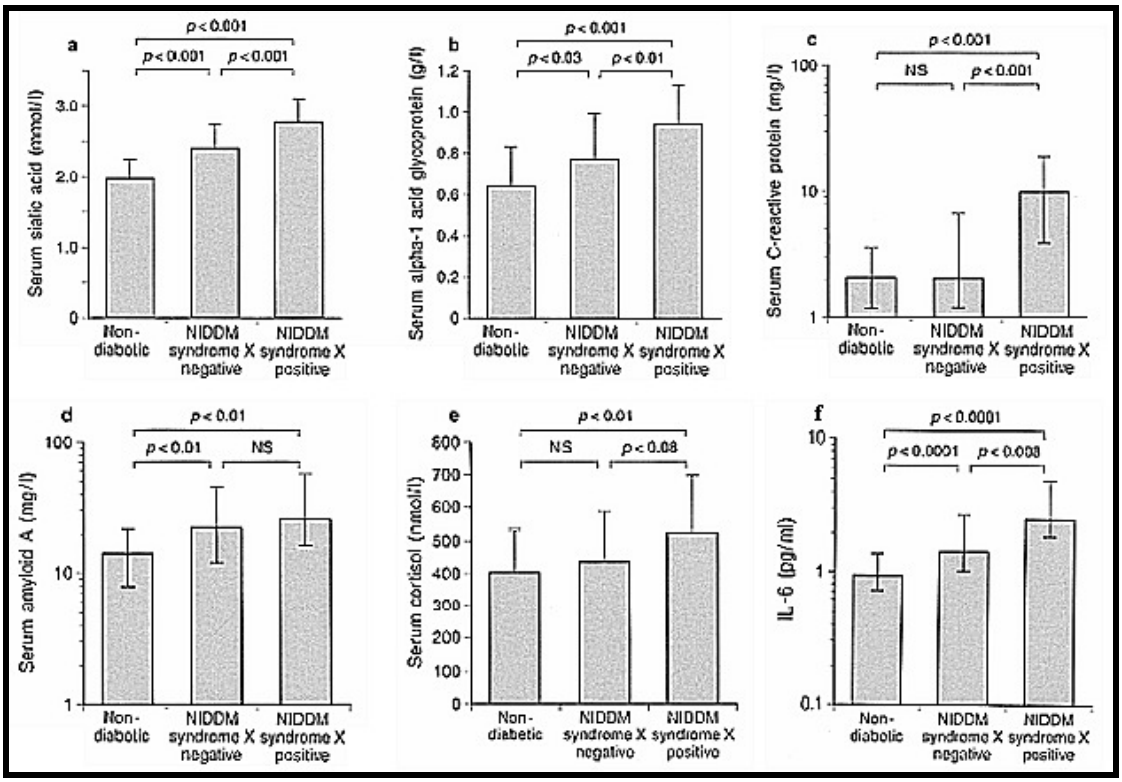

Figure 29 Six markers of acute phase response and the associations of their serum concentrations with 3 metabolic classifications. Columns are mean $\pm$ SD except for CRP and SAA which are median $\pm$ interquartile range. "NS"= non-significant, from [119].

and e) interleukin-6 (IL-6) [119]. Serum sialic acid concentration is included here because many acute phase proteins are glycoproteins with sialic acid at the terminus of their oligosaccharide chains [120]. The graphs show several quite significant as well as some marginally positive associations of the markers with the metabolic classifications.

One marker of inflammation, which was not included in the previous experiment, tumor necrosis factor-α (TNF-α) has come to be regarded as one of the most important mediators of low-grade, chronic inflammation, and studies of TNF-α have been seminal

to the proposal of a non-classical, lipocentric mechanism of IR and T2DM. We will now briefly review some of the relevant primary studies of TNF-α

Human adipocytes are cells where large energy reserves are stored as triglycerides, which can be mobilized for distribution through the circulation as FFA. Adipocytes normally respond relatively weakly to the stimulatory effect of insulin on their uptake of glucose [101] when compared to skeletal tissue or hepatocytes. In non-obese people, less than 1% of infused or ingested glucose is taken up by adipose tissue. In obese people, up to 3% can be taken up by adipose tissue [43]. In either case, little of the defect of systemic glucose disposal could possibly be directly attributed to a defect in glucose uptake in adipose tissue. However, while the direct acute role of adipocytes in the body's glucose economy is small, research on the indirect chronic role of adipocytes on glucose uptake, as regulators of whole-body lipid homeostasis, has illuminated their profound importance within the context of the lipocentric pathogenesis of insulin resistance. In addition to their important, direct role in lipid metabolism, adipocytes have been shown to mediate elements of the innate immune response by secreting several hormones, collectively known as adipocytokines [121]. This hormone secreting activity confers the role of endocrine organ [122] to adipose tissue and puts adipocytes at the interface of the nutrient- and pathogen-sensing pathways [117]. When chronically defective, this bi-functionality of the adipocyte is believed to provide, at least partially, long-sought connections, from predisposing genes and/or obesity to insulin resistance, metabolic syndrome and T2DM.

One of the early contributions that illuminated some of the connections between metabolism and immunity came in a 1993 report, by Hotamisligil et al., studying TNF-α expression of mRNA and protein in various tissues of genetically obese mice and rats [93]. The TNF family is a group of several pluripotent cytokines that have long been studied for their tumor necrotizing activity [123] and are believed to be primarily expressed by macrophages. In this study, mRNA for TNF-α was found to be elevated 5- to 10-fold in the adipose tissue of several obese models of mice and rats relative to the lean models [93]. In contrast, no difference in expression of TNF-α mRNA was found in liver, kidney, skeletal muscle or spleen tissues of the same animals. Increased expression of the TNF-α mRNA positively correlated with local expression of the TNF-α protein cytokine. Though at low levels, ~100pg/mL, the circulating concentrations of TNF-α protein were also positively correlated with obesity, and were 30% higher in the obese animals ($p < 0.05$). The genetically obese, insulin resistant rats were administered doses of chimeric TNF-α receptor-IgG, intravenously, to scavenge the circulating TNF-α. An insulin clamp study revealed that insulin sensitivity was significantly improved by scavenging TNF-α, over genetically identical control rats, which were administered vehicle alone. Further, it was shown that the improvement in insulin sensitivity was the result of increased muscle glucose uptake and not a result of improved suppression of HPG, as there was no difference in this latter parameter.

Since the 1993 report, it has been shown [109] that high levels of serine phosphorylation occurred on IRS-1 in murine adipocytes treated with TNF-α. The serine phosphorylation of IRS-1 was shown to inhibit the insulin receptor tyrosine kinase

autophosphorylation that is important for GLUT-4 mobilization, following *in vitro* insulin stimulation. Importantly, macrophages have been found to increasingly infiltrate adipose tissue in obese mice and humans [124, 125] and the percentage of infiltration of the adipose tissue is proportional to the body mass index [124].

Recent studies, summarized in Figure 30 [126] have elucidated a pathway of intracellular crosstalk between the TNF-α receptors and IRS-1/IRS-2, that results in the serine phosphorylation of IRS-1 and the inhibition of insulin action. This crosstalk has been described as an evolutionary integration of the metabolic and the innate immunity pathways, as the inflammatory response relies upon energy redistribution, especially the

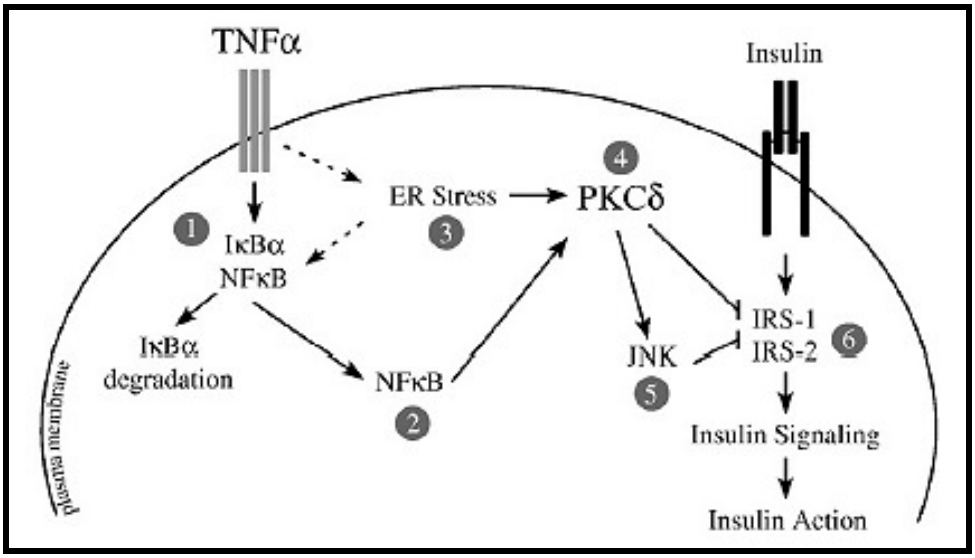

Figure 30 Proposed model of the crosstalk between the TNF-α and insulin sensing pathways, from [126].

mobilization of stored lipids [127]. Accordingly, the insulin signaling pathway, essentially an energy storing (anabolic) pathway, is partially suppressed when in conflict

with the basically catabolic inflammatory response. Historically, under-nutrition included the risk of immunosupressive infection because of this linkage between these two pathways. With the historical advent of chronic over-nutrition, this linkage presents pathologically with chronic inflammation, which according to this model, leads to insulin resistance [117, 127].

A "big picture" model that incorporates the interactions between adipose tissue and the immune system is shown in Figure 31. On the left of the figure is an adipocyte that has reached a threshold for the storage of triglycerides. This overload may result in

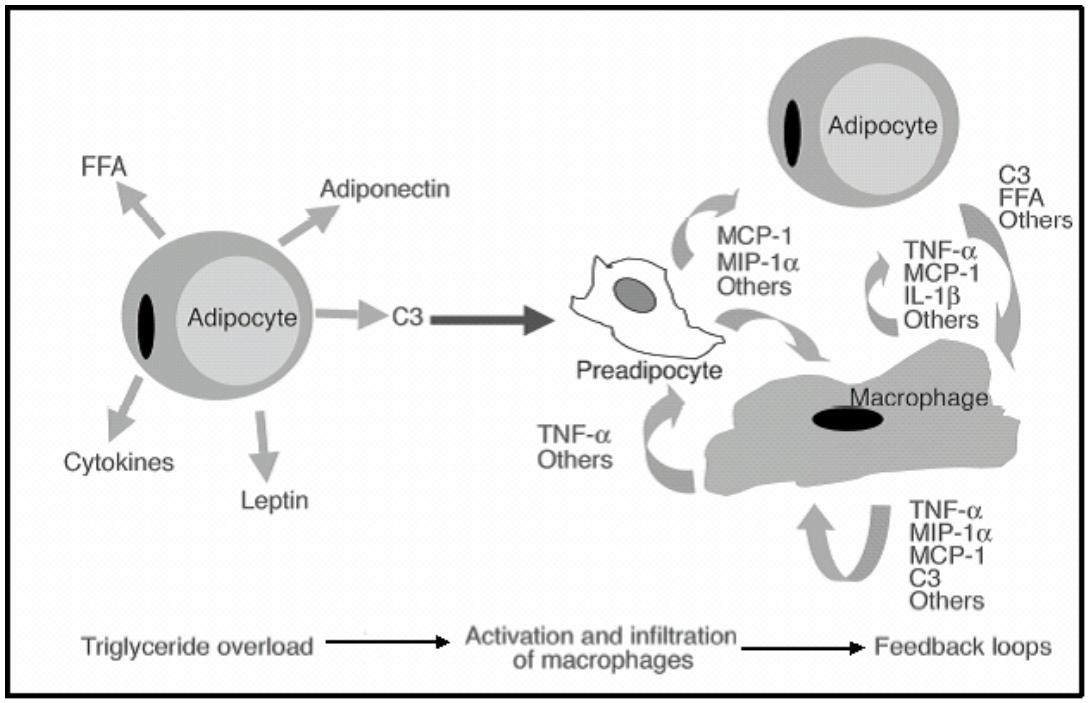

Figure 31 Model of chronic inflammation and adipocyte IR. C3 is complement factor-3 and represents activated innate immunity. Adapted from Xu et al [125].

the loss of the adipocyte's normal ability to suppress lipolytic activity in response to insulin. At the threshold, factors derived from adipocytes, possibly including the

cytokine TNF-α, induce macrophage activation and infiltration into the adipose tissue, as seen on the right side of the figure. According to this model, the activated macrophages secrete cytokines that further impair the adipocyte's insulin sensitivity and a positive feedback loop is created in which more macrophages and peripheral monocytes are activated and infiltrate the adipose tissue. The amplifying feedback loop of signal is proposed to increase the adipocyte insulin resistance and eventually the leakage of TNF-α into the circulation, in addition to the augmented circulating FFAs, causes the systemic insulin resistance [114, 117].

The idea that fat produced a substance which excessive fat overproduced, with local and systemic pathological metabolic consequences was a paradigm shift from the classical lipotoxicity concept in diabetes research [128]. Studies of adipocytokines and other fat-produced bioactive species have since been extended beyond TNF-α to include leptin, IL-6, resistin, monocyte chemoattractant protein-1 (MCP-1), plasminogen-activator inhibitor-1 (PAI-1), angiotensin, visfatin, retinol-binding protein-4, serum amyloid A (SAA), adiponectin and others [128].

While the linkage of inflammation to IR is believed to be of paramount importance, *in vivo* human experiments have failed to show that scavenging or blocking TNF-α improves the metabolic parameters of T2DM. One such experiment [129] showed that treatment of T2DM patients with etanercept, a TNF-α scavenger, resulted in significant decreases in the markers of inflammation, IL-6 (~30% decrease, $p = 0.03$) and C-reactive protein (50% decrease, $p = 0.04$), but there was no concomitant improvement

in B-cell response, serum lipid profile or insulin sensitivity, in the 4 week course of the experiment [129].

A class of insulin sensitizing drugs called the thiazolidinediones (TZDs) has yielded valuable insight into other possible non-classical mechanisms, linking cellular FFA to IR. TZDs are selective agonists of the nuclear transcription factor, peroxisome-proliferator-activated receptor-γ (PPARγ), one of three known PPARs. The PPARs are a subfamily of the 48-member nuclear-receptor superfamily. The PPARs regulate gene expression in response to ligand binding of various FFAs and bioactive eicosanoid lipid products [130]. PPARγ is expressed most abundantly in adipose tissue and is also found in pancreatic B-cells [131], vascular endothelium, and macrophages [132]. It was first identified as a regulator of adipogenesis, but it also plays a role in cellular differentiation, atherosclerosis, cancer, as well as insulin sensitization [130]. In adipocytes, PPARγ promotes fat storage by increasing adipocyte differentiation and the transcription of lipogenic enzymes. Well differentiated adipocytes are smaller than less differentiated adipocytes and their expression of TNF-α is lower [133]. Also, the expression of adiponectin, a cytokine that is produced exclusively by adipose tissue [132], is regarded as beneficial for insulin sensitivity [125] and is found to be reduced in the circulation of T2DM, and is higher in well-differentiated adipocytes [133].

Evidence that TZDs act as insulin sensitizers comes from *in vivo*, clinical studies that show them to consistently lower fasting and postprandial glucose concentrations as well as FFA concentrations [132]. In one such study [134], the treatment of persons with the TZD, rosiglitazone, increased insulin-stimulated glucose uptake in the peripheral

tissues, increased hepatic insulin sensitivity and increased the insulin sensitivity in adipose tissue, as measured by the ability of insulin to suppress circulatory FFA concentrations. Interestingly, these improvements in metabolic function were attended by weight gain and an increase in the subcutaneous adipose tissue mass, a consistent finding for thiazolidinediones [132].

So, the TZD's are hypothesized to have a classical insulin sensitizing mode of action in their ability to promote FFA uptake and storage in the adipose tissue, and consequently reducing the harmful ectopic deposition of the FFA to the liver, muscle and possibly the pancreatic B-cells [132]. The TZDs appear to also have an indirect, non-classical mode of action, as shown in gene profiling studies on adipocytes, showing that TZDs affect the expression of more than 100 clustered genes, including the familiar adipocytokines, adiponectin and TNF-α [132].

I hope that the intended larger points have been made, that the role of circulatory FFA is a modern focus in the large field of T2DM research and may have an important role in the natural history of T2DM. While this model incorporates much, it does not answer questions of apparent variable individual susceptibility regarding the imperfect concordance of T2DM with body mass index (BMI). Specifically, why do some overweight people never get T2DM? And why do 10-20% of people who get T2DM have normal BMI? [135]. Research on the gene associations with T2DM is devoted to answering these questions, but has not been markedly successful to date [42], and thus an in-depth discussion of the genetics of T2DM is outside of the scope of this paper.

β-Cell Dysfunction

We have seen how early researchers such as Opie recognized morphological changes in the insulin secreting B-cells of the Islets of Langerhans in the pancreases of human T2 diabetics. It is now known that in most cases, a defect in both the B-cell function and insulin sensitivity is required for hyperglycemia to exist in T2DM [62]. However, pancreatic pathology in T2DM is extremely variable, and although an average of approximately 50% reduction in the B-cell mass has been shown in postmortem studies of T2DM subjects [136, 137], this alone can not account for the hyperglycemia associated with the disease [138]. This conclusion is corroborated by the observation that the surgical removal of up to 70% of the pancreas in pancreatectomies, seldom leads to permanent hyperglycemia [137]. Also, the same degree of B -cell reduction and islet disorganization can be found in elderly subjects without clinical evidence of diabetes [138].

Beside showing decreased overall insulin secretion in advanced stages of T2DM [139], there are also disturbances in the temporal patterns of insulin secretion following glucose stimulation, suggestive of a defect in the β-cell mechanism that is responsible for the temporal coordination of insulin response. Insulin secretion from β-cells occurs in pulses and decreased insulin secretion in advanced T2DM is manifested as blunted and erratic insulin pulsatility following meals [140]. Figure 32, from a 1988 study by Polonsky et al. [140] shows effects on insulin pulsatility in concatenated traces of post-breakfast (4 hour increment), post-lunch (5 hour increment) and post-dinner (5-hour increment) insulin secretion rates (shown as percentage of mean) for 8 controls and 8

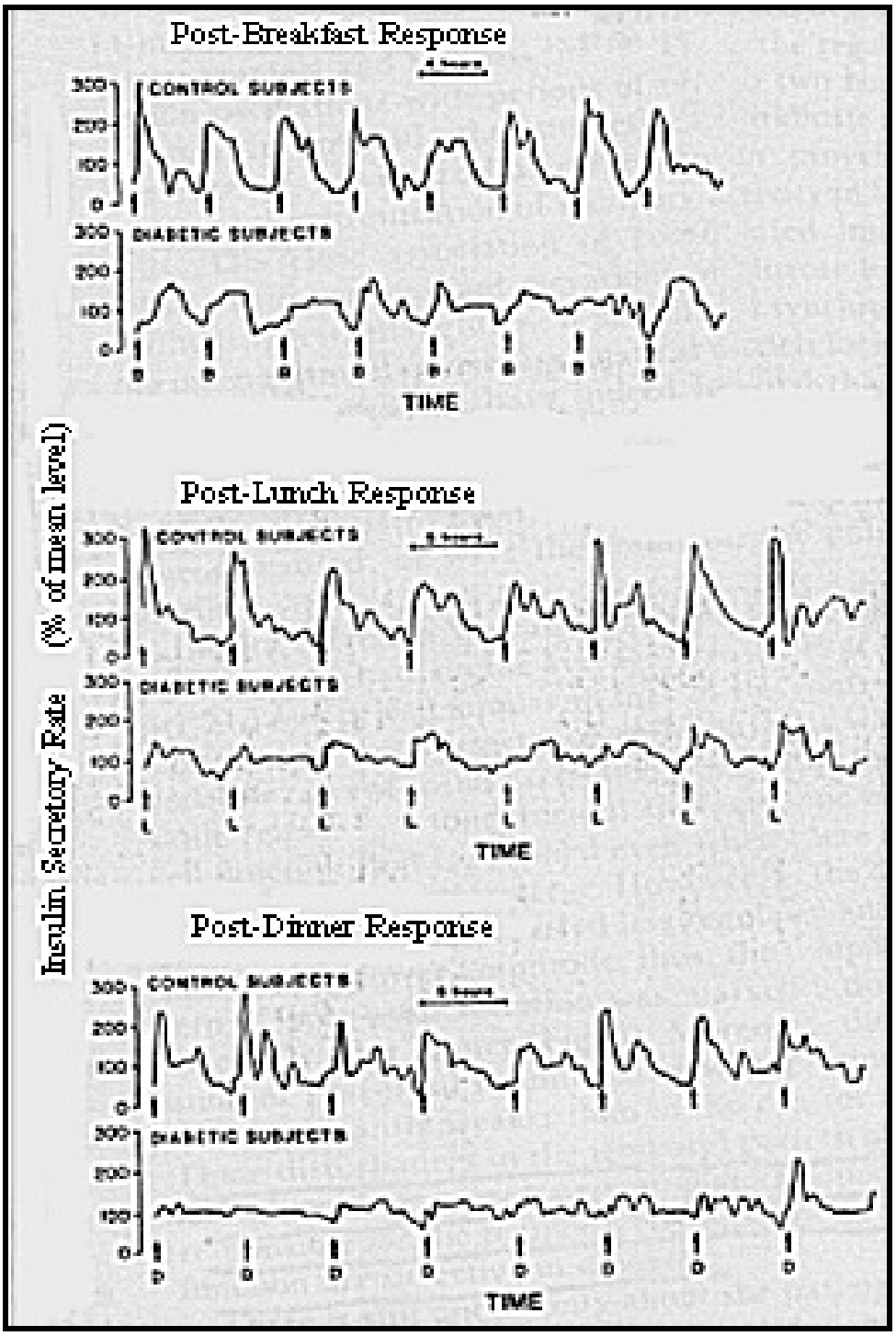

Figure 32 Loss of insulin pulsatility in T2DM, from [140].

diabetics. The times of the meals are shown by the small arrows below the traces. In the post-breakfast response of the T2 diabetics, the first pulse after the meal was delayed and blunted. This delay was not statistically demonstrated for the other meals. In the controls, the sharp peaks in response to each meal allow each subject to be inferred from the profile of the trace, while in the diabetic traces, the erratic nature of the pulses makes it more difficult to identify the transition from one subject to the next. This disturbance is most evident after dinner where the pulses are almost non-existent for some T2DM subjects. A similar loss of oscillatory insulin secretions was found in the non-diabetic, first-degree relatives of T2DM patients, after intravenous injection with a bolus of glucose, leading to the hypothesis that the loss of pulsatility is fundamental, not only to diminished B-cell function but also to peripheral insulin sensitivity [141] which has been shown to benefit from pulsed infusions [142] of insulin in comparison to continuous flow infusions.

There is also an abnormality in the efficiency of conversion from proinsulin to insulin that takes place in the B-cells and leads to an increased proportion of the relatively inactive, incompletely processed proinsulin to insulin in the plasma of T2 diabetics [143].

We have seen that hyperglycemia in T2DM is a manifestation of more or less coexistent impairments in the action and secretion of insulin [5]. Hyperglycemia is also self-perpetuating, since hyperglycemia *per se* has deleterious effects on insulin action and secretion [144]. Evidence that hyperglycemia can cause insulin resistance comes from patients with poorly controlled T1DM, where insulin resistance is a characteristic feature,

secondary to the loss of insulin secretion [144]. The recognition of the "vicious cycle" between insulin's secretion/action effects on plasma glucose concentration and plasma glucose concentration's effects on insulin secretion/action has led to the concept of "glucose toxicity" in B-cells [144]. While the precise biochemical mechanisms that are responsible for defects in insulin secretion and B-cell pathology remain to be discovered, studies have provided evidence for the involvement of hyperglycemia, dyslipidemia, cytokine, leptin, and autoimmunity induced pathways [145]. These defects may be amplified to pathology through mechanisms of phosphoinositide metabolism [144], ATP-sensitive K^+ channel, IRS-2, oxidative stress, nuclear factor-κB, endoplasmic reticulum stress and mitochondrial dysfunction [145]. It isn't necessary to present details of the studies on these potential tissue damaging pathways here, but particular pathways that provide a context for our experimental findings will be elucidated in the final discussion.

Complications of Type 2 Diabetes Mellitus

As we will see in more detail in the section on diagnosis, T2DM is defined by the level of circulatory glucose (the diagnostic cutpoint) above which will statistically lead to increased risk of complications, specifically retinopathy, 5 years later [2]. While the association of diabetes with its complications has long been known [146], 2 clinical trial studies in the 1990s: the Diabetes Control and Complications Trial (DCCT) [147] and the United Kingdom Prospective Diabetes Study (UKPDS) [148] strengthened evidence that hyperglycemia *per se* is the principle determinant of vascular damage.

In the DCCT, a study of 1441 T1DM patients, it was shown that each percentage increase of non-enzymatically glycosylated hemoglobin (Ha1c), an index of glycemic control for the preceding 3-4 weeks [149], was associated with a substantially larger concomitant risk of developing retinopathy. For example, a patient with a 6.0% Ha1c, indicating well-controlled glycemia, had a mean relative risk comparable to a non-diabetic after 6 years of follow-up. A patient with a 10% Ha1c, indicating poorly controlled glycemia, had a mean relative risk of showing retinopathy that was approximately 8-fold higher [149]. Importantly, patients randomly assigned to intensive insulin therapy groups showed significantly lower incidence of retinopathy than those assigned to a conventional insulin therapy group. A similar relationship between the degree of therapy and the incidence of albuminuria as a marker of nephropathy was also demonstrated [147].

In the UKPDS, a similar therapy intervention study to the DCCT, it was shown that T2DM patients who were treated intensively, with insulin or hypoglycemic drugs of the sulphonylurea class, or conventionally, by diet alone, had a 37% decreased chance of microvascular complications for every 1% decrease in Ha1c over the 10 year course of the study [150]. The intensively treated group had a median Ha1c of 7.0% and the conventionally treated group had a median Ha1c of 7.9% during the course of the study [150].

A relatively recent line of research has sought to discover how and why hyperglycemia causes microvascular and macrovascular pathological consequences. Every cell in every tissue is awash with hyperglycemic blood in all forms of diabetes

[151]. So what causes microvascular tissue damage to occur in relatively few tissues, most strikingly in the retina, renal glomerulus and peripheral nerves: leading to well-known T1DM and T2DM associated blindness, end-stage renal disease and debilitating neuropathies [152]? Also, how does hyperglycemia cause the macrovascular dysfunction that causes 80% of all diabetics to die from a thrombotic event, 75% of which are cardiovascular (stroke and infarction) and the remainder of which are a cerebrovascular event (stroke) or peripheral vascular complications [153].

Four hypotheses have gained credence as explanations of the linkages between hyperglycemia and tissue damage [152]. They are: increased polyol pathway flux (Figure 33A); increased advanced glycation end-product (AGE) formation (Figure 33B); activation of protein kinase C (PKC) isoforms (Figure 33C); and increased hexosamine pathway flux (Figure 33D). Each of these will be considered briefly below.

In the polyol pathway model, aldose reductase (AR) uses cellular NADPH as a co-factor to reduce reactive oxygen species (ROS)-generated toxic cellular aldehydes to inactive alcohols. In the presence of high levels of glucose, NADPH-regeneration of reduced glutathione (GSH) becomes depleted, thus leaving the cell vulnerable to oxidative stress [151].

Results of studies on the contribution of the polyol model have been inconsistent [151]. In heterozygous transgenic mice, however, that overexpress AR in the eye lens, chemically induced diabetic mice showed approximately 3-fold reduced levels of GSH ($p < 0.001$) concomitantly with 2-fold increase in the lipid peroxidation product malondialdehyde, compared to chemically induced diabetic, non-transgenic mice [154].

Also, clinical studies have shown significant improvement in subjective and electrophysical measures of nerve function, as well as nerve regeneration and reduced sorbitol accumulation in human T2 diabetics with peripheral neuropathy after AR inhibitor treatment [155, 156]. However several of these agents have not achieved use because of unacceptable hepatic dysfunction (tolrestat), renal toxicity (zenarestat) and subjective hypersensory effects (sorbinil) [156], and worldwide, only one such polyol pathway inhibiting drug, epalrestat, is in clinical usage [155].

Regarding the increased production of advanced glycation end-products (AGEs), proteins non-enzymatically [149] react with reducing sugars, primarily glucose and fructose, adding to lysine side-chains in a concentration dependent manner (Figure 34), and forming a relatively unstable Schiff base [157]. As shown in Figure 34, the Schiff base can rearrange to the Amadori product to form the first stable glycation product. Glycated hemoglobin (Ha1c) that is used to monitor glucose concentration is a specific ketoamine [158] glycation of the NH_2-terminal valine of the B-chain [149]. Before the Amadori protein product is removed by protein turnover, it may be further converted by a series of ill-defined reactions to produce advanced glycation end-products (AGEs). Alternately, AGE precursors can be formed when sugar oxidation products directly attack proteins [157].

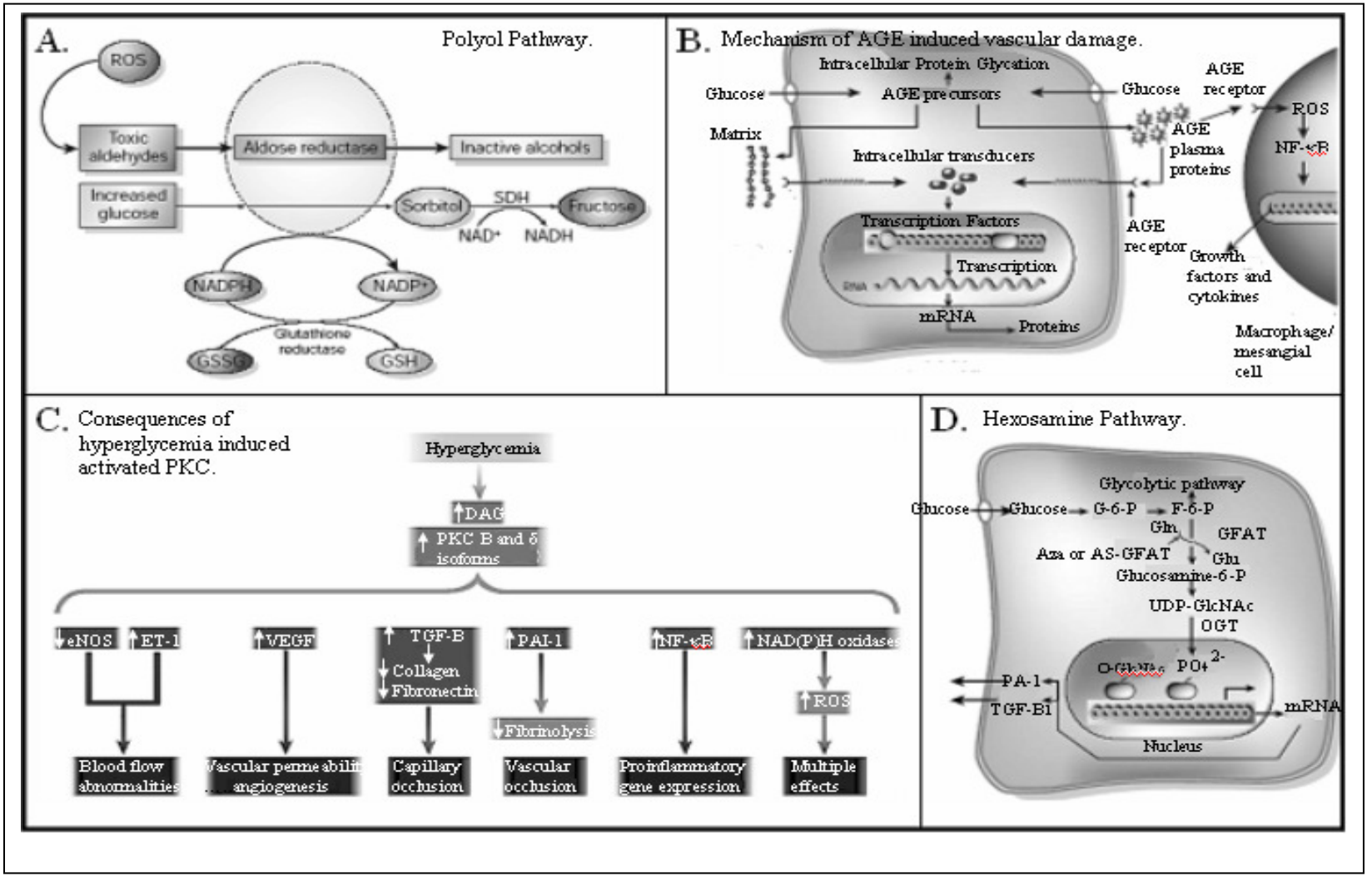

Figure 33 Four pathways hypothesized to cause diabetic complications, from [152].

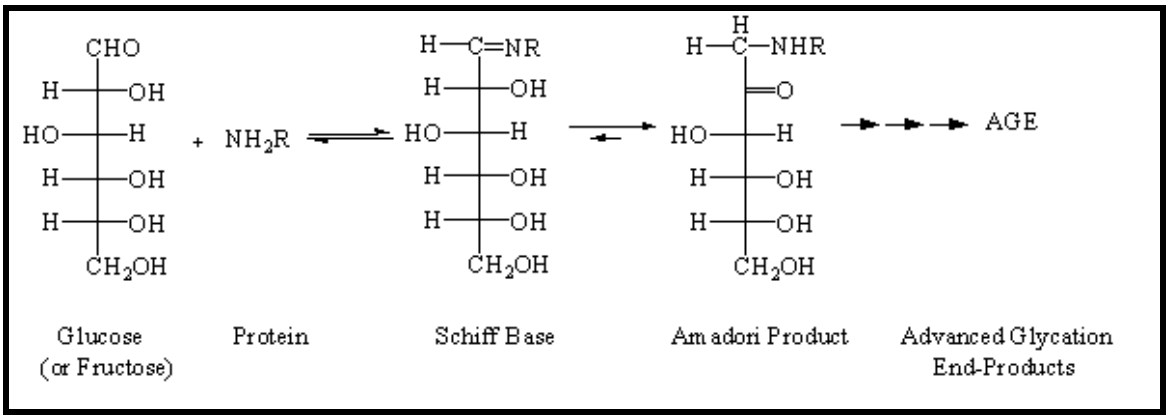

Figure 34 The sequence of reactions that produce advanced glycation end-products (AGE).

AGE precursors, shown schematically in Figure 33B can modify intracellular proteins and possibly change gene transcription [151]. AGE precursors may diffuse from the cell to modify long-lived structural proteins like collagen of the extracellular matrix causing damage to the extracellular matrix and cellular dysfunction [151] or damage to the crystallin in the eye [157]. AGE precursors can also modify circulatory proteins, such as HSA, changing their structure, function and potentially leading to systemic pathological consequences [159-162]. Modified circulatory proteins may also bind to cell surface receptors for AGEs (RAGEs), triggering the inflammatory response through the NF-κB pathway [151].

A bifunctional AGE scavenging molecule, aminoguanidine, has been shown to effectively ameliorate or abrogate the pathological effects of hyperglycemia on the retinae of rats with chemically induced diabetes [163]. In a randomized 2-4 year, clinical trial of 690 T1DM patients, administering either a placebo, low dose (150 mg) or high dose (300mg), aminoguanidine was shown to have efficacy in lowering proteinuria,

reducing the progression to retinopathy and improving lipid profiles. However, the non-placebo groups had aminoguanidine associated adverse events, including the induction of autoantibodies, flu-like symptoms, mild liver enzyme elevations, anemia, and three subjects in the high dosage group (n=225) suffered glomerulonephritis, two of whom required maintenance dialysis [164]. Thus, aminoguanidine has not been adopted as a therapy for reversing complications of T2DM.

The third mechanism that contributes to hyperglycemia-associated pathology is the mechanism by which increased levels of diacylglycerol (DAG) leads to increased activation of various isoforms of protein kinase-C (PKC), the serine-threonine kinases that interfere with proper phosphorylation of insulin receptor substrates, as was discussed in the Insulin Resistance section (Figure 19 and Figure 26). As seen in Figure 33C, increased DAG leads to a variety of changes in gene expression, and in each case, expression that is beneficial to the cell is decreased and unhealthy expression leading to inflammation, oxidative stress and atherogenic processes is increased [151].

Researchers who had previously found that the predominant isoenzyme PKC-B was upregulated in the heart, retina, glomerulus and aortas of chemically induced diabetic rats [165], further showed that oral administration of a specific PKC-B inhibitor improved measures of retinal and renal function. The left side of Figure 35A shows a measure of PKC activity in the glomeruli of non-diabetic (open bars) and diabetic rats (grey bars), as a function of oral dosages of the PKC-B inhibitor, LY333531. The diabetic rats show a dose dependent decrease in PKC activity. The right side of Figure

35A shows a measure of glomerular filtration rate (GFR), an early indicator of increased intra-glomerular pressure and renal abnormality. The decrease in GFR seen in the

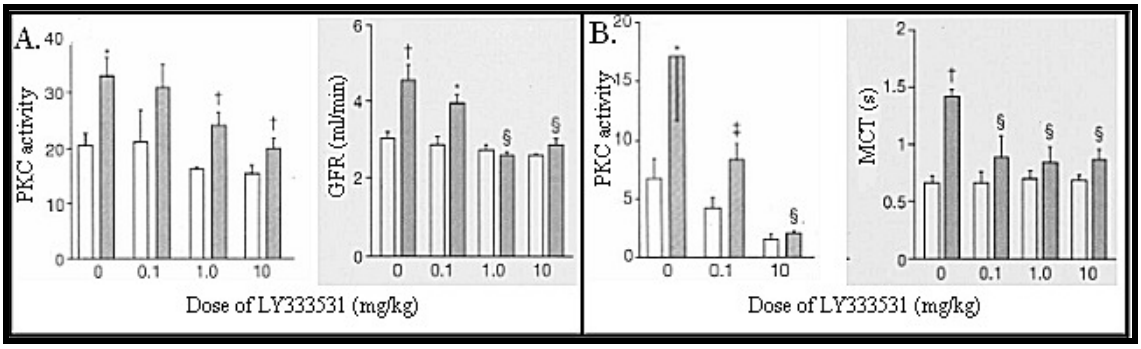

Figure 35 The PKC-B inhibitor, dose-dependent normalization of glomerular and retinal functions in diabetic rats, from [165].

diabetic rats parallels their PKC activity and in both cases the levels are nearly normalized at high dosages, to those seen in the non-diabetic. The authors suggest that the lack of effect in the non-diabetic rats was an indication that PKC-B is not activated in the tissue under normal circumstances. Figure 35B shows a similar experiment showing the parallel dose responses due to PKC-B inhibitor in rat retinae in PKC-B activity and mean circulation time (MCT), an indicator of microvascular resistance to blood flow [165].

The last of the four proposed contributors to diabetic complication is the increase flux through the hexosamine pathway (Figure 33D). Where hyperglycemia exists, an increase of superoxide radical from the electron transport chain in mitochondria (Figure 37A) can cause an inhibition of glyceraldehyde-3-phosphate dehydrogenase (GAPDH, Figure 37B) in the glycolytic pathway, leading to presumed increase of fructose-6-phosphate (F6P) levels [166]. An increase of F6P leads to an increased diversion of F6P

into a signaling pathway in which an enzyme called glutamine:fructose-6 phosphate amidotranferase (GFAT) converts F6P to glucosamine-6 phosphate and finally to uridine diphosphate N-acetyl glucosamine (UDPGlcNAc). High amounts of UDPGlcNAc results in the glycosylation of serine and threonine residues by the GlcNAc moiety, catalyzed by the enzyme O-GlcNAc transferase (OGT). Increased glycosylation of transcription factors in this manner may cause pathological O-GlcNAc modifications of normally phosphorylated sites [152].

Evidence for the seeds of pathogenesis by the hexosamine mechanism has been shown in cultured bovine aortic endothelial cells [166]. In an experiment by Du et al in 2000, GAPDH activity was shown to be inhibited by high (30 mM) glucose, compared to low (5mM) glucose (Figure 36A). GAPDH activity was completely recovered by all of 5 methods that were used to prevent the production of, or to quench superoxide radical. No recovery was seen with an anti-sense uncoupling protein (UCP) vector or with a vector containing AZA cDNA, a hexosamine pathway inhibitor. In accord with the model, these effects on GAPDH activity were generally anti-correlated with the production of UDP-GlcNAc, as determined by UV RP-HPLC (Figure 36B). This is consistent with hyperglycemia increasing superoxide, which inhibits GAPDH, and which then leads to high cellular levels of UDP-GlcNAc. Further, anti-GlcNAc, anti-phosphoserine and anti-phosphothreonine western blots of Sp-1, a transcription factor that is believed to regulate transcription of plasminogen activator inhibitor 1 (PAI-1) showed competitive interference of O-GlcNAcation with phosphorylation (not shown here) [166]. Luciferase plasmids, that signal promoter activity, showed activation of transforming growth factor-

B (TGF-B) (Figure 36C), as well as PAI-1 (Figure 36D), parallel to that of the cellular UDP-GlcNAc production.

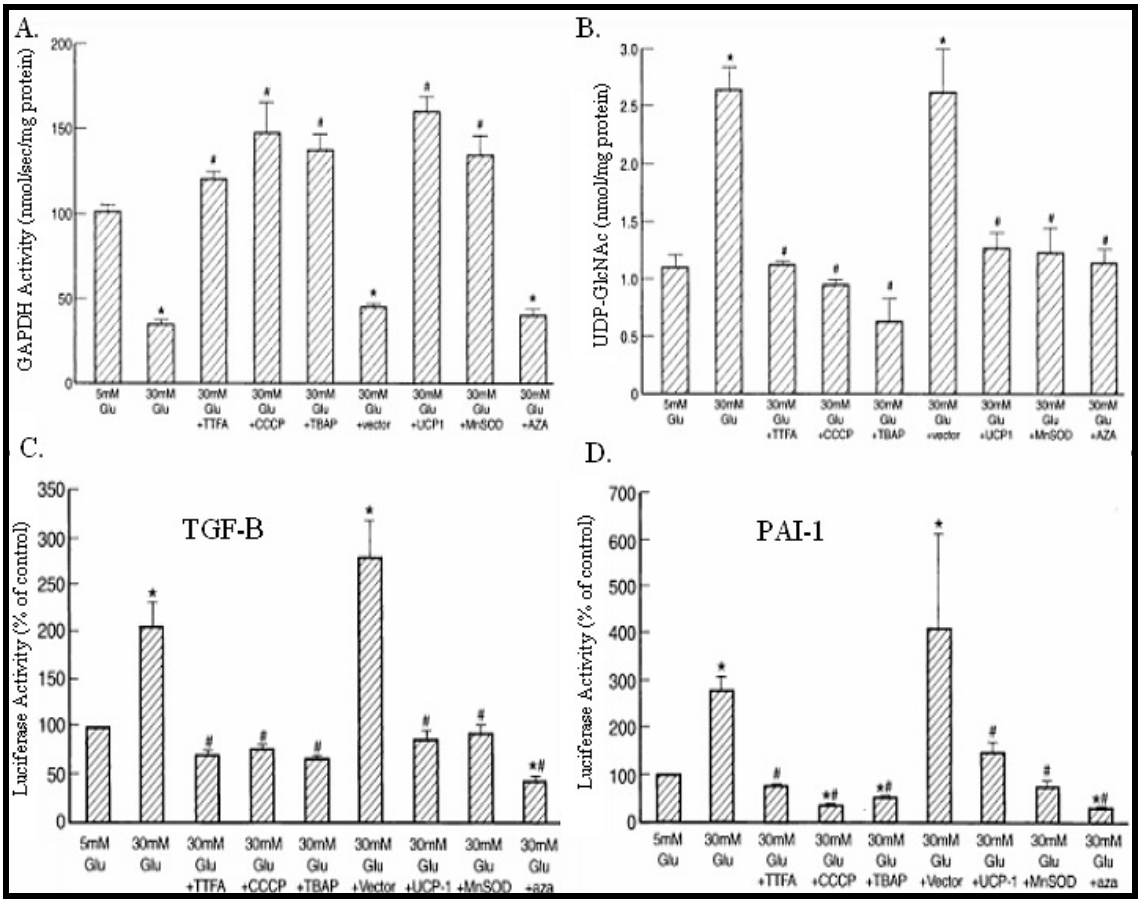

Figure 36 The effects of glucose and superoxide inhibitors. From [166].

As seen in Figure 33C the superoxide mediated pathway may be an alternate path to the PKC-activated pathogenesis of capillary and vascular occlusion caused by TGF-B and PAI-I, respectively, although no measurements of PKC or DAG levels were made in this experiment.

Also in 2000, Nishikawa et al. [167] showed that the first 3 pathways to diabetic complications: increased PKC-activation, increased AGES and increased aldose

reductase flux could be abrogated by blocking the production of superoxide in the electron transport chain (Figure 37A). In 2001, Michael Brownlee, because of what he considered the disappointing effectiveness of individual inhibitors which targeted individual pathways, added the hexosamine pathway flux to the 3 pathways of Nishiwaka. Brownlee proposed the superoxide mechanism of GAPDH inhibition as a "unifying mechanism" [152] resulting from the hyperglycemia-induced overproduction of superoxide in the mitochondrial electron transport chain (Figure 37A) to explain all four pathways.

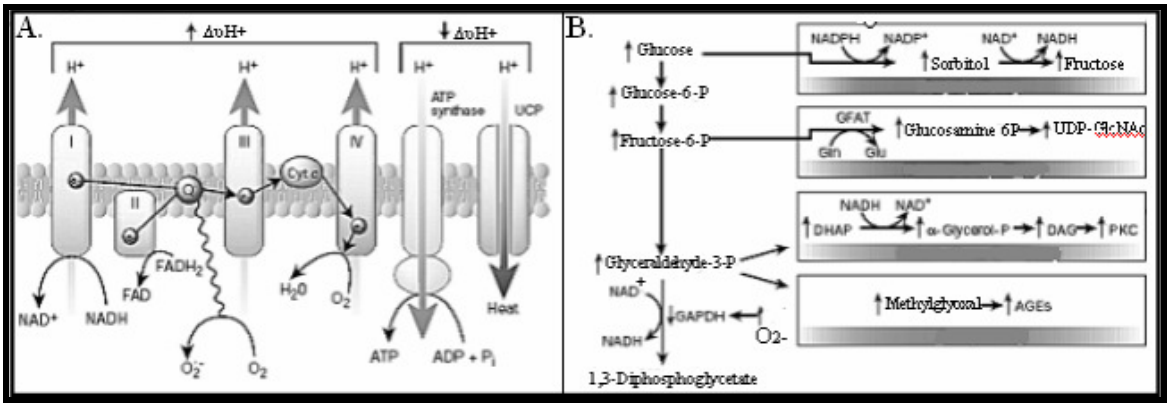

Figure 37 Brownlee's unifying mechanism for the four hyperglycemia-induced pathways to diabetic complications, from [152].

As seen in Figure 37A, increased levels of the electron donors, NADH and $FADH_2$ from the tricarboxylic acid (TCA) cycle, result in a high mitochondrial membrane potential ($\Delta\upsilon_{H+}$). This inhibits the electron transport at complex III, which increases the levels of free-radical intermediates of coenzyme Q (ubiquinone), which in turn leads to increased levels of reduced O_2, (superoxide radical) and the consequent inhibition of GAPDH.

Figure 37B is a schematic showing how the inhibition of GAPDH leads to Brownlee's proposed "unified" increased flux into each of the four previously discussed mechanisms.

Brownlee explained that the reason why diabetes associated complications occur in a relatively few and specific tissue types is that these tissues have relatively constitutively active glucose transporters and therefore are internally exposed to higher glucose concentration than the cell types that are more dependent upon insulin stimulation for glucose transport [151]. The role of hyperglycemia induced oxidative stress is currently a very active line of research. Brownlee's 2001 publication [152], which proposed the unifying mechanism, has been cited by Web of Science publications 1,892 times, about 300 times a year since 2006.

Epidemiology of Type 2 Diabetes Mellitus

Diabetes mellitus has attained the status of a global pandemic [168] . According to the 2003 International Diabetes Federation's (IDF) Diabetes Atlas, 195 million people between the ages of 20 to 79 years, worldwide, were considered diabetic and it was predicted that by the year 2025, 333 million people would be diabetic. This predicted increase, considered alarming at the time, was approximately 4% per year [169]. This year (2010) the 2009 Diabetes Atlas reported that 285 million people were expected to be diabetic, an increase of 10% per year since 2003. 90% of these cases are T2DM. Of the T2DM cases, at least 90% are the "common" type, of multifactorial pathogenesis, as opposed to the relatively rare monogenic forms such as maturity onset diabetes in the young (MODY) and mitochondrial diabetes [170].

The geopolitical trend of the epidemic is consistent with the thrifty gene hypothesis [45]. The regions of the world that are becoming "westernized" by moving away from an agrarian lifestyle are experiencing the most rapid increase in T2DM. The prevalence of T2DM has shown itself to evolve in association with rapid cultural and social changes, aging populations, increasing urbanization, dietary changes, reduced physical activity and other unhealthy lifestyle and behavioral patterns [169]. Asia , Africa and South America were therefore, as of 2003, expected to experience 57%, 50%, and 44% growth, respectively, in the prevalence of T2DM in their populations from 2000 to 2010 [107]. This is to be compared with the lower 23% and 24% growth for North America and Europe.

The modern day consumption of the sugar fructose, mostly as high-fructose corn syrup sweetener, warrants special mention as a dietary change that may be a large contributing factor to obesity as well as insulin resistance [171]. Fructose, compared with glucose, is preferentially metabolized to lipid in the liver. And fructose consumption in animal models has been shown to induce insulin resistance, impaired glucose tolerance and hypertension [171].

Diagnosis of Type 2 Diabetes Mellitus

The plasma samples for the 2D-PAGE proteomics analysis experiments to be described were from subjects who were classified as having normal glucose tolerance (NGT) or T2DM. The classifications were made using the WHO diagnostic criteria that were first recommended in 1999 [2]. The details of this classification are included in the

Materials and Methods section. Briefly, the WHO recommends a diagnosis of T2DM for persons with FPG ≥ 126 mg/dL or 2 hour plasma glucose ≥ 200 mg/dL after oral administration of 75 gm glucose [2].

For the follow-up experiments to the 2DGE proteomics experiment, samples were also included from subjects who were classified as having impaired glucose tolerance (IGT). These subjects have FPG < 126 mg/dL and their glucose levels were between 140 and 199 mg/dL two hours after the 75 gm glucose drink.

The cut-points for diagnosis of T2DM are primarily derived from the results epidemiological studies that show the occurrence of diabetes-specific complications, particularly retinopathy, across a range of plasma glucose levels. Figure 38A shows an

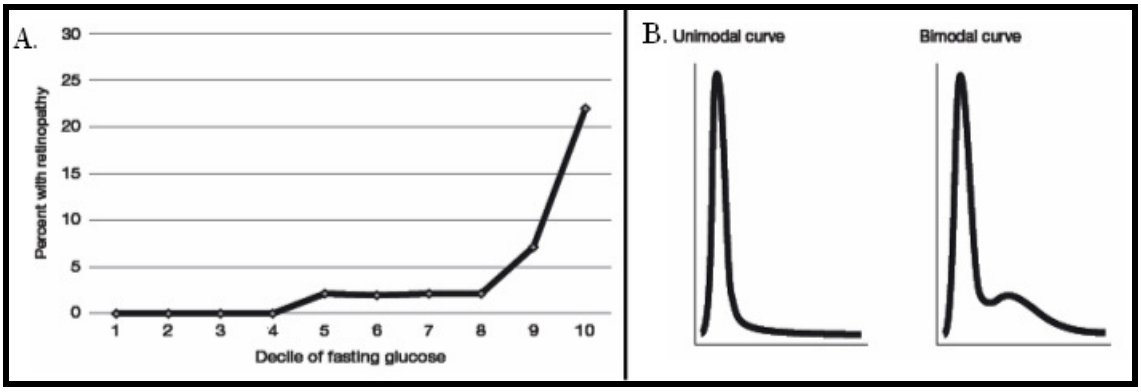

Figure 38 Examples of epidemiological studies used to define T2DM. A) Percentage of 5-year risk for retinopathy vs. deciles of fasting plasma glucose. B) Unimodal (left) and bimodal (right) population distributions of fasting plasma glucose. Both distributions are numbers in population vs. fasting plasma glucose. From the 2006 WHO/ IDF report Definition and Diagnosis of Diabetes Mellitus and Intermediate Hyperglycemia: Report of a WHO/IDF Consultation [2].

example of such data in which deciles of FPG are plotted against the prevalence of retinopathy for a population. The diagnostic cut-point is determined as the level at which

the risk of retinopathy increases significantly. Figure 38A shows that the prevalence of retinopathy rises dramatically in the 9th decile of plasma glucose. Most studies have used the lower limit of the 9th decile as the cutpoint for T2DM diagnosis [2].

Studies that are based upon diabetic complications, such as was shown in Figure 38A, have been combined with "population distribution of plasma glucose" studies to derive diagnostic cut-points. An example of data from such a study is shown in Figure 38B. Two different distributions of plasma glucose, with plasma glucose on the x-axis and numbers of people on the y-axis are shown in this figure. In the left curve the entire population is represented by a unimodal distribution. On the right is an example of a bimodal distribution in which two groups are represented in the population. In the bimodal distribution, the cut-point that is used to discriminate normal from abnormal is where the two component curves intersect. In this case the cut-point that separates the two components of the population doesn't necessarily indicate any pathogenic implications for adverse health outcomes that could be attributable to diabetes. Such bimodal distributions of plasma glucose have been found in populations with a high prevalence of diabetes, including Pima Indians, Pacific Islanders, Asian Indians, Mexican Americans, Egyptians, Malaysians and an elderly white population of Southern California [2].

The combination of different types of studies to derive the cut-points for diagnosis of T2DM is likely a reflection of the WHO report's observation that there were limitations in the data and methodologies used to determine at which level the harm was specifically increased and which clearly differentiated diabetes from non-diabetes.

However, the WHO report states that the chosen cutpoints distinguish a group with significantly increased premature mortality and increased risk of microvascular and cardiovascular complications.

Clearly, biological markers that more closely associate with hyperglycemia related complications would better discriminate T2 diabetes from non-diabetes. This statement is close to the heart of the reason why the NIH program announcement for the grant that funded this experiment, PROTEOMIC AND METABOLOMIC APPROACHES TO DIAGNOSE DIABETES AND PRE-DIABETES (NIH PAR-04-076) stated,

> "Clinical trials have demonstrated effective interventions for preventing or delaying complications in those with diabetes and for preventing or delaying onset of diabetes in those with pre-diabetes. However, millions of Americans are not receiving effective therapy, in part due to the limitations of current methods of diagnosing diabetes and pre-diabetes. The oral glucose tolerance test (OGTT), the gold standard for diagnosis of diabetes and pre-diabetes is inconvenient, requires fasting, and is not highly reproducible. The fasting blood glucose (FBG) is less burdensome but much less sensitive, particularly in older Americans who have the highest prevalence of diabetes and pre-diabetes…
>
> (a) simplified, less burdensome approach to the diagnosis of diabetes and pre-diabetes would facilitate increased recognition and improved care of these conditions. Many proteins and other blood components may be modified in individuals with elevated blood glucose. Identification of these molecules or of identifiable correlates of hyperglycemia would facilitate development of potential new laboratory tests for diagnosis of diabetes and pre-diabetes. With this initiative we are encouraging scientists with expertise in proteomics and metabolomics to develop new tests to detect pre-diabetes and diabetes that correlate with the results of the OGTT but do not require fasting or administration of glucose."

The forgoing chapter had very little discussion on blood and plasma. As delineated by the program announcement above, our experiment investigated plasma

proteins for differences related to T2DM. We will now briefly discuss human plasma and the proteomics technologies that will be used for this investigation.

INTRODUCTION TO HUMAN PLASMA PROTEOMICS

Our experiment utilized a novel combination of technologies to subfractionate and separate citrated human plasma proteins by differential two-dimensional gel electrophoresis (2DGE) for the comparative analysis of the relative concentrations of the individual protein isoforms from human non-diabetic (NGT) controls and newly diagnosed, untreated T2 diabetics. An overview of the workflow of the experiment is shown in Figure 39. Briefly, in Figure 39A, citrated plasma from subjects is immunodepleted of the 14 most abundant proteins. In Figure 39B, the many remaining low-abundance proteins are taken forward for fractionation into 6 fractions by reverse phase (RP) HPLC and the control, T2DM samples and internal standards are labeled with different colored fluorescent Z-dyes. In Figure 39C, the 6 fluorescently labeled RP-HPLC fractions are separated on 2D gels for comparison of individual protein isoform spot volumes between the diseased and non-diseased states using multiple color, fluorescence-detection. Protein spots changes between the experimental groups that met the statistical criteria employed were then identified by in-gel digestion, mass spectrometry and database searching.

The sections that follow will describe the plasma sample and summarize the individual technologies to provide the rationale for their use, as well as for the methods used to adapt them to the experimental flow. Details of the protocol are given in the Materials and Methods section.

Human Blood, Plasma and Serum in Research

The liquid, non-cellular part of blood is known as the plasma [172]. Blood is routinely collected as a clinical specimen world-wide and regularly separated into its cellular components and plasma or serum by centrifugation. The cellular component comprises the hematocrit, or red blood cells, and the buffy coat. The buffy coat comprises the white blood cells and platelets. Within plasma are all of the soluble components of blood including proteins, electrolytes, metabolites, drugs and toxins.

To prepare plasma from blood, common anti-coagulants, such as citrate or EDTA [173], are added to chelate divalent calcium cations [172], thereby preventing the coagulation cascade via the fibrinogen activation pathway. Heparin may also be used to catalyze the function of anti-thrombin to much the same anticoagulant effect [174, 175]. Serum is created by allowing plasma to undergo coagulation and then removing the precipitated fibrin mesh by centrifugation [172] . In this respect serum may appear to be a simpler sample than plasma as a starting material for a proteomics study but, as a biochemical process, serum generation is subject to variable proteolysis that accompanies coagulation, as well as ex vivo parameters such as temperature and time of sample processing. During the process of coagulation necessary for serum generation, platelets, leukocytes and erythrocytes secrete proteins and enzymes that may contribute to artifactual variation [172]. Also proteins can become trapped within fibrin clots in a variable manner. For these reasons serum is regarded as a more artifactually heterogeneous sample of peptides and should generally be avoided for biomarker discovery [173].

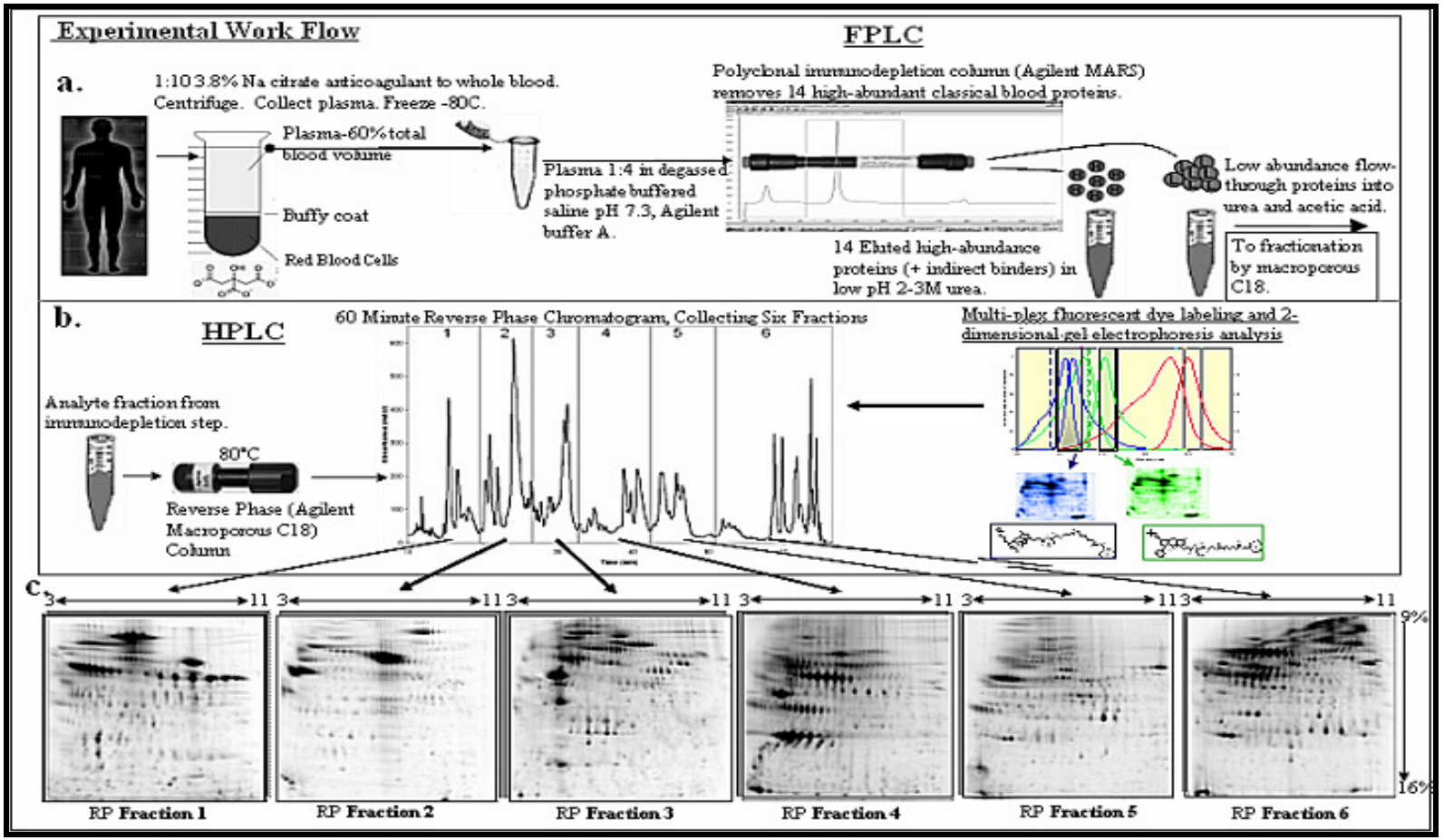

Figure 39 Experimental work flow for the 2-D differential fluorescence detection experiments of this thesis.

Plasma has powerful allure as a sample for the discovery of biological markers because of its ease of accessibility and because it is in contact with every tissue in the body, carrying the secreted proteins and proteolytic degradation products of those tissues as subsets [176, 177]. Plasma is believe to carry tens of thousands of proteins in their intact, cleaved and modified forms [178]. Routinely administered clinical tests for immunoglobulins indirectly detect exposure to many pathogens, for example, HIV and influenza. And there are several diagnostic ELISA tests for circulating tissue "leakage" [176] proteins, such as: γ-glutamyl tranferase for detecting liver disease; troponin T, myoglobin and creatine kinase MB to diagnose myocardial infarction; prostate-specific antigen for warning of prostate cancer [179], and CA125 for detecting ovarian cancer [180].

Plasma contains over 10 orders of magnitude in dynamic range of concentration between it most abundant protein, serum albumin (HSA), and the least abundant clinically measured proteins [176]. For this reason, and the extreme heterogeneity of its predominant glycoproteins, the immunoglobulin family, plasma is considered the most difficult proteome to characterize [181]. At present, four orders of magnitude is the largest estimate for the linear dynamic range of detection for global proteomics experiments using fluorescent dyes [182]. As can be seen in Figure 40, if the protein evidence of a disease exists in a protein class other than the most abundant "classical" plasma proteins, one will need to analyze proteins of concentration at least four orders of magnitude lower than the most prevalent plasma protein, which is HSA (disregarding hemoglobin which is separated from the plasma with the red blood cells). However, with

the removal of HSA alone, it can be seen that plasma protein concentrations two orders of magnitude lower may be brought into the purview of the four log dynamic range, which begins to reach into the "tissue leakage products, etc." class, but not into the interleukins and the lowest level proteins.

Sample Handling

Sample handling is a primary concern for all expression proteomics experiments. Generally, experiments with fewer sample handling steps will introduce fewer experimental variations and, all other things the same, are ultimately more likely to detect

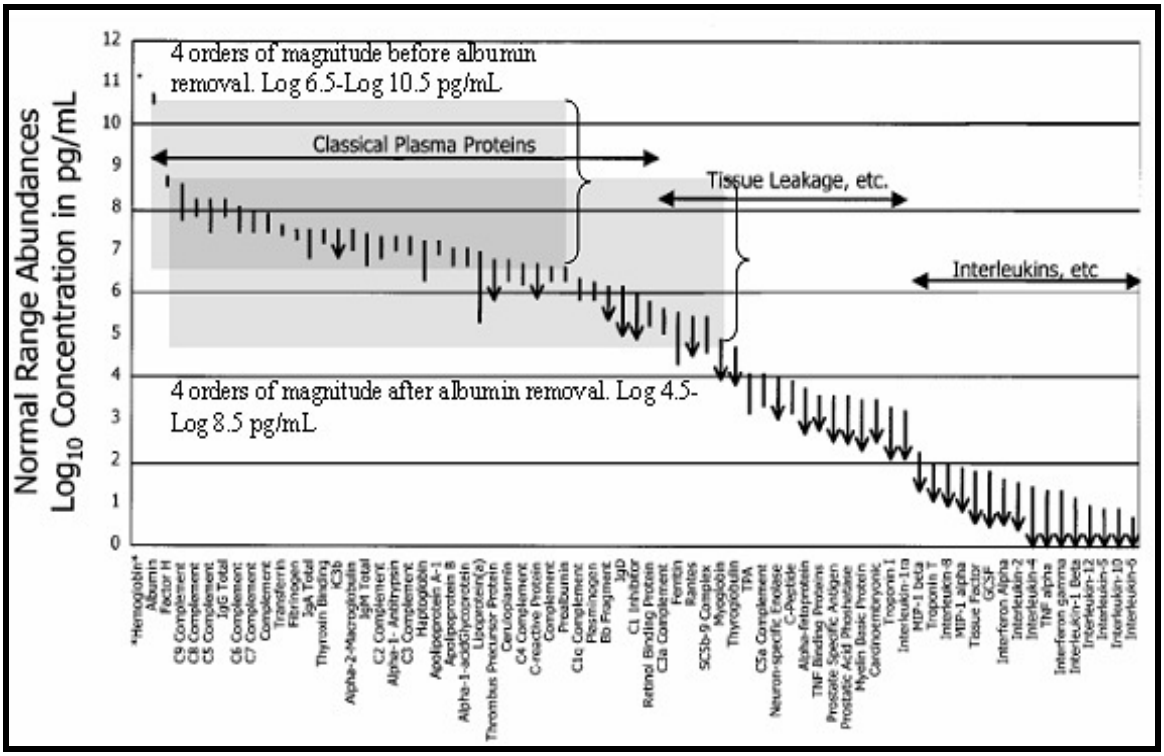

Figure 40 Plasma protein concentration range. Adapted from [176].

true biological changes. But clearly, with the amount of previous research done on blood and diabetes, an approach to this experiment without steps to subfractionate and simplify the protein analyte, before displaying it by two-dimensional gel electrophoresis (2DGE), would likely have been fruitless. So a tradeoff approach, to gain depth in the dynamic range of plasma protein concentration, in exchange with the acceptance of some increased technical variation, was devised. Our efforts to reduce the effect of experimental variation will be discussed in the HPLC fractionation section of Materials and Methods. Many expression proteomics experiments utilize specific protease inhibitors in the attempt to diminish artifactual variation caused by *ex vivo* proteolysis. This strategy is of greatest benefit for cellular preparations where proteases are liberated when protease- sequestering subcellular compartments such as lysosomes are disrupted during sample preparation. However, some specific protease inhibitors, specifically the widely used 4-(2-aminoethyl) benzenesulfonyl fluoride (AEBSF) [173] have been shown to be a source of variation in 2D gel experiments, as they change the pI of proteins to which they are bound.

Plasma doesn't experience such high levels of proteolysis as typical lysed cells and evidence of the usefulness of protease inhibitors in stabilizing proteins in global serum proteomics is ambiguous [183]. This is due in part to the presence of a large class of endogenous circulatory protease inhibitors [184]. In contrast to cellular lysates, it has been observed that even very long term exposure to room temperature in serum only marginally degrades proteins [173] and there is no evidence that protease inhibitors offer protection against the generation of low molecular species on 2D gels [185]. Chemical

denaturants and altered pH environment have been shown to be general methods for reducing protein alterations, although these are also imperfect methods for the inhibition of *in vitro* enzymatic activity [175, 186]. Also, it has been shown that the addition of protease inhibitors, in denaturing solutions, such as are used in this experiment, does little to abolish the residual activity [186].

In order to control proteolysis in this experiment, which includes multiple solvent exchanges, we relied on the addition of sodium citrate at the time of the blood draw to inactivate calcium-dependent proteases, chemical denaturation, alteration of the pH, and low temperature storage. Except for the time during the blood draw and aliquoting the samples, the plasma that was used in this experiment was stored at -80 C. At the time of the first injection of sample for immunodepletion, the bench time for dilution of the thawed samples, centrifugation and the FPLC injection in this experiment was 3 minutes. Although the sample was kept on ice until the 2 minute centrifugation, this pre-injection time may have been the most vulnerable step to proteolysis in our procedure. After injection onto the FPLC immunodepletion column, the flow-through proteins were collected directly onto denaturing urea and acetic acid that resulted in final concentrations of 6M and 1%, respectively. This immunodepleted, flow-through protein solution was then immediately loaded onto the C18 column for reverse-phase fractionation, where the proteins were exposed to the acidic mobile phase containing 0.1% TFA and a gradient of eluting concentrations of acetonitrile in the RP-HPLC step that followed. The respective RP fractionated solutions were frozen to -80C and lyophilized. The dried, subfractionated

proteins then were washed from the vials with 8M urea and 4% CHAPS detergent before aliquoting, refreezing, lyophilizing, dye-labeling and iso-electric focusing.

The low pH environment resulting from the addition of acetic acid, after immunodepletion also suppresses the formation of mixed disulfides that may result from the exposed cysteines in the denatured proteins. The rate of oxidation is proportional to the concentration of thiol anion and is therefore strongly pH-dependent. The pK of the cysteine thiol is about 8.3, so disulfide formation and oxidation can be severely diminished at pH 4 or below [187]. If mixed disulfides were to occur, they would cause artifactually different elution times in the RP-HPLC, for the protein subunits forming the mixed disulfide bridges. Protein disulfides were reduced and alkylated between the first and second dimension of the 2D gel preparation to improve separation but we wished to retain the native disulfides during the RP-HPLC step. Any native disulfides are regarded as providing potential information on the oxidative state of proteins that could reflect the diseased state, and which could become evident in the gels if the samples were not reduced and alkylated before the isoelectric focusing step in the sample processing.

Below is an explanatory justification of the several steps in the experimental protocol. For more experimental details see the Materials and Methods section.

The Immunodepletion Strategy.

The first step in our strategy to analyze lower abundant proteins was the depletion of the plasma of its 14 most abundant proteins. This benefits the 2D gel analysis in several important ways. The most important protein to remove is HSA. HSA is such a

predominant protein that it often creates a disruption of the pH gradient in the first dimension separation. It occupies up to 7 isoelectric positions near pH 5.6 and M_r = 66000, so it occupies a large and central position in 2D gels as shown in Figure 41, directly occluding the visualization of other proteins with a similar molecular weight and pI. As can be seen in Figure 41, the HSA is also accompanied by horizontal and vertical streaks, even extending below it, likely indicating the co-precipitation of proteins with pI values that are similar to HSA [188] and interfering with the quantitation of proteins located far, in pI and M_r, from HSA.

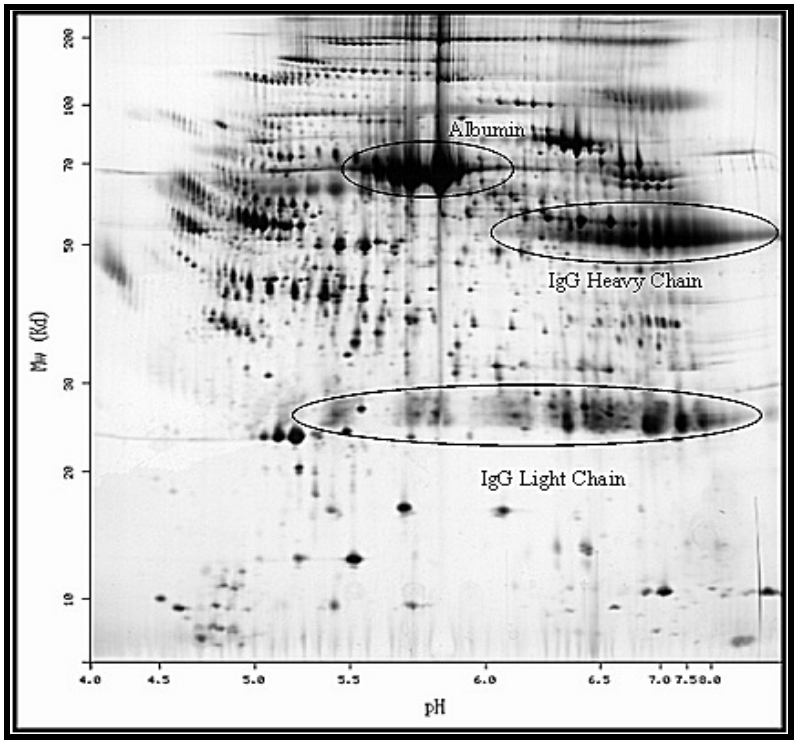

Figure 41 From ExPASy Swiss 2D page viewer-Human plasma. HSA and the heavy and light chains of IgG are in the ovals, demonstrating the extreme heterogeneity of their pIs and horizontal positions, obscuring and interfering with the quantitation of similarly migrating proteins.

Perhaps even more profoundly for expression proteomics, is the indirect way that HSA and other abundant proteins suppress the signals of all the less abundant proteins in 2D gels. Because of the quantitative analysis requirement that no protein fluorescent signal should saturate the detection capability of the scanner, the reduction of the photomultiplier voltage of the gel scanner, to bring intense protein signals to sub-saturation, becomes necessary and the signals of all proteins are reduced, with potential for the loss of detection of the large number of proteins that would fall below the sensitivity limit.

There is a third important benefit resulting from the immunodepletion step, involving the practicability of the fractionation step that followed immunodepletion. In our protocol, the step following immunodepletion was the fractionation of the low abundance proteins by reversed-phase high-pressure liquid chromatography (RP-HPLC). The column used for this step (Agilent, macroporous reversed-phase "mRP" Hi-recovery protein C18, 4.6 x 50mm, part # 5188-5231) has a loading capacity of 380 μg. The depletion of 40 μL of plasma yields a flow-through protein mass from one immunodepletion injection that is compatible with the capacity of the mRP column, but undepleted plasma would saturate the column capacity, primarily with abundant proteins.

The immunodepletion column (Agilent 4.6 x 100 mm IgG polyAb multiple affinity removal system "MARS-14" LC column) combines polyclonal antibodies and low molecular weight "affibody" ligands [189] to bind 14 abundant proteins in plasma including HSA, IgG, antitrypsin, IgA, transferrin, haptoglobin and fibrinogen, alpha2-macroglobulin, alpha1-acid glycoprotein, IgM, apolipoprotein AI, apolipoprotein AII,

complement C3, and transthyretin [190]. These proteins are known as the "bound" fraction that are eluted in a later step and on average comprise about 94% by mass of the total plasma protein content [189]. Healthy human plasma contains 60-80 µg /µL of protein [185, 191]. Therefore, using the high estimated value of 80 µg /µL, the 40 µL plasma capacity of the MARS-14 column will be injected with approximately 40 µL x 80 µg protein/ µL = 3200 µg of protein. The remaining protein mass after depletion by 94% is 3200 µg protein x 0.06 = 192 υg. This is well below the 380 υg capacity of the mRP column, so each immunodepletion can be coupled with a RP-HPLC fractionation, without the need for any additional sample manipulation.

The pie chart in Figure 42 shows the relative amounts of the most abundant

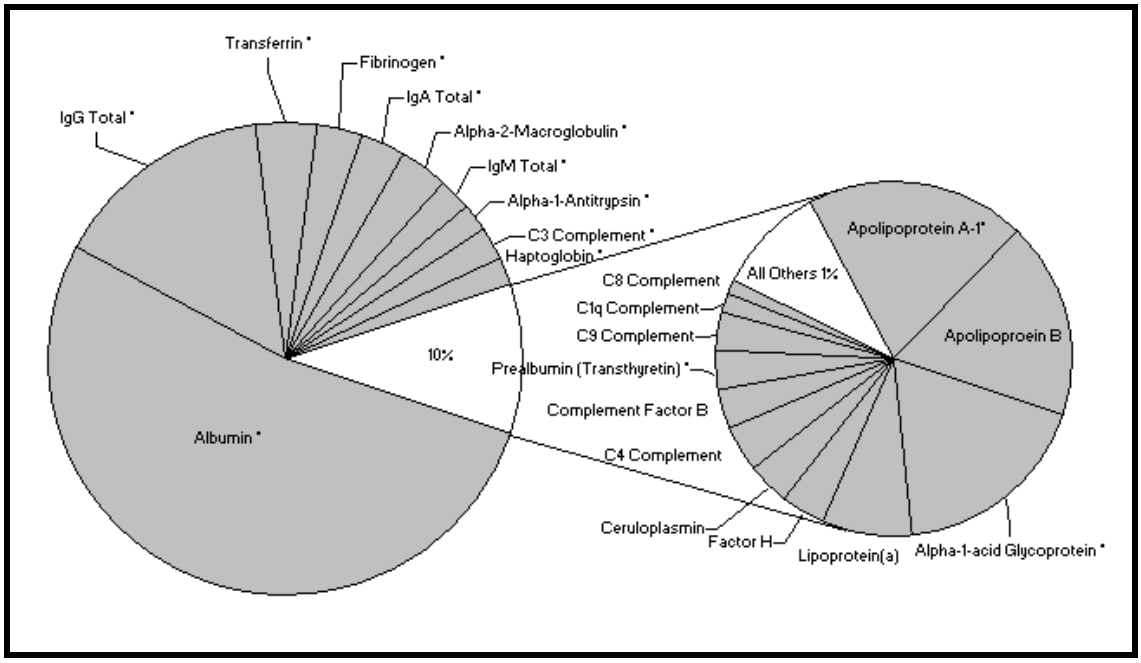

Figure 42 Pie charts representing percentages of total plasma protein mass of several individual abundant proteins. Proteins with asterisks are targeted for removal by the MARS 14 immunodepletion column. Apolipoprotein A-II is the only targeted protein not included in the figure. Modified from [192].

plasma proteins. 22 proteins make up roughly 99% of the total protein mass in serum [176, 192, 193]. In the case of plasma, fibrinogen has not been activated nor precipitated out of solution, so 23 proteins comprise a bit more than 99%. 13 of the 14 proteins removed by the immunodepletion column are shown and are marked with an asterisk. Apolipoprotein A-II is the only targeted protein not included in the figure. According to Agilent specifications, the proteins are reproducibly bound and removed from the "flow-through" with 97.5-99.9% efficiency, for up to 200 injections (Figure 43) [189]. The

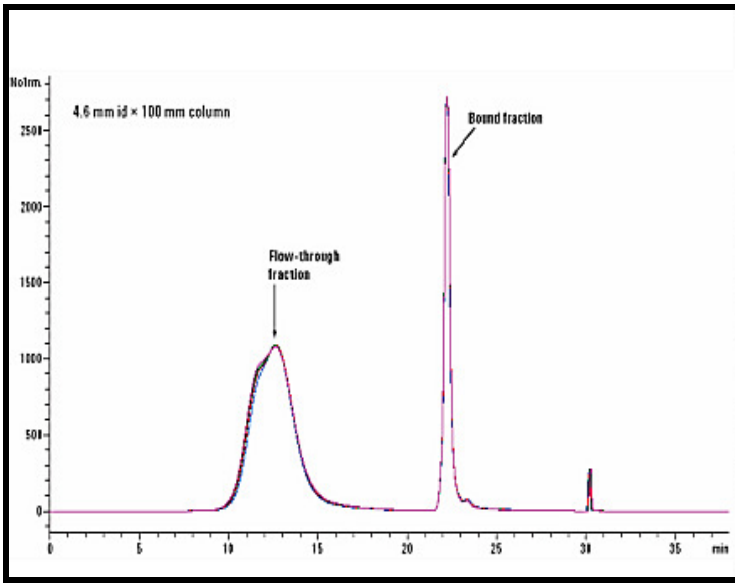

Table 1. Depletion Efficiency of High-Abundant Proteins from Human Serum and Human Plasma on the Human 14 Column

Sandwich ELISA immunoassays described in the Experimental section were used to measure the concentration of high-abundant proteins in flow-through fraction after 200 runs of immunodepletion.

Target protein	Depletion in serum (%)	Depletion in plasma (%)
Albumin	99.9	99.9
Haptoglobin	99.0	98.9
Transferrin	99.7	99.9
IgG	99.9	99.9
IgA	99.9	99.9
a1-Antitrypsin	99.7	99.5
a2-Macroglobulin	99.6	99.3
a1-Acid glycoprotein	99.0	99.0
Apolipoprotein AI	99.2	98.5
Apolipoprotein AII	98.0	98.0
Complement C3	99.0	99.0
IgM	99.7	99.5
Transthyretin	98.3	97.5
Fibrinogen	N/A	97.6

Figure 43 Agilent figures on the reproducibility and efficiency of removal for targeted proteins. The chromatogram shows different color trace overlays for the 1st, 50th, 100th, 150th and 200th runs. No information on the absorbance wavelength used for the Y-axis was given. The optical absorbance of the eluted bound fraction exceeds the dynamic range of the detection so the relative areas of the two peaks do not reflect the amount of protein depletion, from [189].

myriad of lower abundance proteins, comprising the remaining ~6% by mass are found in the flow-through fraction. These low abundance proteins were the proteins that went forward to RP fractionation to be used for the 2D gel experiments to be described.

While no differential proteomics reports, using the MARS-14 column, have been published to date, several groups have reported greater proteome coverage by removing HSA and other highly abundant proteins [179, 194]. Using coomassie staining of 2D gels, Pieper et al. found that, after the removal of 10 abundant proteins from human plasma, 650 protein spots were visible, compared to only 220 in unfractionated serum [195]. Using covalent labeling of proteins with fluorescent dyes on 2D gels, Chromy et al. were able to detect over 1500 spots after immunodepletion of human serum with a MARS-6 column, compared with only 850 from crude serum [196].

Although the quantitative benefits of plasma depletion are established, some groups have reported the non-specific binding of proteins and the removal of proteins associated with HSA, a known carrier of other proteins. In a mass spectrometry based experiment, Yocum et al. showed that more peptides of protein species that were not targeted by the immunodepletion could be detected in digests of undepleted serum than in MARS-6 depleted species [178], although the ion-suppression effects due to the presence of highly abundant species was not ruled out. Granger et al. showed that low abundance cytokines are non-specifically, and reproducibly removed from plasma, apparently by binding to the column matrix of a Montage albumin deplete kit (Millipore) [188]. However, this latter method used a blue dye hydrophobic affinity resin which is a different resin than is used in the MARS columns. Other studies have shown that HSA

is a specific carrier of many abundant, intact, high molecular weight proteins [197], forming a sub-proteome called the "albuminome" which would be expected to be removed with HSA, by HSA targeting methods.

In a side-by-side comparison of 2D gels of MARS-6 targeted proteins with methods that used combinations of dye-base HSA removal (Cibacron blue) with IgG removal (protein A and G), the MARS-6 system was shown to have the least non-specific proteins in the bound fraction gel [198]. Another study directly compared 8 depletion/enrichment strategies, including; N-linked glycopeptide enrichment, cysteinyl-peptide enrichment, 3 magnetic bead separations (Bruker ClinProt C3, C8 and weak cation exchange-WCX), size fractionation, MARS-6 column and protein A/G depletion in a bottom-up, tandem-MS, ion-trap analysis [199]. The authors claimed that the "MARS column depletion was unique among the methods tested in demonstrating comparatively high performance both in terms of proteome coverage and reproducibility". Figure 44 shows the comparison of the 8 methods and unfractionated

	cumulative peptide identifications			cumulative protein identifications[b]		cumulative protein identifications[c]		cumulative protein identifications[d]	
scheme	total	unique	unique to scheme	total	unique to scheme	total	unique to scheme	total	unique to scheme
Gly	10420	505	307	153	35	83	6	61	0
Cys	14807	478	57	135	26	64	1	45	2
C3	8439	968	25	157	12	88	0	76	0
C8	7800	716	17	140	13	72	0	60	0
WCX	15724	1328	145	203	29	110	2	93	2
Size	10269	625	90	130	23	73	4	52	2
A/G	4379	291	24	76	10	41	1	30	0
MARS	24283	1958	868	252	92	138	23	117	24
Unfract	8882	761	50	147	9	78	4	57	1

Figure 44 Comparison of 8 serum fractionation methods and unfractionated serum. The numbers indicate "high quality" peptides or proteins identified from 1 (b), 2 (c), or 3 (d) peptides, from [199].

serum, by their abilities to yield unique peptides. Going from left to right under the 4 groups labeled "cumulative…identifications"; the first group (3 columns) are "high confidence" peptides (PeptideProphet score > 0.95). The 2nd, 3rd and 4th groups are protein identifications using an increasing required number of peptides (1, 2 and 3 respectively) to identify proteins. In each case the MARS-6 method has the highest numbers, obtaining the highest unique number of proteins after sample processing. This bottom-up approach show significantly decreased sequence coverage for most of the 6 depleted proteins, including HSA, transferrin, antitrypsin and haptoglobin, which went from 12% to 0% sequence coverage after depletion. The specificity of the haptoglobin antibody for haptoglobin was shown by no diminishment of sequence coverage of haptoglobin-related protein after immunodepletion.

The fact that other species are partially co-depleted from plasma by binding to HSA is not necessarily a weakness of the method. The concentrations of the unbound fraction of these species may provide information on the changed binding character of HSA due to other factors. For example changes in fatty acid binding to HSA or changes in populations of other HSA binding protein species, such as acute phase proteins might change with health and disease. Nevertheless, the bound fraction of the MARS-14 column may show itself to be an interesting analyte and it was collected and stored at -80 C for future investigation.

RP-HPLC of Depleted Human Plasma

The first priority of the sample preparation after immunodepletion was the removal of ionic contaminants that would interfere with the iso-electric focusing step of the 2D-PAGE[5]. The flow-through proteins of the immunodepletion step are prepared in the very salty proprietary Agilent buffer A. We chose to follow the immunodepletion step with a reverse-phase step using a high protein recovery 4.6 mm X 50 mm macroporous C18 column (Agilent mRP-C18) operated at high-temperature (80° C),. This strategy has the advantage that it integrated the cleanup of the sample from the ionic interferences of buffer A and endogenous salts, with the added ability to subfractionate the proteins using a gradient of organic mobile phase. The Agilent mRP-C18 is marketed for use with depleted plasma proteins and has been shown to have high (> 99%) recovery and reproducibility [200, 201] when used under the recommended conditions of elevated temperature and with the recommended chemical additives (urea and acetic acid).

Figure 45 shows an overlay of the absorption and fluorescence traces of the effluent from 80° C mRP-C18 HPLC trace of the MARS-7 (Agilent, removes HSA, IgG, antitrypsin, IgA, transferrin, haptoglobin, fibrinogen) depleted plasma from our early pilot investigations. Samples were loaded n the RP column in 3 sequential injections to approach the capacity of the column. During the time between 0-12 minutes, 3 large flow-through peaks that saturated the diode-array detector (DAD) are seen in the black trace of the 210 nm ultraviolet (UV) signal. These peaks correspond to the flow-through species of the 3 sequential column loading injections of sample. In the first 2 peaks can

[5] The method development phase of this experiment owes a debt of gratitude to Mr. Navid Movahed who was particularly deeply involved in the RP-HPLC development.

be seen small sharp peaks on the right shoulders. These are due to artifactual drifting of the signal while the flow of the mobile phase through the column and detector is stopped during the loading of the injection loop for injection of the next portion of sample. Because the RP-HPLC column binds species based upon their hydrophobicity, the salts, urea, acetic acid and the water soluble small molecules of the plasma flow through without binding to the column. While these peaks strongly saturate the UV detector, there can also be seen some small fluorescent signal (red trace- 280 nm excitation/ 330 nm emission). A part of this signal is believed to be light-scatter into the 330 nm wavelength, but a bicinchoninic acid protein assay (Pierce, catalog # 23224/23221) was positive for proteinaceous material in these peaks. However, a one-dimensional gel that was stained with a sensitive fluorescent post-stain, Sypro Ruby (Bio-Rad), showed no protein bands. For this reason, it was decided that any peptide material that was in the peaks that caused the low fluorescence, was in low amounts and in primarily either amino acid form or from such small peptides as to be not separable in the 2D gel experiments.

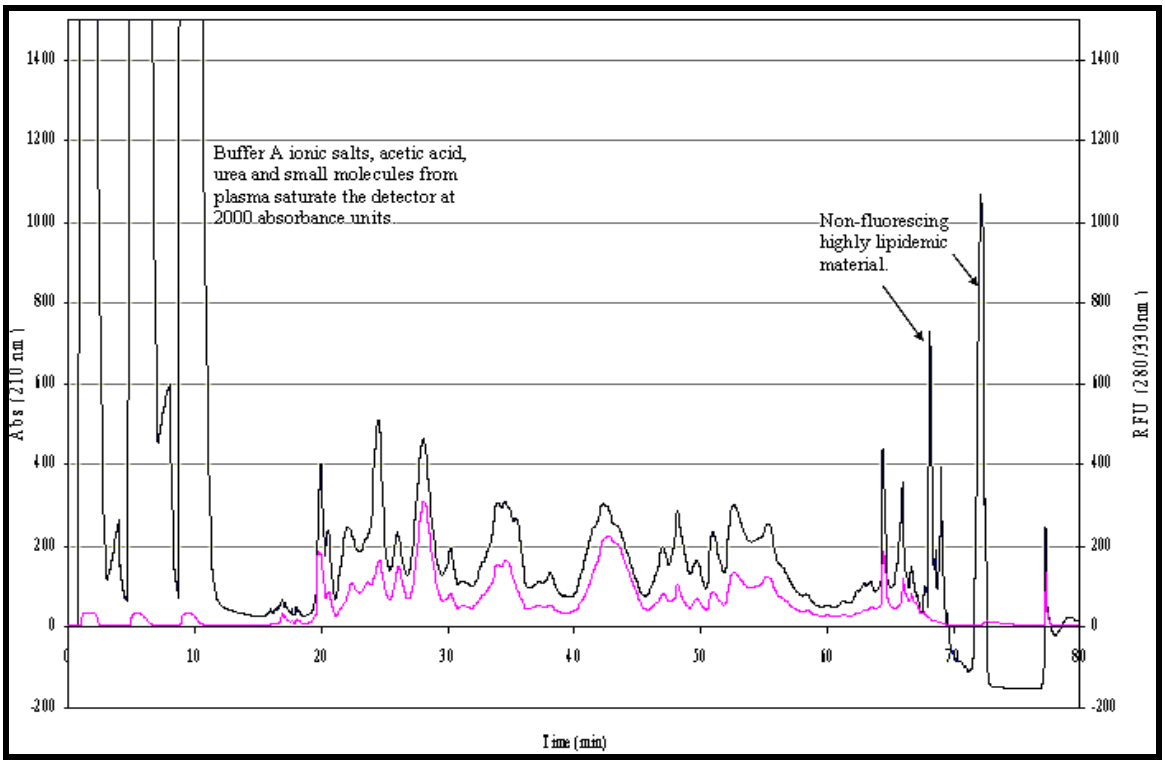

Figure 45 Comparison of the UV signal (210nm-black trace) and the fluorescent signal (280nm excitation/330nm emission) for a MARS-7 depleted plasma mRP C18 HPLC run at 80 C with three sequential sample column loading injections before elution with the solvent gradient.

On the other end of the trace of Figure 45, from approximately 67-73 minutes, there appear several large peaks in the UV trace that also have very little fluorescence. Because these peaks have such little fluorescence, relative to the UV signal, compared with the proteins throughout the midsection of the trace, and because they elute during the 95-100% organic phase, it is believed that they are composed of primarily highly lipemic material that might include carotenoids and some very hydrophobic lipoproteins. For this reason, proteins were collected only until the local minimum occurring just before the large UV peak at 73 minutes, to avoid the introduction of lipids to the sample.

Lipids can interfere with iso-electric focusing by consuming detergent [202]. The rehydration buffer used for the most hydrophobic fraction #6 was also modified to include an additional chaotrope, thiourea [202, 203], and a different, more powerful surfactant, ASB-14 [204]. ASB-14 is known to better solubilize more hydrophobic proteins or protein samples with high lipid content (see Materials and Methods-*Immobiline strip rehydration and cup-loading for iso-electric focusing*).

The RP-HPLC column was tested for carry-over of sample. The black trace of Figure 46 is a run on the column in which a MARS-7 immunodepleted plasma sample

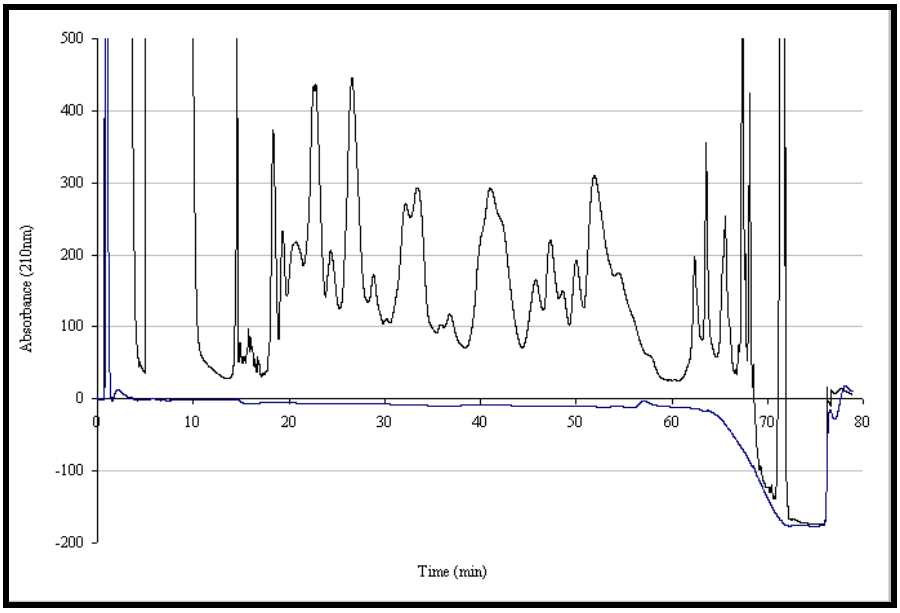

Figure 46 Two RP-HPLC runs (020407b and 020407c) showing a MARS-7 depleted plasma sample (black trace) and the blank injection that followed (blue trace).

was injected. The blue trace is the blank RP-HPLC run immediately following. Some very small carryover peaks are seen at 40 minutes and 58 minutes that amount to less than 1% of the area under the trace of the previous injection. The program that was used

for the experimental samples was lengthened to integrate a 12 ½ minute column cleaning step at the end of the run that swept once from 3%-100% mobile phase B (see Figure 59 in the Materials and Methods section of PROTEIN MARKERS OF T2DM IN HUMAN PLASMA). This was intended, not so much to prevent carryover, which seemed negligible, but to extend the reproducible lifetime of the column. The blue trace is largely the absorbance of the water/0.1% TFA which dips around 70 minutes as the mobile phase composition sharply climbs to 100% acetonitrile/0.08% TFA.

Figure 47 show a comparison of plasma protein gel images. In the top middle image is a gel with MARS-14 immunodepleted proteins that were desalted on the mRP-C18 column but were not subfractionated. Because of the high-dynamic range of the plasma proteins, there is a relatively low spot count, for 2D gels of 610 spots from the total depleted proteins. The 6 lower gel images show the spot patterns and raw spot counts from MARS-14 immunodepleted plasma samples that were mRP-C18 fractionated into 6 fractions, using the chromatographic cutoffs that were also used in the T2DM experiment (see Figure 60 in Materials and Methods of PROTEIN MARKERS OF T2DM IN HUMAN PLASMA). We estimated, from visually inspecting the patterns of abundant proteins that were shared between "neighboring" gels, with respect to the chromatogram, that 10% of proteins were shared and thus counted twice in these numbers. So, after summing the raw spot counts from the 6 fractions and multiplying the total by 0.9 to approximately account for doubly counted spots, the fractionation method is shown to yield approximately 3400 spots, or roughly a 5.5 fold increase in the spot count compared to the unfractionated samples. This indicated that the method of

fractionation is a promising way to increase the number of analytical spots and would increase the chance of finding a marker of T2DM.

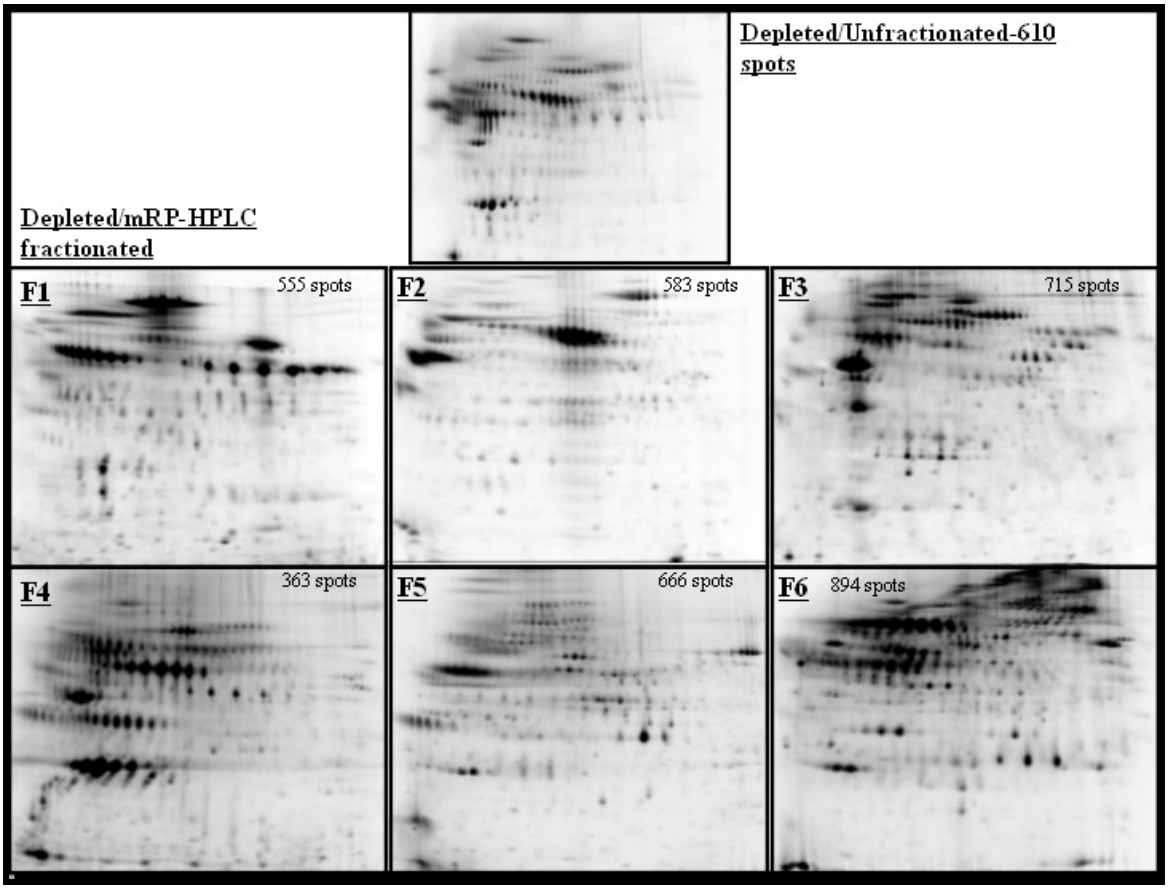

Figure 47 Comparison of immunodepleted plasma 2D gel spot counts before and after RP fractionation.

Two-Dimensional Gel Electrophoresis

In 1975, O'Farrell [205] showed the power of combining two protein separation technologies, creating two-dimensional gel electrophoresis (2DGE). Today, 2DGE is an established technology that is used to separate and quantify the intact proteins of complex biological samples. It couples a first-dimensional protein separation that exploits the protein's charge carrying character (isoelectric focusing-IEF) with a second-dimensional

separation by sodium dodecyl polyacrylamide gel-electrophoresis (SDS-PAGE), a mobility dependent separation that correlates well with the protein's molecular weight (MW). The relative, MW-dependent position of a protein after SDS-PAGE is known either as its "apparent MW", and it is expressed in kilodaltons (kDa), or it is expressed as relative mobility (M_r), which is a unitless measure of apparent MW, in which the kDa unit is implied.

Of great practical importance to the science of 2D gels was the introduction of "immobilines" by Bjellqvist et al. [206] in 1982. Immobilines are acrylamide derivatives of weak acids and bases that are covalently incorporated into the acrylamide gel of the 1st dimension to create an immobilized pH gradient (IPG). This innovation overcame early difficulties with gradient drift, allowed more robustness to the presence of ionic contaminants [206], allowed the advent of narrow range IPG strips [207] and is used today in all of the commercial IPG strips.

2DGE's definitive strength results from the ability of IEF to separate intact proteins and to resolve many biologically important post-translational modifications that affect the charge state of the protein, such as phosphorylation or deamidation. This separation is known as isoform resolution. For example, in the case of deamidation the net change of the molecular weight of the protein is 1 Da [208], not enough mass difference to detect as a change in the second dimension SDS-PAGE. However, as is seen in blood proteins, which are believed to have wide-spread deamidation [208], the loss of one charge is typically a large enough change in the total charge of the protein, relative to the pH gradient of the first-dimension, to resolve a new spot in the horizontal

dimension. Each deamidation adds a net negative charge unit, creating a discrete shift [209] in the protein's final focused position or isoelectric point (pI), toward the positively charged electrode (anode). A series of spots that appears to be modifications of a single protein is called a "horizontal spot train".

Because 2DGE is not inherently selective with respect to the proteins that are analyzed, it is called a "global" expression technology. This is in contrast to "targeted" technologies such as antibody based assays. The use of the word "global" shouldn't be interpreted to mean "universal" however, because of the known biases of the gel-based platform for abundant proteins, proteins of molecular weight between about 10 kDa and 200 kDa, non-basic proteins and non-hydrophobic proteins [210].

Successful 2DGE is a largely sample dependent endeavor. Many options are available to optimize the two-dimensional space of the gel to improve the resolution for the individual protein species of a particular sample. These options are summarized in Angelika Gorg's "The Current State of Two-Dimensional Electrophoresis with Immobilized pH Gradients" [207, 211]. Briefly, one can target protein pI ranges by selecting commercial IEF strips with narrow range (1 pH unit), medium range (3-4 pH units) or broad range (7-8 pH units). Also for the first dimension, a variety of commercial non-linear or linear gradients in IEF strips of 7 cm, 18 cm or 24 cm lengths can be used, increasing the resolution of spots with longer strips. For the second-dimension, one should determine whether the resolution of a sample is high enough in a uniform composition of acrylamide, which, all other factors the same, will provide the lowest variability between sets of gels. Or, if a uniform gel composition shows a

congestion of high MW proteins, it may be desirable to increase the resolution of the higher MW proteins, at the expense of lower MW proteins, with a top-to-bottom gradient of acrylamide, say 9-16%, which will have a greater relative slowing effect on the migration of low MW species. This was the rationale behind our choice to use a 9-16% gradient gel for our experiments, as plasma contains many high MW proteins.

Several methods are in general use to apply the sample/rehydration buffer to the IEF strips, such as: passive or active (under electrical potential) rehydration, cup-loading, and wick-loading. Cup-loading has been shown to be superior to active rehydration for increasing the entry of high MW proteins [202], such as are found in plasma, into the gel matrix, so we adopted this method.

One can also select different rehydration buffer compositions with respect to their denaturant/chaotrope and detergents. This choice depends on whether it is desirable to denature ionic complexes of proteins, or on the solubility that is required to match a particular sample's hydrophobic nature.

In our experiment, for HPLC fractions #1-#5, a standard rehydration buffer for soluble proteins was used, including: water, 8 M urea, 4% CHAPs zwitterionic detergent, and 1% ampholines (pH 3-11). For HPLC fraction #6, a standard rehydration buffer recommended for lipemic and hydrophobic proteins was used, including 7 M urea, 2 M thiourea, 2% ASB-14 zwitterionic detergent and 1% ampholines (pH 3-11). While the 2 M addition of thiourea has been shown to enhance solubility for hydrophobic proteins, this enhancement can't be extended by its inclusion in the equilibration buffer, as it

scavenges the alkylating agent, IAA, and is thought to interfere with the saturation of proteins by SDS [212], causing streaking [213].

For the first-dimensional separation, since there was no desire to target a smaller pI range in the planned experiments, we chose to use the broadest commercially available IEF strip of pH range 3-11. Focusing of proteins in the far basic region of 3-11 strips can be problematic, since mixed disulfides can form between various protein species at pH near and above the pI of the cysteine side chain, pH ~ 8.3, and causing streaks and perhaps artifactually higher numbers of spots [214]. Commonly used reducing agents, dithiothreitol (DTT) and dithioerythritol (DTE) are typically used in excess, but because they are weak acids, the charged species migrate out of the pH gradient and become depleted at pH greater than 7 [204]. Thus, in this already denaturing condition, the inclusion of DTT or DTE may actually promote, or at least not prevent the formation of mixed disulfides in this pH range.

One strategy that is used to reduce basic-region streaking, by preventing the formation of a heterogeneous population of disulphides, is the addition of excess species of a small, uncharged organic disulphide that is symmetrical around the disulphide bond. One such species is hydroxyethyl disulfide (HED, Destreak™-GE Healthcare). When HED is added in excess, the exposed, free thiols of the denatured proteins are oxidized to mixed disulfides with half of the HED instead of with other proteins, effectively preventing the formation of protein-protein mixed disulfides. With excess HED, the equation:

Equation 1 $Prot\text{-}S^- + HO\text{-}CH^2\text{-}CH^2\text{-}S\text{-}S\text{-}CH^2\text{-}CH^2\text{-}OH \Longleftrightarrow Prot\text{-}S\text{-}S\text{-}CH^2\text{-}CH^2\text{-}OH + HO\text{-}CH^2\text{-}CH^2\text{-}S^-$

is pushed to the right [215] of the equilibrium. We found that the combination of cathodic cup-loading of the sample and the inclusion of HED [202] in the rehydration buffer, gave good resolution of proteins in the far basic region and across the entire range of the strip, eliminating problems with resolution on the basic end.

The inclusion of HED in the first dimension obviated the necessity for the reduction and alkylation prior to IEF and, therefore, the reduction was done afterward, "between dimensions", in the equilibration step. The equilibration buffer that was used for all six fractions was a standard buffer recommended by Gorg [216], modified to include 4% SDS, instead of 2% SDS. The recipe was 6M urea, 4% SDS, 30% glycerol, and 50 mM Tris-HCl pH=8.8, with 1% DTT added in the first equilibration, and 2.5 % IAA added in the second equilibration. The equilibration steps wash out the CHAPS detergent and equilibrate in the SDS detergent. In the case of fraction #6 they also wash out the thiourea, before equilibrating with IAA, which is then in approximately 10-fold excess. Detailed protocols for all experimental steps are in the Materials and Methods section of the chapter PROTEIN MARKERS OF T2DM IN HUMAN PLASMA.

After running the 2nd dimension, our method included a 5 hour fixation of the gels to remove an artifact of the ZBB dye, which was used to label internal standard samples. All of the dyes in the 2D gel experiment used the lysine reactive N-hydroxysuccinimidyl ester (NHS-ester) chemistry to covalently derivatize the proteins with their fluorescent

moiety. This particular dye, ZBB, was found to leave a large fluorescent "blob" in the midsection of the gels before fixation. In Figure 48, the artifact is clearly visible in the

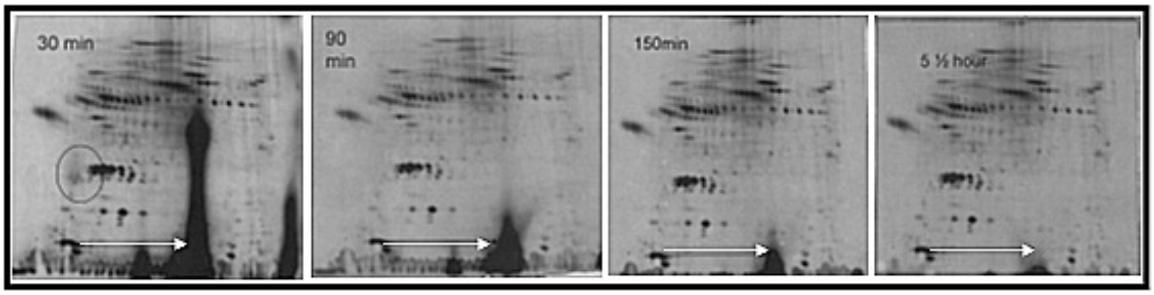

Figure 48 The "blue blob" artifact of ZBB. Cathodically cup-loaded ZBB labeled plasma proteins showing the time course of the artifact's removal with fixation. From left to right: 30 minutes, 90 minutes, 150 minutes and 5 ½ hours of fixation. It was essentially removed from the experimental gels by 5 hour fixation.

"30 min" image on the far left, as the large dark vertical streak. This artifact has been shown to result from this dye's relatively hydrophilic structure. (See Zdye structures in Figure 52 of the chapter SPECTRALLY RESOLVED FLUORESCENT DYES FOR PROTEOMICS. The portion of the dye which results from hydrolysis, without reacting with proteins (free carboxylic acid) focuses to a position at about pH 7 on the IPG strip, corresponding with the position of the streak on the gel. A percentage of all NHS-ester dyes will hydrolyze to the free carboxylic acid without derivatizing a protein, and the fluorescent piece will focus to its specific pI. The other fluorescent Zdyes that were utilized partitioned into the SDS micelles and effectively migrated off the gels by electrophoresis. But because ZBB has a less hydrophobic structure than the other dyes, it is believed that its free acid incorporates to a lesser degree within the micellar SDS, during the second dimension separation. Therefore ZBB fails to migrate off the gel effectively, as one would predict for a small peptide and is found for the other more

hydrophobic Zdyes. In a later generation of this Zdye, (see Figure 57, ZBB dipropyl NHS-ester of the chapter SPECTRALLY RESOLVED FLUORESCENT DYES FOR PROTEOMICS) the two methyl groups on the conjugated fluorophore structure were replaced with more hydrophobic propyl groups, and the artifact was ameliorated, obviating the need for fixation before fluorescence scanning.

After the completion of over half of the gels for this experiment it became clear that the red dye was not producing consistent data. In Figure 49 is an illustration of the justification for the rejection of all the HBO-187 data from the final analysis. In Figure 49A are the densitometric images from the Progenesis spot matching software for a

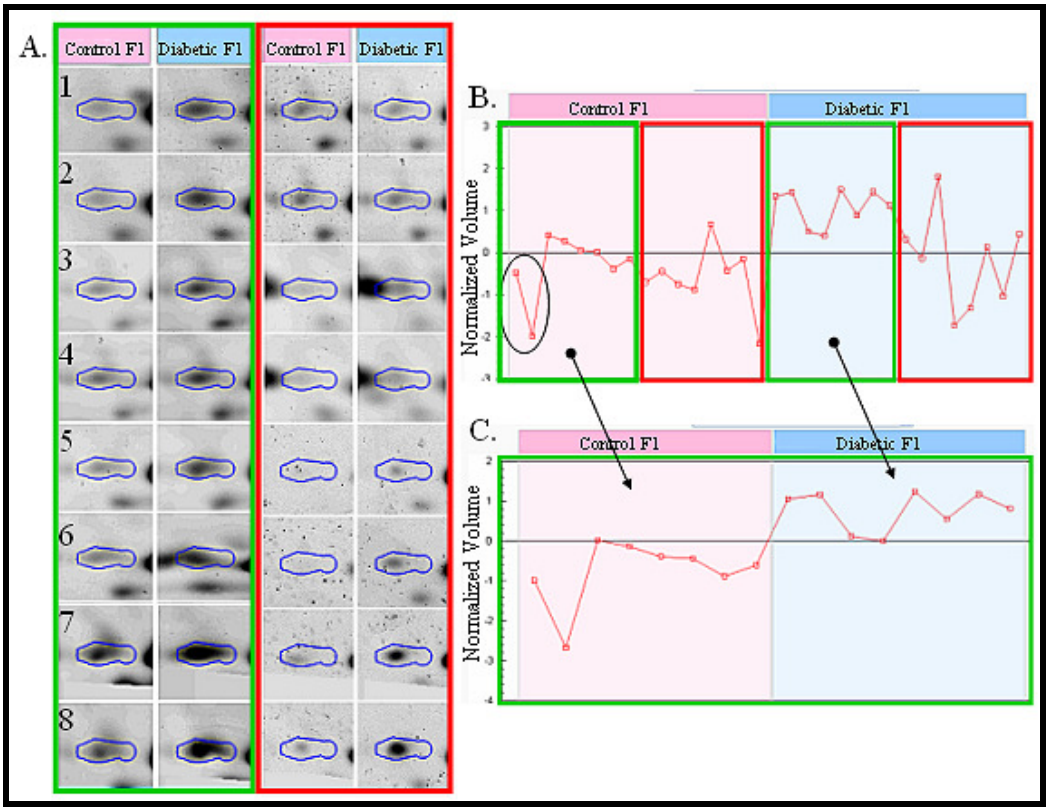

Figure 49 Justification for rejecting the red data set.

protein spot identified as serum amyloid A in fraction 1 (F1). (See Results and Discussion in PROTEIN MARKERS OF T2DM IN HUMAN PLASMA). The images produced using the green dye, ZGB, are outlined with a green border and the images from red dye, HBO-187, are outlined with a red border. The non-diabetic sample images are shown under pink heading and the T2DM sample images are shown under the blue headings. In several of the images from HBO-187 a high amount of artifactual noise can be seen in both the control and diabetic images, appearing as dark speckles around the protein spot. The Progenesis spot quantitation software attempts to identify these "spikes" in intensity and subtract their intensity from the final quantitation, but for low intensity spots, this is apparently not completely effective. In Figure 49B is a graphical representation of the quantified normalized spot intensities for the complete data set in Figure 49A, including the data from the red dye. The intensities from the ZGB images are enclosed in a green border and the intensities from HBO-187 are enclosed in a red border. Going across from left to right, the technical replicates are paired. The first technical replicate pair of spots is in the oval enclosure. The problem can be clearly seen in the red data where the pair-wise matched intensities are much less similar, compared to the pairs of the green data spots, giving the graphical representation of the red data a much sharper saw-tooth character than the green data. In other words, the jumps in intensity between paired members of technical replicates are much larger in the red data than the green data. This, as well as the artifactual speckling, was seen in many spots. In Figure 49C is the same kind of representation of the data, using only the spot intensities given by ZGB. The members of the technical pairs are consistently much better matched

in intensity. In light of these observations, it was decided that the experiment would be likely to yield more "true positive" results if the HBO-187 data set was omitted from the final analysis.

Mass Spectrometric Identification of Proteins

To identify proteins-of-interest (POI) from the 2DGE experiment, the spots were picked from the gels and trypsin digested. The digested polypeptides were extracted from the gels and either analyzed by matrix-assisted laser desorption ionization mass spectrometry time-of-flight (MALDI-TOF, Bruker Biflex) or liquid chromatographic tandem mass spectrometry (Agilent Technologies 6340 LC/MS/MS ion trap) using nano-chip (Agilent Technologies 40nL trap 75µm x 43 mm 5µm C-18SB-ZX, catalog #G4240-62001) LC and alternating between collision induced dissociation (CID) and electron transfer dissociation (ETD) ionization.

MALDI-TOF uses the assistance of an acidic crystal matrix that must be a good solvent for the analyte, to promote co-crystallization of it with the matrix, and a good absorber of the light energy from the MS laser to desorb the incorporated peptides [217]. The choice of matrix is largely empirical but ACHA is a widely used matrix for peptides and proteins [218]. The process of MALDI desorption and ionization of the peptides has been well summarized by Knochenmuss and Zenobi [219].

In MALDI-TOF, the positively charged gas-phase peptide ions with mass (m) and charge number (z) are extracted in a pulsed electric vector field (E) and experience an accelerating vector potential (V) that will give the ions energy = ezV. This energy is

equal to the kinetic energy $1/2mv^2$. Assuming that all the accelerated ions attain the same kinetic energy and converting v to L/t, where L is the length of the flight chamber and t is flight time, then for all ions $m/z= [2eVt^2]/L^2$ [220]. In the general case, the equation for m/z can be collapsed to an expression with a linear term and a squared term involving t, or $m/z = B(t-A)^2$, where A and B are calibration constants determined by the measurement of ionic species with known m/z . The mass spectrometer measures the time between the initiation of the electric field pulse and the detection of ionic species, and converts the time to m/z using this relation.

Internal calibrations of the peptides in the digests utilized the known m/z of several prominent auto-digestion peptides of the methylated porcine trypsin used for the digestions [221], whenever possible. If enough high-quality internal standard peaks were not present in a particular spectrum, external mass calibration, using a prepared peptide mixture on a separate spot on the MALDI sample plate, was used. The specifics of sample preparation and MALDI measurement parameters are given in the Materials and Methods section.

The LC/MS/MS used in this experiment was an Agilent 6340 XCT Ultra ion trap with chip LC nano electrospray ionization (nESI) [222]. In this method, the digested peptide sample is withdrawn from a sample vial and loaded onto the C18 RP column of the chip LC “nanochip” by the autoinjector. Using MS-compatible solvents for the RP gradient (see Materials and Methods), the peptides elute from the column in turn, according to their hydrophobic character. A nebulizing needle continuously injects the peptide solution into the mass spectrometer, at atmospheric pressure, under high electric

potential between the needle and the mass spectrometer. Hot nitrogen gas facilitates the evaporation of the solvent droplets, leaving the total charge of each shrinking droplet conserved while loading the charges onto the peptides as the droplet size diminishes. Electrostatic repulsion between the droplets causes the formation of a "Taylor cone" and eventually electrostatic repulsion of the peptides within each evaporating droplet generates enough force between the peptides to overcome the surface tension of the droplets. This is believed to create a "fission" event leaving single ions in nanometer sized droplets [223] and ultimately desolvated molecules in the gas phase of the mass spectrometer.

Under electrostatic force, the ions leave the nebulizing chamber and enter the "ion optics" comprising voltage gates, octopoles, lenses, and skimmers, which are used to select the range of m/z for introduction to the ion trap, and move the ions into lower pressure necessary for the function of the ion trap. Once in the ion trap, the peptide ions experience an oscillating electric field of radio frequency (RF) and a superimposed potential between the electrodes, which constrain the ions in stable trajectories near the center of the trap. In an ideal ion trap the motions of the ions in the radial and axial directions are independent. The important outcome of this independence is the ion trap's ability to perform "resonant ejection" of selected ranges of m/z values [220]. By scanning through a range of voltages, the trajectories of a range of m/z values can be sequentially destabilized and ejected from the trap to the detector. The voltage that destabilizes an ionic species can be used to determine its m/z through calibration. This gives the m/z of the peptides in their digested forms, referred to as the "MS" of the ions.

For amino-acid sequence information of the peptides, the trap can be used to select ions, usually those that meet pre-set priorities, such as a threshold of intensity, for further analysis. If a peptide meets the criteria, all other species can be selectively destabilized and scanned out of the trap. The remaining peptide, now of known m/z, can be targeted for high-energy collision induced dissociation (CID) while being excited by a supplementary RF voltage. The energized ions collide with helium atoms in the trap and dissociate into a statistical distribution of daughter ions. The "MS/MS" fragments that result from CID are cleared from the trap by a voltage scan and detected just as the ions were in the "MS" scan.

The Agilent 6340 can also use electron transfer dissociation (ETD) to gain increased sequence coverage of the peptides. The method of the present experiment analyzed the daughter ions by alternating between CID and ETD to seek complementary sequence information. CID works in positive ion mode since the daughter ions are fragments of the positive precursor ions. In ETD, when a precursor ion has been selected, as before in positive ion mode, negatively charged fluoranthene ions enter the trap, transfer electrons to the positively charged peptides and destabilize them, causing their dissociation [224]. Because ETD is reducing the net charge of the precursor ion, it requires highly positively charged ions to yield positive ion fragments.

The dissociated peptides in MS/MS provide sequence information by yielding a distribution of daughter ions that can be analyzed for the loss of masses which correlate to the losses of known species such as amino acids, water, ammonia or post-translational modifications. The typical CID dissociation breaks the peptide backbone at the peptide

bond, between the nitrogen and the carbon of the carbonyl group. In Figure 50 this is represented by the blue lines. A fragment can only be detected if at least one charge localizes to the fragment. If the charge localizes to the N-terminal fragment, then the detected species is known as a b-ion. If the charge localizes to the C-terminal it is known as a y-ion. ETD tends to dissociate peptides between nitrogen and the α-carbon. In Figure 50, this is represented by the orange lines. In this case, if the charge localizes to the N-terminal fragment, then the detected species is known as a c-ion. If the charge localizes to the C-terminal it is known as a z-ion.

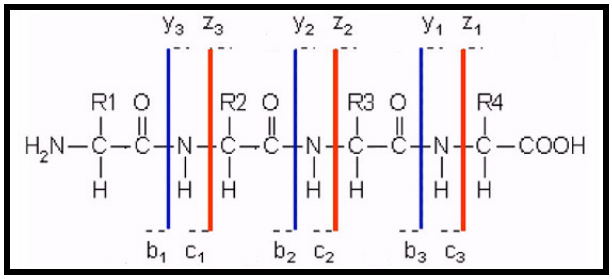

Figure 50 The peptide backbone fragmentations that cause b and y ions of CID (blue) and the c and z ions of ETD (orange).

In Figure 50 is an example of the MEWNKEAAANAQK tryptic peptide from a in-gel digest of a spot identified as cysteine-rich glycoprotein-3 (CRISP-3, see Results and Discussion of PROTEIN MARKERS OF T2DM IN HUMAN PLASMA). The top spectrum is the CID MS/MS with the b-ions represented in blue and the y-ions in orange. The position of the parent ion at ~497 m/z (z = +3) is marked with a red dot on the m/z scale and is not represented by a peak in the spectrum because it has undergone targeted fragmentation. A relative dearth of any peaks around 497 m/z indicates the m/z values within in the targeted CID range. The bottom figure is the ETD spectrum of the same

peptide with the c-ions in blue and the z-ions in orange. In this case the precursor m/z has not been fully fragmented, is still present in several charge states and is represented in green. In addition to the singly and doubly charged ions, note the presence of peaks representing m/z of water and ammonia losses. In this case, the ETD spectrum was unusual among the spectra of this experiment in that it provided greater coverage, 23 out of 25 possible ions, than the CID spectrum which yielded 21 out of 25 ions.

As can be verified in the APPENDIX A: Supplementary Figures section, the identification scores of several proteins were strengthened by ETD sequence data.

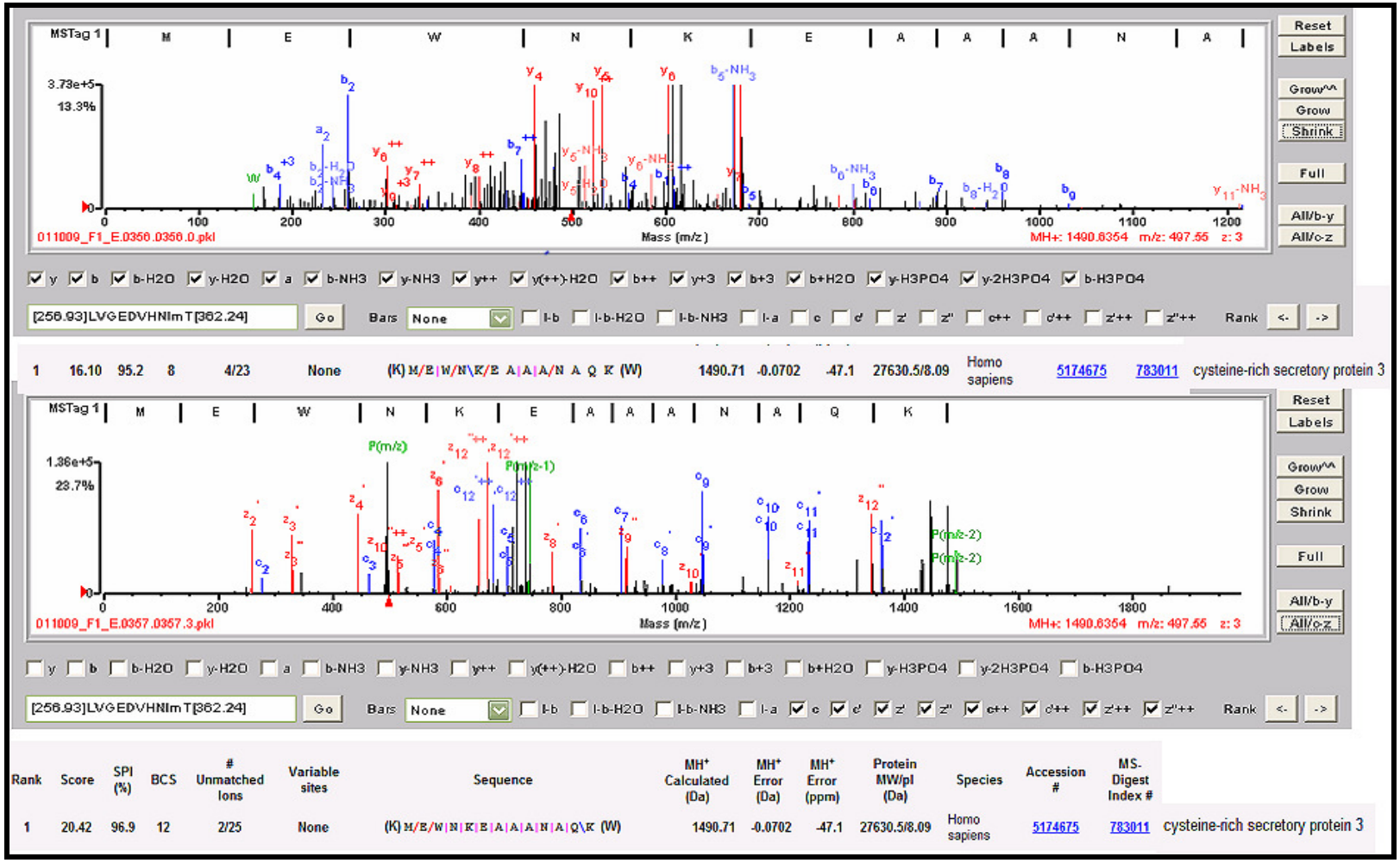

Figure 51 Comparison of CID (top) and ETD (bottom) fragment ions spectra for a CRISP-3 peptide.

SPECTRALLY RESOLVED FLUORESCENT DYES FOR PROTEOMICS

Introduction

Figure 52 shows the 3 NHS-ester dyes that were used in these 2 DGE experiments. They were designed by Dr. Dratz and Dr. Grieco and synthesized by the laboratory of Dr. Grieco at MSU Department of Chemistry and Biochemistry to meet

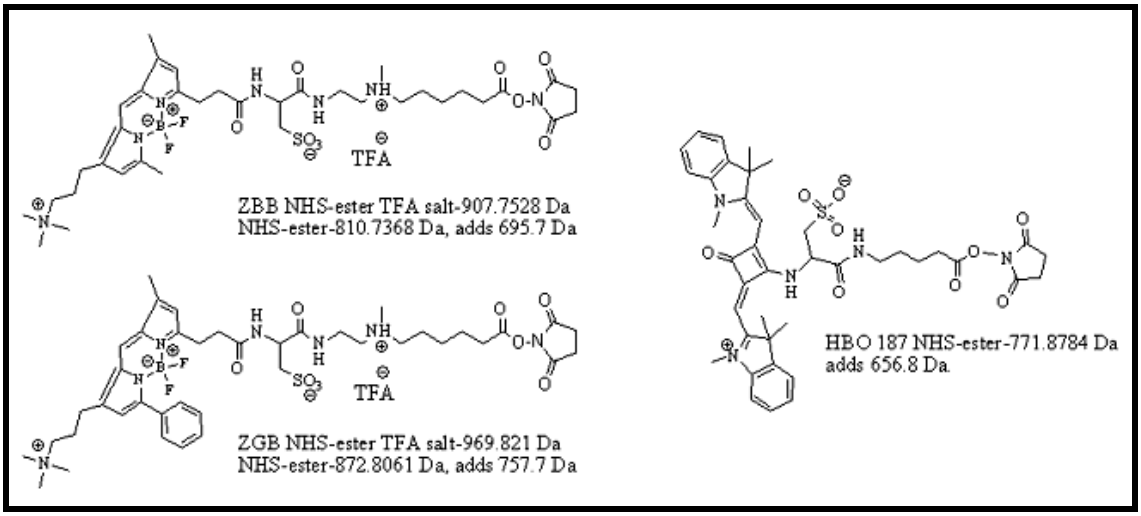

Figure 52 The 3 spectrally resolved Zdyes used in the 2D gels of this experiment.

required specifications of charge, excitation/emission wavelengths, stability, solubility and reactive chemistry.

The spectral characters of the fluorescent dyes owe their properties primarily to the heterocyclic aromatic structures in each. The two "Zxx" named molecules have an aromatic, boro-fluoridate known as the "Bodipy" core. The HBO-187 dye was synthesized with a "squarene" center conjugated with two indole groups. Initial trials of a red boro-fluoridate dye found that it was reductively unstable, and therefore, unsuitable

for 2DGE. The HBO-187 dye, while having a quantum yield that was considerably lower than the other two Zdyes, was shown to be stable and that dye-labeled proteins nearly co-migrated with the boro-fluoridate labeled proteins, so these Zdyes were adopted for experimental use. These are version 2.0 Zdyes that were the best available when these experiments were begun and so we used them throughout. When improved Zdyes were developed we had proceeded too far with the experiments to go back and repeat the experiments with the newer Zdyes, and we also had limited plasma to work with. All three of these Zdyes have been replaced in V 3.0 and V 4.0. For example, the current Zdyes no longer require fixation before scanning, leading to stronger fluorescent signals. The red Zdye in particular has undergone the most changes and improvements, and the current green Zdye has stronger signals when attached to the most basic proteins.

With respect to the spectral character, candidate dyes were required to have excitation and emission wavelengths that were well-separated on the color spectrum so that, with the available laser excitations (at 488nm, 532nm and 633nm) and choice of emission filters, they could be excited and detected independently of one another (spectral resolution). If spectrally resolved, dyes can be used to label different samples, mixed and applied to a single gel, effectively eliminating the variation that is introduced by using multiple gels, as well as the work and use of resources to create them. This method was introduced in 1997 by Unlu et al. [225] and is commonly referred to as two-dimensional difference gel electrophoresis “2D DIGE”, discriminating it from 2DGE. Labeling of multiple samples with spectrally resolved dyes for use on a single gel is referred to as “multiplexing”.

Published 2DGE protocols are in wide use that react 50 µg of protein with 400 pmoles of NHS-ester fluorescent dyes in 10 µL, pH ~ 8.0 reactions on ice for 30 minutes. To "quench" the labeling reaction after 30 minutes, the protocol calls for the addition of 1µL of 10 mM lysine to react with unreacted NHS-ester dye, before mixing the differently colored reactions [226]. This prevents the cross-labeling of samples with the "wrong" dye. Our protocol used from 2 to 5-fold higher concentrations of dye to increase the signal of lower abundance proteins (Table 9). Chromatographic experiments were

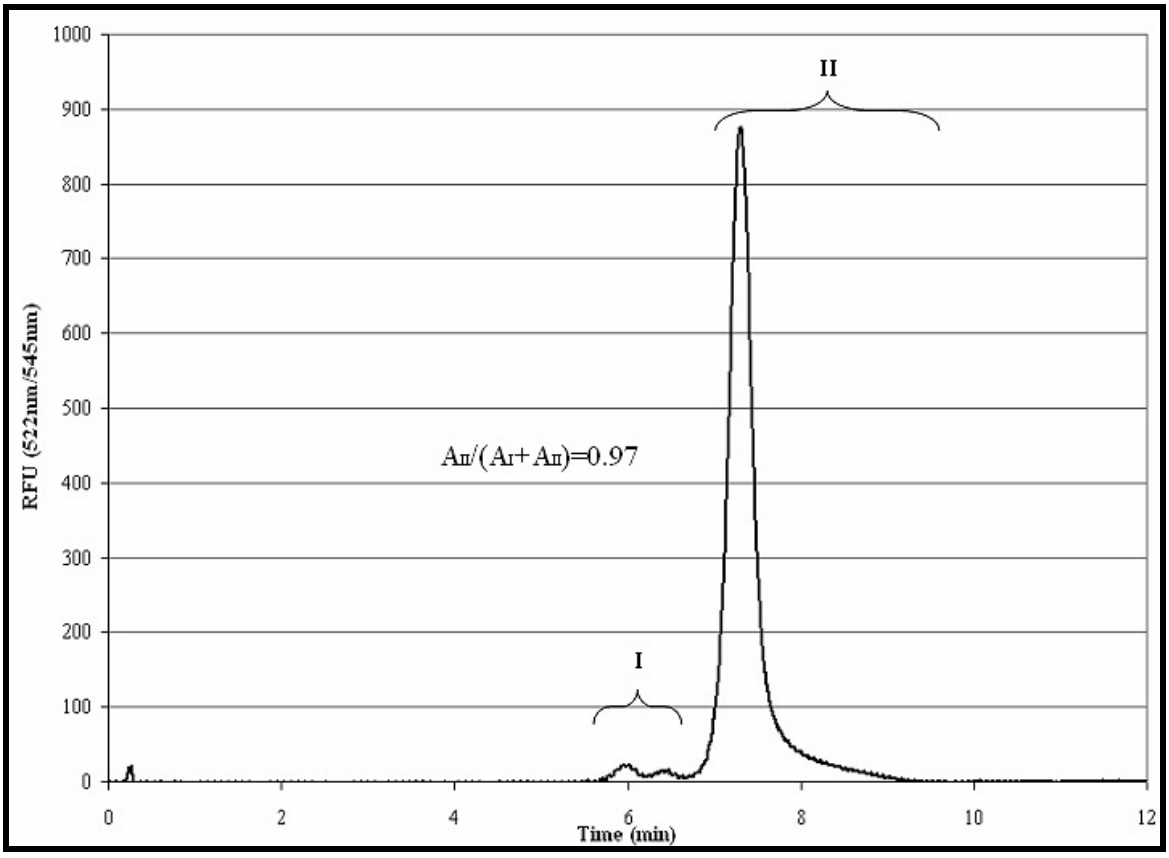

Figure 53 Fluorescence chromatogram of ZGB dye. Using a Waters Atlantis dC16 RP 4.6 X 150 mm 5u column, 0.6 mL/min flowrate, 35% mobile phase B isocratic. A= 0.1% TFA in H_20, B= 0.08% TFA in ACN.

conducted to show that the NHS-ester dye (ZGB) was being effectively quenched by lysine. Figure 53 is a RP fluorescence chromatogram (Ex=522 nm/Em=545) of ZGB. This ZGB dye had been dissolved as a stock solution in DMF and stored at -80 C for over 30 days and removed for use several times. Before loading onto the injection loop the dye was added to 25% mobile phase B. In this acidic solution the dye is stable and hydrolysis was retarded. Figure 53 shows a large peak, "II", at ~7.5 minutes, which is the intact active dye, and two smaller peaks, "I", representing the hydrolyzed NHS-ester (free carboxylic acid) and an unknown fluorescent species. After integrating the areas beneath the curves, for both I and II, the proportion of the intact dye, II, to the total, I + II, was found to be 0.97 for this vial of dye.

This quantitation method was used to monitor the kinetics of dye reactivity under 2 temperature conditions; on ice and at RT, and 2 reactive conditions; with lysine quenching and without lysine quenching. For these reactivity experiments 30 mM bicine buffer, pH=8.4 was used. If the bicine buffered reaction was to be at RT, the pH of the buffer was adjusted at RT. If the bicine buffered reaction was to be on ice, the pH of the buffer was adjusted on ice. For the unquenched experiments, no lysine was added and so

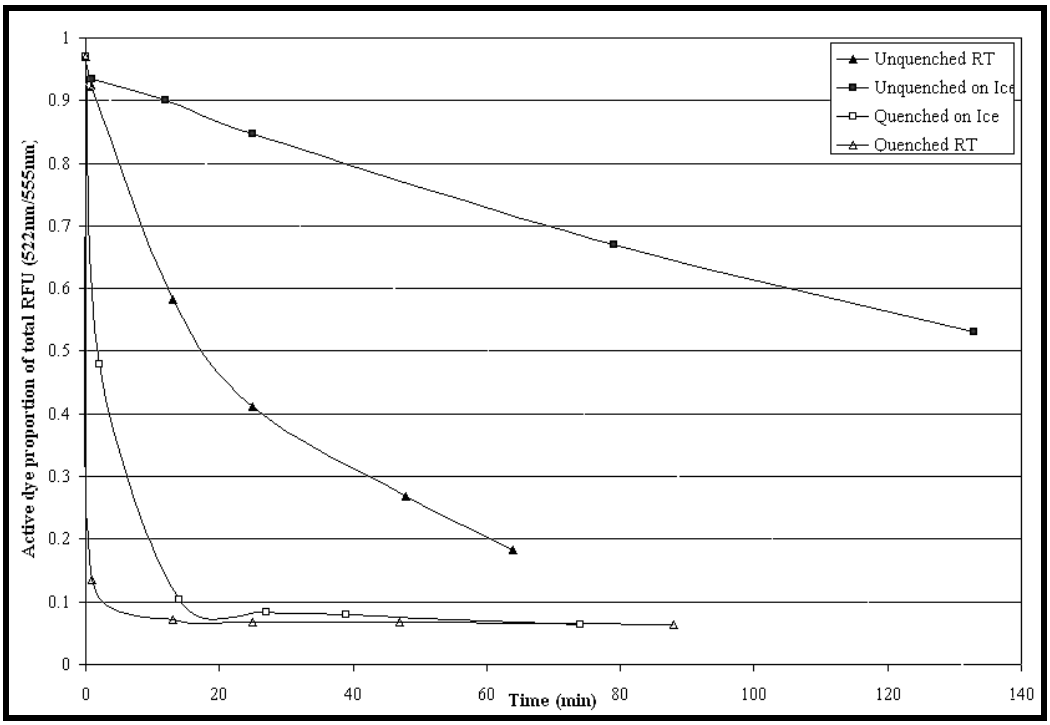

Figure 54 Time courses of active ZGB NHS-ester under different conditions of temperature and lysine quenching.

hydrolysis of the dye to the free carboxylic acid was the main reaction. Figure 54 shows the normalized kinetic data for the unquenched (hydrolysis) of ZGB, on ice (closed squares) and at RT (closed triangles). Also shown are lysine quenching reaction data in which dye (1.2 nmoles) and lysine (20 nmoles) were combined in a 10 µL reaction. This reaction used approximately a 3-fold increase of dye and a 2-fold increase of lysine over the widely used protocol [226], although here it was without any prior dye-protein reaction, which is commonly done with 50 µg of protein for 30 minutes. These experiments were also done on ice (open squares) and at RT (open triangles). The traces in Figure 54 clearly show the effectiveness of lysine quenching. The half-life of the active dye, on ice, without quenching is ~3 hours, whereas with quenching it is ~2

minutes. At RT, without quenching, the half-life of active dye is ~20 minutes, whereas with quenching it is on the order of a few seconds. This experiment showed that a 3 fold increase of dye could be effectively quenched with a concomitant fold increase in lysine. In order to assure effective quenching of the additional dye, either 1 µL of 30 mM lysine or 1 µL of 50 mM lysine was added, according to the concentration of fluorescent dye that was used (Table 9).

Spectral Character of Dyes

In Figure 55 is the normalized absorbance in EtOH (thin traces) and emission (thick traces) spectra of the 3 protein labeling Zdyes utilized. The blue spectra are for ZBB. The green spectra are for ZGB. The red spectra are for HBO-187. The vertical

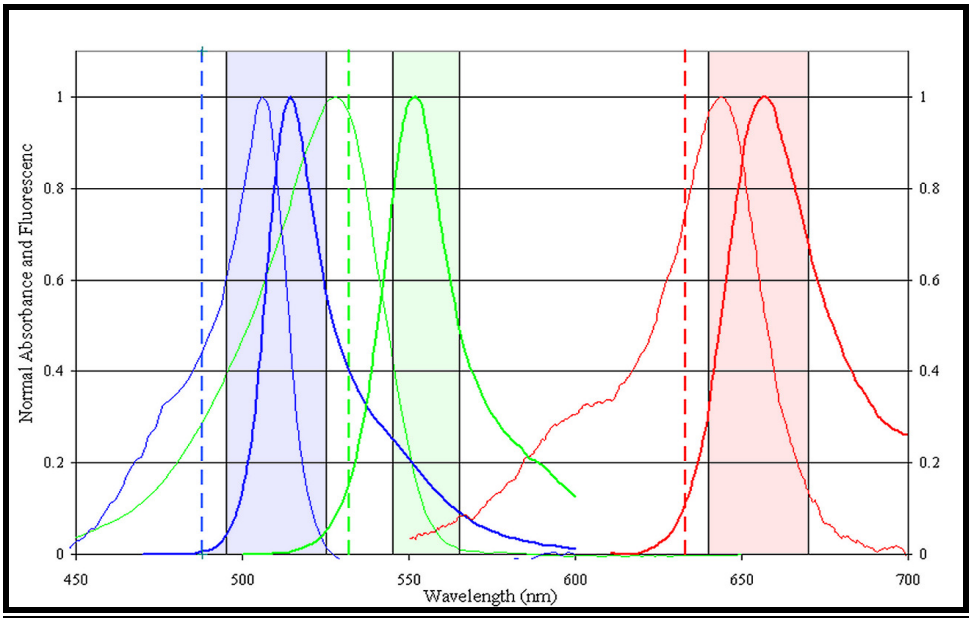

Figure 55 The normalized EtOH absorbance (thin traces) and emission (thick traces) spectra of the 3 protein labeling dyes. The dashed lines mark the wavelengths of the excitation lasers at 488nm (blue), 532nm (green), and 633 nm (red).

dashed lines represent the dye excitation light emitted by the blue (488 nm), green (532 nm) and red (633 nm) scanner lasers. The emission filters, shaded to correspond with the dyes for which they were used, are: 510nm 30nm band-pass, 555 nm 20nm band-pass and 655nm 30 nm band-pass.

Internal Standard

The mixed internal standard method described by Alban et al. [226] was used in this study. This method employs a mixture of all the samples to be used in the experiment to create enough identical standard aliquots to include one as an internal standard in each multiplexed gel, along with the experimental samples. Each internal standard is labeled with the same spectrally resolved fluorescent dye. In Alban's case a blue fluorescent dye, Cy2, was used. In our experiment the blue dye, ZBB was used for the internal standard channel. Although any color could theoretically be used for the internal standard channel, we used the blue channel because the background fluorescence of the acrylamide gels is the highest in the blue channel and the lower background channels were reserved for experimental samples, where sensitivity was of first importance.

The motivating principle of the internal standard is to provide a means of mathematically correcting for the gel-to-gel variability in the of protein abundances that is due to variations in protein migration. The internal standard spot volumes for each particular gel are compared by the Progenesis software to a "master" or "reference" gel, chosen by the researcher from among the set of gels as a best representative gel of the

overall group. The Progenesis spot matching software attempts to "warp" all of the other digital images of gels within an experimental set so that spots representing the same protein match the coordinates of the protein on the reference gel. It then uses the same spot outlines for all of the images for quantitation. Figure 56 schematically demonstrates how the internal standard works. In Figure 56A is a 3 gel experiment with no internal standard, focusing on a single protein spot across the 3 gels. In gels 1 and 2 the protein spot is 100% quantified as its intensity is well enclosed by the perimeter (black irregular enclosure). Gel 3, however, shows that about 25% of the spot intensity lies outside of the perimeter. Without the internal standard correction, the spot intensity is not accounted for and it contributes to technical variation. A similar experiment, but now done with another color channel with the internal standards included in each gel, shown in Figure 56B, can be used to correct each of the experimental spot intensities of Figure 56A by multiplying them by the ratio of the internal standard spot volume of the reference gel (gel #1) and the co-migrating internal standard spot volume. So, in the case of gel #2,

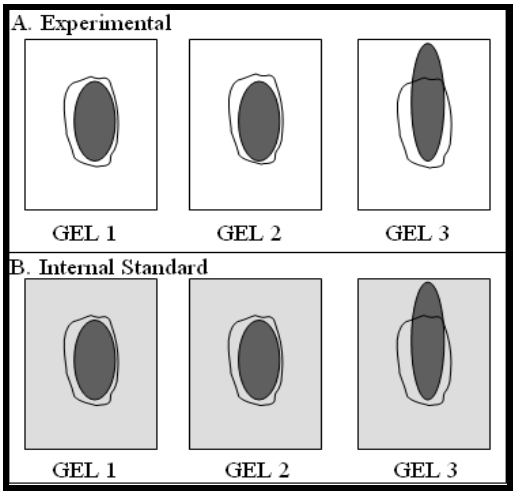

Figure 56 The internal standard strategy primarily aids gel-to-gel reproducibility when spot migration is sub-optimal.

where there is no loss of spot intensity, the co-migrating internal standard spot volume is theoretically identical to the internal standard spot volume of the reference gel, so the correction factor (cf) =1/1 is multiplied by the co-migrating spot volume of the experimental channel, leaving it unchanged. For gel #3, where the spot volume of the internal standard is 75% of the reference gel, the cf=1 / 0.75= 1.33, which, when multiplied by the experimental spot volume, creates the technically corrected experimental value. For equal protein loading from the two experimental groups, 45 µL internal standard aliquots were prepared after mixing 1:1 portions of the 12 mixed NGT controls and the 8 T2DM samples.

In a subsequent experiment that probed the oxidation state of HSA's Cys-34, (see ASSESSMENT OF MODIFICATIONS OF HUMAN SERUM ALBUMIN) we compared the non-diabetic and T2DM plasma on 1D gels using a red fluorescent Zdye with cysteine-specific maleimide labeling chemistry (KJS-IX103 Maleimide, Figure 57). This was done simultaneously in a single reaction-pot with a blue lysine-reactive NHS-ester dye used as protein loading control (ZBB Dipropyl NHS-ester, Figure 57).

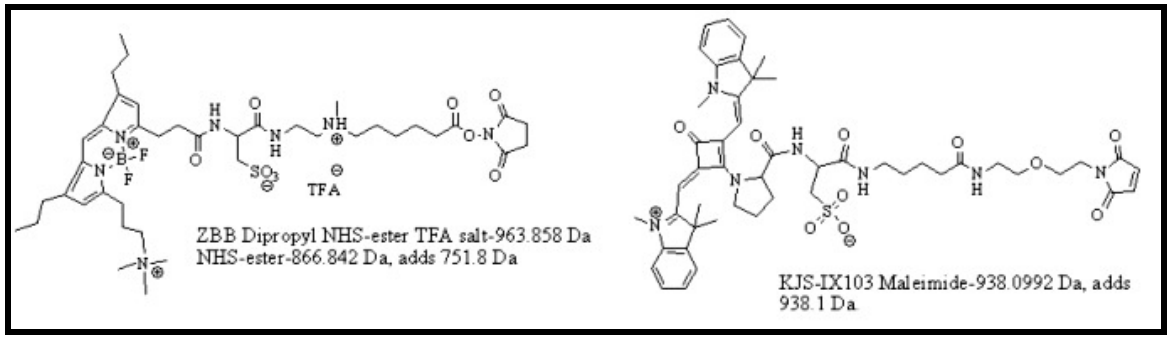

Figure 57 Dyes used in cysteine oxidation probe experiment.

PROTEIN MARKERS OF T2DM IN HUMAN PLASMA

Introduction and Method Development

Our sample preparation prior to 2D gel electrophoresis combines the removal of the 14 most abundant proteins by immunodepletion with reverse-phase fractionation of the remaining lower abundance proteins into six fractions according to the hydrophobicity of the proteins as briefly explained previously. An overview of the work flow is shown in Figure 39.

Materials and Methods

● *Human plasma samples.* Human citrated plasma samples were provided by the National Institutes of Health (NIH) and National Institutes of Diabetes and Digestive and Kidney Diseases (NIDDK) as part of an R21 grant to develop new diagnostic tests and/or to identify new biomarkers for the diagnosis of pre-T2DM and/or T2DM (PAR-04-076). The plasma samples prepared by NIH were from adult subjects who met all of four exclusion criteria. These criteria were:

1) Subjects were not previously known to have T2DM.
2) Subjects did not have an illness that caused them to miss work during the week prior to the blood draw.
3) Subjects did not have an acute infection or illness during the week prior to the blood draws (in the opinion of the subject).
4) Subjects were not known to be pregnant.

NIH administered two glucometric measurements to assign patients with normal glucose tolerance (NGT), impaired glucose tolerance (IGT), orT2DM. Together, the two measurements are referred to as the oral glucose tolerance test (OGTT). In the OGTT, after a fast of 8 to 12 hours, a person's blood glucose was measured before and two hours after drinking a solution containing 75 grams of glucose. Persons were categorized as NGT, IGT or T2DM according to World Health Organization (WHO) criteria. These criteria are as follows:

NGT- FPG < 126 mg/dL and glucose rises to no higher than 140 mg/dL two hours after the glucose drink.

IGT- FPG < 126 mg/dL and the glucose level is between 140 and 199 mg/dL two hours after the glucose drink.

T2DM- FPG > 126 mg/dL and/or the blood glucose rises to 200 mg/dL or above.

In addition to providing the quantitative glucometric data for each subject, the NIH also provided several anthropometric and metabolic measurements of the patients. The anthropometric measurements are: height, weight, body mass index (BMI), blood pressure, waist circumference, and waist/hip ratio. For the metabolic profile, prior to the OGTT, venous blood was drawn for the measurement of hemoglobin A1c (Ha1c), plasma total cholesterol, triglycerides, HDL cholesterol, LDL cholesterol, and C-reactive protein.

- *Protocol for the preparation of citrated plasma samples.* Prior to the collection of blood, each donor signed an NIH institutional review board (IRB) approved informed consent form. Subjects were seated for at least five minutes prior to blood collection.

Under the direction of a qualified and licensed physician, trained phlebotomists collected blood from each donor into evacuated blood collection tubes (BD Glass Sodium Citrate, 0.105M, 10 mL, catalog # 366007). After a discard tube was drawn to prime the tubing, approximately 30 mL of blood was collected from each donor into 3 tubes by venipuncture. Immediately after collection, the tubes were inverted four times. All tubes were kept always in wet ice or refrigerated at 4 C. Specimens were centrifuged in a swinging bucket centrifuge at 1,500 g for 15 minutes at 4 C. The resultant plasma was then pooled into a secondary 50 mL conical Falcon tube. The secondary Falcon tube containing the plasma was then centrifuged at 1,500g for 15 minutes at 4 C to remove all potentially remaining cellular material. The top 90% was removed into a new tube to ensure that no cellular material was collected. Plasma was then aliquoted (0.33 mL each) in labeled 0.5 mL cryovials and stored at -70 C. The above protocol was completed within 75 minutes from the time of specimen collection. After shipping on dry ice, the specimens were stored at -80 C until aliquoting for the experimental procedure.

The following samples were provided to us by the NIH/NIDDK:

1) 1 mL (3 x ~330uL) from 12 NGT patients. These specimens were used as controls.

2) 1 mL (3 x ~330uL) from 13 IGT patients. These specimens were not used in the expression proteomics portion of this experiment but were used in some of the analyses to be described.

3) 1 mL (3 x ~330uL) from 10 patients with newly-diagnosed, untreated (NDU) T2DM. These specimens were used as the diseased experimental samples.

4) The corresponding blood cell pellet and buffy coat from each NGT, IGT and T2DM patient were also aliquoted and frozen at -80° C. These specimens were not used in this experiment.

● *Plasma aliquots for the immunodepletion step of the 2D gel sample prep.* The volume of plasma to be used for each immunodepletion was determined to match the rated capacity of the immunodepletion column (Agilent 4.6 x 100 mm IgG polyAb multiple affinity removal system "MARS-14" LC column, gift of Agilent Industries). This capacity was stated as 40 µL of plasma. According to the LC column instructions [189], 40 µL of plasma should be diluted four-fold in buffer A (Agilent part # 5185-5987-equilibration, loading and washing buffer) and filtered in a 0.22 υm spin filter to remove particulates, prior to injection. There was a concern about protein losses and variation during spin filtering and this step was replaced by a short centrifugation with no spin filter. Our modified protocol (see below) diluted 45 µL of plasma four-fold with 135 µL of buffer A, centrifuged and only the top 160 µL was collected for injection into the MARS-14 column. This was found to adequately remove particulate material, as little increase in back pressure was observed over the course of approximately 200 LC injections.

In order design an experiment of a manageable size and to yield a reasonably sufficient statistical comparison we elected to make four pooled samples of control plasma. Each non-diabetic pool comprised equal amounts of plasma from 3 non-diabetic subjects unique to their pool, to compare with four pooled samples of T2DM plasma, each one comprised of equal amounts of plasma from 2 diabetic subjects, also unique to their pool. Pool analysis was also intended to "smooth" individual differences and enhance the characteristic traits that are related with the disease status affecting the constituent individuals [227]. For each of four pools, eight 45 µL aliquots of each, control and experimental group, were prepared. In addition, approximately thirty 45 µL aliquots comprised of equal amounts of all 20 plasma specimens combined were prepared for an internal standard to be included with all gels. All plasma samples were thawed and kept on ice during mixing. After the respective mixtures were made, the samples were vortexed and dispensed in 45 µL aliquots into labeled low-retention 1.7 mL microfuge tubes (Axygen Scientific, INC. Maxymum Recovery microtubes) and stored at -80 C until the time of use.

● *Experimental pool constituents and NIH sample data*. The following tables (Table 3-Table 7) contain the biometric and metabolic data provided by the NIH for the subject samples that were provided for this experiment. Table 3 - Table 5 contain the data for the T2DM and non-DM subjects, with the calculated averages for the pools used in the 2D-PAGE part of this study. They also show the individual subjects that were included in each pool. Table 6 and Table 7 contain the data for the IGT subjects. The

IGT subject samples were only used as individual samples and only in experiments following the 2D-PAGE portion.

The abbreviations and units that are used in the tables are as follows: "CAT_WHO"-World Health Organization diagnostic categorization number, 0 = normal glucose tolerance, 1 = impaired glucose tolerance, 2 = type-2 diabetic; "V" – visitation number, ex. V2= visit number two, referring to the patients visitation to the clinic; "HT." – height, units are centimeters; "CNGE" – change; "BMI" – body mass index, units are kg/m^2; "BP_DIAS" – average diastolic blood pressure from 3 measurements; "BPDS" – diastolic blood pressure; "SIT" – measurement #, "BP_SYS" – average systolic blood pressure from 3 measurements; "BPSYS" – systolic blood pressure, units of pressure are centimeters of mercury; HIP and WAIST measurements are in centimeters; "SAG_ABL_DIAM" – average sagittal abdominal diameter; "SAD" – sagittal abdominal diameter, units are centimeters; "CAP_1HR" – capillary glucose concentration 1 hour post 50 gram glucose challenge test, units are milligrams per deciliter; "_RAND" – random, for the capillary glucose concentration this is not necessarily fasting, pre- 50 gram glucose challenge test, units are milligrams per deciliter; "LAST_MEAL_DTIM" – date and time of last meal; "GLU_FAST" – Fasting venous glucose concentration, pre 75 gram oral glucose tolerance test (OGTT); "_1HR" – 1 hour post-OGTT venous glucose concentration; "_2HR" – 2 hours post-OGTT venous glucose concentration, all units of glucose concentrations are mg/dL; "_CHOL" – cholesterol, units are mg/dL; "_HDL" – high-density lipoprotein, units are mg/dL; "_LDL" – low-density lipoprotein, units are mg/dL; "_TRIG" – triglycerides, units are

mg/dL ; "_A1c" – hemoglobin A1c, glycated hemoglobin, units are percentage of total hemoglobin; "_ALT" – serum alanine aminotransferase concentration, units are IU/L; "_CRP" – high sensitivity measurement of serum C-reactive protein concentration, units are mg/L; "_ALB" – urine albumin concentration, units are mg/L; "_CREAT" – urine creatinine concentration, units are mg/L; "ALB_CR" – urine albumin/creatinine ratio, units are μg /mg; "CAT_5_ADA" – American Diabetic Association diagnostic categorization number, 0 = normal glucose tolerance, 1 = impaired glucose tolerance, 2 = type-2 diabetic, 12 = impaired glucose tolerance with unimpaired fasting glucose, 13 = impaired glucose tolerance and impaired fasting glucose; "_WHO" - World Health Organization diagnostic categorization number, 0 = normal glucose tolerance, 1 = impaired fasting glucose, 2 = type-2 diabetic, 12 = impaired glucose tolerance with unimpaired fasting glucose, 13 = impaired glucose tolerance and impaired fasting glucose.

Diabetic sample #26800204 was flagged by NIH as "blood draw incomplete" and the sample was missing. Diabetic sample #26700453 was flagged as "very high lipid or patient not fasted". This sample was not included in the study. In the following tables each of these is indicated as a "problem sample".

Table 3 Metabolic and Biometric Parameters for NGT and T2DM NIH Samples.

	SAMPLE_ID	CAT_WHO	AGE_V2	SEX	RACE	HT.	V1_WT	WT CNGE	V2_WT	BMI	BP_DIAS	BPDS_SIT_1	SIT_2	SIT_3	BP_SYS	BPSYS_S.T1	SIT2
Pool #1 Control	26800013	0	47	F	BLACK	151.4	0	0	65.7	29	83	77	84	81	113	116	113
Pool #1 Control	26800016	0	57	F	WHITE	156.6	0	0	67.6	28	74	77	72	75	128	139	127
Pool #1 Control	26800017	0	36	F	WHITE	167.9	0	0	52.5	19	80	78	81	78	116	121	117
Pool #2 Control	26800046	0	48	F	WHITE	170	82.3	-1	81.4	28	87	93	88	85	125	142	124
Pool #2 Control	26800055	0	55	M	WHITE	175.4	0	0	79.7	26	79	80	77	81	134	142	135
Pool #2 Control	26800060	0	61	F	WHITE	168.7	0	0	68.5	24	66	74	67	64	108	107	105
Pool #3 Control	26800063	0	53	F	WHITE	151.8	0	0	49.9	22	90	87	90	89	128	125	128
Pool #3 Control	26800079	0	48	F	WHITE	167.2	0	0	69.9	25	80	85	79	81	133	137	134
Pool #3 Control	26800091	0	55	F	WHITE	150.4	0	0	55.5	25	91	95	93	88	159	175	158
Pool #4 Control	26800106	0	55	F	WHITE	169.1	79.7	0	79.3	28	71	68	73	69	126	129	123
Pool #4 Control	26800122	0	50	F	WHITE	163.6	67.2	0	67.5	25	75	84	75	74	118	139	121
Pool #4 Control	26800273	0	56	M	WHITE	182.9	0	0	68.6	21	62	67	63	60	113	130	115
	26800431	0	44	F	WHITE	162.2	64.4	0	63.8	24	71	70	70	71	110	117	110
Control Pool #1 Average						158.6			61.9	25	79	77	79	78	119	125	119
Control Pool #2 Average						171.4			76.5	26	77	82	77	77	122	130	121
Control Pool #3 Average						156.5			58.4	24	87	89	87	86	140	146	140
Control Pool #4 Average						171.9			71.8	25	69	73	70	68	119	133	120
	SAMPLE_ID	CAT_WHO	AGE_V2	SEX	RACE	HT.	V1_WT	WT CNGE	V2_WT	BMI	BP_DIAS	BPDS_SIT_1	SIT_2	SIT_3	BP_SYS	BPSYS_S.T1	SIT2
Pool #1 T2DM	26800077	2	56	F	WHITE	162.6	0	0	109.4	41	66	65	64	68	147	159	145
Pool #1 T2DM	26800101	2	58	F	BLACK	149.6	75.8	0	75.6	34	78	81	75	81	136	136	131
Pool #2 T2DM	26800134	2	57	M	WHITE	180.6	0	0	89.6	27	83	83	85	81	136	141	136
Problem Sample	26800204	2	50	F	BLACK	164.5	75.9	0	76.1	28	86	84	85	86	118	125	121
Pool #2 T2DM	26700304	2	61	F	WHITE	153.9	66.9	0	66.9	28	70	68	70	69	118	123	117
Problem Sample	26700453	2	36	M	BLACK	172.8	110.7	0	110.9	37	82	85	85	79	129	137	125
Pool #3 T2DM	26700457	2	56	F	BLACK	158.3	66.5	-2	65	26	70	69	70	69	110	107	110
Pool #3 T2DM	26800552	2	61	M	WHITE	162.9	87.6	-1	85.9	32	81	79	82	80	144	140	149
Pool #4 T2DM	26800581	2	40	M	WHITE	179.1	102	0	101.8	32	93	93	95	90	126	135	123
Pool #4 T2DM	26700586	2	59	F	BLACK	170.7	132	-1	130	45	56	62	57	54	142	149	147
T2DM Pool #1 Average						156.1			92.5	38	72	73	70	75	142	148	138
T2DM Pool #2 Average						167.3			78.25	28	77	76	78	75	127	132	127
T2DM Pool #3 Average						167.9			98.4	35	82	82	84	80	137	139	137
T2DM Pool #4 Average						174.9			115.9	39	75	78	76	72	134	142	135

Table 4 Metabolic and Biometric Parameters for NGT and T2DM NIH Samples.

	SIT3	HIP	WAIST	SAG_ABL_DIAM	SAD_1	SAD_2	V1_CAP_1HR	_RAND	V1_GLU_1HR	_RAND	1_LAST_MEAL_DTIM	V2_GLU_FAST	1HR	2HR
Pool #1 Control	113	103	88.2	21	21.4	21.6	96	93	88	77	2/2/2005 12:37:00 PM	87	94	98
Pool #1 Control	129	103.2	97.2	22	22.2	22.7	173	72	96	76	2/27/2005 8:43:00 PM	89	122	90
Pool #1 Control	115	93.5	64	14	14	14	134	111	94	95	1/12/2005 12:54:00 PM	80	68	75
Pool #2 Control	125	114.1	92	22	22.7	22.8	181	93	152	97	3/20/2005 8:00:00 PM	94	158	95
Pool #2 Control	133	97	96.5	19	19.8	20	116	105	110	76		90	127	83
Pool #2 Control	111	101.5	83.5	16	16.7	16.3	171	105	163	101	1/3/2005 6:46:00 AM	94	119	71
Pool #3 Control	127	90	66.1	16	16.4	16.5	177	87	140	77	2/22/2005 3:17:00 PM	84	87	79
Pool #3 Control	131	101	97.5	19	19.5	19.7	186	79	176	85	3/1/2005 12:29:00 PM	91	77	76
Pool #3 Control	160	96.5	70.7	18	18.1	18.1	178	86	158	91	3/7/2005 11:41:00 AM	88	114	80
Pool #4 Control	128	112.8	89.1	21	21.8	21.6	177	101	135	92	4/20/2005 12:15:00 PM	85	134	84
Pool #4 Control	115	106.9	88.2	20	20.3	20.8	170	94	129	86	4/28/2005 9:00:00 PM	82	112	54
Pool #4 Control	111	79.1	73	16	16.5	16.6	169	83	145	85	2/16/2005 10:34:00 AM	89	119	78
	109	100.1	77.6	19	19.2	19	206	92	85	129	4/13/2005 7:30:00 AM	88	149	90
Control Pool #1 Average	119	99.9	83	19	19.2	19.4	134	92	93	83		85	95	88
Control Pool #2 Average	123	104.2	91	19	19.7	19.7	156	101	142	91		93	135	83
Control Pool #3 Average	139	95.8	78	18	18.0	18.1	180	84	158	84		88	93	78
Control Pool #4 Average	118	99.6	83	19	19.5	19.7	172	93	136	88		85	122	72
	SIT3	HIP	WAIST	SAG_ABL_DIAM	SAD_1	SAD_2	V1_CAP_1HR	_RAND	V1_GLU_1HR	_RAND	1_LAST_MEAL_DTIM	V2_GLU_FAST	1HR	2HR
Pool #1 T2DM	148	134.5	115.3	26	26.8	26.7	193	114	175	103	2/24/2005 11:03:00 AM	138	266	216
Pool #1 T2DM	141	109	103.5	25	25.9	26	184	130	197	129	3/23/2005 9:30:00 AM	131	231	272
Pool #2 T2DM	136	102	100.5	21	21.9	21.8	231	180	239	179	2/1/2005 6:45:00 AM	131	249	234
Problem Sample	114	110	94	23	24	23.7	231	112	193	109	7/15/2005 7:45:00 AM	134	238	241
Pool #2 T2DM	118	109	86.2	22	22.9	22.7	217	148	191	131	6/13/2005 12:40:00 PM	109	254	202
Problem Sample	133	118.6	116.2	28	28.1	28.1	257	113	244	118	4/13/2005 9:30:00 PM	113	248	230
Pool #3 T2DM	110	102.7	90.4	21	21.7	21.6	254	142	223	138	4/15/2005 11:15:00 AM	122	262	212
Pool #3 T2DM	138	106.1	105.1	24	24.8	24.5	223	172	224	175	5/4/2005 9:00:00 AM	115	314	204
Pool #4 T2DM	128	109.2	103.6	24	24.3	24.2	155	168	163	167	7/12/2005 12:30:00 PM	130	258	208
Pool #4 T2DM	137	145.1	113	33	33	33.3	295	219	272	206	8/2/2005 6:30:00 AM	171	366	279
T2DM Pool #1 Average	145	121.8	109.4	26	26	26.4	189	122	186	116		135	249	244
T2DM Pool #2 Average	127	105.5	93.4	22	22	22.3	224	164	215	155		120	252	218
T2DM Pool #3 Average	136	112.4	110.7	26	26	26.3	240	143	234	147		114	281	217
T2DM Pool #4 Average	133	127.2	108.3	29	29	28.8	225	194	218	187		151	312	244

Table 5 Metabolic and Biometric Parameters for NGT and T2DM NIH Samples.

	V2_CHOL	HDL	LDL	TRIG	A1C	ALT	CRP	ALB	CREAT	ALB_CR	V1_VISIT	V2_VISIT	CAT_5_ADA	WHO	IFG_ADA	WHO
Pool #1 Control	138	65	66	35	5.2	14	0.3	0.4	26	15	2/2/2005	2/10/2005	0	0	0	0
Pool #1 Control	148	52	82	70	5.3	38	3.2	0.5	20	25	2/28/2005	3/9/2005	0	0	0	0
Pool #1 Control	135	51	78	30	4.6	17	0.2	0.6	122	5	1/12/2005	1/19/2005	0	0	0	0
Pool #2 Control	120	23	84	67	5.2	22	2.3	0.3	42	7	3/21/2005	4/4/2005	0	0	0	0
Pool #2 Control	192	57	117	90	5.1	21	0.7	0.4	178.4	2	12/20/2004	12/23/2004	0	0	0	0
Pool #2 Control	162	57	92	66	4.9	26	0.2	1.4	249	6	1/3/2005	1/13/2005	0	0	0	0
Pool #3 Control	218	85	124	43	5.2	25	1.7	0.3	110	3	2/22/2005	3/2/2005	0	0	0	0
Pool #3 Control	179	55	117	35	4.6	18	0.8	0.2	55	5	3/1/2005	3/18/2005	0	0	0	0
Pool #3 Control	199	93	99	35	4.5	49	0.4	0.6	84	7	3/7/2005	3/17/2005	0	0	0	0
Pool #4 Control	237	62	150	124	5	19	5.7	0.3	13	23	4/20/2005	4/27/2005	0	0	0	0
Pool #4 Control	210	69	126	74	5.1	13	1.1	0.2	130	2	4/29/2005	5/13/2005	0	0	0	0
Pool #4 Control	140	48	80	61	5.2	16	0.3	0.7	111	6	2/16/2005	2/23/2005	0	0	0	0
	165	46	110	44	5	15	0.8	0.2	10	30	4/13/2005	4/21/2005	0	0	0	0
Control Pool #1 Average	140	56	75	45	5.0	23	1.2	0.5	56	15						
Control Pool #2 Average	158	46	98	74	5.1	23	1.1	0.7	156	5						
Control Pool #3 Average	199	78	113	38	4.8	31	1.0	0.4	83	5						
Control Pool #4 Average	196	60	119	86	5.1	16	2.4	0.4	85	10						
	V2_CHOL	HDL	LDL	TRIG	A1C	ALT	CRP	ALB	CREAT	ALB_CR	V1_VISIT	V2_VISIT	CAT_5_ADA	WHO	IFG_ADA	WHO
Pool #1 T2DM	194	75	99	98	5.7	23	9.3	0.8	164	5	2/24/2005	3/8/2005	2	2	2	2
Pool #1 T2DM	164	26	120	92	6.7	34	9.2	1	151	7	3/23/2005	3/31/2005	2	2	2	2
Pool #2 T2DM	118	22	68	142	5.5	23	6.8	0.5	143	3	2/1/2005	2/9/2005	2	2	2	2
Problem Sample	223	50	146	137	6.1	19	2.8	1.4	121	12	7/15/2005	7/27/2005	2	2	2	2
Pool #2 T2DM	250	38	194	91	5.5	44	4.3	0.1	40	7	6/13/2005	6/27/2005	2	2	1	0
Problem Sample	187	24	96	334	6.3	28	3.5	3.7	158	23	4/14/2005	4/28/2005	2	2	1	1
Pool #3 T2DM	164	32	121	55	5.5	21	3.1	1.6	146	11	4/15/2005	4/25/2005	2	2	1	1
Pool #3 T2DM	191	35	118	191	5.9	42	5.2	1.7	117	15	5/4/2005	5/12/2005	2	2	1	1
Pool #4 T2DM	201	52	106	213	6.4	36	1.6	0.3	49	6	7/12/2005	7/19/2005	2	2	2	2
Pool #4 T2DM	170	43	106	105	7.5	22	17.2	1.9	157	12	8/2/2005	8/8/2005	2	2	2	2
T2DM Pool #1 Average	179	51	110	95	6.2	29	9.3	0.9	158	6						
T2DM Pool #2 Average	184	30	131	117	5.5	34	5.6	0.3	92	5						
T2DM Pool #3 Average	189	30	107	263	6.1	35	4.4	2.7	138	19						
T2DM Pool #4 Average	186	48	106	159	7.0	29	9.4	1.1	103	9						

Table 6 Metabolic and Biometric Parameters for IGT NIH Samples.

	SAMPLE_ID	CAT_WHO	AGE_V2	SEX	RACE	HT.	V1_WT	WT CNGE	V2_WT	BMI	BP_DIAS	BPDS_SIT_1	SIT_2	SIT_3
MetSyn Individ.	26800019	1	52	F	WHITE	169.2	0	0	67.9	24	72	68	74	70
MetSyn Individ.	26800025	1	50	F	WHITE	159.2	0	0	108.3	43	92	95	86	97
MetSyn Individ.	26800038	1	61	F	WHITE	161.6	0	0	75.3	29	90	82	95	85
MetSyn Individ.	26800050	1	65	F	WHITE	159.2	0	0	75.6	30	73	80	79	66
MetSyn Individ.	26800066	1	57	F	WHITE	166.7	79.6	-3	77.1	28	94	95	91	96
MetSyn Individ.	26800068	1	55	F	WHITE	152	0	0	79.8	35	78	87	76	79
MetSyn Individ.	26800112	1	33	F	WHITE	167	57.5	1	58.5	21	65	67	66	63
MetSyn Individ.	26800209	1	44	F	WHITE	170.3	61.4	0	61.5	21	80	97	78	82
MetSyn Individ.	26800213	1	45	F	BLACK	158.7	98.4	1	100.2	40	76	83	80	72
MetSyn Individ.	26800237	1	61	M	WHITE	169.5	90.7	-2	88.6	31	69	69	68	70
MetSyn Individ.	26800454	1	58	F	WHITE	157.6	96.6	-1	95.2	38	64	65	62	65
MetSyn Individ.	26800548	1	68	M	WHITE	174.8	90.4	0	90.9	30	95	98	96	93
MetSyn Individ.	26800753	1	60	M	WHITE	172	91.1	2	93.6	32	98	92	104	92

	SAMPLE_ID	BP_SYS	BPSYS_SIT1	SIT2	SIT3	HIP	WAIST	SAG_ABL_DIAM	SAD_1	SAD_2	V1_CAP_1HR	_RAND	V1_GLU_1HR	_RAND
MetSyn Individ.	26800019	128	117	134	121	102	87	18	18.75	18.75	213	92	180	92
MetSyn Individ.	26800025	143	150	145	140	130.8	120.5	29	29.4	29.2	162	98	175	102
MetSyn Individ.	26800038	141	132	142	139	110	95.3	21	21.2	21.2	176	99	113	64
MetSyn Individ.	26800050	116	137	105	126	104.8	93	19	19.5	19.2	215	110	195	107
MetSyn Individ.	26800066	127	127	127	127	105.5	93.5	22	22.5	22.3	190	115	163	106
MetSyn Individ.	26800068	133	135	136	129	111	102.9	24	24.8	24.9	208	79	199	86
MetSyn Individ.	26800112	100	100	105	94	95.9	70.6	14	14.1	14	212	111	139	104
MetSyn Individ.	26800209	119	122	123	115	98.5	80.9	18	18.6	18.4	253	96	240	91
MetSyn Individ.	26800213	126	122	132	119	127	107.2	26	26.9	27	188	99	168	97
MetSyn Individ.	26800237	114	126	111	117	106.7	109.5	22	22.2	22.9	181	95	153	94
MetSyn Individ.	26800454	116	113	117	114	116	117.1	28	29	28.9	222	107	202	106
MetSyn Individ.	26800548	156	157	153	158	109.5	103.4	24	24.9	24.8	174	107	181	105
MetSyn Individ.	26800753	143	157	134	152	108	109	25	25.4	25.7	196	94	211	98

Table 7 Metabolic and Biometric Parameters for IGT NIH Samples.

	SAMPLE_ID	V1_LAST_MEAL_DTIME	2_GLU_FAST	1HR	2HR	2_CHO	HDL	LDL	TRIG	A1C	ALT	CRP	ALB	CREAT	ALB_CR	V1_VISIT
MetSyn Individ.	26800019	1/12/2005 8:23:00 AM	94	204	191	208	63	117	138	5.2	23	2.7	1.6	223	7	1/12/2005
MetSyn Individ.	26800025	2/7/2005 1:04:00 PM	112	221	170	253	41	190	110	5.2	49	6.5	0.3	13	23	2/7/2005
MetSyn Individ.	26800038	1/25/2005 3:10:00 PM	97	194	171	151	34	93	119	4.9	22	4.5	1	59	17	1/25/2005
MetSyn Individ.	26800050	1/13/2005 8:48:00 AM	99	219	159	245	80	155	48	4.9	21	3.3	0.4	54	7	1/13/2005
MetSyn Individ.	26800066	4/25/2005 8:30:00 PM	109	231	173	237	64	157	81	4.7	52	1.2	0.2	15	20	4/26/2005
MetSyn Individ.	26800068	2/23/2005 4:59:00 AM	95	213	167	344	54	259	153	5.3	36	4.3	0.3	59	5	2/23/2005
MetSyn Individ.	26800112	6/15/2005 11:30:00 AM	76	169	159	216	73	133	51	5.4	30	0.5	0.2	11	27	6/15/2005
MetSyn Individ.	26800209	7/18/2005 12:30:00 PM	92	196	170	183	85	88	49	5.3	17	2.1	0.2	14	14	7/18/2005
MetSyn Individ.	26800213	7/14/2005 8:15:00 AM	100	178	168	233	49	172	60	5.8	19	1.2	0.1	46	4	7/14/2005
MetSyn Individ.	26800237	3/21/2005 12:00:00 PM	93	173	142	203	44	127	159	5.4	21	3.7	0	64	5	3/21/2005
MetSyn Individ.	26800454	4/25/2005 11:45:00 AM	104	230	173	263	54	187	109	4.9	54	28.6	0.3	67	5	4/25/2005
MetSyn Individ.	26800548	6/23/2005 9:00:00 AM	108	251	167	159	29	93	187	5.5	47	1.2	1.4	183	8	5/23/2005
MetSyn Individ.	26800753	6/28/2005 8:00:00 AM	98	202	152	179	45	119	74	5.8	24	0.2	0.4	28	14	5/28/2005

	SAMPLE_ID	V2_VISIT	CAT_5_ADA	WHO	IFG_ADA	WHO
MetSyn Individ.	26800019	1/18/2005	12	12	0	0
MetSyn Individ.	26800025	2/16/2005	13	13	1	1
MetSyn Individ.	26800038	2/7/2005	12	12	0	0
MetSyn Individ.	26800050	1/20/2005	12	12	0	0
MetSyn Individ.	26800066	5/5/2005	13	12	1	0
MetSyn Individ.	26800068	3/8/2005	12	12	0	0
MetSyn Individ.	26800112	6/22/2005	12	12	0	0
MetSyn Individ.	26800209	7/28/2005	12	12	0	0
MetSyn Individ.	26800213	7/21/2005	13	12	1	0
MetSyn Individ.	26800237	3/30/2005	12	12	0	0
MetSyn Individ.	26800454	5/6/2005	13	12	1	0
MetSyn Individ.	26800548	6/30/2005	13	12	1	0
MetSyn Individ.	26800753	7/7/2005	12	12	0	0

The compositions of the experimental sample groups, broken down into sex, BMI, age and race are shown in Table 8.

Table 8 The breakdown of some important demographic and biometric classifications within the experimental groups. F=female, M=male, B=black, W=white.

	NGT (12)	T2DM (8)
Sex (F/M)	10/2.	5/3.
BMI	25 ± 3	33 ± 7
Age	52 ± 7	56 ± 7
Race (B/W)	1/11.	3/5.

- *The order of sample preparation.* The samples were prepared for 2D-PAGE beginning with pool 1 and cycling through the sample types within each pool: internal standard, control, T2DM, internal standard, control, etc. We decided on this cycling progression of preparation instead of a randomized progression in the anticipation of possible systematic changes in the binding of both the reversed-phase column and the immunodepletion column over the long term and many runs of the experiment. Although a seemingly small effect, the systematic, gradual loss of binding capacity of the MARS-6 column for IgG, from 99.9 to 99.7%, and IgA, from 99.9 to 99.1, over the stated 200 run lifetime of the column has been demonstrated by others [228]. Also, in the case of the reverse-phase column, if there was an increasing accumulation of irreversibly binding species such as lipids or oily proteins, it was reasoned that by cycling the sample preparation, each sample type would "see" more similar column conditions than if the sample preparation was left to chance, as in a random progression. The same argument is made for the binding characteristics of the immunodepletion column. Even though the

column was shown to be reproducible in its gross binding characteristics (Figure 43), by rotating the sample types, subtle systematic changes in specific antibody binding characteristics, over the course of the experiment, could be equally "distributed" between the sample types.

● *Immunodepletion of abundant plasma proteins.* Previously pooled and aliquoted 45 µL plasma samples were thawed on ice immediately prior to each column injection. After thawing the plasma, 135 µL of degassed Agilent buffer A was added to make a four-fold dilution. This was briefly vortexed and centrifuged at 2000 rcf (Eppindorf MiniSpin Plus fixed angle bench top centrifuge) for two minutes at room temperature. The upper 160 µL was aspirated using a 250 µL Hamilton syringe and immediately injected into the AKTA FPLC system for immunodepletion. The remaining ~20 µL solutions were discarded.

The FPLC system (P-920 pump and UPC-900 UV detection at 214nm, Amersham Biosciences) was fitted with a 4.6 x 100 mm IgG polyAb MARS-14 LC column (Agilent part #5118-6558). After loading the sample into a 2 mL PEEK tubing sample loop (Upchurch part # 1533, O.D. 1/16", I.D. 0.030") via the 7 port automatic injection valve (INV-907, Amersham Biosciences) the run was begun. The timed method of flow-rate and percentage compositions of degassed Agilent buffer A and buffer B can

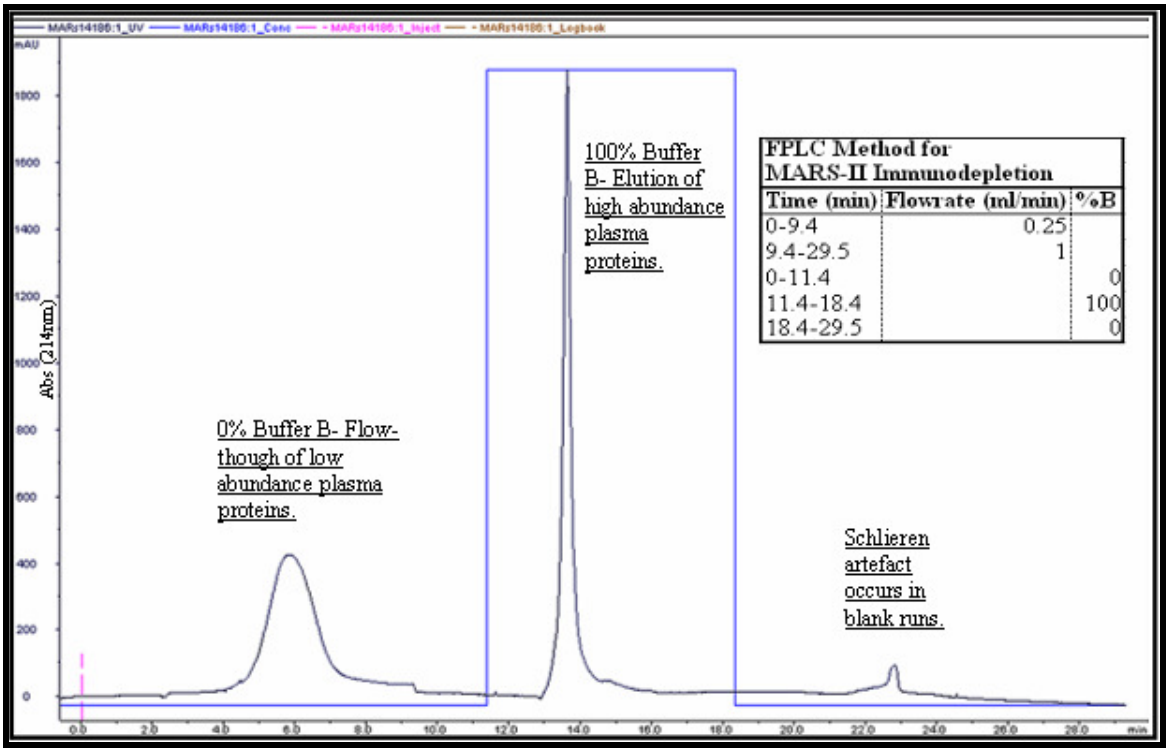

Figure 58 A representative chromatogram of the FPLC immunodepletion using the MARS-14 column.

be found in the inset box of Figure 58. The flow-through proteins were collected between the times 2.4 and 9.4 minutes, with the flow rate of 0.25 mL/min. The flow-through proteins were collected into a 15 mL conical tube into previously added 0.82 gm urea (Sigma, SigmaUltra catalog # UO631) and 23 µL glacial acetic acid (EMD Chemicals Cat. # AX0073-9) for a final concentration of 6M urea and 1% acetic acid after the fraction collection was complete. The solution was gently mixed during the collection to completely dissolve the urea. 100% buffer B was started at 11.4 minutes

and the eluted high-abundance proteins were collected between 13-16 minutes and frozen for future use.

In Figure 58, the "eluted" peak at 14 minutes represents greater than 90% of the injected proteins and the "flow-through" peak at 6 minutes represents less than 10%, based upon the stated 94% depletion for this column [189]. The area of the peaks appears to be inconsistent with this as the eluted peak seems too small. This under-representation is believed to result from the relatively high concentration of the eluted proteins, far beyond the limit of concentration for a linear response of the detector according to the Beer-Lambert law.

● *Reverse-phase fractionation of the "low-abundance" plasma proteins.* For the RP fractionation of the low-abundance proteins, the collected flow-through fractions from the immunodepletion step were loaded using a manual analytical injector (Rheodyne part #9725) and a 2.5 mL PEEK tubing sample loop (Upchurch part # 1538, O.D. 1/16", I.D. 0.040"). An Agilent 1100 series binary pump (Agilent part # G1312A), column heater (Agilent part # G1316A) and diode array detection (Agilent part # 1315A) with a 6mm flow cell (Hewlett-Packard part # G1315-60015) was used. Mobile phase compositions were: mobile phase A-MilliQ (Millipore) H_20/0.1% TFA (Fisher Scientific catalog # 04902-100) and mobile phase B-95% acetonitrile (J.T. Baker HPLC grade)/0.08% TFA. The mRP column was heated and separations were run at 80 °C. For approximately the first half of the experiment a heated water bath was used and the temperature was controlled by adding cool water as needed. For the second half of the experiment a column heater (Agilent 1100 G1316A) was used.

The approximately 2.3 mL solutions of collected proteins from each immunodepletion, in buffer A, 6M urea and 1% acetic acid, were immediately loaded on to the mRP column in two 1.15 mL injections. After loading the first half at a flow rate of 0.75 mL/min, the HPLC run (Figure 59) was started and the second half of the sample

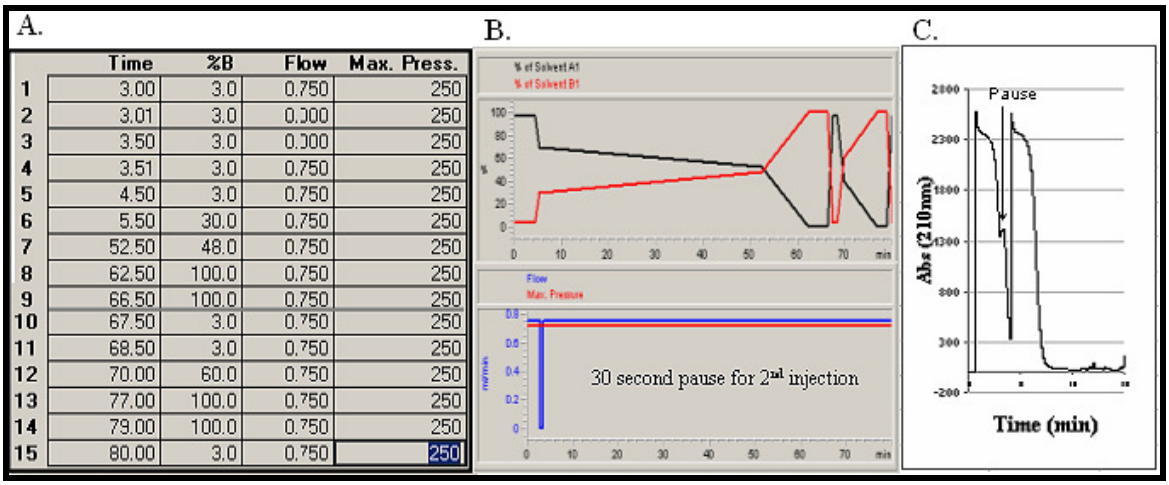

Figure 59 A) The HPLC Method for fractionation of depleted plasma peptides. B) Upper figure- Solvent composition traces for elution of proteins with added column wash from 68 to 80 minutes. Lower figure- Effluent flow-rate trace-blue with 30 second column loading "pause" from 3-3.5 minutes to load the sample loop with the 2nd injection and maximum allowed pressure-red. C) First 15 minutes of a representative depleted plasma trace showing two large peaks corresponding to the two injections. The flow-through peaks are primarily urea, acetic acid and other small molecules in plasma, including amino acids.

was loaded into the injection loop during a programmed 30 second pause at 3 minutes.

Six protein fractions were collected from the RP separations with fraction #1 beginning at 9.0 minutes, a starting time that allowed the ionic contaminants and urea to flow through uncollected (Figure 59C). The cutoffs for each fraction were executed at local minima for fractions #1, #3, #4, #5 and #6 and at the local maximum for fraction #2 (Figure 60). The fraction cutoffs were determined to provide approximately equal

amounts of protein to each fraction, with four technical replicate analytical gels per fraction, after pooling the fractions from six such runs. The net area under the UV trace,

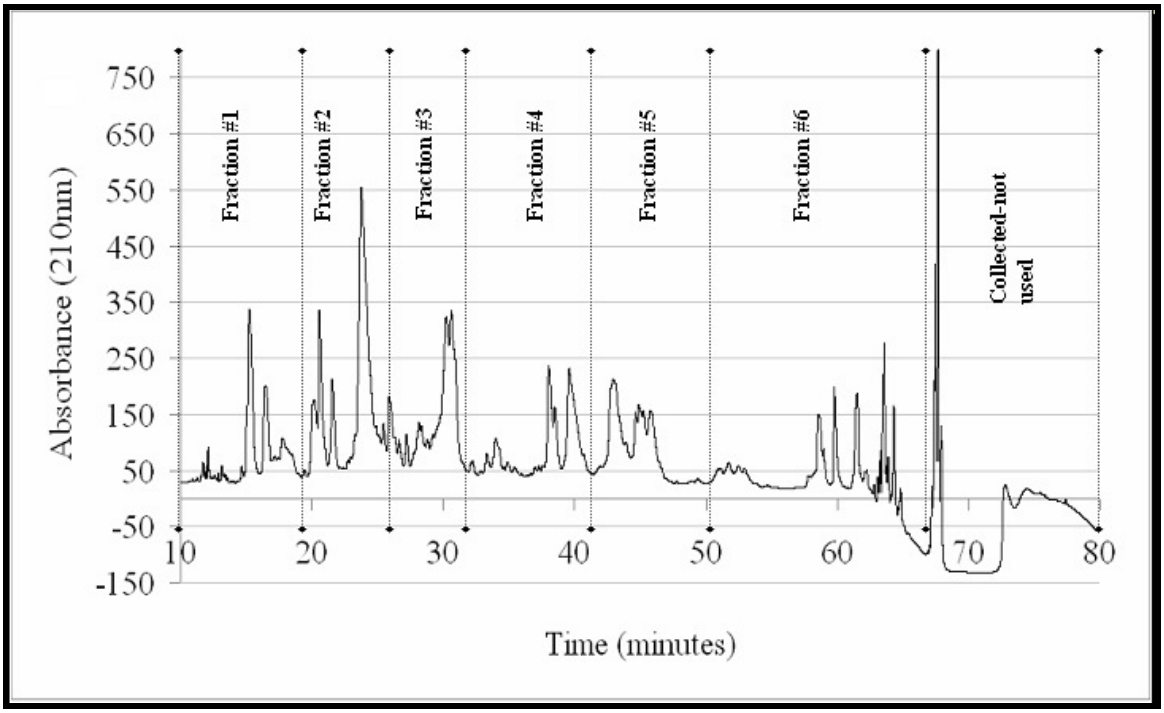

Figure 60 A representative chromatogram from the RP-HPLC fractionation of MARS-14 immunodepleted plasma proteins at 80° C run as described in the text.

(210nm) after subtracting that of a blank run, was used to quantify the percentage of the estimated average total mass of protein in the flow-through of the immunodepletion, (based upon 94% immunodepletion [189] of 80 µg /µL protein in plasma) which eluted during each HPLC fraction. Based on this calculation, the approximate amounts of protein produced for each of the gels from their respective fractions are: fraction #1-42 µg, fraction #2-74 µg, fraction #3-53 µg, fraction #4-46 µg, fraction #5-43 µg. As was discussed in the RP-HPLC of Depleted Human Plasma section, the UV trace over-represents the amount of proteinaceous material in fraction 6 by an estimated 30%. So a

correction was made to the percentage of the total represented by area under the trace for this fraction. When the fractional area under the trace in fraction #6 is multiplied by 0.70, the calculated amount of protein is 42 μg. Fractions #1-#5 were collected in 15 mL conical vials. Fraction #6 was collected in a 50 mL conical vial (Becton-Dickinson Falcon Tubes). Fractions were immediately frozen after collection and lyophilized until dry. It should be emphasized that these protein estimates were used relatively to one another to choose fraction cutpoints, so that the amounts of protein were divided approximately evenly between the gels. These fraction cutpoints were found to produce gels with sub-saturating but strong fluorescence signals within the Typhoon User's Guide [229] recommended 400-800V range of scanner PMT voltages, so the protein loadings were empirically determined to be appropriate.

● *Pooling and aliquoting of RP-HPLC fractions for labeling.* In order to produce enough protein for the gels, it was necessary to combine corresponding fractions from multiple HPLC runs. However, the fraction combination was likely to also be beneficial in that it served to "average out" run-to-run variations introduced by the HPLC fractionation, as well as the immunodepletion steps.

Figure 61 shows a modular schematic describing the fractionation and aliquoting scheme for one experimental group type (out of three) within one pool (out of four). The scheme follows the work flow of 6 immunodepletions and 6 RP sub-fractionations for each of pool 1 groups; controls, patients and internal standards. Each of the 6 F1 sub-fractions for the groups were combined, realiquoted to 4 samples, lyophilized and frozen until the day of labeling. The bottom of the figure shows the colors of dye that were used

for each of the samples and how they were combined to run on each of the 4 gels. The 4 controls and 4 experimental samples were "cross-labeled"; 2 green and 2 red, to prevent artifactual differences in intensity resulting from "dye- bias", as some proteins may react differently or have different effects on the quantum yields of the dyes. So, pool 1 yielded 24 (samples) x 1/3 gels/sample x 4 pools x 3 experimental groups = 96 gels, for the overall experiment.

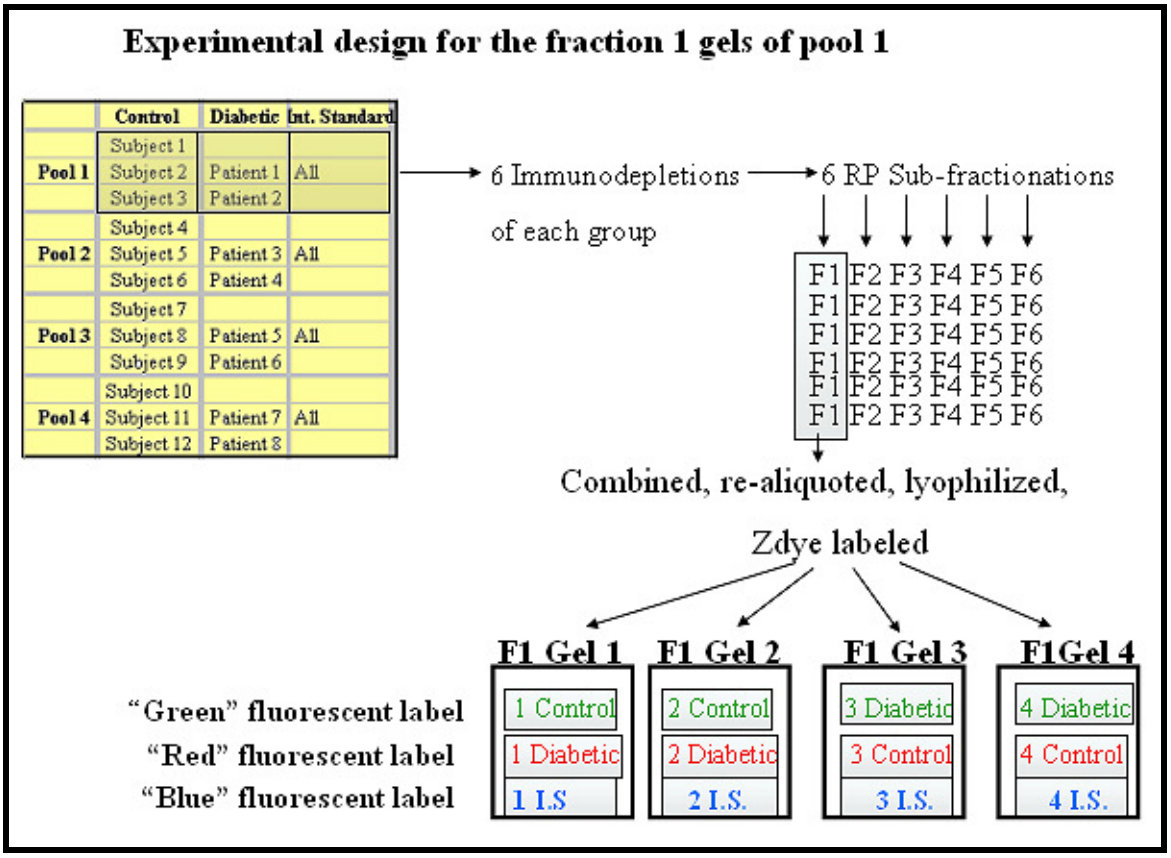

Figure 61 The aliquoting scheme used in the 2D gel experiment representing the F1 gels from 1 of the 4 pools.

To combine the respective fractions from 6 RP runs, 40 µL of 8 M urea and 4% CHAPS was used with a Pipetteman tip to carefully wash the lyophilized samples from

interior surface of each conical vial. After each wash the vial was centrifuged at 1000 rpm to bring the wash to the bottom of the vial and the wash was serially transferred to each vial to wash and combine the proteins. After transferring the final wash to a 1.7 mL microfuge tube on ice, the six conical vials were washed sequentially a second time by vortexing, centrifuging and transferring 1560ul of MilliQ water (Millipore Corp.) from one tube to the next in series. This wash was combined with the first wash in a 2.0 mL microfuge tube, vortexed and aliquoted equally to four labeled 1.7 mL microfuge tubes. These samples were then frozen and lyophilized. The resulting approximately 400 µL volume of proteins suspended in a matrix of urea and CHAPS was stored at -80 C until the time of fluorescent dye labeling.

- *Fluorescent Zdye labeling of proteins for two-dimensional gel electrophoresis.*

Dye labeling of the aliquots was empirically determined to produce gel images with strong but sub-saturating fluorescence signals (with a scanner PMT voltage between 400-700V) and to produce few multiply labeled proteins, as evidenced by lack of vertical spot trains.

To label the protein fractions, 7ul of 45 mM Bicine (Bicine-Calbiochem, catalog # 391336, HCl-EMD chemicals, catalog # HX 0603-3) adjusted to pH 8.6 with NaOH, was gently stirred into the previously prepared 400 υl matrix of solid protein, urea and CHAPS, using a 10 υL Pipetteman tip, until the solid was dissolved. After centrifuging, and placing on ice, 1 µL of the covalent labeling dye dissolved in dry dimethylformamide (DMF-Thermo Scientific, catalog # 20672) was added (Table 9). For fractions #1, #3, #4, #5, and #6, 1ul of 1mM ZBB or ZGB in DMF was used. For fraction #2 1ul of 0.8

mM was used. For the red dye HBO-187, for fractions #1, #3, #4, #5, and #6, 1ul of 2mM was used. For fraction #2 1ul 1.6 mM was used. These reactions were gently vortexed, centrifuged and placed on ice, in the dark, for 30 minutes for the protein

Dye labeling and lysine quenching			
Fraction	ZBB/ZGB	HBO-187	K Quench
F #1	1000 pmole	2000 pmole	30/50 mM
F #2	800 pmole	1600 pmole	30/50 mM
F #3	1000 pmole	2000 pmole	30/50 mM
F #4	1000 pmole	2000 pmole	30/50 mM
F #5	1000 pmole	2000 pmole	30/50 mM
F #6	1000 pmole	2000 pmole	30/50 mM

Table 9 Dye labeling and lysine quenching of different RP protein fractions.

labeling reaction. After 30 minutes, the amine reactive NHS-ester dye reaction was quenched by adding 1 µL of lysine solution (Table 9). Fraction #2 was labeled with 20% less dye than the fractions #1, #3, #4, #5, and #6 to compensate for the higher amount of protein in the fraction. To stop the protein labeling reactions after 30 minutes, the reactions received either 30 mM lysine (Fluka catalog # 62840) for the less concentrated blue and green dye labeling, or 50 mM lysine for the more concentrated red dye labeling. These lysine quenching solutions (K-quench) also contained 0.02% sodium azide (Sigma catalog # S2002). The NHS-ester quenching reaction was allowed to proceed for at least ten minutes, on ice, before the labeled samples were washed out of the tubes and combined in IEF rehydration buffer.

- *Immobiline strip rehydration and cup-loading for iso-electric focusing.* The rehydration buffer that was used for fractions #1-#5 was MilliQ water, 8 M urea, 4% CHAPS, 1% Destreak™ (GE Healthcare Life Sciences, catalog # 17-6003-18), 1% pH 3-

11 NL IPG buffer, (GE Healthcare Life Sciences, catalog # 17-6004-40) and a trace of bromophenol blue (Sigma-Aldrich, catalog # B-6131) to visually confirm electrical conductivity through the individual strips during IEF. For fraction #6, which is believed to contain a relatively high percentage of lipids, the rehydration buffer was prepared as the buffer for fractions #1-#5, but 7 M urea and 2 M thiourea (Sigma-Aldrich, catalog # T8656-50G) was substituted for the 8 M urea [204], and 2% ASB-14 detergent (Calbiochem, catalog # 182750) was substituted for 4% CHAPS.

Approximately 9 hours before the protein labeling, the immobilized pH gradient (IPG) strips (24 cm Immobiline™ Drystrips, non-linear pH 3-11, GE Healthcare Life Sciences catalog # 17-6003-77) were rehydrated according to the manufacturer's instructions. Strips were thawed and placed gel-side down in 350 µL of rehydration buffer in a gel rehydration tray and covered with biotechnology grade mineral oil (Bio-Rad catalog # 163-2129). The strips were allowed to rehydrate for approximately nine hours at 4 °C.

To load the labeled proteins for the 1st dimension isoelectric focusing, each of the 3 matched 12 µl labeled and quenched labeling reactions (control, diseased, and internal standard proteins) were combined with each other and 114 µL of rehydration buffer was added to make approximately 150 µL total volume, for cup-loading. [6] Rehydrated IPG

[6] For approximately 80% of the designed experiment, three dye-labeled samples were added per gel, so approximately 36 µL of combined sample was mixed with 120 µL of rehydration buffer to be cup-loaded. When it was realized that the red dye was introducing a high amount of artifactual variation, use of this dye was discontinued, its data rejected and thenceforth only two dyes were used, ZBB for the internal standard and ZGB for both the control and diseased samples. For these gels, approximately 24 µL of combined sample was mixed with 130 µL of rehydration buffer.

strips were placed in the Ettan™ IPGphor II™ ceramic manifold (Amersham Biosciences) with the gel sides up and the paper electrodes (GE Healthcare Life Sciences catalog # 80-6499-14), each wetted with 125 µL of water, were emplaced on each end of the gels. Sample cups (GE Healthcare Life Sciences catalog # 80-6498-95) were emplaced at the cathodic end of each strip. The strips and electrode wicks were then covered with mineral oil. The 150 µL mixture of rehydration buffer and multiplex labeled proteins was added to the cup and covered with a few drops of mineral oil. Strip numbers were recorded to match with sample numbers.

The proteins were focused at 20 °C according to the following method (Table 10).

Table 10 Method for iso-electric focusing on IPGphor II.

	Step/Grad	Voltage (V)	Hrs or Vhrs?	Hrs/Vhrs
Step #1	Step	500	Vhrs	1000
Step #2	Gradient	1000	Hrs	2
Step #3	Gradient	8000	Hrs	3
Step #4	Step	8000	Hrs	2

All steps were limited in current to 50 uA per strip and kept a constant temperature of 20 °C by thermoelectric Peltier cooling of the IPGphor.

● *Preparation of gradient 2D-polyacrylamide gels.* To resolve the iso-electrically focused proteins in the 2nd dimension, 24 cm x 1.5 mm, gradient 9%-16% acrylamide gels were used. Prior to pouring gels, 5X Tris buffer (1.87 M Tris base-Bio-Rad, catalog # 161-0719) pH 8.8 was prepared by adjusting the pH with concentrated HCl (HCl-EMD chemicals, catalog # HX 0603-3). Also, gel casting plates with inserted paper labels were assembled in the Dalt II gel casting chamber (Amersham Pharmacia Biotechnology).

To prepare eight gels, the 9% and 16% buffered acrylamide solutions were prepared as follows. In two labeled 500 mL vacuum flasks, 5X Tris pH 8.8, 40% acrylamide (Bio-Rad, catalog #161-0148), MilliQ water, 50% glycerol (Sigma-Aldrich, SigmaUltra, catalog # G6279-1L) and 10% w/v ammonium persulfate ("APS"-Bio-Rad, catalog #161-0700) were mixed according to the recipe in Table 11.

Table 11 Buffered acrylamide compositions for 9%-16% acrylamide gels.

9% Acrylamide	Volume	16% Acrylamide	Volume
5X Tris	80 mL	5X Tris	80 mL
40% Acrylamide	90 mL	40% Acrylamide	160 mL
Water	240 mL	50% Glycerol	160 mL
10%APS (w/v)	670 uL	10%APS (w/v)	670 uL
TEMED	67 uL	TEMED	67 uL

The solutions were alternately degassed by creating a vacuum using a mechanical pump (Gast Manufacturing) and submerging the vacuum flask in a water bath sonicator (Branson model # 2510) for 10 minutes each while the other solution was refrigerated at 4 °C. When the solutions were degassed, the polymerization catalyst N,N,N',N',-tetra-methyl-ethylenediamine ("TEMED" Bio-Rad Laboratories, catalog #161-0800) was gently mixed in and the solutions were poured into the gradient maker (SG series-Hoefer Scientific Industries). In order to prevent non-uniform polymerization in the upper corners of the gels, the gel-casting chamber with assembled plates was gently flushed with argon and a thin layer of mineral oil was applied to the rim of the top opening to create a "gasket" with food-service film placed over the opening to prevent diffusion of the argon from the chamber. With both chambers of the gradient maker opened, the solutions linearly mixed, creating gels with an upper acrylamide concentration of 9% and bottom concentration of 16%, by using a peristaltic pump (Masterflex ® Easy Load ® II-

Cole-Parmer Instrument Co.) to fill the plates in the casting chamber. The setting for the flow-rate dial was 60 and the peristaltic tubing inner diameter was 0.25". The casting chamber required 10-15 minutes to fill. After pouring the gels, the fill tube was clamped shut to prevent the reverse flow of the solutions and approximately 1 mL of 0.1% SDS was applied to the top of each gel to impede capillary effects at the surface of the gel solution. The polymerized gels in glass plates were wrapped in food-service film and stored laying flat in 4 °C until the time of use.

● *Reduction and alkylation of the focused proteins.* Before running the 2nd dimension, iso-electrically focused proteins were reduced and alkylated to break intra-chain and inter-chain disulfide bridges. The IPG strips with focused proteins were each placed, gel side up, in channels of a 24 cm strip tray and 5 mL of reducing equilibration buffer was added to each strip. After gently rocking for 15 minutes in the dark (aluminum foil cover), the reducing buffer was poured off and 5 mL of alkylating equilibration buffer was added to each strip. This was also rocked gently for 15 minutes in the dark. The composition of the equilibration buffer was 6 M urea, 4% sodium dodecyl sulphate (SDS-Sigma-Aldrich, catalog # L3771-500G), 30% glycerol, and 50 mM Tris-HCl, pH 8.8. To make the reducing equilibration buffer; 0.1 gm of dithiotheitol (DTT-Bio-Rad catalog # 161-0611) was dissolved per 10 mL of equilibration buffer. To make alkylating equilibration buffer; 0.25 gm of iodoacetamide (IAA-Sigma-Aldrich, catalog # I1149-25G) was dissolved per 10 mL of equilibration buffer.

● *2D-polyacrylamide gel electrophoresis (PAGE) of focused proteins.* After the reduction and alkylation of the proteins, the strips were removed from the trays, drained

and carefully emplaced on the upper edge of the correspondingly labeled gradient gels. The strips were sealed in position by the addition of melted 0.5 % w/v agarose (Bio-Rad, catalog # 162-0100) dissolved in 1x running buffer (0.025 M Tris base, 0.192 M glycine, 0.1% SDS) with a trace of bromophenol blue. The assembled gels were inserted into a 24 cm PAGE tank (Ettan Dalt II-Amersham Pharmacia Biotechnologies) and "dummy" gels were inserted into any empty slots to equalize the current per gel from run to run. The tank was filled with 1x running buffer and the PAGE run was begun. The 2nd dimension PAGE was run at constant power of 1 watt (W) per gel for the first hour and 2 W per gel thereafter, until the end of the run. When the bromophenol blue dye-front had migrated to the bottom of the gels (18-25 hours), the plates were removed from the tank. The gels were removed from the plates and placed, 2 gels per container, in fixing solution (10% MeOH/7% acetic acid) and gently rocked for 5 hours with one change of fixing solution after 1 hour. After 5 hours the gels were placed in water until the time of scanning.

● *Fluorescent imaging of 24 cm 2D analytical gels.* The gels in water were immediately taken for fluorescent imaging on a Typhoon™ Trio scanner (GE Healthcare Life Sciences). After cleaning the platen with water and isopropanol, a gel was carefully placed directly on the scanner platen lengthwise (24cm) along the Y axis, and a small amount of water was added to its surface. A clean low-fluorescence glass plate was placed on top of the gel so that the gel-pressing feature of the scanner could be used without coming into direct contact with the gel.

In order to assure a quantifiable image with sub-saturating intensity for all the protein spots, it was necessary to adjust the voltage on the photomultiplier tube (PMT) to keep the most intense protein spot(s) below saturation for each scanned channel. To do this, the gels underwent a 2 step pre-scan. First, using a 500 μm resolution of the entire gel, the coordinates of the most intense protein spot(s) could be quickly located. Saturated spots appear red on the "real-time" image of the scan. Then, scanning just within those coordinates and using a 100 μm resolution, the appropriate voltage of the PMT was found by trial-and-error to produce images with sub-saturating intensity for that spot and therefore the entire image.

Using the PMT voltages determined from the pre-scans and consistent with the linear range of the scanner (400V to 700V), all gel images were scanned at 100 μm resolution. For scans of proteins labeled with ZBB blue dye (internal standard) the 488nm laser (argon) with an emission filter of 510 nm, bandpass 30 nm (Chroma Technology) was used. For scans of proteins labeled with ZGB green dye (control or diseased samples) the 532 nm frequency doubled (Nd:YAG, neodymium doped yttrium aluminum garnet) laser with an emission filter of 555 nm, bandpass 20 nm (Typhoon standard R6G filter). For scans of proteins labeled with HBO 187 red dye (control or diseased samples) the 633 nm laser (helium-neon) with an emission filter of 655 nm, bandpass 30 nm (Chroma Technology) was used. After scanning, the platen was cleaned with water and isopropanol prior to scanning the next gel.

Image data stored as .gel files by the Typhoon™ were imported into ImageJ image processing software (National Institutes of Health, v. 1.41o) and processed as

"stacks". This feature allows all files of identical file size and dimensions to be processed simultaneously and identically. The stacked images were cropped identically to exclude extraneous marginal regions and to reduce the file sizes. The "unstacked" files were saved as .tif files to be imported into the Progenesis™ software that was used for spot matching and quantification.

● *Spot matching and quantitation using Progenesis SameSpots software.* The cropped 2D-PAGE .tif image files were analyzed using Progenesis SameSpots software (Nonlinear Dynamics). All gels within a particular fraction, #1-#6, were warped to matched a representative "master" gel. Matching, after entering up to 50 "seed" landmarks, was automatic but were verified manually. After automatic spot detection and background removal, the images were edited manually using the spot adding, splitting and removing features of the software. Artifacts, or spots that could not be confidently verified as true matches, were removed from the analysis, and misalignments were corrected by manual warping by adding landmarks when appropriate.

● *Statistical Exclusion Criteria.* In order provide exclusion criteria for technical variation, only the spots that were accepted by the Progenesis software as significantly changed within each fraction (8 replicates of each sample type, $p < 0.05$, fold change $\geq$ 1.4) prior to averaging the 2 technical replicates in each pool, were taken forward for further consideration. The values for these spots were then transferred to an Excel spreadsheet and the 2 technical replicates within each of 4 pools for each sample type were averaged to produce 4 biological replicates for the control subjects and 4 biological replicates for the T2DM subjects within each fraction. The assumption of normal

distributions of the data was made. An ftest (Excel- "ftest" function) tested the null-hypothesis, namely, that the variances of the compared distribution of spot values were not different. The ftest returns the probability that the variances of 2 distributions are not significantly different. If the ftest calculated that the two compared sets of values had a greater than 50% probability that the variances were not different, then an unpaired ttest with equal variances was used. If there was a less than 50% probability that the variances were not different then an unpaired ttest with unequal variances was used. These spot values were then considered significantly changed ($\geq$ 1.4 fold change between groups) if the null-hypothesis of the unpaired t-test was rejected at 95% confidence ($p < 0.05$) comparing the 4 pooled biological replicates of non-diabetic samples with 4 pooled biological replicates of the diabetic samples. Gel images of the spots that met these criteria were further assessed for spot quality and alignment.

- *Colloidal coomassie staining and in-gel tryptic digestion of polypeptides.* Some proteins showing a significant change in expression were abundant enough that they could be detected and picked after colloidal coomassie staining of the multiplexed analytical gels and identified by mass spectrometry. But for most of the significantly changing proteins, their abundance was too low to see by this method and preparative gels were required, loaded with up to 10 of the reversed-phase fractions, to enable the visual detection of the coomassie stained spots. The preparative gels were prepared identically to the analytical gels, except for the combination of more fractions in the preparative gels than in the analytical gels, and the proteins were only labeled with one

fluorescent dye, ZGB. The gels were fluorescence scanned before coomassie staining to provide a reference image for spot picking.

To prepare 1 L of colloidal coomassie stain [230], immediately before use, 16 mL of 85% ortho-phosphoric acid (Fisher Scientific, catalog #A242-1) was added to 768 mL MilliQ water. 16 mL of a 5% coomassie brilliant blue G-250 solution (Fluka, catalog #27815) in MilliQ water was added to the acidic solution. Stirring rapidly, 200 mL of MeOH was very slowly added over approximately 10 minutes. Single gels were placed in 0.5 L of the staining solution and gently rocked overnight. Gels were destained with several changes of water until the background was removed.

The stained and destained gels were transferred to a clean light table in a HEPA-filtered, positive pressure, dust-free hood for spot-picking. The spots were picked using the fluorescent reference image to compare with the visible coomassie spot pattern, using a clean scalpel. The excised spots were diced into roughly $1mm^3$ pieces and placed in a low-retention 1.7 mL microfuge tubes (Axygen, Inc., catalog# MCT-175-L-C).

To prepare the gel pieces for digestion [231], they were washed by vortexing for 10 minutes with approximately 5 times their volume of 25 mM NH_4HCO_3 (Fisher Scientific, catalog #A643-500) in 50% acetonitrile. This was repeated, usually only once, discarding the supernatant, until the gel pieces were opaque, slightly shrunken and no longer blue. They were then speed-vacuumed or lyophilized to dryness. No reduction or alkylation was necessary at this point because the proteins were previously reduced and alkylated.

To digest the proteins, 1 µl of 1 µg/µl (previously prepared and stored at -80 °C) sequencing grade modified porcine trypsin (Promega, catalog #V5111) in 50 mM acetic acid was diluted with 100 µl 25 mM NH_4HCO_3. Enough of the trypsin solution was added to the dried gel pieces to just cover them and, if necessary, more was added after the pieces soaked up the solution to just cover them again. The digestion reaction was incubated at 37 °C for 8-12 hours.

To extract the trypsin digested peptides, approximately 3 times the gel volume of 50% acetonitrile/5% formic acid (Fischer Scientific, catalog # $A118^P$-500) was added. This was vortexed for 10 minutes and water-bath sonicated for 5 minutes. The supernatant was transferred to a low-retention 0.5 mL microfuge tube (Phenix Research Products, catalog # MAX-805S) and the extraction was repeated a second time. The two combined extractions were concentrated by speed-vacuuming to approximately 10 µl. This was stored at -80 °C until the time of mass spectrometric analysis.

● *Mass spectrometric analysis of polypeptide digests.* To identify proteins of interest from the 2DGE experiments, digested polypeptides from gels were either analyzed by matrix-assisted laser desorption ionization mass spectrometry time-of-flight (MALDI-TOF-Bruker Biflex) or liquid chromatographic tandem mass spectrometry (Agilent #6340 LC/MS/MS ion trap) using alternation of the CID/ETD modes for collision induced dissociation (CID) and electron transfer dissociation (ETD) so that both types of spectra were generated for each single sample analysis.

To prepare a sample for MALDI-TOF MS, a saturated solution of α-cyano-4-hydroxycinammic acid (ACHA) matrix was prepared by adding excess ACHA to 50%

acetonitrile/1% TFA and vortexing for 2 minutes. The solution was then centrifuged for 1 minute at 2000 rcf to pellet the solid ACHA. 1 µl of the digested protein solution, described above, was added to the MALDI plate (Bruker AnchorChip 384, catalog #209513 and 1 µl of the matrix supernatant was then mixed with the digested proteins with a 2 υL Pipetteman. A 1:1 combination such as this was found to generally yield a good result for moderately abundant (easily visible by coomassie staining) spots. This solution was dried in a 37° C oven. The dried crystal/peptide spot was then washed to remove salts by adding 2 µl of 0.1% TFA in water and aspirating 4-5 times with a Pipetteman. The crystals were then allowed to re-dry at RT before mass spectrometry.

For the MALDI-TOF MS, data was acquired using the method RP_0_2kDa_Peptidegetter.par. This method was initially developed by Dr. Rachel Neal for peptides less than approximately 2000 Da. It uses positive ion mode, matrix ion suppression of species less than 400 Da and pulse delayed ion extraction of 200 υs in reflectron mode. Internal calibration of the mass spectrometer was utilized whenever possible, using trypsin autolysis peptides.

Raw MALDI datafiles were imported into flexAnalysis (version 3.0 Bruker-Daltonik GmbH) software. The spectra were assessed for quality and peak lists comprising only the non-autolytic, monoisotopic peaks with signal-to-noise ratios (S/N) greater than 5 and m/z greater than 800 (Figure 62) were exported to an Excel spreadsheet. To filter out peaks that were non-specific m/z values, an exclusion list was compiled from multiple spectra from unrelated spots that included common m/z values. These are believed to be primarily trypsin autolysis peptides and matrix clusters [221]. If

trypsin autolysis peptides were recognized they were used for internal mass calibration. After these exclusion peaks were removed from the peak list, the refined peak list was submitted for mass fingerprint database searching.

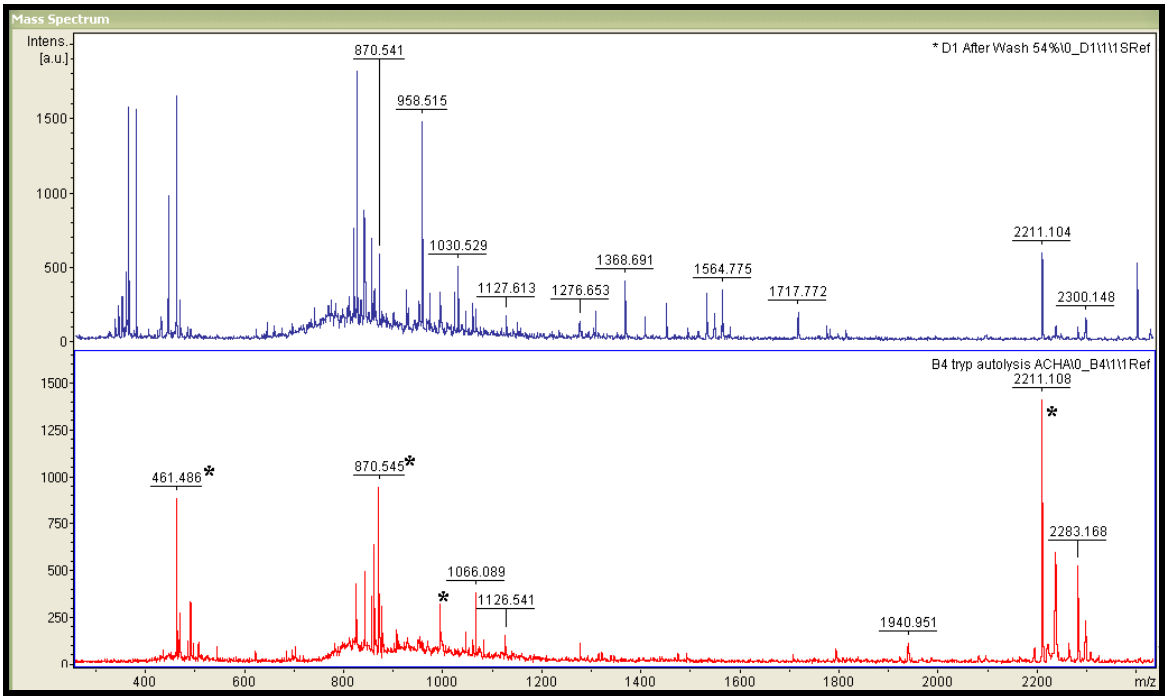

Figure 62 Top-Representative MALDI "mass fingerprint" spectrum-Zinc-α-Glycoprotein (ZAG) tryptic peptides. Bottom- MALDI spectrum of Promega methylated porcine trypsin and α-cyano-4-cinnamic acid matrix clusters. Peaks with asterisks were also found in the ZAG spectrum and those peaks with masses given in [221] provided a convenient means for internal mass calibration.

For the mass fingerprint database searches, the refined peak list was submitted to the MASCOT online search engine (Matrix Science Ltd.). The National Center for Biotechnology Information non-redundant (NCBInr) database was used for searches with Homo Sapiens as the selected taxonomy. One missed cleavage was allowed, using trypsin cleavage and a mass tolerance of 200 ppm. Because iodoacetamide was used to alkylate the cysteines during the 2DGE, the fixed modification, carbamidomethylated

cysteine, was chosen. Two allowed variable modifications were chosen: oxidized methionine and deamidated glutamine (Q) and asparagine (N) [208]. The peaks were submitted as monoisotopic, protonated masses (MH+).

As supporting evidence, in addition to MASCOT scores, nominal molecular weights and predicted pIs that were returned from the database searches were cross-checked against the actual positions of the respective spots in the 2D gels.

MASCOT returns a probability-based score after evaluating the probability that the number of "hits" and "misses" in the submitted peak list occurred by chance, considering the number of *in silico* peptides in the selected database search. The algorithm calculates an absolute score S, based upon the absolute probability P where S = - 10 Log (P) [232]. A score of 82 corresponds to the absolute probability, $10^{-8.2}$ that the observed match is a random event. However, considering the size of the selected database, the algorithm also calculates an objective significance threshold and expectation value, which it reports. Significance is, by convention, a value below 0.05. Table 13 shows the obtained results.

For the LC/MS/MS runs, the LC method parameters of "SL_121808_ETD_15minLC_Getter", include 2 υl autoinjections (Agilent) of the above-described digested protein solutions. These digests were automatically loaded onto an HPLC "nano-chip" (Agilent Technologies 40nL trap 75µm x 43 mm 5µm C-18SB-ZX, catalog #G4240-62001) using the HPLC-Chip/MS cube interface (Agilent #4240A). The LC gradient of mobile phase A (0.1% TFA, 5% ACN in MS grade water) and mobile phase B (0.1% TFA in ACN) was as shown in Table 12 with a stop time at 15 minutes.

A blank run of the same method was run between each sample injection to minimize cross-contamination of samples.

Table 12 LC method for ion trap with 43 mm chip LC.

	Time (min)	%B	Flow	Max. Pressure
1	0.0	0	0.6 ul/min	200 bars
2	10.0	75	0.6 ul/min	200 bars
3	11.0	100	0.6 ul/min	200 bars
4	12.0	100	0.6 ul/min	200 bars
5	13.0	0	0.6 ul/min	200 bars

The mass spectrometer data acquisition part of the method, SL_121808_ETD_15minLC_Getter, used an alternating combination of CID, in which b and y ion fragmentation predominates, and ETD, in which c and z ion fragmentation predominates in an attempt to gain additional sequence information from sometimes complementary sets of fragmented peptide daughter ions. The use of ETD requires a pre-run set-up procedure which is described in the Electron Transfer Dissociation User's manual, which is available online [224] and will not be described in detail here. Briefly, after the fluoranthene reagent heater is ignited the methane gas flow-rate, maximum ion accumulation time, MS/MS triggering threshold, and the "SmartTarget" parameter controlling the quantity of ions to be stored in the trap must be optimized daily to attain good resolution of the ions.

The ion trap parameters for the acquisition of ion data were previously part of a method that was optimized by an Agilent technician for trypsin digested peptides by using a target mass of 922 m/z. 922 m/z is an abundant value found in the calibration

mixture. The parameters described here have not been changed from the recommended "canned" method. Briefly, the general ion trap mode included a standard-enhancement, positive ion polarity, scanning in the range of 50-2200 m/z in a speed of 8100 m/z/s. No averaging of scans was used, by entering "1" in the "Averages" parameter, and the rolling average mode was disabled. Ion optics electrical settings were as follows: capillary: -1680 V (adjusted to yield ~ 90 nA with proper spray), end-plate offset: -500V, skimmer: 40.0V, cap-exit: 160.0V, octopole 1 DC: 12.00V, octopole 2 DC: 2.53V, trap: 96.2, octopole RF: 200Vpp, lens 1: -5.0V, lens 2: -60.0V. The dry gas was 325° C. with a flow-rate of 5.0 L/min.

The ETD parameters were optimized for the MS(n) acquisition. MS(n) was limited to n=2 (MS/MS). The number of precursor ions was set at "3" to trigger fragmentation, but the other threshold parameters were part of the daily pre-run set-up. Precursor ions below 300 m/z were excluded and active exclusion parameters were set to exclude precursor ions from MS(n) after accumulating 3 spectra within a 0.5 minute period. The MS/MS fragmentation amplitude was 1.3 V.

To pre-process the MS/MS data, the raw data were imported into DataAnalysis (Bruker Daltonics-version 3.3) and the line spectra were smoothed and baseline subtracted, using the default algorithms. The smoothing algorithm used a single cycle with a smoothing width of 0.2 m/z to produce Gaussian curves. The baseline subtraction used a flatness of 0.8 from a range of 0-1. A compound list was then compiled using the default autoMS(n) algorithm and the baseline-subtracted, smoothed compound list was exported as a Mascot generic file (.mgf) to an in-house Spectrum Mill server data

directory (http://sm.chemistry.montana.edu/msdataSM/Scott) to be analyzed by Spectrum Mill (SM) software (Spectrum Mill MS Proteomics Workbench version A.03.03, Agilent).

To process and run database searches on the .mgf files that were imported into the SM directory, a desired file was "selected" from the SM Data Extractor window. For the data extraction, the Agilent Spectrum Mill Application Guide [233] states that for data extraction, the fixed modifications are set according to the chemistry that was used to prepare the samples. Since our samples had been reacted with iodoacetamide between dimensions of the 2D gels, carbamidomethylation was chosen. The default settings of data extraction were retained, including: the fixed carbamidomethylation of cysteines, sequence tag length > 1, MH+ inclusion range from 600.0 to 4000.0 Da for MS/MS, scans with precursor m/z = $\pm$ 0.5 within $\pm$ 15 seconds were merged, maximum z = 7, and minimum S/N of MS was 25.

After data extraction, a database search was performed from the SM "MS/MS Search" page. The previously processed extracted data file automatically opens from this page. The validation filter setting was "spectrum-not-marked-sequence-not-validated". The default batch size of 81 was used. The maximum number of reported hits/search was 5. The search parameters were as follows: Database- "NCBInr", Digest- "trypsin", Species- "Homo Sapiens", Maximum # missed cleavages- "1", and "All" protein pIs were allowed. No required or disallowed amino acids were selected. The modifications that were chosen were: fixed carbamidomethylation of cysteines, variable deamidation of asparagine and glutamine [208], and variable oxidation of methionine [234, 235]. Under

"Matching Tolerances" the parameters were: Minimum scored peak intensity- "50%", Instrument- "Agilent ESI ion trap MIX-CID-ETD, Masses are- "Monoisotopic", Precursor mass tolerance- "$\pm$ 2.5 Da", Product mass tolerance- "0.7 Da", Maximum ambiguous precursor charge- "3". For "Spectral Quality" the parameters were: Sequence tag length- ">3", and Minimum detected peaks- "4". For "Search Mode", the "calculate reversed database scores" and "variable modifications" with a precursor mass shift range from "-18.0" to "177.0" Da was chosen. This is believed to represent the range of mass shifts resulting from a water loss (-18.0 Da) and oxyglycosylation (+177.0).

After the database search, the results were validated in the "Protein/Peptide Summary" page of SM. Validation of the individual peptides involved 2 quantitative criteria: peptide score and % scored peak intensity (%SPI). The %SPI is the percentage of the MS/MS peak-detected spectral ion current that is explained by that search interpretation. Agilent literature recommends that peptides with scores that are greater than 13, and with an %SPI of 70 or greater, are almost certain to represent valid results. Peptide scores between 8 and 10, (%SPI $\geq$ 70) generally represent good results but the spectra should be checked for quality. And peptides with scores lower than 6 seldom represent valid interpretations [236]. Agilent also recommends that, based upon the summation of the constituent peptides scores, valid proteins must have a cumulative score greater than 20 and comprise 2 or more distinct peptides. Even though 2 or more distinct peptides were required, the cumulative score for a protein may include multiple peptide scores from a single peptide, if multiple charge states of that peptide were detected. Also a peptide that was fragmented by both modes of fragmentation, CID and

ETD, would contribute both peptide scores to the cumulative protein score. Keratin peptides/proteins were excluded from consideration. The proteins identified by this method are tabulated in Table 14 of the Results and Discussion section of this chapter and details of the identifications are shown in APPENDIX A: Supplementary Figures.

Results and Discussion

The following figures (Figure 63-Figure 68) show representative gels from each of the fractions #1-6 produced by the previously described method. In each figure the top and bottom images are the same fluorescence image scan but the contrast is adjusted to show the lower abundance proteins in the bottom image. Protein spots that were identified as significantly changed between the sample types are enclosed in red ovals.

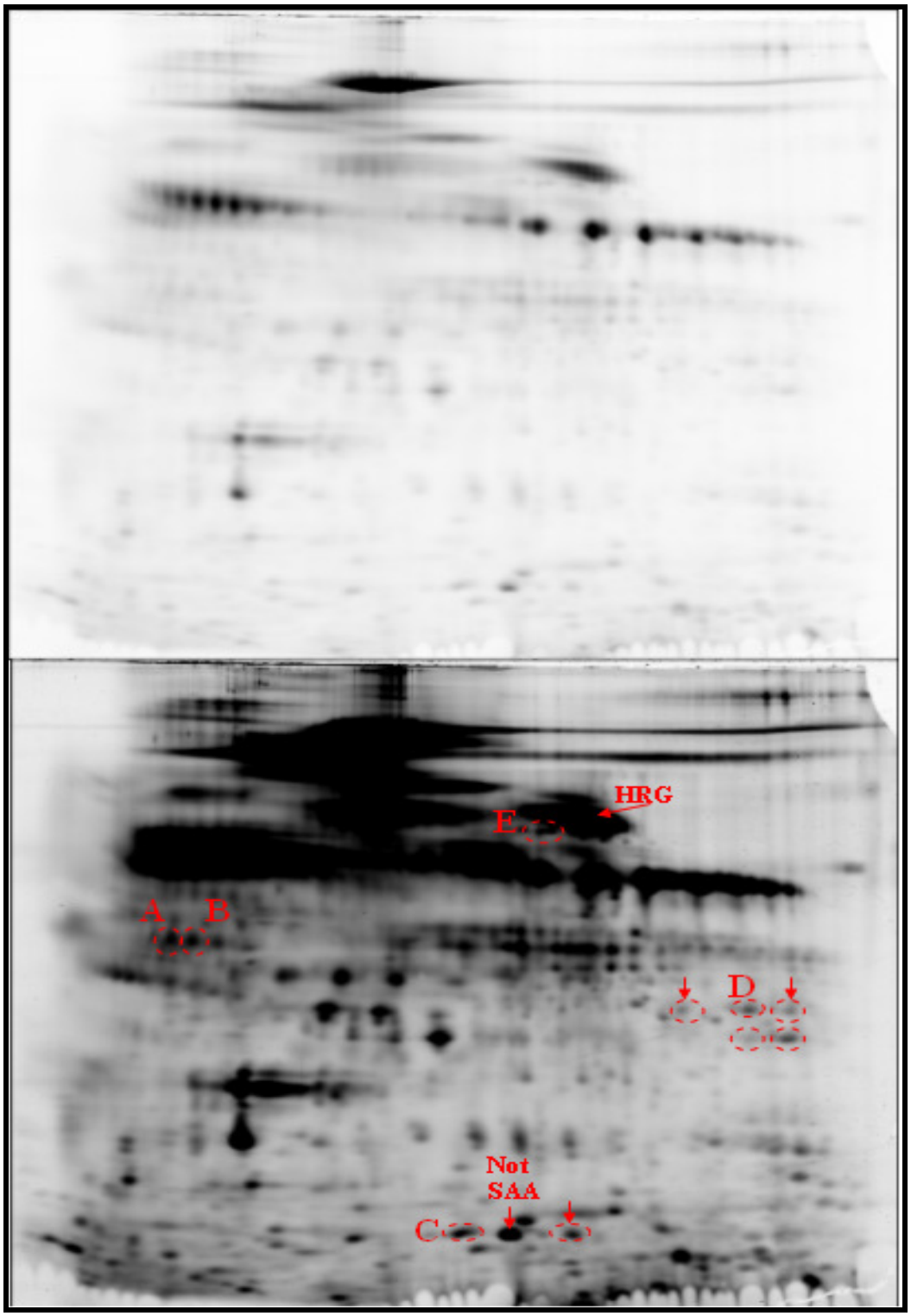

Figure 63 Representative fraction 1 gel image at low and high contrast settings.

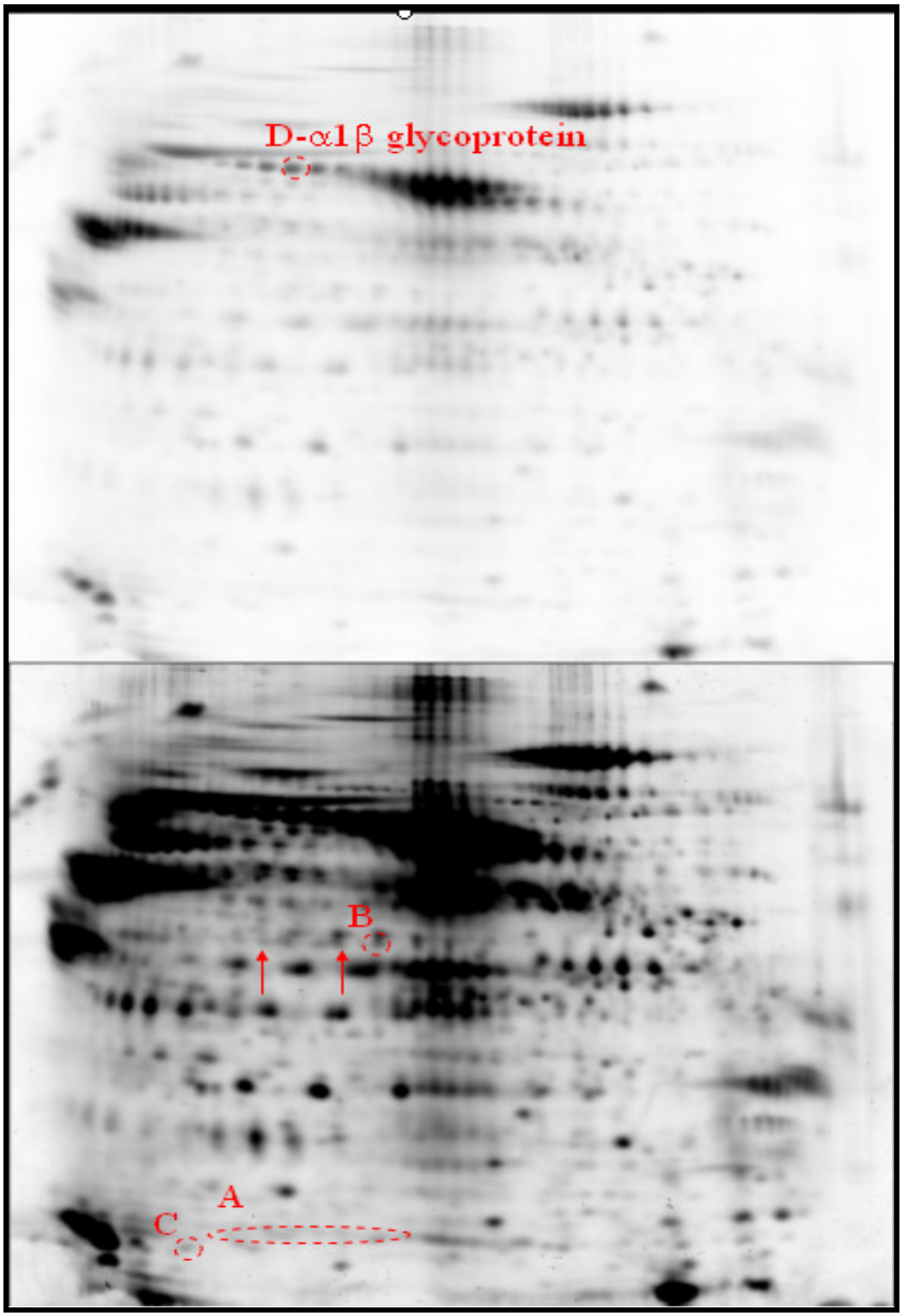

Figure 64 Representative fraction 2 gel image at low and high contrast settings.

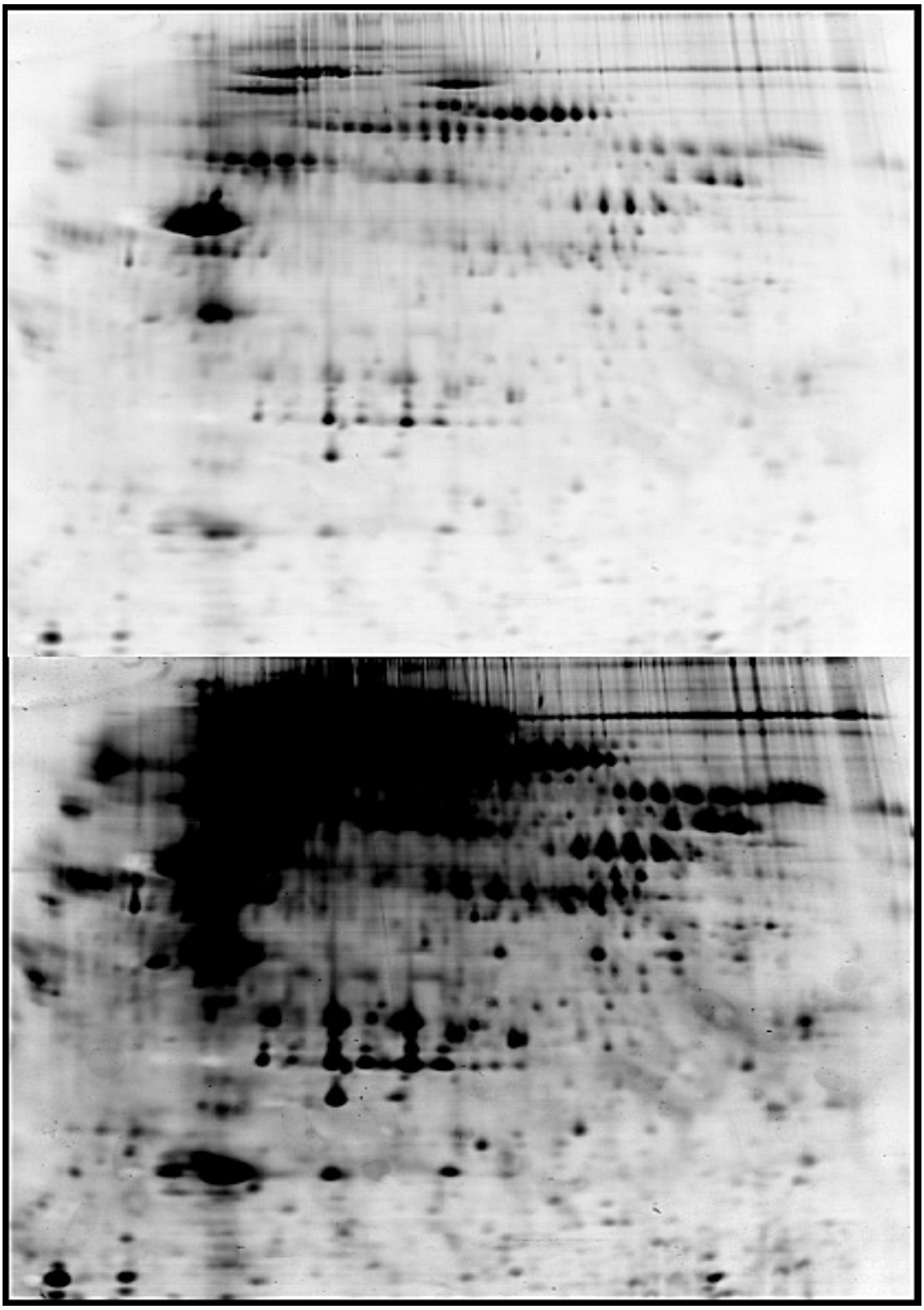

Figure 65 Representative fraction 3 gel image at low and high contrast settings.

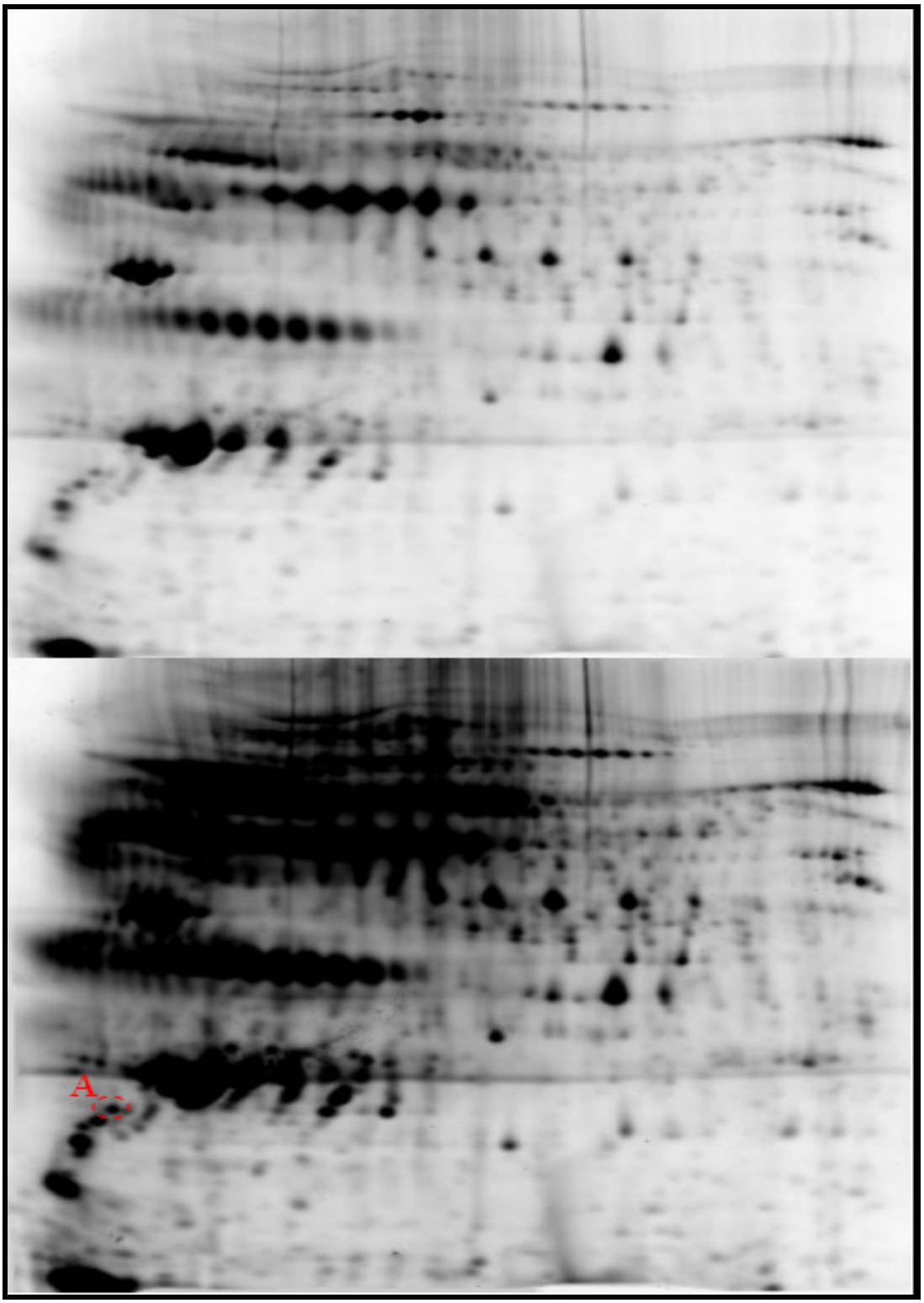

Figure 66 Representative fraction 4 gel image at low and high contrast settings.

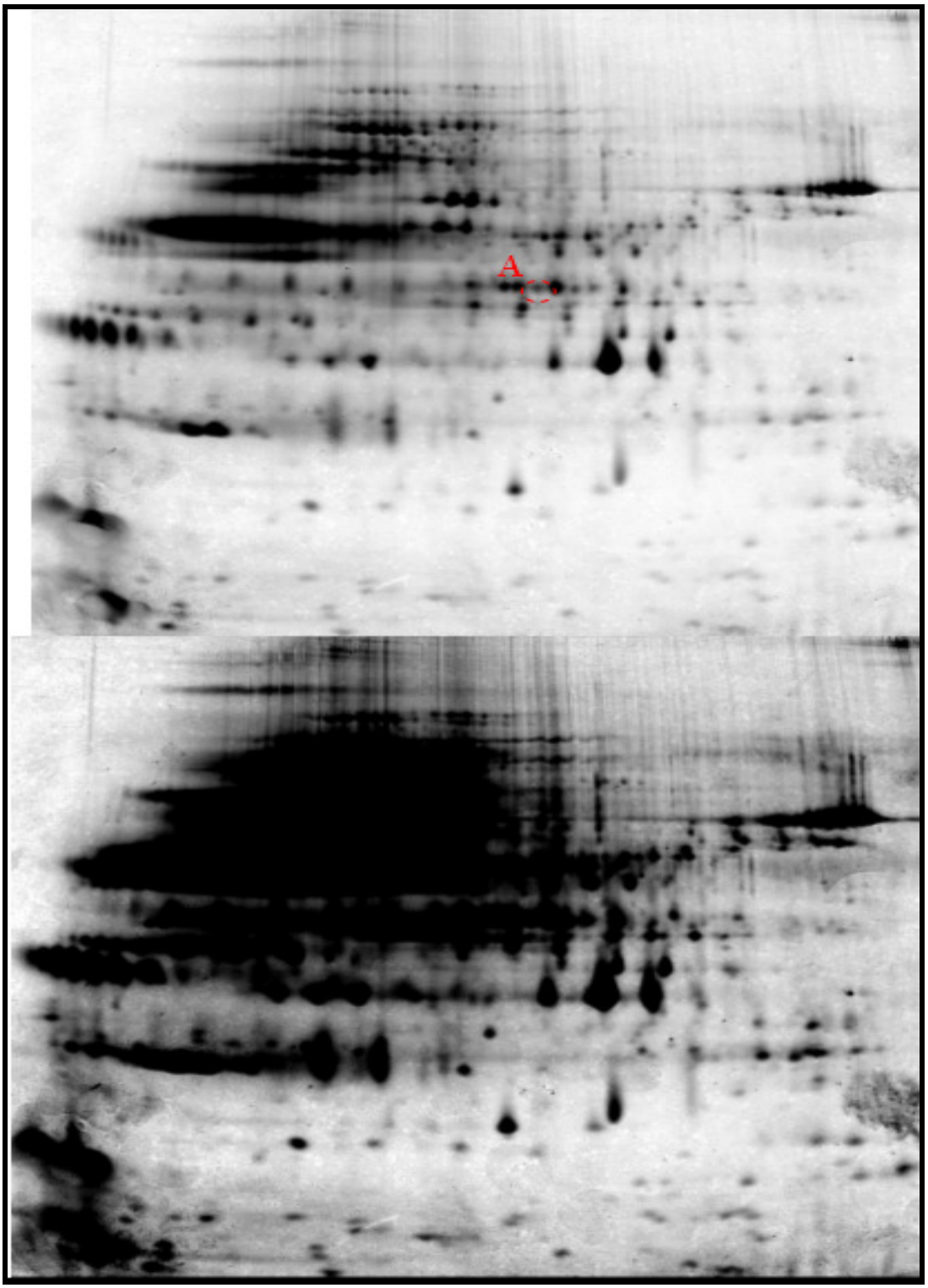

Figure 67 Representative fraction 5 gel image at low and high contrast settings.

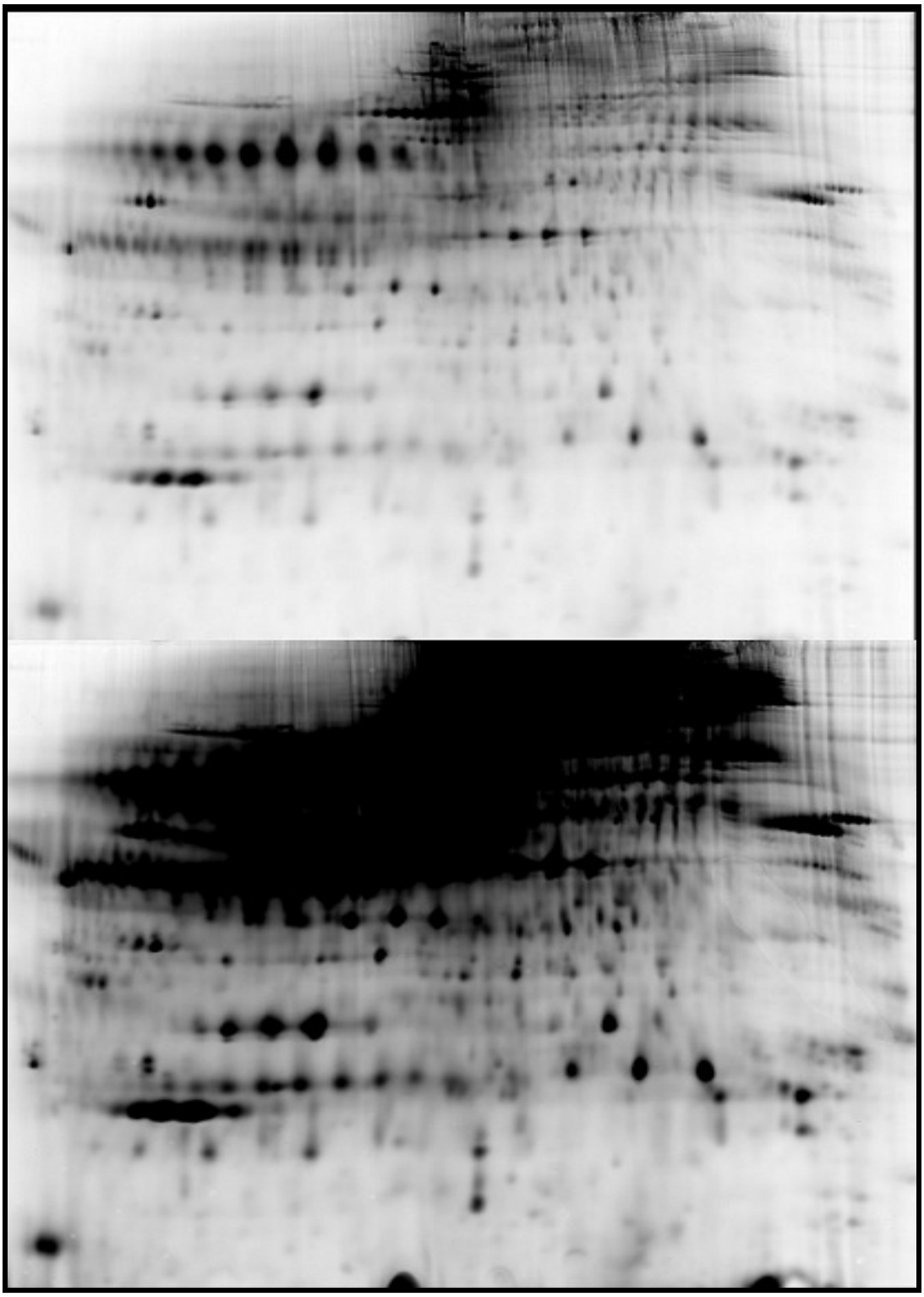

Figure 68 Representative fraction 6 gel image at low and high contrast settings.

Protein Identifications of In-Gel Digests-Table 13 shows the identities and MASCOT scores of differentially quantitated proteins that were submitted for MALDI MS. Table 14 shows the identities and Spectrum Mill scores of differentially quantitated proteins that were submitted for ESI tandem MS.

Table 13 MALDI MS/MASCOT protein identification data.

				MALDI		
MS File	Gel ID			MASCOT	Expect.	Masses
		Protein	Abbreviation	Score	Value	Matched
032408 D1	F1-A	Zinc-α-Glycoprotein (Chain B) Isoform	ZAG	82/66	0.0016	10 out of 22
032408 D2	F1-C	*Serum Amyloid A (1 Preprotein) Isoform	SAA	No Match	na	na
032408 D4	F1-E	Histidine-Rich Glycoprotein Precursor	HRG	70/66	0.021	9 out of 16

Table 14 ESI ion trap/ Spectrum Mill protein identification data.

			ESI MS/MS Scores > 13 %SPI=70			ESI MS/MS Scores > 9 %SPI=70					
			Distinct	Protein	%AA	Distinct	Protein	%AA	Database	Nominal	Nominal
MS File	Gel ID	Protein	Peptides	Score	Coverage	Peptides	Score	Coverage	Accession	MW	pI
			(>2)	(>20)		(>2)	(>20)				
011009_F1A	F1-A/B	ZAG	9	161.82	32	12	195.87	40	52790422	34244.9	5.71
031708A	F1-C	SAA1	4	85.68	40	4	85.68	40	40316910	13532.1	6.28
011009_F1D	F1-D	CRISP-3	4	73.84	19	4	73.84	19	5174675	27630.5	8.09
120308_A	F1-E	CFHR-5	4	64.04	8	8	106.41	18	13540563	64419.8	6.81
120308_A	F1-E	HRG	1‡	13.87	3	3	37.04	8	4504489	59578.6	7.09
092208A	F2-A	*HPT	13	238.79	43	13	238.79	43	3337390	38233.7	6.14
010909_F4	F4-A	Apo-AI	4	64.09	17	5	74.92	20	4557321	30778	5.56
		* Identified from unreduced preparative gel									
		‡ Not considered a sufficient protein identification									

In the center-right box of Table 14 are the distinct peptides, cumulative protein score and residue coverage for the indicated protein when the peptide scores are required to be over 9. The Spectrum Mill application guide [236] states that scores from 8-10 are generally good but that the spectra should be reviewed manually. In the center-left box

of Table 14 are the distinct peptides, cumulative protein score and residue coverage for the indicated protein when the peptide scores are required to be over as stricter criteria of 13. The Spectrum Mill application guide states that scores over 13 almost always represent valid results. The spectral details for each protein and protein coverage maps are given in APPENDIX A: Supplementary Figures.

● *Proteins of Interest (POI) from the 2D-PAGE experiment.* Following is a discussion of some of the interesting known properties of the POIs from the 2D-PAGE experiment.

● *Zinc-α-2-Glycoprotein (ZAG)* – The relative plasma concentration levels of the acidic, circled isoform of this protein, (Figure 63, fraction 1 gels, labeled "A") was found to be present at 1.4 fold lower concentration in the T2DM pools (Figure 69- "ZAG A"). The neighboring, more basic isoform, (circled, to the right of ZAG A in Figure 63, "ZAG B" in Figure 70) was also 1.4 fold down in the T2DM patients. For isoform ZAG A, a statistical f-test determined that there was a 32% chance that the variances between the two groups were not different. Because of the relatively low probability that the variances were similar, a two-sided t-test with unequal variances was used, which yielded a p-value of 0.04. For isoform ZAG B, an f-test score determined a 26% chance that the variances were not different. A two-sided t-test with unequal variances yielded a p-value of 0.03. As two-sided, t-tests with equal variances, the p-values were 0.03 and 0.02, respectively. The averaged values of ZAG A and ZAG B was down 1.4 fold in the T2DM patients. The f-test determined that there was a 33% chance that the variances between the two groups were not different. A two-sided, t-test with unequal variances

yielded a p-value of 0.02 for the averaged values. A two-sided, t-test with equal variances yielded a p-value of 0.01 for the averaged values. These p-values ($p < 0.05$) are considered statistically significant.

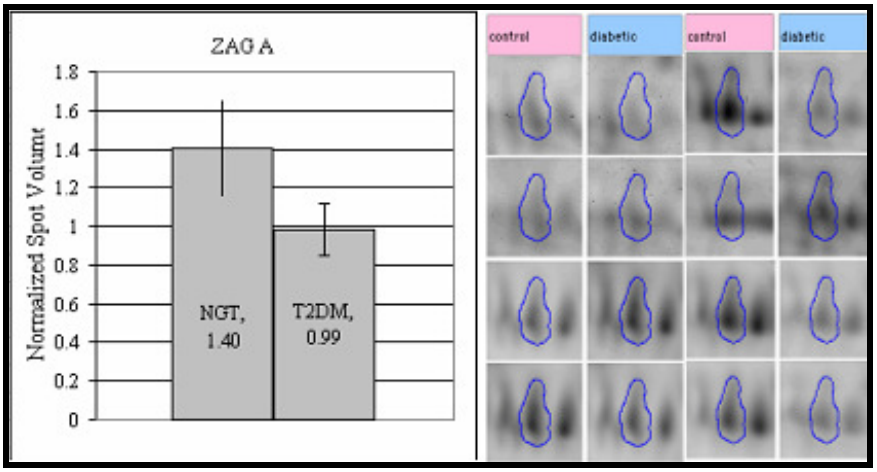

Figure 69 ZAG A relative expression histograms, expressed as pool averages ± standard deviation, and spot images from the fraction #1 gels.

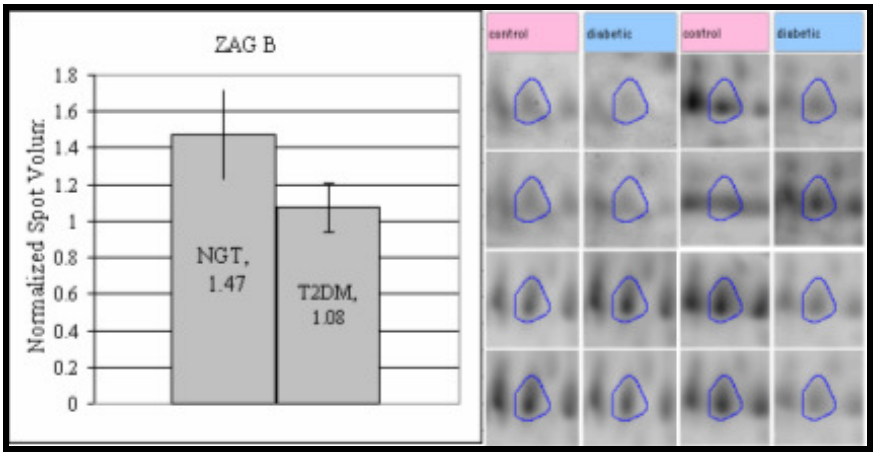

Figure 70 ZAG B relative expression histograms, expressed as pool averages ± standard deviation, and spot images from the fraction #1 gels.

ZAG has many features that make it potentially very interesting to diabetes research. An important recent finding supports ZAG as a new member of the family of adipocytokines along with leptin, resistin, TNF-α, IL-6 and adiponectin [237], having endocrine-like functions and showing changes in plasma concentration associated with obesity and possibly insulin resistance [237-239]. Also, it is the first of an unusually high percentage of POIs in this experiment that are known to be specific HSA binders [197]. Aspects of HSA binding will be discussed in greater detail as its own section below.

ZAG is a 40 kDa, single chain glycoprotein [240] that was originally purified from human blood plasma in 1961, by Buergi and Schmid, using its insolubility in the presence of added zinc ion [241], hence its name. These researchers showed that the experimental isoelectric point of the protein is between pH 3.8 and 3.9. Although much is known about the structure, location, and disease associations of ZAG, the specifics concerning its function are still unknown [237, 240]. ZAG has 30 – 40% amino acid sequence identity with the extracellular portions of major histocompatibility complex class I (MHC-I) heavy chains. ZAG is regarded as the only bona fide soluble MHC-I class protein, as it has no transmembrane sequences [242, 243]. The MHC-I like groove of recombinant ZAG doesn't bind peptides [244], but was found to bind exogenous polyethylene glycol (PEG) used in the crystallization process [245]. The ZAG groove is hydrophobic with an arginine cap, which is believed to confer it with endogenous fatty acid binding ability [240]. PEG also can displace fluorescently labeled lipid from the binding site [245].

In humans, the primary locations of ZAG in the body are the blood plasma and seminal fluid. The seminal ZAG has been proposed to have a role in fertility and is at a 6-fold higher concentration than in the plasma. Seminal ZAG is synthesized in the prostate. The typical circulating ZAG concentration is 1.5 μM [237], and is synthesized in the liver [240] and adipocytes [237].

ZAG is also known to be highly expressed by certain types of tumor cells. The overexpression of ZAG can lead to the general depletion of fat stores, a kind of wasting syndrome known as cancer cachexia [243]. This function of ZAG was discovered when a known tumor-associated lipid mobilizing factor (LMF), isolated from the urine of cancer patients [246], was shown to be identical to ZAG in its molecular weight (both intact and chymotryptic fragments), amino acid sequence, presence of carbohydrate, antigenicity and the *in vitro* ability to stimulate lipolysis in isolated murine adipocytes. ZAG was found to be the responsible agent for the fat-depleting activity of the cachexia, and is now believed to normally function regulating lipid degradation, which increases to a pathological extent in cachexia [243].

A study that compared homozygous ZAG KO mice [242] with wild type mice showed that the knockouts, while viable, fertile and displaying no grossly abnormal phenotype, had significantly ($p < 0.05$) more body weight. The excess body weight at 23 weeks was seemingly moderate, about 5% on a normal diet, and about 10% greater in mice on a high-fat diet. This weight gain was attended by a significant reduction of lipolysis in the adipocytes of the ZAG KO mice and was not a result of food intake, as there was no significant difference in food uptake between the groups. Also there was no

difference between the groups in their basal levels of glucose, triglycerides, insulin, FFAs, or leptin.

Recent research has come out of interest in ZAG's specific lipolytic activity and its possible role in human obesity and insulin resistance. One such study [247] explicitly investigated whether a ZAG ELISA could differentiate 132 healthy subjects from 92 subjects with metabolic syndrome. Even though the metabolic syndrome group had a significantly higher average BMI (healthy mean BMI= 23.9, MetSyn mean BMI= 30.3, $p < 0.01$) they found that ZAG was unable to discriminate the groups. They did find a modest correlation of ZAG with FPG ($r= 0.18$, $p < 0.05$).

Two recent studies on Spanish cohorts come to conflicting conclusions about the relationship between blood serum ZAG levels and BMI. In a study by Selva et al. [239] with a relatively wide range of BMIs, the comparison was made between a group of 10 non-obese subjects with 20 obese subjects (non-obese mean BMI=25.1, obese mean BMI=42.8 kg/m^2, $p < 0.001$). Serum ZAG did discriminate the groups ($p = 0.002$) and there was a negative correlation between BMI and serum ZAG concentrations ($r= -0.65$, $P < 0.001$). In this study, no correlation was found between ZAG levels and insulin resistance-related parameters. In a less obese group of 73 subjects with a BMI range of 23.1-32.6 kg/mg^2, Ceperuelo-Mallafre et al. [248] found that there was no correlation of circulating ZAG levels over the range of BMIs, but that there was significant correlation with parameters of insulin resistance, thus there seem to be large cohort effects, as are often seen in human studies.

Very recently it has been demonstrated *in vitro* that ZAG mRNA expression by human adipocytes is down regulated (> 2-fold, $p < 0.01$) by 24 hour exposure to macrophage conditioned (MC) medium [249]. ZAG release by the adipocytes was down regulated (by 47%, 0.001), by 48 hour exposure to the MC medium. The researchers showed that ZAG mRNA expression by the adipcytes was completely recovered by the addition of anti-TNF-α antibodies.

Interestingly, ZAG levels were also found to be changed in a 2008 T1DM global proteomics study by Metz et al. [250] at Pacific Northwest National Laboratory. No mention was made as to the relative BMIs for the subjects in this study (all subjects were under 30 years old, 10 newly diagnosed T1DM and 10 non-diabetic controls). Metz used MARS-6 (Agilent Industries) immunodepleted plasma of T1DM and non-diabetic controls, and a "bottom-up" approach (in which complex protein samples are first digested and the peptides are quantified by their MS peak intensities), to deduce the relative protein quantities. Estimating protein-level relative abundances as the median value of peptide relative abundances for all peptides originating from a given protein, Metz et al. found 5 proteins ($\geq$2-fold change, t-test $p < 0.05$) evidenced by at least 2 unique peptides (t-test $p < 0.1$) that were changed between patients and controls. Perhaps the point of greatest interest is not that they also found ZAG changed, but that they found it up 2-fold in type-1 diabetics, whereas we saw it down 1.4-fold in type-2 diabetics. However, Metz suggested that ZAG may have been elevated in the diabetic group because they were newly diagnosed and may recently have been ketotic, a situation

where ZAG would be deployed to mobilized fatty acids for energy production. T1DM and T2DM are very different diseases, to be sure.

In the present experiment, there was a possible trend but not a significant correlation between the 8 pool-averaged, (4 T2DM, 4 NGT) normalized spot volumes for ZAG A and 8 pool-averaged BMIs, r = - 0.66, P=0.075, using n-2 degrees of freedom (dF). Using the average normalized spot volumes of the two ZAG isoforms yielded P=0.063. Table 15 shows the pool averaged BMIs, the averages of which do not reach significant difference (p = 0.06) between the experimental groups.

Table 15 The two-tailed, unequal variances, t-test for the BMIs, p=0.06.

	Pool #	Av. BMI	Group Av.	StDev
NGT	1	25		
	2	26		
	3	24		
	4	25	25	0.9
T2DM	1	38		
	2	28		
	3	29		
	4	39	33.1	5.7

Notwithstanding the apparent ability of ZAG to bind zinc ion, no evidence that ZAG is involved in the transport of circulating zinc, which is also down in T2DM [120], nor of any connection between ZAG and research involving intracellular zinc as a regulator of pancreatic islet function, [251] was to be found in the literature. It would be desirable to investigate the correlations between ZAG and the metabolic parameters of T2DM in a larger cohort of subjects.

● *Serum Amyloid A 1* (SAA1) *preprotein* - The relative plasma concentration levels of SAA1 preprotein, (Figure 63, fraction 1 gels, labeled "C") was found to be 1.8 fold higher in the T2DM pools (Figure 71). The standard deviations of the experimental groups appeared similar, and an ftest calculated that there was a 76% probability that the variances were not different, so a two-tailed t-test with equal variances was used, which yielded a p-value of 0.008. The relatively dark protein spot to the right side of SAA1 preprotein (labeled "not SAA" in Figure 63) was suspected of being an unchanging isoform of the same protein and was tested by in-gel digestion and MS identification. However, the spot to the right didn't yield any SAA peptides. Another weak spot further to the right of SAA (labeled with an arrow in Figure 63) was also changing (2.1-fold, p = 0.02 with unequal variances). This is likely to be an isoform of SAA1, but unfortunately, because of its relatively low abundance, the spot could not be accurately located in the

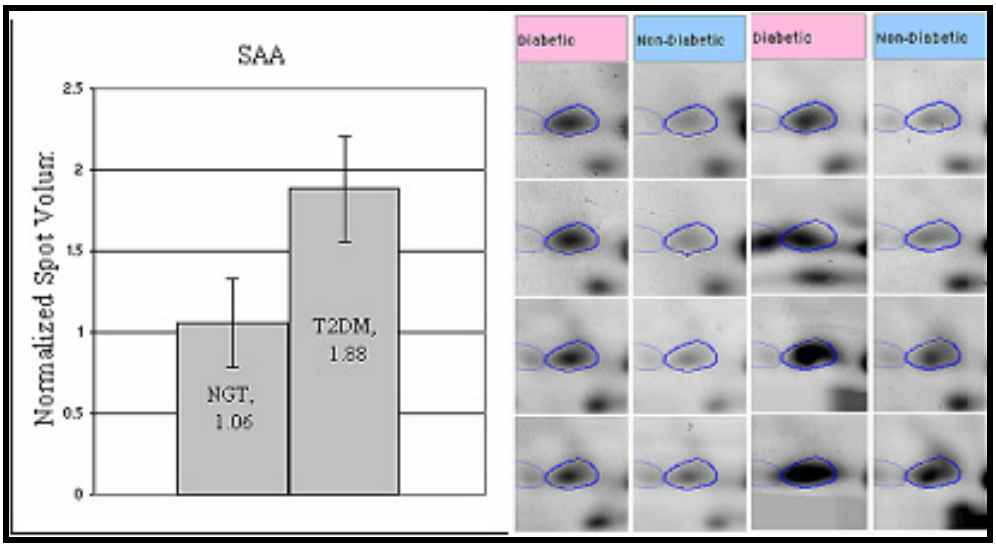

Figure 71 Serum amyloid A-1 preprotein relative abundance histogram, expressed as pool averages ± standard deviation and spot images from the fraction #1 gels.

preparative gel of F1, and no SAA1 peptides were identified from gel pieces estimated to be from its region.

In humans, the serum amyloid A (SAA) family comprises 3 differentially expressed apolipoproteins, two of which are acute-phase SAAs (SAA1 and SAA2) [118, 252] and which share greater than 90% sequence identity [118]. Most of SAA1 and SAA2 are bound to high density lipoprotein (HDL) in the circulation [252]. The third SAA (SAA4) is constitutively expressed in several tissues and shares 53% and 55% identity with the acute phase SAAs [252]. SAA3 is a gene with no known mRNA or protein [118].

The acute phase response is part of the innate immune response [120] and is characterized by a set of immediate inflammatory reactions that ameliorate acute challenges to the host, such as trauma and infection. Although most pronounced in acute episodes of inflammation, the acute phase response also accompanies chronic inflammatory disorders [1]. The acute phase response induces a cascade of inflammatory mediators, initiated through activated blood monocytes and tissue macrophages, which act on the local vasculature, as well as systemically.

The most important primary inflammatory mediators are proteins of the interleukin-1 (IL-1) and the TNF cytokine families [118] (see the earlier section Inflammation and Insulin Resistance in Adipocytes in INTRODUCTION TO TYPE II DIABETES). These inflammatory mediators begin a cascade of secondary cytokines and chemokines from local stromal cells, attracting neutrophils and other leukocytes to deal with the initial intrusive stimulus, the cellular debris and to reinforce the pro-

inflammatory cytokine cascade [118]. Systemic effects include biosynthetic changes in the expression profiles of circulatory proteins that often originate in the liver. The acute phase SAA proteins are mainly produced by the liver under the regulatory influence of the inflammatory cytokines IL-1 and TNF-α [253] and the SAA proteins have been called the "major vertebrate acute phase reactant" [118] .

C-reactive protein (CRP) is the most clinically monitored circulatory acute-phase protein. It was discovered in 1930 by Tillett and Francis as a species in the plasma of patients with pneumonia that reacted with a newly discovered fraction (fraction C) of carbohydrate from pneumococci [254]. The circulating concentrations of both CRP and SAA can increase up to 1000-fold [255] during the time of acute response, such as in response to infection or tissue injury [256]. Although concentrations of the multiple components of the acute phase response often correlate in expression with each other, (or

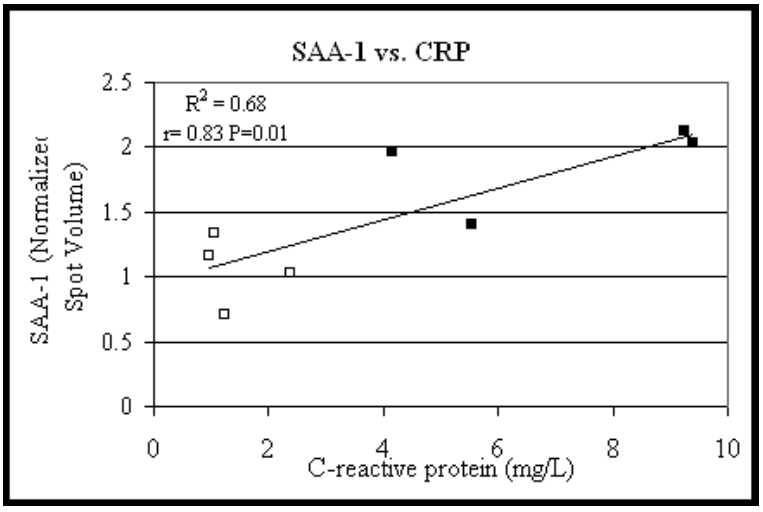

Figure 72 The correlation of the 8 pooled SAA normalized spot volumes with the 8 pool averages of C-reactive protein, from the NIH measured metabolic parameters-Table 5 (P = 0.01, dF =6). Open boxes (□) represent NGT samples and the closed boxes (■) represent T2DM samples. Average CRP values are NGT-1.4 ± 0.6 mg/L, T2DM-7.1 ± 2.6 mg/L, p = 0.006.

in the case of negative acute-phase reactants, anti- correlate), not all of them are in concordance in all patients with the same illness [1]. Figure 72 shows the positive correlation of the SAA normalized spot volumes from the pooled samples of the 2D-gel experiment with the pool averages of the NIH measured values of CRP ($r = 0.83$, $P = 0.01$). This correlation matches very well with a 2000 study by Ridker et.al [257] that had a correlation coefficient of $r = 0.81$ between CRP and SAA in 366 women. Although closely correlated in Ridker's study, only CRP, and not SAA, was found to be an independent predictor of future cardiovascular disease. The acute phase SAA proteins are the precursors of the amyloid A (AA) protein which is the main component of amyloid deposits found in several disorders known as the amyloid A amyloidoses [252]. These amyloidoses are complications of chronic systemic inflammation in which the levels of plasma SAA are consistently high, although the mechanism that determines the sites of deposition are unknown [252]. Rheumatoid arthritis and tuberculosis are two examples of the clinical consequences of chronic and recurrent acute inflammation, respectively, and both involve amyloid depositions [118]. The predominant amyloid protein species that is found in the amyloid deposits is the 8 kDa, 76 amino acid, N-terminal cleavage product of the ~12 kDa SAA protein [118, 258], thus the identified SAA-1 is called the "preprotein" form. The 8 kDa species, if it is present in plasma, is not likely to be well resolved on standard 2D gels.

As a side note, there is a progressive pancreatic amyloidosis found in T2DM that appears to be unrelated to the SAA protein. The pancreatic fibril component that is often

found in T2DM is a 37 amino acid peptide known as the islet amyloid polypeptide (IAPP or amylin) [259].

The precise role of SAA is still largely unknown [1, 255]. Recent research on acute phase SAA has been directed on its reported pro-inflammatory/immune-related functions and its lipid transport/metabolism-related functions.

First addressing its immune related functions; SAA has been shown to induce extra-cellular matrix degrading enzymes that are important for tissue remodeling after injury [253]. Acute phase recombinant SAA1 (rSAA1) has chemoattractant activity for immune cells, including monocytes and leukocytes, at concentrations corresponding to those found during the acute phase (>0.8 υM), as shown by *in vitro* studies by Badolato et al. [255]. Also, rSAA1 was shown to induce significant infiltration by monocytes and polymorphonuclear leukocytes *in vivo* into the tissue around the injection sites in the dermis and adipose tissues of BALB/c mice, which was not detected when only HDL in medium was injected [255] .

A 2007 study by Hatanaka et al. [260] compared the plasma SAA levels by ELISA in 18 treated and untreated T2DM patients with 20 age and BMI matched non-diabetics. The T2 diabetics had been treated by diet or oral hypoglycemics for at least 10 years. The plasma concentrations of SAA in the T2 diabetics was 3.4 ± 1.2 υg/mL vs. 1.2 ± 0.3 υg/mL for controls ($p < 0.001$). This ratio of SAA in T2DM to controls is 2.8-fold, a higher value than the 1.8-fold measured in our 2D gel experiment (Figure 71). This higher value they found may be related to the longer duration of the disease, as the subjects in our 2D gel experiment were newly diagnosed and untreated. But, as will be

seen in the discussion below, no relation of SAA with the duration of T2DM was found in a larger study [261].

Hatanaka also compared the *ex vivo* secretion of several cytokines from neutrophils and monocytes, including: proangiogenic and chemotactic interleukin-8 (IL-8), pro-inflammatory interleukin-1B (IL-1B), TNF-α, and interleukin-1 receptor antagonist (IL-1ra) [260]. It was shown that the cytokine secretions from both cell types significantly increased not only if the cells were stimulated with 17 μg /mL rSAA but also if the cells had been purified from T2DM patient's blood. Figure 73A shows the relation with SAA for two of the tested cytokines IL-1B (top) and TNF-α (bottom). The bar graphs in Figure 73A on the left of each figure for neutrophils and monocytes, labeled "spontaneous" represent the supernatant cytokine concentrations that were not stimulated by SAA. The bar graphs on the right of each half Figure 73A are SAA stimulated cells. Additionally, the cross-hatched regions represent the concentrations of cytokines secreted

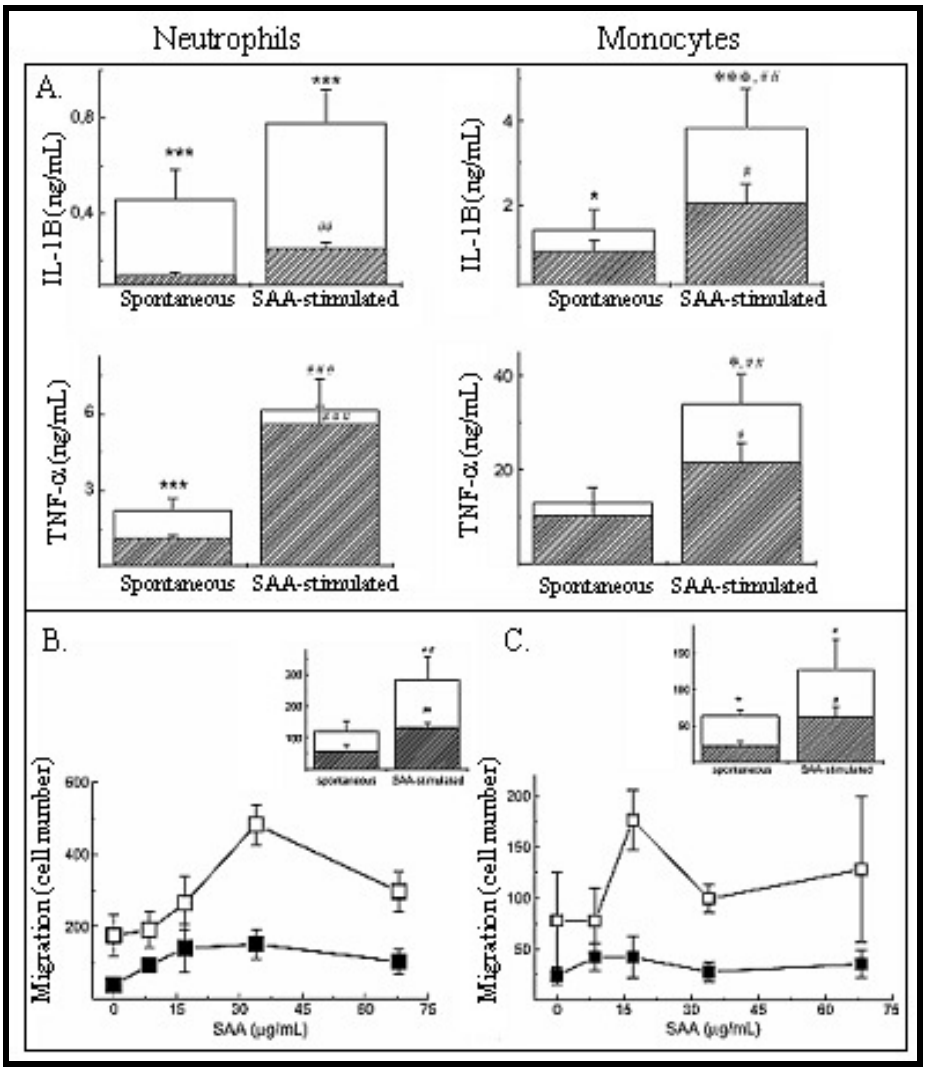

Figure 73 A) SAA induction of cytokine secretion from cultured neutrophils and monocytes of non-diabetic (cross-hatched) and T2 diabetic (white) subjects. B and C) SAA concentration dependence of neutrophils and monocytes from T2 diabetics (white boxes) and non-diabetics (black boxes). * $p < 0.05$, **$p < 0.01$, *** $p < 0.001$ for comparisons between cells from diabetics and non-diabetics. # $p < 0.05$, ## $p < 0.01$, ### $p < 0.001$ for comparisons between the SAA-stimulated and spontaneous cytokine release. Modified from Hatanaka et al [260].

from cells of the non-diabetics, and the white regions represent the additional concentration secreted by the cells from T2DM patients. The symbols regarding the significance of the differences are explained in the caption.

Hatanaka also investigated the migration of neutrophils and monocytes, using 96-well chemotactic plates to measure cell migration through a membrane toward varied concentrations of SAA. Figure 73B shows the SAA concentration dependence of diabetic (white boxes, n=5) and non-diabetic (black boxes, n=5) neutrophil migration. Figure 73C shows the same experiment for monocyte migration. The inset figures show the mean + S.E.M. of 15 non-diabetics and 15 T2DM at a fixed concentration of SAA (30 μg /mL).

These results were interpreted by Hatanaka as indicative of "hyper-responsiveness" of the diabetic leukocytes to SAA, in relation to their production of cytokines and cellular migration. Specifically, they stated that the link between the hyper-responsiveness of neutrophils and SAA concentrations may be important to understanding the progression of diabetes, especially with regard to the stimulatory effect of IL-8, TNF-α and IL-1B on endothelial cells. The activation and proliferation of endothelial cells has been shown to be strongly related to vascular complications in diabetes [260]. Additionally the increased production of cytokines is related to insulin resistance, central obesity and hypertension [260]. Thus, Hatanaka proposed the "activation axis" scheme in Figure 74 to model SAA's potential role in a feedback loop with leukocyte activation, release of cytokines and the progression and complications of diabetes. This figure also shows a linkage of SAA to the amyloidosis of the pancreas, but there was little explanation as to how this could arise. It is not likely to occur as a plaque

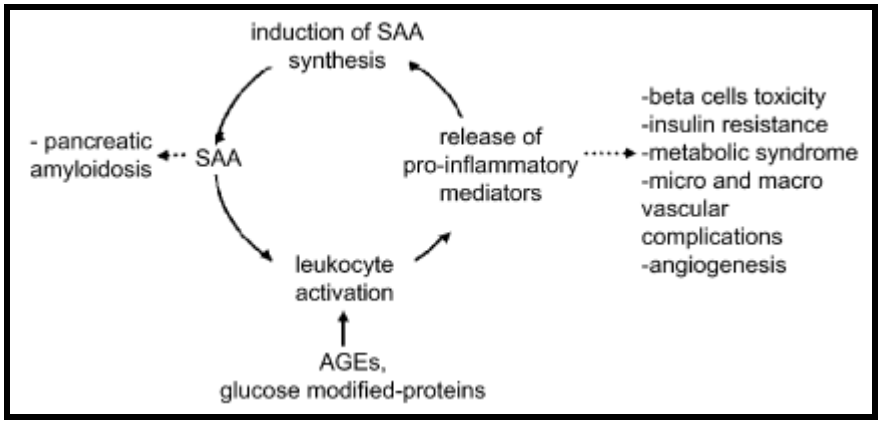

Figure 74 Hatanaka's SAA "activation axis" scheme, from [260].

of AA protein, but may arise from the cytotoxic effect of SAA induced, inflammatory IL-1B preferentially binding to the pancreatic B-cells [262, 263].

Regarding SAA's role in lipid metabolism, it has been shown that 90% or more [258] of the SAA apolipoprotein associates with HDL in the blood and that SAA dissociates apolipoprotein A-I (apo A-I) from HDL in the process of acute phase response [264, 265]. This process of changing equilibria of the exchangeable apolipoprotein components is called HDL "remodeling" [264]. HDL particles containing apo A-I are the most efficient reverse transport (efflux) agents for cholesterol from the periphery to the liver for catabolism [264]. Thus, SAA may have a deleterious effect on HDL's anti-atherogenic properties, but the relative roles of the individual exchangeable apolipoproteins to cholesterol efflux are controversial.

Total blood concentrations of the primary HDL constituents, apo A-I and apo A-II lipoproteins, have clearly been shown to be protective against heart disease and have an inverse relationship to the risk of myocardial infarction [266]. The apolipoproteins are

structural constituents of the HDL particle and are beneficial independently of whether they are associated with HDL or not [267]. However, the relative contributions of the subfractions of HDL to this cardio-protective benefit are unknown [267]. The relative concentrations of total HDL, as measured by NIH, in the 12 NGT samples were significantly higher (1.5 fold, $p = 0.03$-unpaired, 2-tailed ttest) than the 8 T2DM samples. This point will be discussed in more detail in the discussion on the POI, apo A-I fragment, below.

A 1995 study by Banka et al. showed a decrement in the ability of HDL to transport cholesterol at high levels of apo A-I displacement from HDL by SAA *in vitro,* but only when 50% or more of the HDL was constituted of SAA [264]. The SAA level employed in this experiment was too high to be of biological relevance except in extreme cases of acute phase response when the composition of HDL could reach 80% SAA [264].

The study by Pickup et al. [119] that was discussed in the section Inflammation and Insulin Resistance in Adipocytes of INTRODUCTION TO TYPE II DIABETES and summarized in Figure 29, showed that SAA was associated with T2DM ("NIDDM") independently of the metabolic syndrome ("syndrome X") status of the patients. SAA has also been found in elevated concentrations in T2DM in a larger study by Kumon et al. [261]. This 1994 ELISA study compared the fasting plasma SAA levels in 105 treated and untreated T2DM patients with 91 matched non-diabetics. The T2 diabetics had 2.1 ± 1.3 μg /mL vs. 1.2 ± 0.5 μg /mL for controls ($p < 0.001$). This ratio of SAA in T2DM to controls is 1.75, in excellent agreement with the value of 1.8 that was measured in our 2D

gel experiment (Figure 71). Kumon found no difference in concentrations of SAA between groups of T2 diabetics, depending on the duration of T2DM, FPG, Ha1c levels, grade of retinopathy or the treatment strategies including: diet alone, sulfonylurea, or insulin. However, a significant increase of SAA associated with increased urinary albumin ($p = 0.027$) was found.

- *Cysteine-Rich Secreted Protein-3 (CRISP-3)* - The relative plasma concentration levels of a CRISP-3 isoform, (Figure 63, fraction 1 gels, labeled "D") was found to be 1.5 fold higher in the NGT pools (Figure 75). Additional isoforms to the left and right of the POI (identified by arrows in Figure 63) also yielded strong CRISP-3 identifications and were also higher in NGT but not significantly so. An additional spot

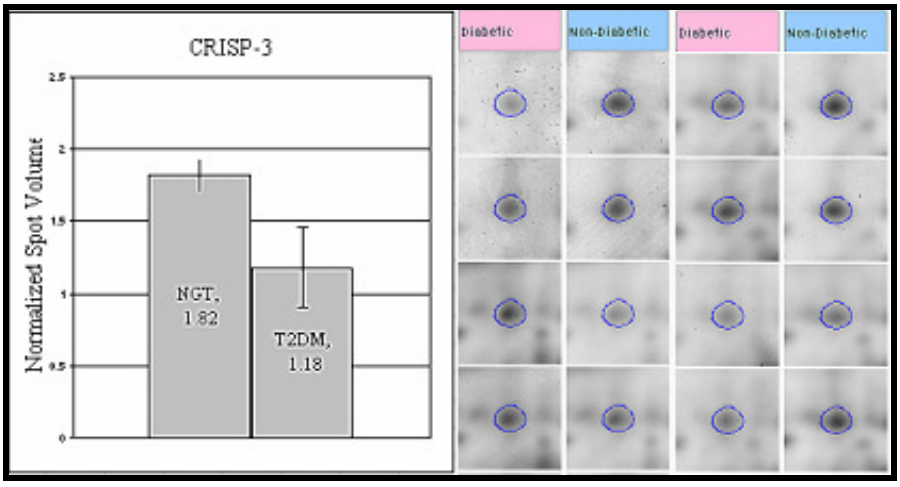

Figure 75 CRISP-3 relative abundance histogram, expressed as pool averages ± standard deviation and spot images from the fraction #1 gels.

of lower M_r also yielded CRISP-3 peptides. This isoform is identified by arrows below and to the right of CRISP-3 spot "D". The lower M_r spots may represent non-glycosylated forms and have MW that is approximately 2 kDa lower. A similar mobility

shift has been affected experimentally by N-glycanase in CRISP proteins expressed by neutrophils, [268] and the circulatory CRISP protein [269] implying the presence of N-linked oligosaccharides. None of the other isoform or presumed glycoform spots showed significant differences between the experimental groups. An f-test of CRISP-3 spot "D" determined that there was a 19% chance that the standard deviations were not different, so a two-sided t-test with unequal variances was used, which yielded a p-value of 0.013. A two-sided t-test with equal variances yielded a p-value of 0.006.

The neighboring fraction, F2, gel image shows several spots in the region of similar pI and MW as the CRISP-3 proteins in F1. A search for a spot pattern in F2 with similar pIs and M_r s to match the pattern of CRISP-3 isoforms in F1 found no counterparts that would indicate that the measured difference of concentration might be an artifact of a variable HPLC fraction cutoff. Also, no spots in this region showed differences in expression that reflected a complementary concentration change to those seen in F1, between the diabetic and NGT samples which, if found, would have indicated that the observed changes may have been caused artifactually.

The 3 member human CRISP subfamily is a member of the **C**RISP, **a**ntigen 5, and **p**athogenesis-related 1 proteins (CAP) superfamily [270] that have been found in insects, fungi, plants, mammals, nematodes, yeast and reptiles [271, 272]. Members of the CAP superfamily share signature CAP motifs, a CAP domain and a variety of C-terminal extensions. Figure 76 shows a selection of mammalian CAP superfamily members, including the CRISP subfamily, emphasizing the shared CAP motifs and C-terminal extensions. It has been suggested that the structural conservation among CAP

members results in fundamentally similar functions for all the members and that the diversity outside of the core region alters the target specificity and, as a result, the biological consequences, although these are currently unknown [270].

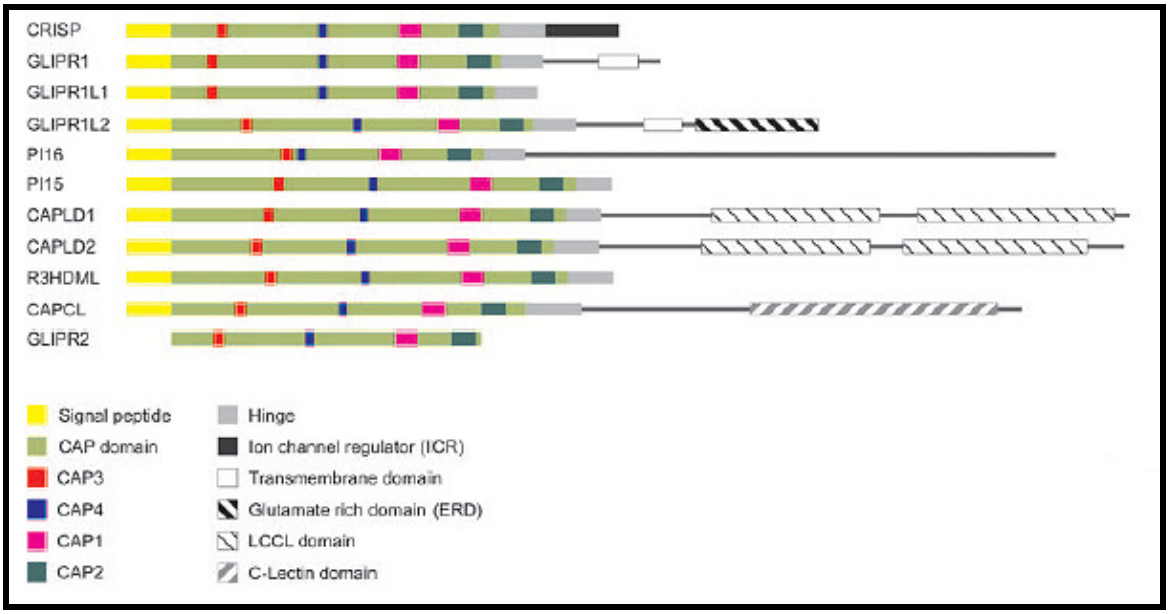

Figure 76 Mammalian members of the CAP superfamily, from [270].

The CRISP subfamily of CAP proteins is distinguished by the cysteine rich C-terminal region of its members [271]. The first CRISP protein in humans was discovered in 1996 by Kjeldsen et al. as a M_r = 28000 granule specific, N-glycosylated protein that was secreted from stimulated neutrophils [268]. Suggesting the name SGP28 (specific granule protein of 28kDa), Kjeldsen noted the sequence similarity of SGP28 to the testes specific human gene (TPX-1) and the sperm coating glycoprotein from the epididymis of mice and rats, which have 72% and 55% sequence identity to SGP28, respectively. Also in 1996, Kratzschmar et al. independently reported the isolation and purification of cDNAs encoding three members of the CRISP family in humans [271]. It was shown

that CRISP-2 corresponded with the TPX-1 form of Kjeldsen. Northern blots on human tissues showed that CRISP-2 transcripts were specific to the testes and epididymis and CRISP-1 transcripts were epididymis specific. CRISP-3 transcripts were far less specific, being found predominantly in the salivary glands, pancreas [273], and prostate and in lower abundance in the epididymis, thymus, ovary and colon [271]. CRISP-3 has 72% sequence identity to CRISP-2.

To Kratzschmar, this glandular localization suggested an exocrine function for CRISP-3. The development of polyclonal antibodies against the denatured N-terminal third of rCRISP-3 by Udby et al. [269] allowed immunoblotting and immunocytochemistry to verify the glandular sources of the protein by finding it in saliva (21.8 ʊg/mL) and seminal plasma (11.2 ʊg/mL). No attempt was made to find it in prostate or pancreatic secretions. Udby also found significant amounts of CRISP-3 in the blood plasma (6.3 ʊg/mL) for the first time [273]. Circulating CRISP-3 was shown to have identical sequence to neutrophil expressed SGP28 and to have the same mobility shift on N-glycanase treatment [269]. Neutrophils are now believed to be the source of circulatory CRISP-3 [270], although it is in higher concentrations in the plasma than most other neutrophil granule proteins [274].

Although the physiological functions of CRISP family proteins in mammals is still not clear [275], they are believed to generally be ion-channel blockers. CRISP proteins are found in a variety of snake and lizard venoms where they are believed to be L-type, voltage-gated Ca^{2+} channel blocking and cyclic nucleotide gated ion-channel blocking neurotoxins [275, 276]. In humans, because of their exocrine and neutrophilic

origins, it has been proposed that CRISPS are involved in innate immunity. In the case of CRISP-3, this has been supported by the finding that it is specifically up-regulated in chronic pancreatitis [273] in which the pancreas has been infiltrated by inflammatory cells.

Ca^{2+} channels are of primary importance for many cellular functions and have been categorized into several groups, designated by the letters: L,P,N,Q,R and T, depending upon their current (L-type is **L**ong lasting when Ba^{+} is the carrier ion) and pharmacological properties (L-type is antagonized by dihydropyridines) [277]. Designations of the L-type channels have been further refined into subtypes, depending upon the combination of subunits that comprise the channel. For instance; the L-type Ca^{2+} channel, $Ca_v1.2$, is a subtype that is found in endocrine cells, neurons and cardiac muscle [277].

Interestingly, insulin secretion by pancreatic B-cells is very dependent upon L-type Ca^{+} gated ion channels, a proposed target of CRISP-3, for stimulus-secretion coupling. It has long been established that increased intracellular Ca^{2+}, from the Ca^{2+} influx across the plasma membrane of the β-cell, is required for glucose-induced insulin secretion [278]. And, although β-cells possess a heterogeneity of Ca^{2+} channels, it has recently been shown, in rats, that the primary Ca^{2+} channel that mediates insulin secretion in pancreatic islets is the L-type Ca^{2+} channel, $Ca_v1.2$ [279].

Ca^{2+} channels are clearly involved in the human insulin response. Sulfonylureas are a class of drugs that have long been in used to treat T2DM by stimulating insulin secretion by the pancreas. The primary target of sulphonylureas is the ATP dependent

potassium (K_{ATP}) channel, which they induce to close. By blocking the K_{ATP} channel, depolarization of the β-cell membrane ensues. Depolarization triggers the opening of Ca^{2+} channels and the influx of Ca^{2+} into the cell, which, in turn stimulates the exocytosis of insulin [280].

Udby and coworkers noted [274] that CRISP-3 was at higher concentration in plasma than other neutrophil secreted species. Because circulatory species with MWs below ≈40 kDa are generally cleared from the circulation by the kidneys [281], they hypothesized that CRISP-3, at ~30 kDa, must be in complex with another protein to bring the MW of the complex above the renal cutoff. They found that CRISP-3 forms a specific, high-affinity complex in 1:1 stoichiometry with α_1B-glycoprotein (A1BG-see Figure 64 labeled "D", mascot score from MALDI=79 /64 significance), a protein also of previously unknown function [274]. Udby claimed that A1BG has sequence homology to several circulatory opossum proteins that form complexes and neutralize toxic proteins, protecting the animal from the effects of snake and reptile venom [274]. The authors suggested that the function of A1BG was as a transport protein, to bind CRISP-3 and inhibit its potentially harmful effect in the circulation.

Because CRISP-3 is normally associated with A1BG, a relationship proposed to protect tissues from the harmful effects of free CRISP-3, then the interpretation of our result, that CRISP-3 is in lower plasma concentration in T2DM, is not obvious. If one accepts Udby's contention that CRISP-3 is potentially a danger to tissues, then the lower concentration of CRISP-3 in T2DM, instead of indicating less total CRISP-3 and less potential for harm, may reflect reduced affinity of CRISP-3 to A1BG. This could result

in more unbound CRISP-3, therefore more flux out of circulation and the increased potential for pathological sequelae in the tissues of T2 diabetics. High blood glucose provides the increased opportunity for structural change to many proteins in the body and circulatory proteins in diabetics have been shown to contain higher levels of oxidative modifications [282], coupling with lipid peroxidation products [283], and glycation [157]. Increased damage to proteins in T2DM may affect the function of receptors, enzymes, and transport proteins [284], and this may also be the case for modified A1BG or CRISP-3. We will show later, in the case of HSA, the binding character can be closely correlated with FPG.

A 2003 effort by Pieper et al. [179] attempted to catalog the identifications of as many plasma proteins as possible from 2D gel separations. The experiment produced 66 coomassie stained gels which were preceded by a multidimensional fractionation strategy, including the immunodepletion of 8 abundant proteins, anion exchange chromatography as well as size exclusion chromatography. 325 unique proteins were identified from an estimated number of gel spots greater than 3700, but the list did not include CRISP-3. This is likely to be because the pI range of the gels was limited to pH 4 – 7 and the isoforms of CRISP-3 have pIs greater than 7. But in a 2004 meta-survey that attempted to create a non-redundant catalog of plasma proteins [181] from 4 global plasma proteomics sources, including the Pieper study, CRISP-3 was absent. It isn't clear why this would be, as CRISP-3 is not an exceedingly low abundance protein.

● *Histidine-rich Glycoprotein Precursor (HRG Precursor)/Complement Factor H-Related Protein-5 (CFHR-5)* - This spot train (Figure 63, fraction 1 gels, labeled "E") was decreased 1.5 fold in the T2DM samples (Figure 77). An ftest determined that there was a 14% chance that the variances were not different, so a two-tailed ttest with unequal variances was used, yielding a p-value = 0.02. The MS for the spot-train yields two passing identifications, HRG precursor and CFHR-5 (see Table 13 and Table 14). We will briefly summarize the known functions of each of these proteins.

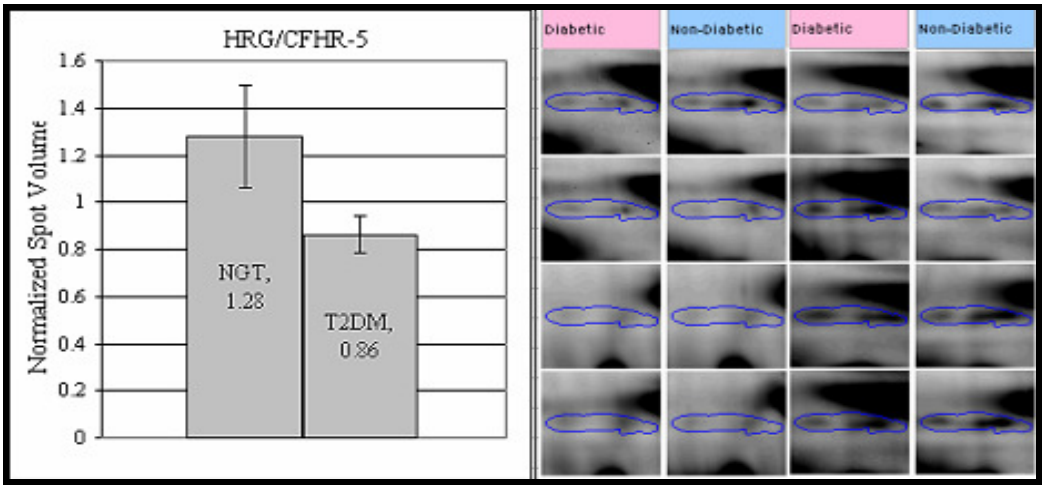

Figure 77 HRG/CFHR-5 relative abundance histogram, expressed as pool averages ± standard deviation and spot images from the fraction #1 gels.

HRG is a fairly abundant plasma protein, reported to be present at 100 ʋg/mL [285] to 150 ʋg/mL [286] . The prominent protein series just above and to the right of this POI was strongly identified as HRG precursor, yielding an excellent Spectrum Mill accumulative score of 321 from peptides with individual scores greater than 13. This prominent spot series is composed of 2 roughly horizontal spot trains that are believed to represent the known N-glycosylated and non-glycosylated species (glycoforms) of Arg

184 [287], due to a P186S mutation that creates a glycosylation site. There was no significant change in the abundance of these HRG isoforms, between NGT and T2DM.

To test the possibility that HRG was identified in the POI spot train because of its proximity to the main HRG spot train, a piece of gel between the coomassie stained POI and the large, coomassie stained, HRG spot series was picked, digested and analyzed by ESI MS. It yielded only 1 HRG peptide, an indication that the 3-peptide, positive identification of HRG within the POI spot was not due to contamination. So, the existence of a minor pI-shifted HRG cleavage product and/or modifications could not be completely ruled out. No evidence of this form could be found in the literature, although ~30 kDa, N-terminal proteolytic fragments of HRG have been found to have some of the same biological activities as the "intact" form [286].

Inspection of the peptide coverage map in the supplementary Figure 128 for HRG shows that none of the identified peptides were from either termini of the protein, and so cleavage of neither terminal to produce a lower MW form could immediately be ruled out. *In silico* cleavage of the C-terminal by 20 amino acids, decreasing the theoretical MW by 2300 Da, which would shift the theoretical pI from 7.11 to 6.93, leaves this cleavage as a possible explanation for the MW and pI shift. *In silico* cleavage of 20 more amino acids did not shift the theoretical pI further to the left. No such acidic shift, by cleaving the N-terminal was predicted within the estimated allowable MW loss of ~4000.

HRG is a 67-75 kDa, multidomain, multi-ligand glycoprotein [285]. It is believed to be an adaptor protein involved in complex formation of diverse proteins regulating multiple biological processes, notably coagulation and both innate and adaptive immunity

[288]. The ligands of HRG include Zn^{2+}, heme, tropomyosin, heparin and heparan sulphate, plasminogen, plasmin, fibrinogen, thormbospondin, IgG, and complement [285, 287].

HRG has several proposed roles as a protective molecule. It may protect against the formation of insoluble auto-immune complexes of complement and IgG, such as occurs to produce the tissue precipitations in lupus and rheumatoid arthritis [286]. HRG may also aid in the clearance of apoptotic cells and in the modulation of angiogenesis [285].

A recent hypothesis by Stewart et al, [288] indirectly links HRG to lipid metabolism and oxidation. These authors showed that Zn^{2+} binding by the plasma carrier protein, human serum albumin (HSA, Zn^{2+} K_d= 30 nM), was diminished when it bound high levels of fatty acids, such as are in circulation in T2DM. (For a description of HSA function, see the section Human Serum Albumin in THE BROMOCRESOL GREEN ERROR FROM POLYCOLONAL HSA ELISA ASSAY (BEPHE ASSAY)). Stewart proposed that HRG, with up to 10 Zn^{2+} binding sites (K_d= 1-4 υM) is protective against the toxicity of otherwise free Zn^{2+} by acting as a "sink" for binding the "overflow" of Zn^{2+} from HSA under conditions of high circulatory FFA.

The forgoing description of HRG and its functions were discussed because HRG appeared as a secondary identification with passing scores by the Spectrum Mill criteria (Table 14). The nearby presence of the main spot series of HRG in F1, the lack of reference in the literature to an HRG cleavage product or variant that would create the necessary shift from the pI and MW of HRG and the relatively weak protein scores,

compared to CFHR-5, suggest that the presence of HRG peptides were likely a result of contamination within the gel from the nearby and abundant HRG spot series.

The presence of complement factor H-related protein-5 (CFHR-5) was strongly supported by its relatively high MS/MS scores and reasonable coverage (Table 14). It is a 65 kDa plasma protein [289] with a nominal pI of 6.81 [290] and is present in normal human plasma at 3-6 μg /mL [289]. These specifications are compatible with its position and intensity in the gels.

CFHR-5 protein was discovered in 1988 by raising monoclonal antibodies against preparations of human kidney with glomerulonephritis [291]. CFHR-5 shares 9 short consensus repeats (SCRs) of the 20 repeats within the sequence of the complement regulator protein, complement factor H (CFH), hence the CFHR name. These SCRs are also found in 5 other structurally related proteins, the CFHRs 1-4 (A/B) [292]. These proteins comprise the CFH family, the genes for which are located within the regulator of complement activation (RCA) cluster on human chromosome 1q32 [292].

The complement system, or simply “complement”, is part of the circulating innate immunity machinery that assists (or complements) adaptive immunity in the recognition and elimination of foreign invading microbes or modified self-cells, including apoptotic and necrotic cells [293]. More than 60 proteins comprise the complement network [293], that become sequentially activated in the presence of offending cells in a complex, cascading response. The initiation of the response can be cell surface bound IgG or IgM (the classical pathway) in which the complement proteins C1q, C1s, and C1r assist antigen/immunoglobulin complexes of IgG and IgM to activate a cascade in the network

of complement effector proteins. Central to this cascade are the C3, C5 proteins that are cleaved and activated by specific convertases. The C3 and C5 cleavage products C3a and C5a are potent mediators of inflammation and of chemotaxis by immune cells [292]. The C3 and C5 cleavage products C3b and C5b mediate phagocytosis in another way. As an illustration of this pathway, complement activation can also be initiated without immunoglobulins, in the fluid phase (the alternative pathway). In this pathway, the offending cells trigger a conformational change in the local, circulating complement proteins C3 and C5. This conformationals change initiates a cascade that results in the indiscriminate coating (opsonization) of nearby cells [293], including host and the offending cells, with the complement protein fragments, C3b and C5b, and their recognition and phagocytosis by macrophages.

Defective regulation of complement can result in a spectrum of diseases involving infectious to non-infectious pathology. Hemolytic uremic syndrome (HUS), dense deposit disease (DDD), age-related macular degeneration (AMD) and lupus are examples of non-infectious pathology, in which mutations produce dysfunctional CFH, which is a negative regulator of the early C3 activation. These defects in the complement cascade cause the subsequent deposition of immunological debris within distinct tissues that are specific to the diseases [294].

Early work on CFHR proteins by Park and Wright [295] found that CFHR-1 and CFHR-2, and several unidentified bands near M_r 66,000 that were consistent with CFHR-5, associated with a minor subpopulation of HDL particle (1.219-1.264 g/mL). The subpopulation of HDL particles also contained phospholipids, apo A-I and

lipopolysaccharide binding protein. The purified particle was shown to enhance the binding of neutrophils to lipopolysaccharide coated plates and was referred to as factor H related protein-associated lipoprotein particles or FHRP-associated lipoprotein particles (FALPs) [295].

The association of CFHR-5 with HDL has since been verified, although the majority of CFHR-5 is not in complex with HDL [289]. The activities of rCFHR-5 have also been shown to overlap with those of CFH, including the inhibition of C3 convertase and binding of acute phase CRP. CRP binding may suggest a means for recruiting CFH and CFHR proteins to sites of tissue damage [289]. Interestingly, while CFHR-1, CFHR-2 and CFHR-5 have been found on HDL, the much more abundant CFH has not been shown to associate with lipoprotein and CFHR-4(A) associates primarily with triglyceride-rich very low density lipoproteins (VLDL) [289], implying diverse functions for the CFH family proteins, despite structural similarities. This has led to the suggestion that the CFHR proteins may have a role in lipid transport [289].

CFHR-5 has been reported to have a novel property among the CFH protein family because of its close association with the pathological deposition of complement complexes in human glomeruli. An immunohistological study of 92 kidney biopsies found that CFHR-5 almost invariably deposited in the tissue when complement was activated [291]. The immunohistochemistry was conducted using an anti-CFHR-5 ("FHR-5" in Table 16) antibody with no cross-reactivity for CFH [296], an anti-C3 antibody, and a neoepitopic anti-SC5b-9 activated complement complex antibody (Table 16).

Table 16 Co-deposition of CFHR-5 with complement in nephropathy, from [291].

	No. of Cases	Incidence of Detection in Glomeruli (cases)			Pattern of FHR-5 Deposition in Glomeruli/Median Intensity of Fluorescence
		C3	SC5b-9	FHR-5	
Thin basement membrane nephropathy	12	0	0	0	
Minimal change disease	4	0	0	0	
Focal glomerular sclerosis	8	2	6	5	Sclerotic lesions/1+
Membranous nephropathy	10	10	10	10	Capillary loop/2+
Membranoproliferative GN type 1	1	1	1	1	Mesangial & capillary/3+
IgA nephropathy	20	19	18	20	Mesangial/2+
Post infectious glomerulonephritis	2	2	2	2	Mesangial & capillary/2+
Lupus nephritis	7	7	6	7	Mesangial & capillary/3+
ANCA-associated GN	6	1	1	0	
Diabetic nephropathy	2	1	2	2	Sclerotic lesions/1+
Hypertensive nephrosclerosis	2	1	1	0	
Interstitial nephritis	3	0	1	0	
Transplant, interstitial rejection	4	1	1	1	Focal capillary loop/1+
Transplant, no rejection	11	1	2	1	Focal mesangial/1+
Total	92				

Abbreviations: GN, glomerulonephritis; ANCA, antineutrophil cytoplasmic autoantibody.

According to the authors, this co-localization of CFHR-5 with complement was a unique property among the CFHR proteins. This study included 2 patients with diabetic nephropathy in which CFHR-5 was found in the deposition and many other types of nephropathy (see Table 16) [291].

This deposition in kidneys fits well with our observation that CFHR-5 is in lower levels in the plasma of newly diagnosed T2DM patients. It also raises the question whether the deposition is an early event in the progression to complications, as none of the subjects within our cohort had measurably impaired renal function, as measured by NIH measured urine albumin/creatinine (see discussion on page 289).

In view of the fact of the relatively strong MS identification for CFHR-5, and that there is no known cleavage or modification of HRG that occurs to produce a shift from the main HRG spots, such as is seen in the gels, the identification of this POI seems highly likely to be CFHR-5. If so, then the secondary MS results leading to the

identification of HRG probably resulted from dispersive contamination from the nearby very abundant HRG spots. Although this explanation doesn't comport well with the lack of HRG protein detected in the intervening space between the spots, it's reasonable to invoke MS run-to-run variability to explain this, especially at these relatively low levels of peptides, and seems preferable to proclaiming a new variant of an abundant protein.

If the changes in presence of this POI are in CFHR-5, and not HRG, then the similar changes seen in the HDL (1.5-fold lower in T2DM) and CFHR-5 (1.5 fold lower in T2DM) may have added significance in light of the reported association of HDL with CFHR-5 [289]. However, since only a minor fraction of the CFHR-5 is believed to exist in circulation as a part of HDL, it isn't a simple matter to speculate on the nature of this dependence.

This POI is illustrative of an important benefit of the RP fractionation used in this study. Comparison of the POI's position in the F1 gel with the nearby position of the abundant central protein of F2 (hemopexin) shows that without the fractionation, the POI would be largely obscured and contaminated by that protein, preventing the accurate quantitation of changes in expression, as well as MS identification.

The last 2 POIs that will be discussed, haptoglobin (Hpt) and apolipoprotein A-I (apo A-I) have been shown to have important functional relationships to HDL. Therefore, a preliminary discussion of HDL will provide context for their respective discussions.

The Framingham Heart Study is a widely cited, long-term epidemiological study of a cohort of Massachusetts residents, that was begun in 1948 "to identify the common

factors that contribute to cardiovascular disease by following its development over a long period of time in a large group of participants." [297] In 1969, baseline measurements of HDL (HDL-C or HDL cholesterol) were begun, and in 1986 Castelli et al. published results [266] validating and extending "limited" earlier results showing that HDL is inversely related to the incidence of coronary heart disease (CHD) including; angina , coronary insufficiency, myocardial infarction and death due to cardiac failure. The study showed that subjects who were at the 80th percentile of HDL concentration had half of the risk developing CHD as those at the 20th percentile. Circulatory HDL is now accepted to have an inverse relationship with atherosclerosis and HDL is routinely measured as a predictor of cardiac risk [298].

HDL is a particle composed of lipids and apolipoproteins [299]. HDL is "high density" because of its high percentage of protein constituent, relative to the

Table 17 Compositions and sizes of the classes of circulatory lipoprotein particles based upon density, tabulated from data in [300].

Density (g/mL)	Class	Diameter (nm)	% Protein	% Cholesterol	% Phospholipid	% Triglycerides
> 1.063	HDL	5-15.	33	30	29	4
1.019-1.063	LDL	18-28	25	50	21	8
1.006-1.019	IDL	25-50	18	29	22	31
.95-1.006	VLDL	30-80	10	22	18	50
< 0.95	Chylomicron	100-1000	<2	8	7	84

percentage of lipids. Table 17 [300] lists the principle classifications of lipoprotein particles and their compositions. The principal protein constituent of HDL is apo A-I, which constitutes ≈70% of the apolipoprotein content [299]. Although the structural mechanism of apo A-I is not clearly understood, it is known to have a key role in cholesterol transport and homeostasis [301]. Because of the high percentage of apo A-I

in HDL, the plasma concentration of apo A-I is expected to correlate closely with plasma HDL concentration [299]. The second most abundant apolipoprotein of HDL is apo A-II, which is found on ≈ 2/3rds of the HDL particles and has an unknown physiological role. Other proteins that are found in HDL are apo A-IV, apo C-I, apo C-II, apo C-III, apoD, apoE, apoJ, apo L-I, apoM, SAA, ceruloplasmin, transferrin and enzymes such as lecithin:cholesterol acyl transferase (LCAT) [299], which will be discussed in the section below on the POI, haptoglobin.

Among the protective properties of HDL are its anti-thrombotic, anti-oxidative and anti-inflammatory activities [302]. The mechanism by which this protective relationship is achieved is still not fully understood [302], but HDL has been shown to have several anti-inflammatory modes. Among the most important are: 1) the reverse transport of cholesterol from cells, possibly abrogating the profusion of inflammatory foam cells in arterial walls, and 2) the inhibition of oxidation of LDL, thereby suppressing its atherogenicity [302]. Oxidized LDL is recognized by the scavenger receptor of macrophages and taken up much more rapidly than un-oxidized LDL. The uptake of LDL promotes the accumulation of cholesterol, foam cell formation and early steps in atherogenesis [283].

As discussed earlier, decreased HDL and elevated triglycerides constitute the dyslipidemic part of the metabolic syndrome. Although “isolated” decreased HDL, that is not a part of the insulin resistant phenotype, is known to occur, IR appears to be associated with the majority of cases of low HDL [298, 299]. The relative concentrations

of total HDL, as measured by NIH, in the 8 T2DM samples of this study were significantly lower (1.5 fold, p = 0.03-unpaired, 2-tailed ttest) than the 12 NGT samples.

● *Haptoglobin*- Haptoglobin (Hpt) was one of the abundant targeted proteins of the immunodepletion step of this experiment. The Hpt binding capacity of the column was exceeded predominately by the T2DM samples and therefore Hpt met the statistical criteria for significantly higher levels of some isoforms. It must be emphasized that the Hpt that was measured in the gels reflects the amounts by which the column capacity for Hpt was exceeded and the true ratio of the differences of concentration between the groups is probably less than the differences measured in the gels. It is also not clear if the measured differences result from real *in vivo* concentrations or, as will be seen, differences in phenotype and the resulting possible differences in column binding, as will be discussed further.

The relative plasma concentration levels of the Hpt isoform, (Figure 64, fraction 2 gels, labeled "B") was found to be 1.6 fold higher in the T2DM pools (Figure 78). An ftest calculated that there was a 47% probability that the variances were not different, so a two-tailed t-test with unequal variances was used, which yielded a p-value of 0.03. Figure 64 indicates two more acidic isoforms to the left of Hpt spot B. These isoforms, while not significantly changed, were 1.6-fold higher (left red arrow) and 3.4 fold higher (right red arrow) in the T2 diabetics group. The low MW Hpt spot train (Figure 64, fraction 2 gels, labeled "A") has several spots that show increased concentrations from 1.9-3.9 fold in the T2 diabetic group.

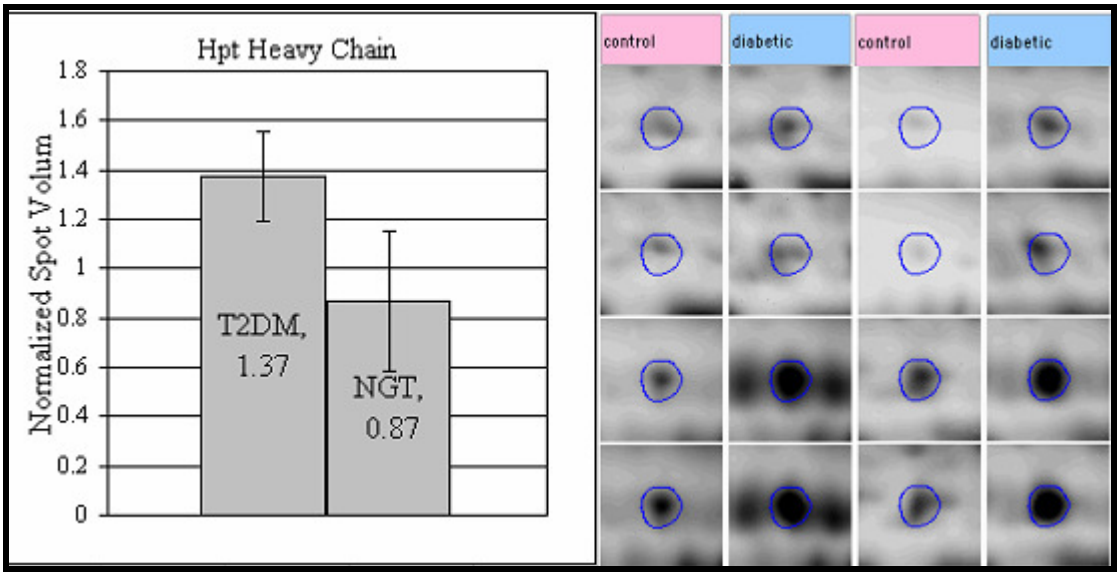

Figure 78 Haptoglobin heavy chain isoform relative abundance histogram, expressed as pool averages ± standard deviation and spot images from the fraction #2 gels.

● *Preparative gel Identification of Haptoglobin*. F2 gels showed a low abundance and low M_r, ~ 15000, spot train (see Figure 79 and Figure 64 spot train "A", for the gel position). Expression analysis of the 6-7 component spots of the train showed 3-4 fold higher concentrations in the T2DM samples, the greatest change in the experiment. Although most of the spots had p-values above 0.05 due to the highly variable concentrations in the T2DM gels, the spot train was of interest because of the relatively high concentration that seemed to be unique to the T2DM samples.

An unusual feature of the spot train is the large number of closely spaced isoforms, for a protein of such low molecular weight. It is believed that most of the spot trains in blood proteins are due to pI shifts resulting from deamidations of Q and N residues [208], as discussed in the chapter INTRODUCTION TO PLASMA PROTEOMICS. Deamidation is a sequence-dependent, non-enzymatic process, that may

provide a measure of the relative time that an isoform has been in circulation, the older isoforms shifted further to the acidic side as they acquire negatively charged E and D residues. The finding of such closely spaced, low MW spots implies that the isoforms are strongly buffered by the presence of many other charged residues. A possible explanation for this, in our protocol, which didn't reduce the disulfides until after IEF, is

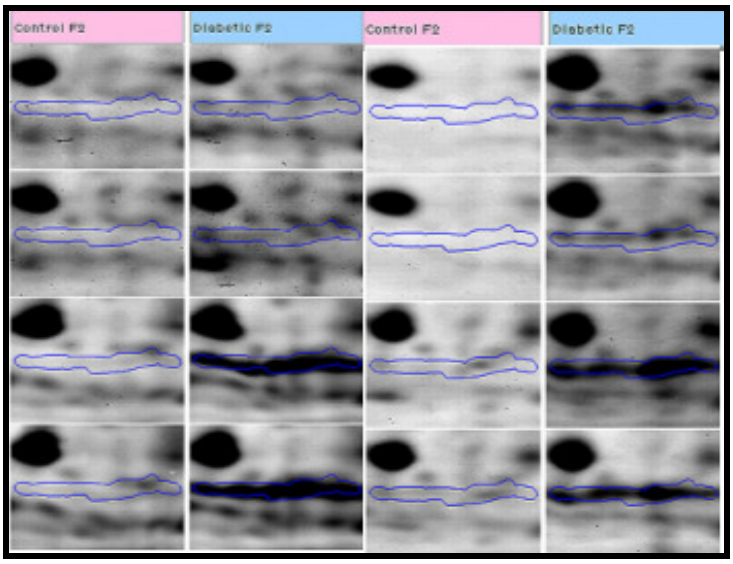

Figure 79 Gel images of the low molecular weight haptoglobin chain, with isoforms circled.

the covalent attachment of the low MW species to a higher MW chain and the pI would be determined by the HMW complex before the reduction between the first and second dimension. This explains how the low MW species can be so closely spaced, and also how it could be in circulation long enough to acquire a high number of modifications, as unbound low molecular weight species are quickly removed from the circulation by the kidneys. The presence of a high MW spot train that corresponded to the low MW spot

train in the gels could not be found, probably because it was relatively low intensity and/or it was obscured by co-migrating spots from other proteins.

Initial attempts to identify the low MW spot train by MS failed. It was decided to make preparative gels combining multiple runs of immunodepletion and RP fractionation to increase the amount of protein in the gel, so that the spots could be visualized by coomassie staining for picking for in-gel digestion and MS. The plasma from a single diabetic subject, whose depleted plasma yielded a large amount of signal for the POI, was used. It was also decided that, if the higher MW chain was obscured by other proteins, there would be better chance of finding it if fraction 2 was subfractionated so that gels could be prepared from only the chromatographic peak that included the POI.

After running 2D gels on the 5 subfractions (far left of Figure 80) of F2, the POI

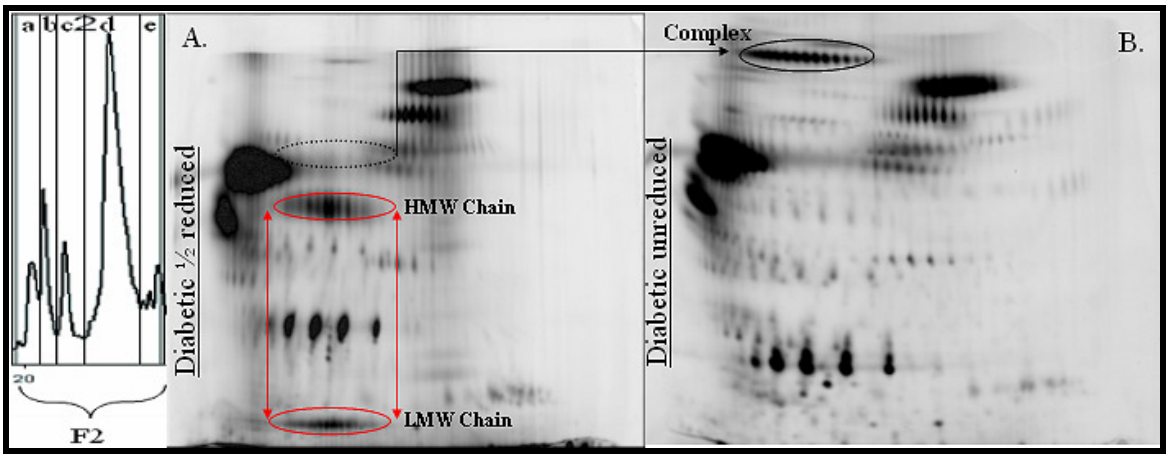

Figure 80 Subfractions, A) sF2a - ½ reduced (reduced between dimensions) and B) sF2b- unreduced.

was found in subfraction 2A (sF2a). An analytical gel of sF2a from a diabetic sample was prepared and heavily labeled with ZGB fluorescent dye. As seen in the gel of Figure

80A a low MW spot train is visible and also a potentially pI correlated high MW spot train is now clearly visible. A preparative gel was also made without reduction alkylation between dimensions using sF2a. The fluorescent image of the unreduced gel is in Figure 80B. With no reduction there is a pI correlated very high molecular weight spot train visible and the low MW spot trains are no longer present. This gel was coomassie stained for spot picking and protein identification.

As a side-note, the spot train in Figure 80B had a much higher M_r than was predicted from the simple summations of the M_rs of the 2 chains seen in Figure 80A. This could be due to intrachain or multiple interchain disulphides that caused retarded mobility in the 2nd dimension. Or, as will be discussed below, there are common polymorphisms of haptoglobin that lead to different disulfide linked multimers, such that healthy people have different combinations of the numbers of disulfide linked subunits. So, in the case of the subject whose plasma was used to produce the gels in Figure 80, the unreduced protein in Figure 80B may include 2, 3, or more pairs (or odd combinations) of the chains seen in Figure 80A. This issue will be discussed in more detail below.

Hpt is an abundant, acute-phase glycoprotein that is synthesized in the liver [303], and is believed to have the primary task of scavenging free hemoglobin ($K_d \approx 1pM$) [304]to prevent iron loss and kidney damage during red cell turnover and hemolysis [305]. Under normal conditions, about 1% of the > 1M hemoglobin is free in the blood [304] and the remainder is in the erythrocytes. In times of injury or otherwise hemolytic episodes, increased circulatory hemoglobin can become highly toxic due to the pro-oxidative property of heme [304] which can create ROS and cellular damage through the

Fenton reaction (see Equation 4 on page 255). The hemoglobin-Hpt complex forms a neoepitope, a recognition site that is formed only when the two species are in complex. The neoepitope is recognized by the acute-phase regulated CD163 receptor of macrophages, which mediates its endocytosis. The engulfed hemoglobin is then metabolized by macrophage into bilirubin and iron [306].

The multiple polypeptide chain structure of Hpt, including an α and β-chain, is a unique feature among the POIs of this experiment. The glyco-β-chain, which has been attributed with the hemoglobin binding capacity , is ~45 kDa [303] and is identical in all the haptoglobins [305]. The smaller α chain consists of 3 common variants consisting of: "slow" and "fast" variants of α^1 (M_r =8900), designated as α^{1S} and α^{1F}, and a α^2 (M_r =16000) variant. The α^{1S} and α^{1F} variants differ only in the replacement of a glutamic acid in the α^{1S} form by a lysine in the α^{1F} form [305]. In addition to the variants of primary sequence, several variants result from 2 common alleles, denoted 1 and 2, and their homozygous 1-1, 2-2, and heterozygous 2-1 genotypes [305].

Hpt is synthesized as a single chain and then cleaved into the α and β chains that are then linked by disulfides to form a monomer [303]. Polymeric Hpt found in blood is made of the monomers linked by disulfides between the α chains [305]. The stoichiometry of these polymers is genetically determined and results in dimeric (Hpt 1-1), linear polymeric (Hpt 2-1) and cyclic polymeric (Hpt 2-2) Hpt, as summarized in Figure 81 (from [305]). The details of oligomerization are beyond the necessary scope

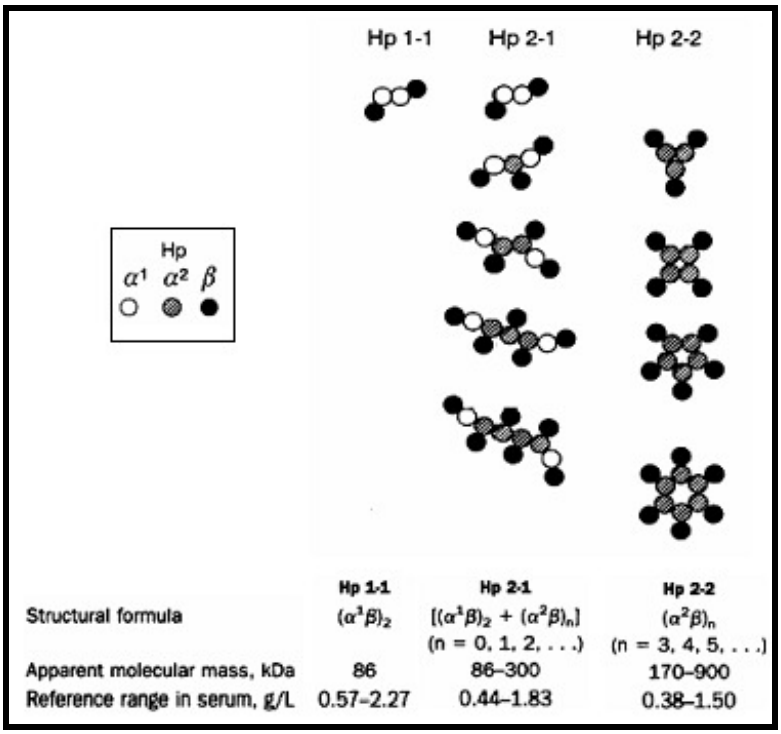

Figure 81 Polymeric Hpt phenotypes, from [305].

of this discussion. However, the phenotypes have been shown to have functional differences that are of interest.

Specifically, the Hpt 1-1 phenotype has been shown to have superior anti-oxidant properties against free hemoglobin *in vitro*, and in T1 and T2 diabetics for the prevention of diabetes associated complications, specifically retinopathy and nephropathy [307]. A 2001 study by Nakhoul et al. [308] looked at the correlation of haptoglobin phenotype with albuminuria, a marker of nephropathy. Among 54 age, sex, age of onset, and duration-of-diabetes matched T1 diabetics, 13 were Hpt 1-1, 22 were Hpt 2-1 and 21 were Hpt 2-2 phenotypes. None of the Hpt 1-1 individuals showed evidence of nephropathy, whereas 23% of the Hpt 2-1 and 38% of the 2-2 did. Among 56 matched

T2 diabetics, 5 were Hpt 1-1, 15 were Hpt 2-1 and 34 were Hpt 2-2. Again none of the 5 Hpt 1-1 showed nephropathy, whereas 33% of the Hpt 2-1 and 33% of the Hpt 2-2 did. After combining the T1 and T2 groups the difference in the incidence of nephropathy between the patients with the 3 phenotypes was found to be statistically significant ($p < 0.015$, chi-squared test).

The M_r of the LMW Hpt chain that was detected in the gels of this 2DGE experiment is not consistent with an 8.9 kDa α^1 chain as it is estimated, by comparing with the position of SAA in the F1 gels, to be greater than 13000. So the phenotype that is associated with this spot train must be either Hpt 2-1 or Hpt 2-2, to be consistent with the presence of the 16 kDa α^2 species. Also, it can't be shown that there is a 1-to-1 correlation between the horizontal positions (pI) or expression patterns of the 16 kDa α^2 spot train and the Hpt β-chain that is detected on the same gels. The evidence suggests that they are not well correlated, since in the 16 kDa α^2 spot train there are spots with 3-4 fold intensity differences between the experimental groups, none of which were significant ($p > 0.05$) and no spot pattern that is similar to this can be found in the 45 kDa β-chain spots. The 45 kDa β-chains that are bound to the 16 kDa α^2-chains may not label as efficiently as the α^2-chains, since there is not a visible ~45 kDa spot pattern that correlates to the α^2 spot pattern in these gels. And the ~45 kDa Hpt spot that was found to be significantly changed was relatively well resolved with greater pI difference between isoforms than the α^2 spot train, suggesting that it comes from a less buffered oligomeric species, consistent with the Hpt 1-1 phenotype.

A trend of increasing risk for the development of T2DM has been found to correlate (P= 0.05) with the quartiles of 6-year follow-up of measured concentrations of Hpt relative to Hpt at baseline in a prospective study 2815 men [309]. Those in the 4th quartile had a 1.7-fold higher risk of developing T2 diabetes than those in the 1st quartile.

Hpt has been found to bind to the HDL apo A-I, and by doing so may link the acute-phase responsewith the interference of apo A-I dependent activity of lecithin:cholesterol acyltransferase (LCAT) [310]. LCAT is a component enzyme of HDL that is critically involved in the intravascular maturation of HDL by esterifying cholesterol and has a major role in the anti-atherogenic process of reverse cholesterol transport [299].

A 2009 publication by Watanabe et al. [304] attempted to illuminate how HDL takes a more complex role than simply a protective one against atherosclerosis and coronary heart disease (CHD), as had been shown by Van Lenten et al. in 1995 [265]. Watanbe's investigations centered on the mechanism which Van Lenten had reported apparently converts HDL from a protective anti-inflammatory agent to a pro-inflammatory one [304]. To do this, "capture" ELISAs were used to prove correlations of complexed proteins with inflammatory states. Capture ELISAs use wells with antibodies that target a specific protein component of the putative complex. After the antibodies were reacted with the samples, a second antibody targeting co-bound species was used to probe for binding partners of the first target. Using capture ELISAs, they demonstrated that Hpt and hemoglobin associated with HDL in patients of coronary heart disease (CHD) and mice fed an atherogenic diet. HDL bound Hpt also positively

correlated with pro-inflammatory properties of HDL as discussed below. The HII assay that was used is a monocyte chemotactic assay that determines the anti-inflammatory/pro-inflammatory property of individuals' HDL. In this assay a standard LDL is used to induce monocyte chemotaxis. The monocyte chemotactic response to the standard LDL is normalized, given a value of 1. When experimental samples of HDL are added, increased chemotaxis, signifiing proinflammatory HDL, yields a value > 1. Diminished chemotaxis signifies anti-inflammatory properties of HDL and yield a value < 1.

Figure 82 collects some relevant figures from the Watanabe publication [304]. In the top panel of Figure 82, A-H, are correlations of individual human CHD plasma samples. "A" shows the non-significant (NS) correlation of direct plasma hemoglobin ELISAs with the lipid peroxide content (LOOH) in the individual samples. In "E" is the

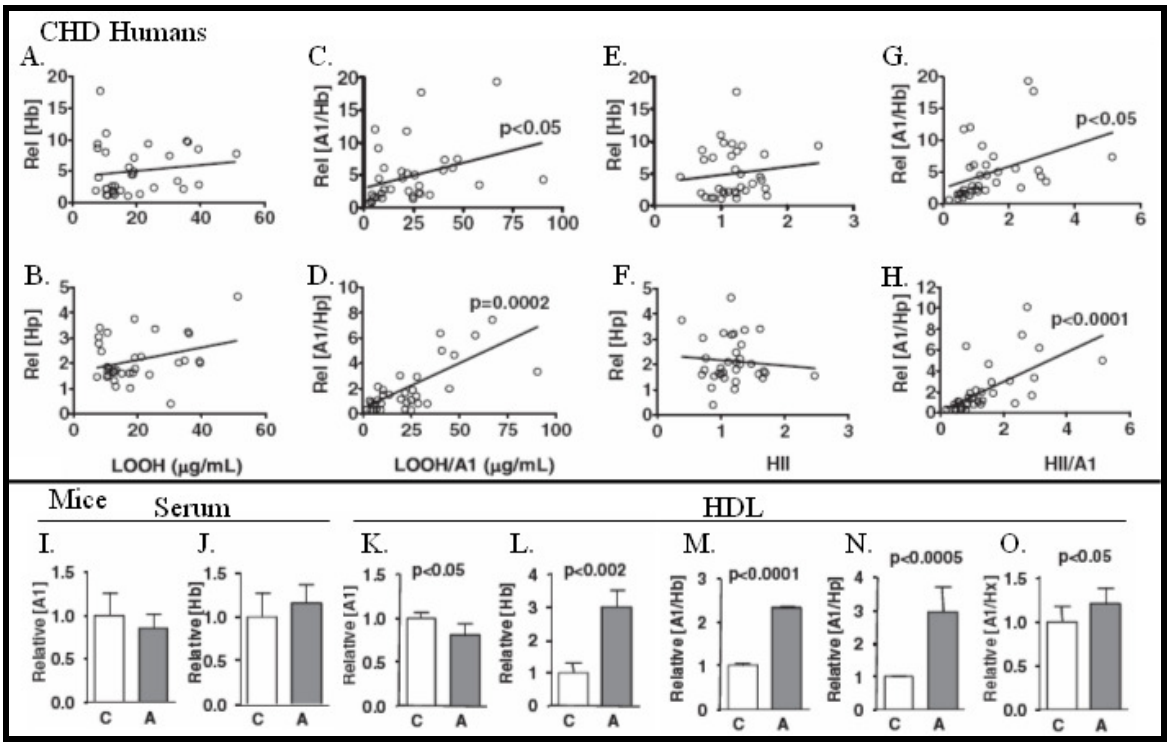

Figure 82 Evidence of the conversion of HDL to a proinflammatory agent. Capture ELISAs (C,D,G,H) show correlations of the indicated complexes ("A1/Hp"-HDL/haptoglobin and "A1/Hb"-HDL hemoglobin) with markers of inflammation ("LOOH"-lipid peroxides and "HII"-monocyte chemotactic assay) in humans, as explained in the text. The mouse study result, I-O, are explained in the text. Bars represent $\pm$1 SD, from [304] .

NS correlation of the plasma hemoglobin ELISAs with HDL inflammatory index (HII) assays. "B" is the NS correlation of direct plasma Hpt ELISAs with LOOH. "F" is the NS correlation of the same plasma Hpt ELISAs with the HII assays. In none of these cases is there a significant correlation. In "C","D","G" and "H" panels show capture ELISAs, in which wells, coated with anti-apo A-I antibodies, were reacted with plasma and then probed with antibodies for the putative complex proteins, either hemoglobin, in "C" and "G", or Hpt, in "D" and "H". These data were then correlated with LOOH in "C" and "D", or with HII in "G" and "H". In these cases the LOOH and HII values were

normalized for individual apo A-I content to correct for differing amounts of apo A-I in individual samples. In each of these capture ELISA cases, the correlations were significant, and especially so with the Hpt targeted samples. These results support the conclusion that the association of HDL with Hpt and hemoglobin switches the HDL from a protective agent to a pro-inflammatory one. Similar results were also shown using hemopexin, a heme-binding protein that also forms complexes with hemoglobin.

The foregoing results didn't show that the Hpt and heme were interacting with HDL while bonded together as a scavenger:ligand complex. But it was shown, by using Hpt $^{-/-}$ mice on an atherogenic diet, that Hpt, but not hemopexin, is required for the accumulation of hemoglobin, as well as heme and ROS, in complex with HDL.

The bottom panel of Figure 82, I-O shows results from WT mouse studies in which the mice were fed a control diet (C) or a high-fat "atherogenic" diet (A) [304]. In direct ELISAs against apo A-I and hemoglobin, there were no significant differences in either apo A-I or hemoglobin, in the whole sera of the controls and atherogenic fed mice (I and J). Within just the HDL fractions (K-O), there is a ≈25% reduction of apo A-I (K), and a very significant 3-fold increase of HDL associated hemoglobin in the atherogenic diet fed mice (L). Within the capture ELISAs of the HDL fractions: apo A-I associated hemoglobin and Hpt were very significantly increased ≈2-fold (M) and ≈3-fold (N) respectively, while hemopexin was not (O)[7].

[7] I modified this figure to correct an obvious misprint. The stated p-values of figures N (previously "$p < 0.05$") and O (previously "$p < 0.0005$") were switched to match the graphs and the stated conclusion in the text, that the apo A-I associated Hpt was significantly different and the apo A-I associated hemopexin was not different between the control and atherogenic diet fed mice.

These data show the pathological potential of acute phase Hpt in changing the normally protective quality of HDL to a pro-inflammatory agent. In light of what is known about the relative effects of the 1-1, 2-1 and 2-2 phenotypes of Hpt, it would seem important in the future to refine this line of experimentation to elucidate the relative roles played by the various phenotypes of Hpt.

● *Apolipoprotein A-I-* The forgoing review of HDL and discussions of SAA and Hpt provided the salient points about apo A-I and won't be reiterated here. Like Hpt, apo A-I was a targeted protein of the immunodepletion column. However, according to Agilent [189], the stated efficiency of its removal, 98.5%, is one of the lowest of the targeted proteins (see Figure 43). This may explain why there is a relatively abundant presence of intact apo A-I in the gel image of F4 (see Figure 66). The spot train immediately above and to the right of the apo A-I spot F4A has been identified as apo A-I, and is believed to be isoforms of intact apo A-I.

This apo A-I spot (Figure 66, fraction 4 gels, labeled "A") was decreased 1.4 fold in the T2DM samples (Figure 83). An ftest determined that there was a 51% chance that the variances were not different, so a two-tailed ttest with equal variances was used, yielding a p-value = 0.03. The MS for the spot yielded a single passing identification, Apolipoprotein A-I (see Table 14 and supplementary Figure 133 and Figure 134).

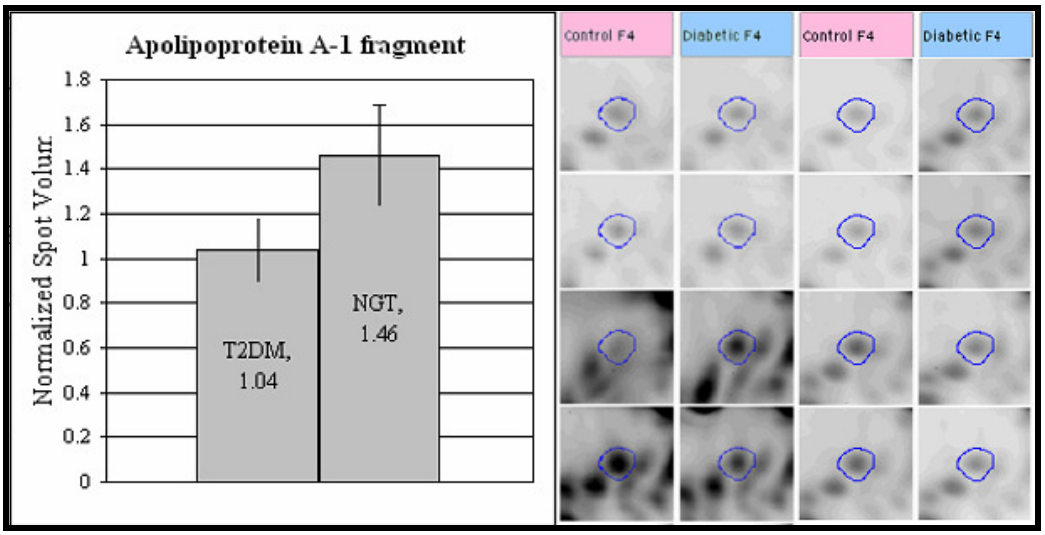

Figure 83 Apolipoprotein AI fragment relative abundances, expressed as pool averages ± standard deviation and spot images from the fraction #4 gels.

While the abundance of apo A-I should reflect the abundance of HDL [299], which, according to our criteria, was reported by NIH to be significantly lower in the T2DM groups, the immunodepletion step likely perturbed the relative concentrations in the intact apo A-I, to the extent that the intact species are not significantly changed in the gel experiment. The NIH tests for HDL showed it to be 1.5-fold lower ($p = 0.03$, two-tailed ttest) in the 8 T2DM samples, as expected for subjects with metabolic syndrome. It is possible that the POI spot F4A (Figure 66), which shows significantly decreased abundance in the T2DM samples, is a cleaved, non-antigenic or less antigenic species of apo A-I. This would explain why its relative abundances were not perturbed by the immunodepletion to the same extent as the intact species. No reported information on biological activity of cleaved species of apo A-I was found in the literature.

● *Unidentified POIs*- Two statistically changed spots were not identified because their low abundances and low molecular weights prevented them from being identified in preparative gels of those fractions. An unidentified spot in F1 was discussed in the section on SAA-1 and is likely to be a lower abundance isoform of SAA-1. It is marked with an arrow in Figure 63, to the right of the spot labeled "not SAA". This unidentified POI was 2.1 fold higher in the T2DM group ($p = 0.03$, unequal variances). A spot in F2 (Figure 64, labeled "C") is also unidentified. It was 1.5-fold higher in the T2DM groups ($p < 0.05$, equal variances). While it has a slightly lower MW than the low MW Hpt chain it is possible that it is an isoform of the α^1 (M_r =8900) chain of Hpt, as was discussed in the section on Hpt. A third unidentified protein is in F5, (Figure 67, labeled "A"). This changing protein was initially not found because of poor alignment in this region of the gel. Upon noticing that several proteins in the spot train were near to significant change, a truer alignment of the individual spots proved that this spot is significantly changing (1.5-fold down in T2DM, unmatched variance ttest $p < 0.04$). This changing protein is possibly adiponectin (AdipoQ, see Conclusion), as AdipoQ is sufficiently abundant to be detected and is also known to be down in T2DM 1.3 to 1.5 fold [311]. AdipoQ has a nomimal pI and MW of 5.4 and 26.4 kDa respectively [312], which, with modifications, is a reasonable match for the detected changing spot. The irregular pattern of the spot train, both in spacing and intensities, suggests that this protein may be approximately comigrating with another species and is significantly obscured by it. Other neighboring spots both to the left and right in the spot train are near to significance, but only show 1.2 and 1.3 fold changes, down in T2DM.

These data and analyses are found on the Progenesis computer in the Dratz laboratory. The respective files for the individual fractions are: F1-"020808 NIH TIID F1B", F2-"030308 F2B", F3-"102008 F3", F4-"022608 F4", F5-"011009 F5, and F6-"040808 NIH TIID F6". Also, the ZAG and CFHR-5 spots were realigned and analyzed in "F1 realigned ZAG 042010".

After removing artifacts and consolidating some spot trains into single intensities, the viable spots in the individual fractions were counted and are approximately as follows: F1-275 spots, F2-450 spots, F3-475 spots, F4- 425 spots, F5-250 spots, F6-550 spots. This is a total of 2425 spots.

The fractions showed a moderately increasing p-value with fraction number which may indicate a relationship of variation with the hydrophobicity of the sub-fractions. The p-values are as follows: F1-0.48, F2-0.50, F3-0.58, F4-0.48, F5-0.57, F6-0.56.

A "volcano" plot (Figure 84), which plots the –LOG (p-value) against –LOG (T2DM/NGT spot ratios) for each spot, provides a convenient overview of the results. In this plot of the 2425 experimental spot values, the significantly changing spots are found only in the upper left and right boxes of the plot. Approximately 10 values in the "significant" regions of the volcano plot were found to be artifactual variations in diffuse, low-intensity regions of the gels, and were removed. Only high-quality spots were included in the significant regions of the volcano plot.

In summary, the proteins ZAG, SAA1, apo A-I and Hpt have established associations with T2DM, and have been shown to have either explicit or implicated roles

in lipid metabolism/inflammation. No previous research has shown a connection of concentration changes of HRG, CFHR-5 or CRISP-3 with diabetes.

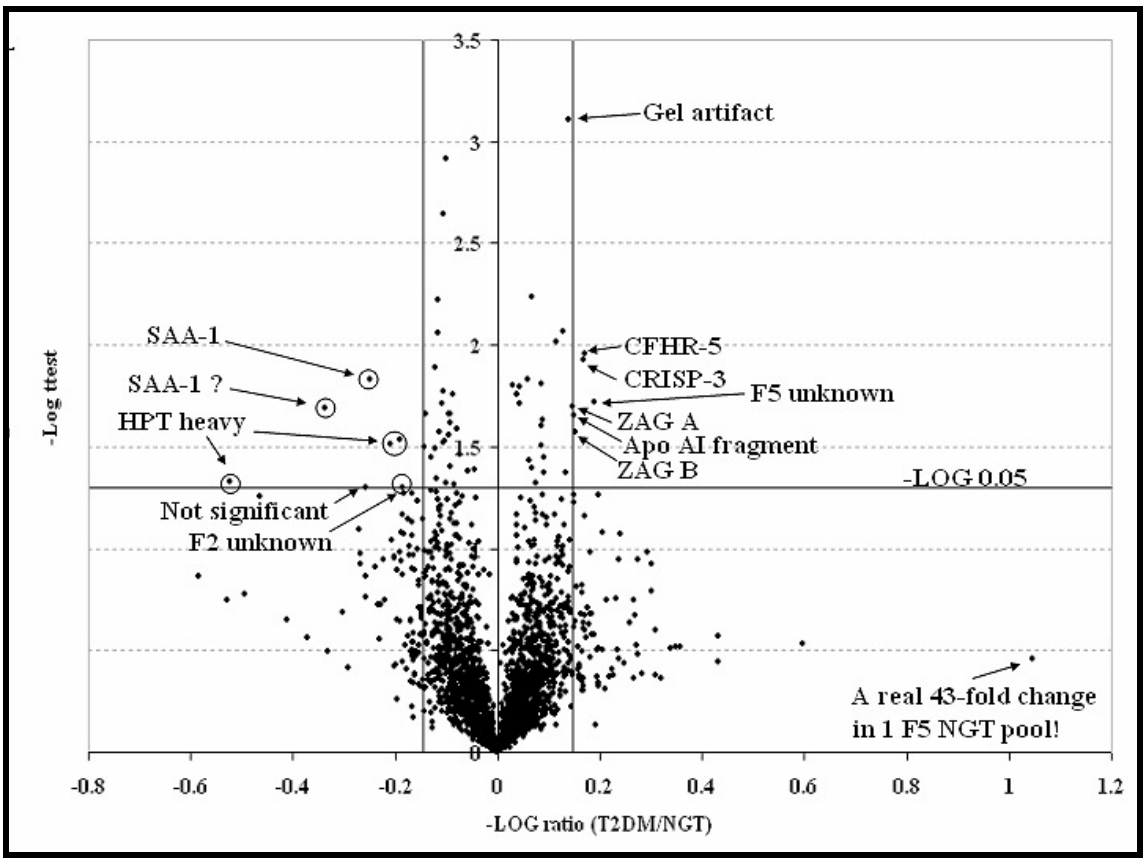

Figure 84 "Volcano plot" of the total spot intensity data from the T2 gel experiment

These results show that the changes seen in POIs are often strongly limited to particular isoforms. In ZAG, SAA-1, CRISP-3, and Hpt the significant changes were limited to 1 or 2 isoforms in each case. This has important implications for proteomics. First, it calls into question the power of methods that don't resolve isoform differences, such as ELISA's and 1D western blots. Clearly, if significantly changing isoforms, such as were found here, are mixed with isoforms that are not changing, insignificantly

changing or significantly changing in the opposite way, then the ability to detect that change is necessarily compromised. Furthermore, specific isoforms may be missed in the "bottom-up shotgun" MS approach. Second, charge-shifting modifications that are enzymatically produced, such as phosphorylation, are very biologically important isoforms. The chemically deamidated isoforms, such as are believed to produce many of the characteristic charge shifts often found in blood proteins [208], also may be biologically important if they change the binding character of proteins or conversely, if the bound interactions of proteins protect potential deamidation sites from the chemistry that produces them. The relative biological activities of the isoforms with associated concentration changes in T2DM need elucidation, compared to other isoforms.

Recent research has attempted to discover the specific protein-protein and peptide-protein interactions of the abundant plasma proteins. This list of interactions has been dubbed the serum "interactome" [180]. Of potential interest is work that found several of the POIs from our experiment specifically bound to the blood carrier protein, human serum albumin (HSA). Figure 85 is the list of proteins that were found in a 2007 investigation by Gundry et al. [197] to be bound to HSA. The authors named this group of proteins the "albuminome". HSA has been briefly discussed at several points in this paper and important features of its structure and function will be discussed in detail in the last chapter, ASSESSMENT OF MODIFICATIONS OF HUMAN SERUM ALBUMIN. Recall that HSA is the most abundant protein in plasma and was ~99% removed from the analyte proteins by the immunodepletion step. HSA is known to be the primary carrier of

NEFAs for their distribution throughout the body, but is also known to bind other proteins, peptides and small molecules [197].

In Gundry's investigation, several methods; size exclusion chromatography (SEC), antibody purification and chemical (NaCl/EtOH) purification were used to assess the proteins that bound HSA. The chemical purification of HSA exploits its 17 internal disulphides, which give it the unusual ability to retain much of its conformation in high percentage organic solvent, and stay in solution. Only proteins that were found to stay in complex with HSA in SEC ("SEC A", "SEC B", "SEC C" in Figure 85) and at least one of either the chemical purification ("Whole fraction" in Figure 85) or the anti-HSA antibody extraction ("Anti-HSA retentate in Figure 85) were considered specifically bound to HSA, and labeled "yes" under the "bound" column. Others were designated "non-specifically bound" and appear as "nc" in Figure 85. SEC fractions were analyzed by both 1D SDS-PAGE and RP-HPLC followed by MALDI-TOF MS and LC-MS/MS to characterize the contents of the HSA bound SEC fractions. In the the far right "coverage" column of Figure 85, the protein sequence coverage is indicated as either: 1) INTACT, when the intact MW was observed by MALDI and greater than 30% sequence coverage was achieved, 2) SINGLE, when a single peptide in multiple fraction was observed, or 3) Percentage, when more than a simgle peptide was observed but there was not enough evidence to conclude the intact form [197].

Table 1. Proteins associated with albumin

Protein	Whole fraction	SEC A	SEC B	SEC C	Anti-HSA retentate	Bound?	Coverage
Retinol-binding protein	✓	✓				Yes[a]	INTACT
Alpha-2-antiplasmin	✓				✓	nc[b]	17%
Apolipoprotein E	✓				✓	nc[b]	18%
Apolipoprotein L1	✓				✓	nc[b]	11%
Beta thromboglobulin	✓				✓	nc[b]	35%
Carbonic anhydrase I	✓				✓	nc[b]	INTACT
Complement component 3	✓				✓	nc[b]	13%
Complement factor B	✓				✓	nc[b]	15%
Desmoplakin	✓				✓	nc[b]	12%
Fibrinogen, alpha chain	✓				✓	nc[b]	SINGLE
Gelsolin *	✓				✓	nc[b]	INTACT
Histidine-rich glycoprotein	✓				✓	nc[b]	9%
Lumican	✓				✓	nc[b]	INTACT
Prothrombin *	✓				✓	nc[b]	SINGLE
Serum Amyloid A4	✓				✓	nc[b]	32%
Vitronectin	✓				✓	nc[b]	6%
Afamin	✓		✓	✓	✓	Yes	18%
Alpha-1-acid glycoprotein 1	✓		✓	✓	✓	Yes	INTACT
Alpha-1-acid glycoprotein 2	✓	✓			✓	Yes	34%
Alpha-1-antichymotrypsin	✓	✓	✓		✓	Yes	INTACT
Alpha-1-antitrypsin *	✓	✓	✓		✓	Yes	INTACT
Alpha-1B-glycoprotein	✓	✓	✓	✓	✓	Yes	INTACT
Alpha-2HS-glycoprotein	✓	✓	✓	✓	✓	Yes	INT.
Angiotensinogen	✓	✓			✓	Yes	21%
Antithrombin III	✓	✓		✓	✓	Yes	INTACT
Apolipoprotein A I	✓	✓		✓	✓	Yes	INTACT
Apolipoprotein A II	✓	✓			✓	Yes	INTACT
Apolipoprotein A IV	✓	✓		✓	✓	Yes	INTACT
Apolipoprotein C II	✓	✓			✓	Yes	INTACT
Apolipoprotein C III	✓	✓			✓	Yes	INTACT
Carboxypeptidase B2	✓			✓	✓	Yes	12%
Ceruloplasmin	✓		✓	✓	✓	Yes	INTACT
Clusterin	✓	✓			✓	Yes	INTACT
Complement component 1 inhibitor	✓		✓		✓	Yes	INTACT
Complement component 4A	✓	✓			✓	Yes	9%
Haptoglobin	✓	✓	✓	✓	✓	Yes	INTACT
Hemoglobin, alpha	✓	✓	✓		✓	Yes	INTACT
Hemoglobin, beta	✓	✓	✓	✓	✓	Yes	INTACT
Hemopexin	✓	✓	✓	✓	✓	Yes	INTACT
Hornerin				✓	✓	Yes	SINGLE
Inter alpha trypsin inhibitor heavy chain H4	✓	✓	✓		✓	Yes	20%
Kininogen	✓		✓		✓	Yes	11%
Leucine-rich alpha 2 glycoprotein	✓	✓			✓	Yes	INTACT
Paraoxonase 1	✓	✓		✓	✓	Yes	26%
Peptidoglycan recognition protein 2	✓	✓		✓	✓	Yes	30%
Plasminogen	✓	✓			✓	Yes	27%
Transferrin	✓	✓	✓	✓	✓	Yes	INTACT
Transthyretin	✓	✓	✓	✓	✓	Yes	INTACT
Vitamin D-binding protein	✓			✓	✓	Yes	INTACT
Zinc alpha 2 glycoprotein	✓			✓	✓	Yes	INTACT

Figure 85 HSA associated proteins from Gundry et al [197]. Bold black boxes indicate proteins found changed in T2DM by us. Fine black boxes with asterisks are 1) HRG-a secondary ID of a T2DM POI with primary ID CFHR-5, 2) SAA-4 with high sequence identity to T2DM POI SAA-1, and 3) A1BG-a protein bound 1-1 with T2DM POI CRISP-3. Proteins in bold red boxes were found changed in T1DM by Metz et al. ZAG was found changed both in our experiment and in Metz [250].

Of note, according to Gundry, 26 out of the 35 specific HSA binders had been found in other studies to be potential biomarkers. 9 out of the 26 previously noted potential biomarkers, including apo A-I, were found exclusively in the anti-HSA albumin-enriched fraction and not in the HSA depleted fraction. Of these 9 proteins, 7 were potential cardiovascular markers.

Part of the motivation for Gundry's work was stated as follows:

"…the ratio of bound to unbound forms of a particular protein could be indicative of disease or immune response. Since this would likely be representative of changes to the intrinsic properties of these proteins and their interactions with albumin, the albuminome…could therefore become a useful tool in biomarker discovery."

In a comparison of the POIs from this 2DGE experiment with the 35 proteins in Gundry's list that met the standard for specific binding, we find that ZAG, Hpt, and apo A-I are included. So, at least half of the POIs in our study are in the albuminome, as defined by Gundry's most stringent criteria. Recalling that CRISP-3 is bound to A1BG with a 1-1 stoichiometry, then a connection to CRISP-3, is represented on this list as Alpha-1B-Glycoprotein. Also, SAA4 (not SAA1) and HRG are included in the non-specifically bound proteins. Of the POIs in our study, only CFHR-5 has no known connection to albumin binding, although several complement factors are included specifically and non-specifically in the albuminome. It's difficult to assign an accurate probability to our finding that a high percentage of T2DM POIs are also HSA binding proteins, primarily because the number of distinct proteins that are represented by the ~3400 spots on the gels is not known. But if one assumes that: 1) 300 distinct proteins are represented on the gels, 2) Gundry's detection capabilities were also sensitive to 300 proteins, and 3) all 35 proteins in Gundry's list are represented by spots on the gels, then

the probability can be calculated as a population-selection (without replacement) problem, or a hypergeometric probability[8]. This probability is used when one is interested in computing the probability for a number of observations that fall into a particular category. In our case we are interested in the number of changed proteins that are in the category of specific HSA binders of Gundry. Each time a protein is found in Gundry's list, that protein is removed from the list and the list is made 1 smaller. This is the "without replacement" character of the hypergeometric probability [313]. With a population of 300, number of successes in the population = 35, sample size of 6, and the number of successes in the sample = 3, then the probability of finding at least 3 of the albumin binders as a random occurrence is:

Equation 2 $$P_6(X \geq 3) = 0.022 \quad [314]$$

and like a p-value, this is considered significant below 0.05. The significance of this probability implies that the POIs in this group are not randomly, but systematically, related, and the simplest hypothesis as to their relationship goes back to changes in HSA. For this reason we chose to investigate the *in vitro* binding properties of HSA, as will be described in the next chapter.

Apparent changes in the stability of HSA have been shown to reflect certain diseased states [315]. Figure 86 compares the differential scanning calorimetry (DSC) profiles (thermograms) of whole plasma from people afflicted with the 3 diseases that were investigated; systemic lupus, Lyme disease, and rheumatoid arthritis. This

[8] My thanks to Ilai Keren of the Department of Mathematical Sciences at Montana State University for guidance on the hypergeometric statistics.

technique involves measuring the excess specific heat capacity of plasma samples while "scanning" through a range of temperatures. The heat capacity is reflective of the denaturation of proteins at their characteristic melting temperatures. In each figure the solid trace shaded in magenta is the averaged thermogram from 15 normal

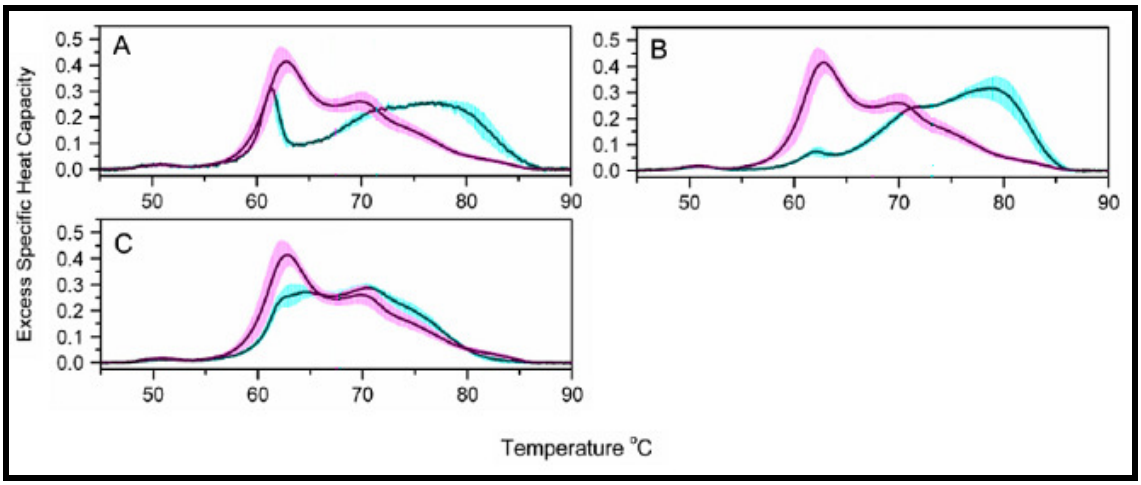

Figure 86 Comparison of normal (n=15, magenta) and diseased (cyan) thermograms in A) systemic lupus (n=2), B) Lyme disease (n=4), and C) rheumatoid arthritis (n=5). The shaded regions represent the standard deviations at each temperature. Figures modified from [315].

control individuals, with the shaded region representing the standard deviation at each temperature. The largest peak, at 62.8° C was shown to be largely the result of contribution from HSA. The thermograms shaded in cyan represent the diseased states. Figure 86A shows the averaged thermogram of samples from 2 patients of systemic lupus. Figure 86B shows the averaged thermogram of samples from 4 patients of Lyme disease. Figure 86C shows the averaged thermogram of samples from 5 patients of rheumatoid arthritis. The authors showed that there were no significant concentration differences of the proteins that were the primary contributors to the thermograms,

between the controls and diseased samples. The observed shifts in the thermograms in the diseased states were explained to be the likely result of differing levels of HSA bound species that led to the thermal stabilization of HSA, although a definitive test of this model was not conducted.

We looked for evidence of HSA's potential involvement in T2DM, in other diabetes studies in the literature. Considering the hypothesis that we detected altered ratios of bound and unbound HSA binding proteins, HSA immunodepletion may have been a critical step. If healthy and diseased samples contained approximately the same total amounts of the HSA bound POIs, but in differing bound to unbound ratios, then the co-removal of HSA bound species may have been important to the observation of significantly altered levels of unbound species in the flow-through analyte. If so, then the immunodepletion was more than an important sample preparation technique; it was also a means to reveal potentially important changes in biological interactions.

While not independently significant, some evidence may suggest HSA's involvement in a study of newly diagnosed patients with T1DM [250]. This study by Metz et al. was previously discussed in the section on ZAG in this dissertation. Metz also used HSA immunodepletion as part of a plasma MARS-6 immunodepletion strategy, prior to a bottom-up LC-Fourier transform ionization cyclotron resonance (FTICR) quantitation strategy. Of the 5 POIs from Metz's T1DM proteomics study: ZAG (up 2-fold in T1DM), corticosteroid-binding globulin (up 2-fold in T1DM), lumican (up 2-fold in T1DM), clusterin (down 2-fold in T1DM), and serotransferrin (down 2-fold in T1DM), all but corticosteroid-binding globulin are on Gundry's list of 50 specific and non-

specific HSA binding proteins [197]. Lumican is listed as a non-specifically bound protein and the others are indicated as specifically bound. The POIs of Metz are shown in red boxes in Figure 85. Unfortunately, this group's stringent filtering criteria only allowed the quantitation of 1930 unique peptides, corresponding to 120 unique proteins. So, calculating the hypergeometric probability with a population size of 120 and 50 of successes in the population, the probability that at least 4 of the 5 POIs in Metz formed a random group was:

Equation 3 $$P_5(X \geq 4) = 0.096$$

which, while suggestive, is not low enough to statistically determine that the 4 POIs formed a group that was significantly associated with HSA.

Of course, despite the similarities of T1DM and T2DM, including chronic IGT and the consequent pathologies, they involve very different metabolic disturbances, and one would expect to find different markers. It is of interest that both diseases have altered ZAG plasma concentrations, although in different "directions"; up in Metz's newly diagnosed T1DM patients and down in our newly diagnosed T2DM patients.

The evidence from our study in T2DM and the weak corroboration by Metz's study in T1DM, that hyperglycemia may involve biologically relevant changes in HSA's binding character, seemed an interesting possibility, so this was pursued, as will be described in the following chapter.

THE BROMOCRESOL GREEN ERROR FROM POLYCLONAL HSA ELISA (BEPHE ASSAY)

Human Serum Albumin

Human serum albumin (HSA) is by far the most abundant protein in plasma. Because of its abundance and its reputation as a "volume expander" [316], a non-specific "molecular sponge" [317] and a specific carrier protein with little enzymatic activity of its own, it has viewed as an obstacle to the analysis of lower abundance proteins in the 2D-PAGE portion of this experiment, as well as other approaches to plasma proteomics analysis. Interestingly, the results of the 2D-PAGE experiment pointed to the possibility that there was something changed about albumin and its protein binding in the T2DM patients. This was based on our observation that a high percentage of the detected changes between T2DM and control plasma were in proteins that are known to bind to albumin [197]. Ironically, whereas our experiment began by viewing HSA as an obstruction, HSA then became the focus of attention for the experiments that followed. For this reason it will be helpful to take a closer look at serum albumin, its known activities, and the means by which its binding properties may be changed in T2DM and hyperglycemic states.

Human serum albumin (HSA) is a highly soluble protein comprised of 585 amino acids with an M_r of 66 K [318]. It is present in healthy human plasma at concentrations between 35 and 50 mg/mL. [319]. HSA has a variety of known physiological roles. One of these is as a key regulator of the osmotic pressure and the distribution of fluid between the different compartments of the body. For this reason, in World War II it was purified

by virtue of its acidic pI and unique solubility in cold ethanol as “Cohn fraction V”. Intravenously administered as a plasma substitute to wounded soldiers as a treatment for shock due to blood loss, HSA is associated with rapid increase in circulating blood volume [316].

Despite the presence of 17 disulfide bridges, albumin has sufficient flexibility to adapt its shape to carry an assortment of biological species, many of which involve hydrophobic interactions [319], as discussed below. In principle, each modification to the structure of albumin, whether it is a result of covalent modification, ionic or hydrophobic interaction, can be expected to modify its binding properties even if the interactions occur at a distance from the binding site [320].

Albumin’s versatile binding capacities involve known sites that transport a variety of cationic, anionic and hydrophobic ligands. The cationic ligands include calcium ion and several divalent metals: Cu(II), Ni(II) Zi(II), Mn(II), Co(II), and Cd (II)) [319]. Among the anionic ligands are several long-chain non-esterified fatty acids (NEFA): oleic acid (18:1), stearic acid (18:0), linoleic acid (18:2), palmitoleic acid (16:1) and arachidonic acid (20:4), which are normally loaded onto circulating albumin at 1 to 2 molar equivalents after food injestion, although albumin has a capacity of 6 fatty acids *in vitro* [319]. Other classes of lipids also are known to bind albumin. The esterified fatty acid, lysolecithin, has been shown to bind to a site that is not competitive with the NEFA sites [319]. Prostaglandins, the steroid hormones cortisol and testosterone, as well as cholesterol and the bile pigment bilirubin have been shown to be carried by albumin. Also, albumin is the primary circulating reservoir (80%) of the biological regulator and

neuromodulator, nitric oxide [321]. The S-nitroso-albumin derivative was shown to retain endothelium derived relaxing factor-like biological activity [321].

Albumin's primary role is believed to be the transport of long chain NEFAs [322]. By binding to albumin, the very low aqueous solubility of the NEFAs can be overcome in blood, and up to mM concentrations of NEFAs can circulate in a non-aggregated form that is readily available to cells [323]. To be efficiently transported, NEFAs must exit the adipocytes, cross the capillary endothelium, travel through the blood stream, and enter the receiving cell.

Lacking evidence of HSA receptors used for the transfer of NEFAs to cells [322], a minimum of three distinct steps are thought to be involved, for transfer from HSA to the cell. First, the NEFA must desorb from HSA and adsorb to the outer leaflet of the cellular plasma membrane. Second, NEFA must cross the bilayer with a "flip-flop" transmembrane movement, in which the carboxylic head group re-orients to the cytosolic face. Third, NEFA must desorb from the cytosolic leaflet for intracellular usage, such as for oxidation or synthesis of cholesteryl esters, phospholipids or signaling molecules like the prostaglandins [324]. The second step, a passive "flip-flop", is an unlikely event in a lipid bilayer if it is assumed that the NEFA exists only as an anion. It has been shown that for a NEFA lying at the aqueous interface, in proximity to the negative charges of phospholipids, the pK is predicted to shift significantly higher. In experiments using small unilaminar vesicles (SUV) it has been shown that the apparent pK of NEFA is 7.5 [323] to 8.4 [325], surprisingly close to physiological pH, so that 50% to 90%,

respectively, of the NEFAs should be un-ionized. Further, it has been shown that NEFAs do undergo flip-flop in SUVs [323] and lipid bilayers of simple lipid vesicles [326].

HSA is also known to be a highly specific carrier of several pharmacological agents. An interesting pair of these ligands are the coumarin-derivative, anticoagulant drugs phenprocoumon and warfarin. As an important illustration of the sensitivity of two similar ligands to the presence of a third ligand, it was shown that the affinity of HSA to warfarin was positively correlated ($P < 0.0001$) with plasma FFA concentration [327]. But this correlation was not found for the very similar phenprocoumon structure, which was shown to have dramatic ramifications for the bioavailability of the two drugs in vivo [327]. Also, recombinant long-lasting insulin detemir, an insulin analog conjugated with a 14-carbon fatty acid chain, has been shown to gain its protracted pharmacokinetic activity *in vivo* because of its association with HSA, both at the subcutaneous site of injection and in the bulk plasma [328].

HSA can be glycated *in vivo* by the same non-enzymatic, glucose concentration dependent means that hemoglobin is glycated. The glycation of HSA alters its binding properties and conformation [329, 330]. A 2008 study [330] showed an interesting protection of HSA from glycation by metformin. Metformin is an "insulin sensitizing" drug with a primary activity on the liver that reduces hepatic glucose production (HGP), mainly by reducing gluconeogenesis [331] and therefore also reduces FPG, by an undiscovered mechanism [331, 332]. This metformin protection was observed even though the hemoglobin A1c levels were <u>not</u> different between the treated and untreated groups. This implies that the difference in glycation of HSA may be due to an unknown

mechanism by which metformin lowered the HSA glycation, apart from the general metabolic effects of metformin [330]. This paper also showed that, when compared to untreated T2 diabetics, the intrinsic tryptophan fluorescence quenching in HSA by acrylamide was significantly changed in metformin treated diabetics, which more closely resembled the tryptophan quenching in the HSA of non-diabetics in the absence of metformin. The difference in quenching between the groups was explained by a difference in accessibility by the acrylamide to the HSA tryptophan, resulting from differences in HSA conformation induced by metformin.

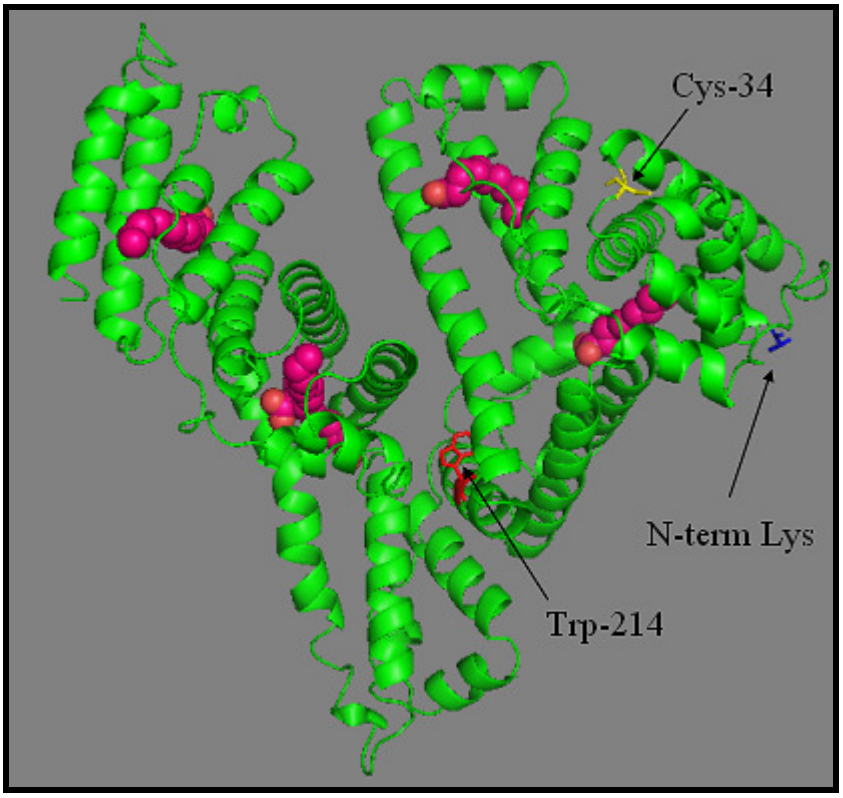

Figure 87 Human Serum Albumin crystal structure complexed with 5 myristates, from [333]. RCSB PDB 1BKE [334].

HSA is also considered to be the most abundant and important [316] anti-oxidant in plasma, and it regulates the redox state of blood by several means. We have already seen that HSA binds several divalent metals. By sequestering Cu(II), and potentially Fe(II) in iron over-loading disease, HSA protects other plasma proteins and lipids from the production of oxidative hydroxyl radical (•OH). Cu(II) can be reduced to Cu(I) by biological reductants such as reduced glutathione (GSH) and ascorbic acid [335]. •OH can be released when these transition metals, Cu(I) and Fe(II), free in solution, react with hydrogen peroxide [336], which can arise from enzymes, oxidizing compounds and activated phagocytic cells [337]. This redox reaction is known as the Fenton reaction [338] (Equation 4),

Equation 4 Fenton reaction $Cu^{1+} + H_2O_2 \rightarrow Cu^{2+} + \bullet OH + OH^-$ [335]

$Fe^{2+} + H_2O_2 \rightarrow Fe^{3+} + \bullet OH + OH^-$

Fenton reactions are known to occur at the sites of metal ion binding, resulting in damage to HSA. Because of HSA's high concentration and rapid turnover, such damage has been regarded as probably biologically insignificant [337, 339]. But this does not consider the possibility that oxidative damage could preferentially occur to a subset of HSA which is involved in particular complexes. Such effects might have little effect on the gross concentration of HSA, but could potentially change the concentration and biological effects of those complexes.

Introduction and Method Development

In order to test for changes in the binding character of HSA, we developed an assay that uses HSA-specific binding of bromocresol green dye (BCG) binding and an anti-HSA polyclonal enzyme linked immunoadsorption assay (ELISA). We reasoned that the BCG assay may be sensitive to changes in the binding character of HSA, whereas the polyclonal ELISA would measure the total protein concentration. BCG is a single species which binds to relatively few sites on HSA, which may have altered binding resulting from protein modifications, whereas the polyclonal ELISA, with many potential epitopes, more effectively measures the total amount of HSA present, regardless of modifications. Therefore, for each plasma sample, we expressed the BCG result as the "observed value" in the canonical "error" equation form:

Equation 5 Error = ("true value" – "observed value") / ("true value")

whereas the "true value" of the HSA concentration was determined by ELISA, and BEPHE is an abbreviation for the unitless "BCG error from polyclonal HSA ELISA", to become:

Equation 6 $BEPHE = ([HSA_{ELISA}] - [HSA_{BCG}]) / [HSA_{ELISA}]$

This calculation allowed the qualitative hypothesis, that the binding character of HSA is altered in T2DM, to be quantitatively assessed by plotting the BEPHE result against certain metabolic measurements associated with diabetes, such as FPG, Ha1c, CRP etc.,

to look for correlations. Before proceeding to the Materials and Methods for this assay we will examine the relevant issues surrounding the dye assay from the literature.

In 1965, Rodkey et al. introduced an "inverse colorimetric" phthalein dye binding assay for HSA that used HSA's versatility for binding amphipathic species, to measure the HSA concentration in serum [340]. This introduction of the assay used a 50 mM phosphate buffer at physiological pH 7.1, a pH which stabilized the conformation of HSA and its binding partners. The assay is called "inverse" because the absorbance of the HSA-bound BCG dye molecule at 616nm decreases from its free absorbance, giving a negative slope to the absorbance vs. concentration standard. The free dye

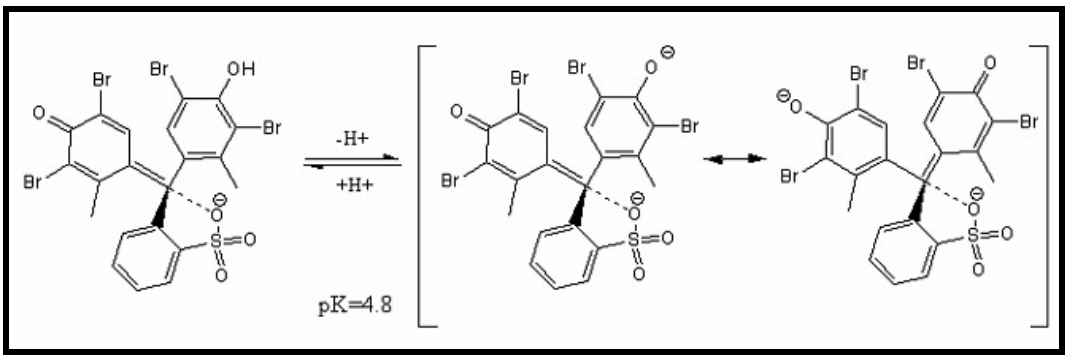

Figure 88 Bromocresol Green structure. From [341] and Wickipedia.

structure at pH=7.1 is predominantly to the right of the equilibrium (pK=4.8 [342]) in the form of the two doubly negatively charged resonance structures in Figure 88.

Rodkey claimed that the method accurately measured HSA with no interference from lipids or bilirubin, known cargos of HSA. A 150-fold dilution of the plasma was shown to be sufficient to decrease the light scattering absorbance of all but highly lipemic, "milky" sera to an insignificant fraction of the total absorbance change. No

detergent was included in Rodkey's method. Our modification included a small amount of detergent and diluted the plasma 250-fold to minimize, light-scattering aggregations, which could confound the HSA-BCG binding with T2DM associated dyslipidemia. An important contribution to our argument will be to control for the triglycerides, which can cause turbidity in high concentrations, and to directly show that light scattering turbidity is not correlated with either the BCG assay or the BEPHE assay, which is the BCG assay normalized by the HSA ELISA value. Also, Rodkey showed that the bile pigment, bilirubin, a known HSA binder, was not an interference at 615nm and was not an effective competitor with BCG for HSA binding sites.

Rodkey investigated the specificity of the neutral pH BCG assay with 3 separate procedures which showed that BCG was not bound by other serum proteins: First, an PAGE separation of serum was stained with the BCG solution, and no evidence of binding by any protein other than HSA was found. Second, a dialyzed serum globulin fraction was prepared by lowering the ionic strength and precipitating the serum globulins. HSA remains soluble in these conditions and was washed from the globulin fraction. The washed globulins were then dissolved in NaCl and added to a BCG solution and no reaction was seen. And third, it was shown that standard HSA solution added to a serum sample was quantitatively recovered from 98.5% to 102% by the BCG measurement, showing that the dye reaction with added HSA was not affected by the presence of serum constituents.

Several groups have made refinements to Rodkey's method in an effort to more accurately measure HSA concentration. The most important modification was introduced

by Doumas et al. in 1971 [343] and is cited in WAKO Pure Chemical Industries literature as the source of the protocol for their current commercial BCG assay [344]. Doumas stated that the main disadvantage of the Rodkey method was the very high absorbance of the working dye solution, which required the use of a sensitive and precise photometer. In their refinement, Doumas took advantage of HSA's pH stability [319] to develop a BCG assay at pH 4.2 in succinate buffer, which used added non-ionic detergent to prevent the protein precipitation that otherwise ensued upon the acidification of proteins. The dye structure at this pH is predominantly to the left of the equilibrium arrows in Figure 88. In the presence of detergent and at this pH, the BCG assay has very low absorbance at 630nm, the wavelength of the analysis. The Doumas assay does not have an inverse relationship between absorbance and dye-binding, as the standard has a positive slope, which is steeper than Rodkey's standard curve, making this assay more sensitive than the Rodkey method. Automated methods using Doumas's method are in clinical use to this day.

Doumas stated that the Rodkey method "not only involved the measurement of high absorbances, but also did not show linear absorbance-concentration relationship and the curve did not intercept the origin." However, as shown in Figure 89 this doesn't

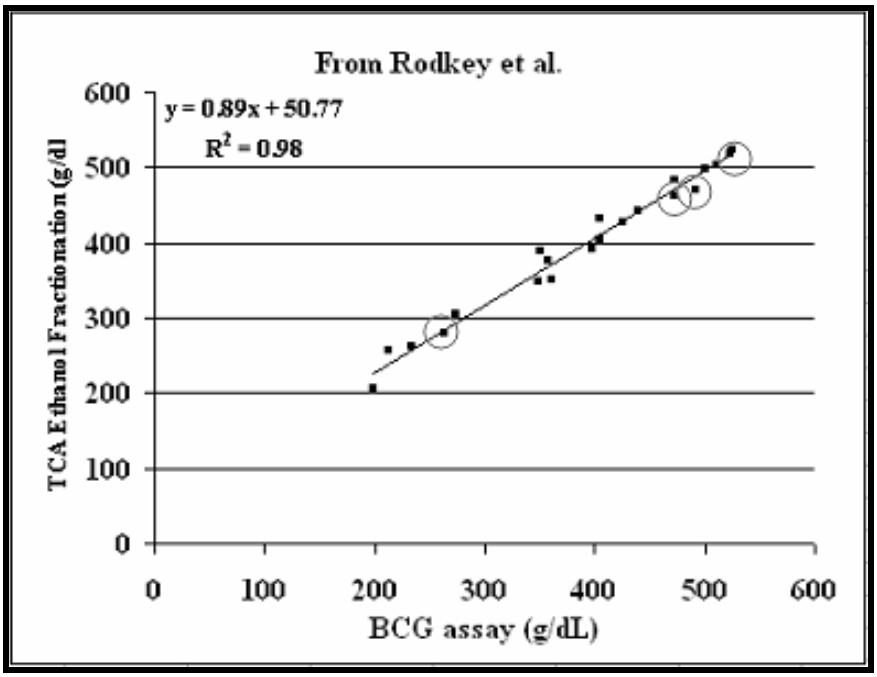

Figure 89 Data from Rodkey et al [340] Table #1 "Serum Albumin Values for Human Serums Obtained By Direct Spectrophotometric Analysis and By TCA-ethanol Fractionation." 4 of these samples were regarded as "extremely lipemic". These data points are circled. There was no correlation of the lipemic status of the samples with BCG error from the TCA-ethanol method.

appear to be wholly true. Figure 89 is a graphical representation, derived from the data listed in Table 1 of the Rodkey paper [340]. Although Rodkey didn't show it graphically, the linear relationship is evident, with an excellent R^2 fit to the line. With the Y-intercept at approximately 51 g/dL, there is a systematic underestimation of HSA by this method that gets worse at low concentrations. An appropriate control will also be given in the Results section, to show that our result is not an effect of this systematic bias.

Unlike Doumas, our goal for the dye-binding assay was not to use a method that necessarily gave the most accurate measurement of the absolute HSA concentration. We wished to preserve any native bound species that could sterically hinder or otherwise alter

the affinity of HSA for BCG binding, as much as possible. The 2D-PAGE experiment highlighted changes in proteins that normally bind to HSA, suggesting that HSA was at the hub of changes seen in T2DM, in a high percentage of known protein associations. Our hypothesis was that the HSA in T2DM was binding protein "passengers" differently for some reason than in control subjects. The list of candidate differences in proteins in the diabetic state that possibly could cause altered binding includes post-translational modifications, bound lipids, oxidation, glycation, protein-protein interactions, bound toxins, bound metabolites, etc. In order to develop an assay that was sensitive to the possibility that the differences in HSA binding resulted from altered levels of protein-protein associations and other conformation dependent or pH dependent ionic interactions, we elected to modify the original neutral pH, Rodkey BCG method that utilized mild conditions, but had less sensitivity than the Doumas method. Rodkey's method, run at pH=7.1 was more likely to preserve protein conformation to the highest degree, and thus report on subject-to-subject alterations of dye affinities to HSA's binding site(s). The Doumas method was clearly not appropriate because it was done at low pH and required detergent to prevent the precipitation of denatured proteins.

Our main modification of the Rodkey assay was the addition of 100 mM NaCl. This was done to make the ionic strength of the assay similar to human plasma to preserve interactions with HSA that depended upon this environment. The average plasma concentration of sodium is about 140 mM [345], but it has been reported that the addition 34 mM of NaCl [343] lowers the sensitivity and the linearity of the Doumas BCG assay. This point is interesting as it may imply that the inclusion of NaCl does

indeed preserve a hindrance to BCG binding by stabilizing native ionic interactions, as would be appropriate for our goal. We found that, with the inclusion of 100 mM NaCl, a linear absorbance vs. concentration standard curve was produced in the 96 well plate reader, yielding R2 values of ~0.97. These are shown in the Results and Discussion section Figure 96 and Figure 97.

Rodkey used a 45 μM BCG solution with a serum dilution factor of 150. They claimed that these conditions prevented any loss in sensitivity for the range of HSA concentration in serum below 50 mg/mL. Our method used 28.6 μM BCG with a plasma dilution factor of 250. The question then arises; did the lowered concentration of reagents create a loss of sensitivity for plasma samples with high HSA concentration, where an effect of a depleted pool of free BCG anions could possibly begin to show? The ability to create linear calibration curves from our plasma standard indicates that it did not cause loss of sensitivity at high HSA concentration. The presence of added NaCl in our protocol may have provided a benefit in this regard since; by preserving suspected BCG antagonizing associations, there would tend to be more free BCG anion concentration than without the added salt. Also, the plasma standard sample, which was used to create the linear calibration curves, bound the most BCG of any plasma sample in the experiment. So, the samples that bound less BCG were assured to be within the linear range.

The other modification that was made in our assay was the inclusion of a small amount of CHAPS, a zwitterionic detergent. The Rodkey assay does not include any detergent. The low pH Doumas assay includes 0.125% of Brij-35 a non-ionic detergent.

We used a concentration 1000-fold less detergent concentration than the Doumas assay, as a "compromise" between the two methods. CHAPS was found to have negligible absorbance at 616nm.

After the publication of Doumas's more sensitive, acidic, denaturing BCG method, Rodkey's method fell from favor, and critical literature has been directed at Doumas's method. In 1974, a group reported that the Doumas (pH 4.8) BCG assay overestimated low values of HSA when compared with capillary electrophoresis. Figure 90A shows this effect [346]. Two controls, shown in Figure 90B, provide excellent agreement of capillary electrophoresis with two other methods of HSA measurement, radial immunodiffusion and Laurell "rocket", at the lower concentrations [346]. Later evidence [347] showed that this overestimation of HSA was caused by a relatively slow interaction of the BCG dye primarily with a class of acute-phase α-globulins including haptoglobin, ceruloplasmin, and orosomucoid [348] that are normally upregulated in times of acute infection. Figure 90C illustrates this effect with a figure from their publication [348]. Shown are the "apparent albumin" concentrations vs. time, with t=0 being the addition of plasma to the BCG reagent. Although the authors did not elaborate,

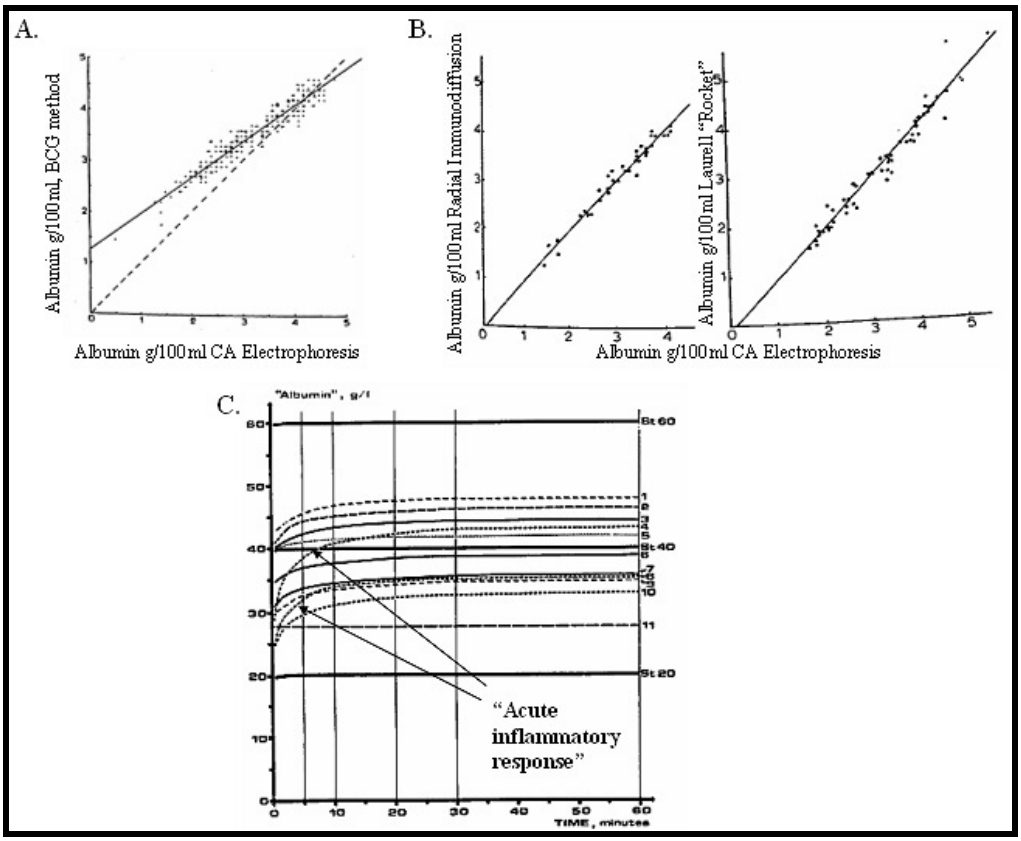

Figure 90 Evidence of systematic errors in the low pH BCG assay. A) Systematic overestimation compared to capillary electrophoresis. B) Comparison of capillary electrophoresis to radial immunodiffusion and Laurell Rocket assay. Data from [346]. . C) Time dependence low pH BCG assay with 2 acutely ill subjects (arrows). Data from [348].

they claimed that the subjects represented by the traces with the greatest change (two arrows) of apparent HSA, between t=0 and t=60 minutes, were acutely ill. They showed that the percentage of this slow change in BCG binding quantitatively correlated with the concentrations of protein markers of acute inflammatory response in all of the subjects. The authors recommended a fast reaction time for the BCG assay, less than one minute,

to overcome this complication and to produce the closest correlation with HSA concentration, as measured by other well validated methods.

In 1968, an assay similar to the BCG assay that used a similar phthalein species, bromocresol purple (BCP), was introduced in a paper to the 20th National Meeting of the American Association of Clinical Chemists [349]. It was later reported that the BCP-HSA reaction at pH=5.2 was immediate and specific for HSA [350] but, as shown below, is more susceptible to biological interference.

As was found in the pH=5.2 BCP HSA binding reaction [350], our investigation found no time dependence of the pH 7.4 BCG reaction, after the earliest possible reading at ~15 seconds. This lack of time dependence in the absorbance signal was as expected from the Rodkey paper [340], since no specification was given with respect to the amount of time between mixing the reagents and reading on the spectrophotometer. Readings were taken at 10 minutes for the experimental samples, although by using the plate reader, precise control of the time was more difficult. To neutralize any effect of time dependence, the BCG-protein reactions were started by alternating the initiation of the reactions between the sample groups. They were then plated and read in the same sequence that they were initiated. The Tecan Safire plate reader contains a double monochrometer, which greatly reduces stray light and allows it to measure high absorbances accurately.

Although there is no evidence that Rodkey's neutral pH assay can be complicated by slow, non-specific interactions with acute-phase proteins, we will provide data to counter the argument that such species might account for the observed differences in the

experimental samples, in the Results and Discussion section. But it should be stated at this point that acute-phase reactants are known to be generally increased in diabetics [119, 351], and all three CRP/SAA/Hpt were increased or had isoforms that were increased in the diabetics that we tested. In contrast to the finding in the literature of increased dye binding by acute phase proteins [346], our neutral pH BEPHE assay showed decreased binding of BCG per HSA in the hyperglycemic subjects. This is counter to what would be expected if the acute-phase reactants predominated by causing the change caused by insulin resistance. In summary, it appears that the BEPHE assay is reflecting the binding capacity of HSA.

There are no high resolution structural studies that show the binding site(s) of BCG to HSA. A 1964 study by Rodkey [352] of BCG binding at pH 6.95 showed 5 lower affinity dye binding sites ($K_a \approx 2.0 \times 10^4$) and 3 higher affinity binding sites ($K_a \approx 7.0 \times 10^5$) on human mercaptoalbumin (free thiol at Cys-34). A biochemical study [353], using the binding conditions of Doumas with various proteolytic fragments of HSA, has shown that a high affinity dye binding site exists near the N-terminal, involving the residues 186-306. This is also the high affinity site for bilirubin binding [353]. Bilirubin has been shown to be displaced by fatty acids and drugs [353].

There are a few studies that utilized a similar concept as the BEPHE assay, for pathological conditions involving the kidney. Studies since the early 1970's had shown reduced binding of dyes to HSA in patients of renal disease or renal transplants [354-356]. Using an anionic dye called methyl orange to show this in 1973, S. Dromgoole suggested that HSA bound NEFAs caused reduced dye binding, but then, in a follow-up

publication, showed that reduced dye binding was not caused by NEFAs [354, 355]. In a 1986 study by Maquire et al. [356] that compared BCG (pH 4.2) with bromocresol purple (BCP pH 5.2 in acetate buffer), the claim was made that BCP, (with lower affinity), detected an inhibition of HSA binding, resulting from a competitive, unknown species in patients of renal failure (Figure 91), which BCG, (with

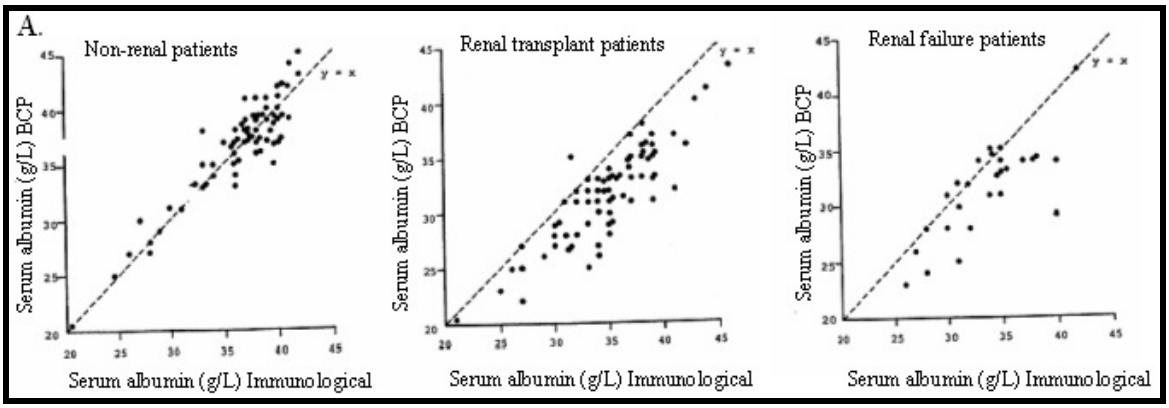

Figure 91 BCP assay detects an unknown HSA bound species in renal patients.

higher affinity), did not detect (not shown). The result was that BCP gave a falsely low HSA concentration in these patients, when compared to an immunological assay and the BCG assay. The lower binding of BCP could detect renal failure but didn't correlate with its severity as assessed by serum creatinine concentration. The reduced binding of BCP by HSA in the renal patients was consistent even when the experimenters adjusted the concentration of BCP 2 and 3-fold, added 135 mM NaCl or adjusted the pH to 4.4 or 4.8. They reasoned that this was because of the relatively low affinity of HSA for BCP.

If BCP has been shown to be more sensitive than BCG to certain competitive binding partners, one may well ask why not use BCP in such an assay as the BEPHE assay? The answer is that a strategy using BCP could well have promise, but there are no

published reports with BCP under native, neutral conditions, as was done by Rodkey with BCG.

Circulating endogenous insulin is not known to bind to HSA to any biologically relevant degree. But because so many other HSA binding species such as circulating FFAs, acute phase proteins, and glucose (glycation) may be related to insulin sensitivity, we wished to investigate whether the fasting concentrations of insulin could be correlated with the BEPHE results. We tested the correlation of the BEPHE results with insulin resistance by calculating insulin resistance, using a method called the Homeostasis Model Assessment of insulin resistance (HOMA-IR). While the gold standard for measuring insulin resistance is the 4-hour hyperinsulinemic-euglycemic clamp [357], HOMA-IR offers a simple, inexpensive way to calculate insulin resistance, using only FPG and fasting plasma insulin concentration (FPI) in an equation that is very simple:

Equation 7 HOMA-IR = FPI (uIU/mL) x FPG (mmol/L)/ 22.5 [358]

This HOMA-IR calculation of insulin resistance has been shown to correlate closely ($P < 0.0001$, $n=115$) with values of the glucose disposal rate as measured by the 4-hour hyperinsulinemic-euglycemic clamp [359]. The calculation was also found to be robust since there were no substantial differences in correlation between men, women, different age groups, obese and non-obese subjects, non-T2DM and T2DM subjects, or normotensive and hypertensive subjects [359]. The diagnostic cutpoint for IR, using the HOMA-IR model is 2 [360]. Using the values of FPG that were provided for experimental samples by the NIH, the calculation of HOMA-IR required the

determination of FPI, which was carried out by sandwich ELISA as described in the Materials and Methods section.

Materials and Methods

● *Competitive ELISA for HSA Concentration.* To quantify HSA in individual plasma samples, we used a competitive polyclonal ELISA kit (AssayMax Human HSA ELISA Kit for plasma and serum-Assaypro, catalog #EA2201) and followed the manufacturer's instructions.

Briefly, to prepare the HSA standard, 500 µg of the HSA standard provided was dissolved in 5 mL of the kit's mix diluent (concentrate provided was diluted 1:10 with MilliQ water) to make a 100 µg/µL standard solution. After vortexing, a portion of the standard stock was subjected to 4-fold serial dilutions 4 more times.

To prepare the individual diseased and control samples, 10,000-fold dilutions of the plasma were created by first adding 4 µL of plasma to 396 µL of the kit mix diluent to create the primary dilution. After vortexing, 10 µL of the primary dilution was further diluted by adding to 990 µL of mix diluent and vortexing.

25 µL of each of the 10,000-fold diluted plasma samples and standards were aliquoted in triplicate to the wells of the 96-well microplate that was pre-coated with polyclonal anti-HSA antibodies. Triplicate wells of mix diluent were also prepared for the assessment of background. Using a multipipetter, 25 µL of the biotinylated standard HSA (the provided stock solution diluted 1:8 with mix diluent) was added to the samples and standards in the wells. After covering with sealing tape, the plate was incubated,

while gently shaking on a rotary titer plate shaker (Lab-line Instruments Inc.), at room temperature. After 1 hour, the wells were washed 5 times with 200 µL of the wash buffer provided (concentrate provided diluted 1:20 with MilliQ water), briskly tapping out the wells of the inverted plate onto a paper towel between washes. After washing, 50 µL of the streptavidin-peroxidase conjugate (the concentrate provided was diluted 1:100 with mix diluent) was added to each well using a multipipetter and the plate was covered with sealing tape and incubated with gentle orbital shaking for 30 minutes. The wells were then washed as described above and 50 µL of the peroxidase substrate provided (tetramethylbenzadine) was added to each well using a multipipetter. After about 10 minutes the evolution of blue color appeared to stop, and 50 µL of the 0.5 N HCl stop solution was added to each well.

Absorbance readings were immediately taken, at 450nm using a microplate reader (Tecan Safire). A 3 x 3 circular reading pattern with 3 flash repeats at each position was used for the standards, NGT and T2DM samples. In a follow-up experiment, in order to speed up the reading, a 2 x 2 circular reading pattern with 3 flash repeats at each position was used for the IGT samples and standards. This departure from our previous standard method is explained and rationalized in the Results and Discussion section.

The mean values for the triplicate readings of absorbance were plotted on the Y-axis in an Excel spreadsheet scatter plot and the standard concentrations on the X-axis to generate the standard curve. The equation for the best-fit line was determined by regression analysis using a 2^{nd} order power series curve-fit. The equation of the standard curve was used to determine the HSA concentrations of the experimental samples using

their averaged absorbance readings. The calculated values were multiplied by 10000 to account for the 10000-fold dilution factor to determine the plasma HSA concentrations.

● *Non-Denaturing Bromocresol Green Assay.* The BCG reagent solution was made in MilliQ water as follows: 28.6 μM bromocresol green sodium salt (Sigma-Aldrich, catalog # 114367-5G), 0.125 x 10^{-3} % w/w CHAPS, 100 mM NaCl, 50 mM NaH_2PO_4, pH=7.4. A similar, non-chromagenic (NC), reagent solution was prepared without the BCG salt to make the standard dilutions (Table 18). Solutions were refrigerated at 4° C until used.

The between-day reference standards were prepared from citrated plasma drawn from a donor (Garry Handelman "GH") at Montana State University Health Center and centrifuged, aspirated and frozen at -80 °C in 120 μL aliquots by our laboratory.

Before the day of the assay, several 6-point serial dilution series were prepared from the standard plasma and NC buffer using the amounts of plasma and NC buffer shown in Table 18. These were aliquoted in the amounts shown under the column heading "Add" in Table 18. The aliquots were frozen at -80° C until the day of the assay.

Table 18 Plasma standard preparation for the BCG assay. "NC"-non-chromagenic.

Standard #	Plasma (uL)	NC Buffer (uL)	Add (uL)	BCG reagent (uL)
1	20	80	4	996
2	20	30	4	996
3	30	20	4	996
4	40	10	4	996
5	100	0	4	996
6	4 uL #1 + 4 uL #5		8	992

On the days of the assays, the prepared standards were mixed with the stated amount of BCG reagent in the last column of Table 18. The standards were prepared in order to relate the results of BCG assays that were performed on different days. GH plasma was also included in the ELISA HSA assay in order to convert the BCG standard results into the units of μg/μL.

To perform the assay, the BCG reagent was brought to room temperature and all standards and plasma samples were thawed on ice. The 6 prepared standards were mixed with the BCG reagent according to Table 18, in 1.7 mL microfuge tubes, vortexed and added to a 96-well plate in 200 μL aliquots, in triplicate. Ten minutes after mixing, readings were taken on the TECAN plate reader. For the experimental plasma samples, 4 μL of plasma was added to 996 μL of the BCG reagent, vortexed and added to the 96-well plate in triplicate 200 μL aliquots. After assuring that no bubbles were present in the microwell plates, readings were taken at approximately ten minutes.

In order to control for read time, the first set of samples that were assayed; the standards, 10 NGT and 8 T2DM samples, were read as triplicate readings in groups of six. So, first, the six triplicate readings of the standards were performed. Then, the first batch of six experimental samples alternating non-diabetic and T2DM, and then the 2nd and 3rd batches were read with the 3rd batch consisting of 4 non-diabetic and 2 T2DM samples. These readings were taken as "3 x 3" circular reads, which is actually only five different well reading positions, arranged like the five spots on a die.

In a later assay, in order to expand the experiment to include the 13 IGT samples, the standard and the samples were read as 2 x 2 circular reads, which is actually just a 2 x

2 square, reading four positions in the well. The 6 standards were read separately and the 13 IGT samples were read as a single batch. The reason for this change, from the reading method used for the T2DM and NGT control sets, was to reduce the amount of variation between technical replicates as it was observed that the menisci were sometimes positioned differently from well to well. By reading closer to the center of the wells, using a 2 x 2 reading pattern in each well, the readings were within the flatter regions of the wells and the menisci had less effect. The effect of the different reading protocols can be seen by comparing the standard charts in the Results and Discussion section, Figure 96 and Figure 97. While both methods give good linear correlation, they are significantly different with respect to the absorbances. This is because the 3 x 3 circular read, reads positions in each well that were on average, significantly closer to the edges of the wells and are reading greater (nearly 50%) average path lengths due to the meniscus effect at the edges.

- *Sandwich ELISA for Human Insulin* - To quantitatively measure insulin concentrations in the plasma samples, a 96-well monoclonal ELISA insulin assay (EIA) was purchased (ALPCO Diagnostics- Catalog # 80-INSHUU-E01). All solutions were prepared according to the manufacturer's instructions and brought to room temperature before use. The cross-reactivity of the assay for C-peptide (an insulin cleavage product), insulin-like growth factor-1 (IGF-1), IGF-2 and proinsulin were stated to be < 0.01%. A diabetes antigen control lyophilized powder was provided with the kit for inter- and intra-assay quality control. It was reconstituted according to the manufacturer's instruction and run in parallel with the samples on each day.

Because of limited sample amounts, 21.5 µL, instead of the recommended 25µL, of plasma samples, insulin standards (0.15, 1, 3, 10, 20 µIU/mL) and antigen control, were pipetted into their respective wells. All standards and samples (n = 9 control, n = 7 T2DM) were run in duplicate. 21.5 µL of each standard, reconstituted antigen control, or sample were pipetted into wells in duplicate. After immediately adding 100 µL of horseradish peroxidase (HRP) labeled monoclonal antibody to each well, the plate was covered and incubated on an orbital microplate shaker at approximately 700 rpm for 1 hour. Using a multipipetter, the wells were washed 6 times with 200 µL of wash buffer, rapping the plate on paper towels between the washes to clear the wells of liquid. 100 µL of chromagenic HRP substrate was then added to the wells and the plate was covered and incubated at room temperature for 30 minutes on the shaker at approximately 700 rpm. After 30 minutes, 100 µL of the stop solution was added to each well and gently mixed. After confirming that no bubbles remained in the wells, the plate was read on the TECAN microplate reader at 450 nm, using a reference wavelength of 650 nm. Each well was read with a 4 x 4 circular read pattern and 3 shots per position.

Results and Discussion

● *Competitive ELISA for HSA.* The standard curve that was used for the NGT and T2DM samples is shown in Figure 92. The standard curve for the IGT samples is in Figure 93. The equations yielded by the regression analyses are shown in the upper left-hand corners of the figures. In each case, it was found that lowest concentration data point, corresponding to the 0.391 µg /mL HSA was of low absorbance relative to its

expected position, based on the an extrapolation from the four higher concentration data points (see insets in Figure 92 and Figure 93). After plate-reading the absorbances for the standard curve used for the NGT and T2DM samples, it was noticed that the 0.391 µg

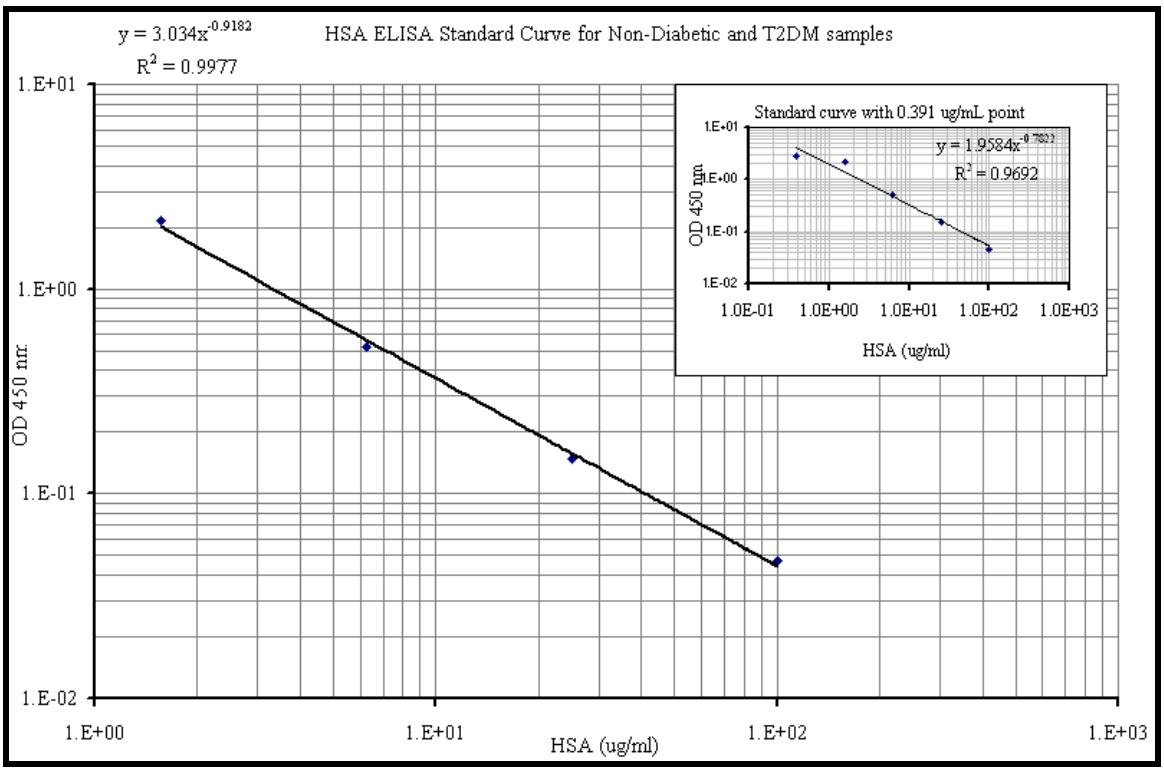

Figure 92 HSA ELISA standard for NGT and T2DM samples.

/mL HSA concentration wells and the wells with just mix diluent for background (i.e. the darkest yellow wells in the standard series) had begun to precipitate. This was consistent with readings of lower absorbances in those wells that did not fit the line of the 4 higher concentration HSA standard points. The Assaypro datasheet that was included with the assay states that the precipitation will reduce the aborbance readings. The datasheet also shows a figure with non-linear lower absorbances in the 2 lowest HSA concentration

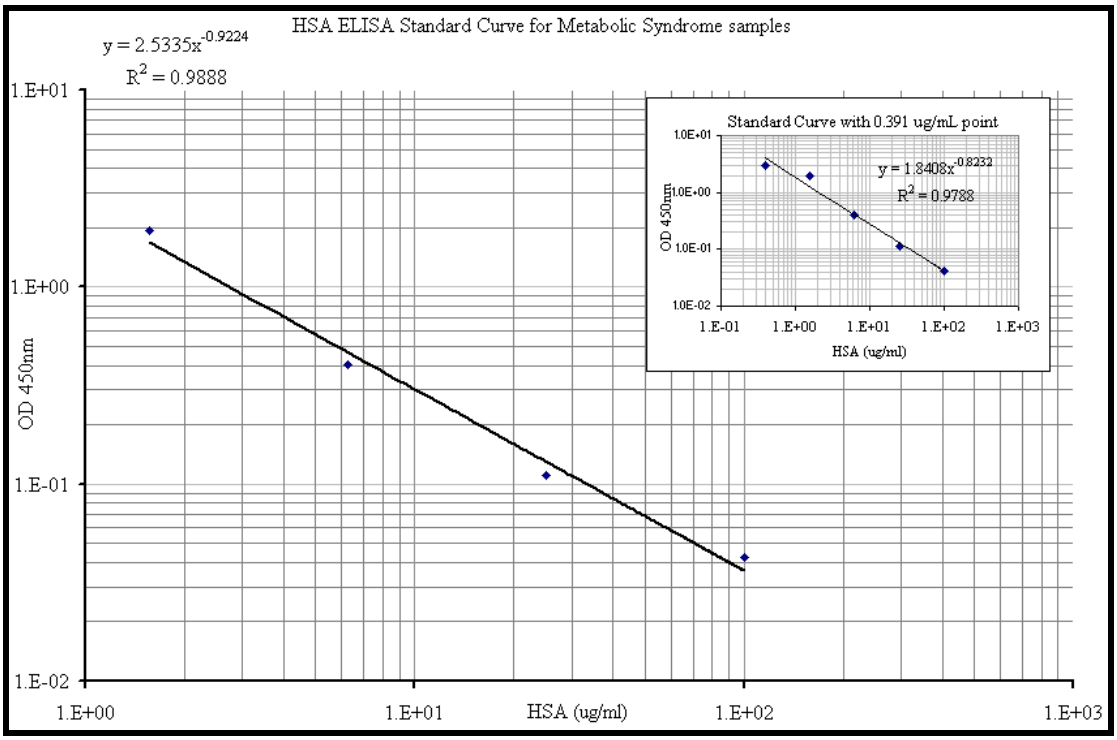

Figure 93 HSA ELISA standard for IGT samples.

points. To attempt to overcome the generation of non-linearity at these concentrations, the time for the absorbance readings was reduced by reducing the number of reads from 5 flashes at each position of a 4 x 4 circular read to 3 flashes of a 3 x 3 circular read in the samples and standard used for the IGT samples. However, this did not change the non-linearity (inset in Figure 93). For this reason there was no blank subtraction in these assays and the lowest HSA concentration point, 0.391 µg /mL, was omitted from both standards. All of the experimental samples were found to have fairly normal levels of HSA and had (undilution corrected) concentrations between the 1.56 µg/mL and 6.25 µg/mL standard points.

Figure 94 shows the ELISA HSA results for the individual NGT and T2DM experimental samples and the GH internal standard sample. Figure 95 shows the ELISA HSA results for the IGT experimental samples.

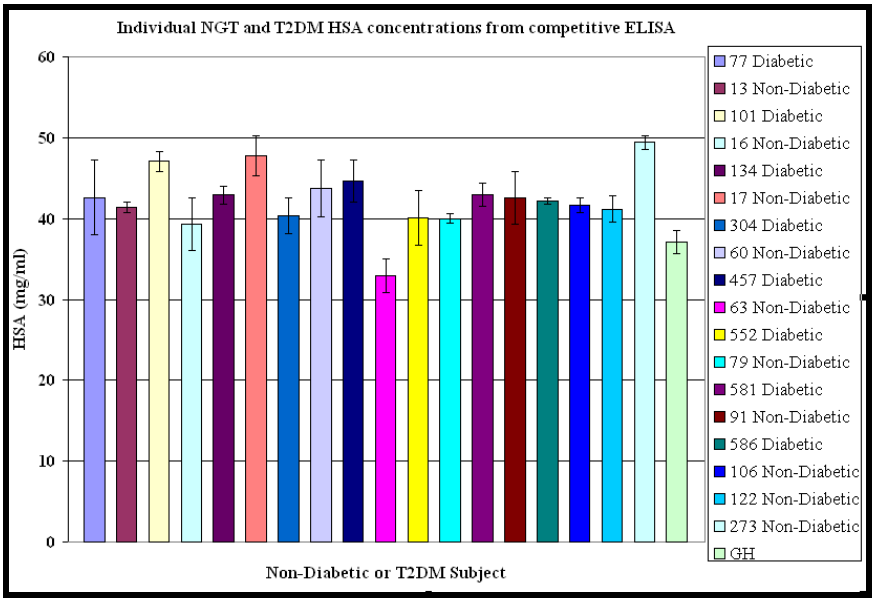

Figure 94 Individual NGT and T2DM HSA concentrations from competitive ELISA.

While there is some variation in the HSA values for different subjects, the average concentrations of the 3 experimental groups are very similar: NGT- 42.0 $\pm$ 4.6 mg/mL, T2DM - 42.8 $\pm$ 2.3 mg/mL, and IGT 42.6 $\pm$ 4.2 mg/mL. These values are not statistically different from each other and are in excellent agreement with stated average plasma HSA concentration (~40 mg/mL) from the literature [361].

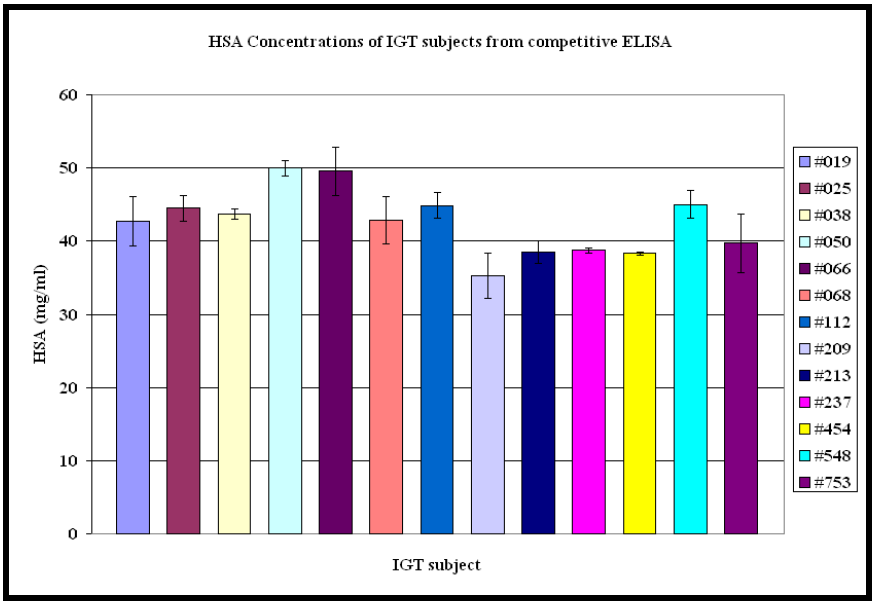

Figure 95 Individual IGT HSA concentrations from competitive ELISA.

● *BCG assay for HSA.* The standard curve, using dilutions of the "GH" plasma, which was used for the NGT and T2DM samples, is shown in Figure 96. The standard curve for the IGT samples is in Figure 97. The Excel equations for the best linear fit by the regression analyses are shown in the upper left-hand corners of the figures.

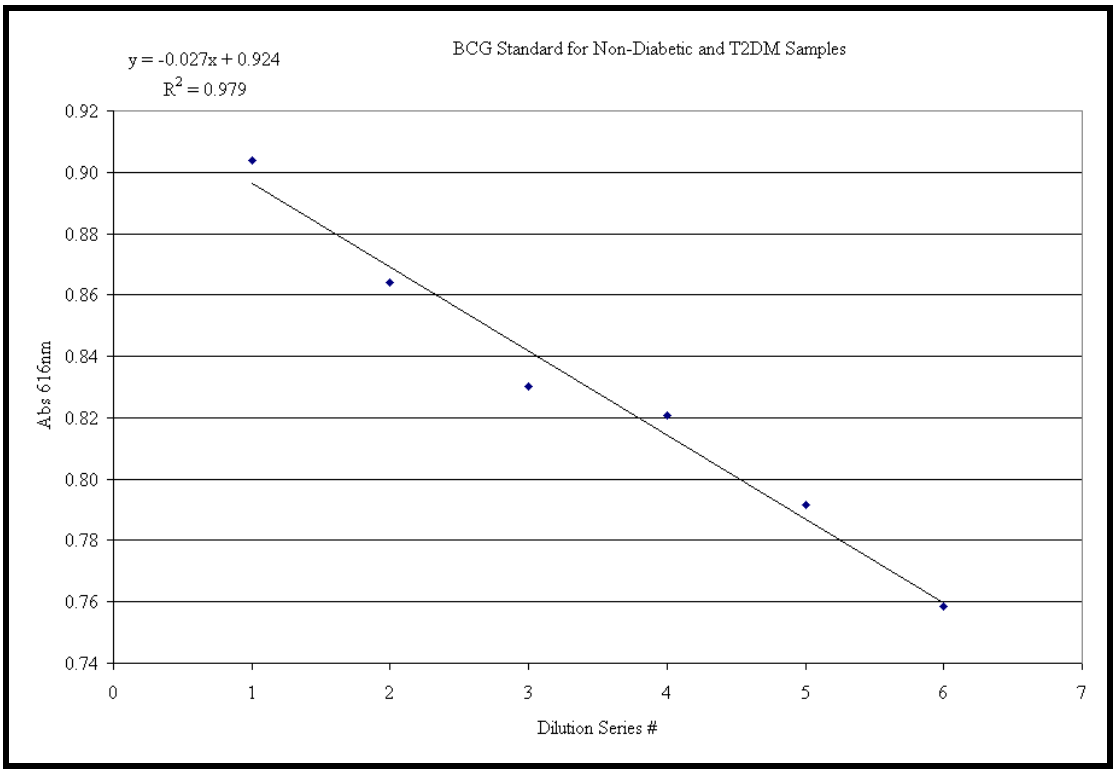

Figure 96 BCG standard curve made from dilutions of the GH plasma and used for the 10 NGT and 8 T2DM samples. 3 x 3 circular reads of each well.

The inset standard of Figure 97 shows the same data points as in the larger figure but with a point at standard #5, which was omitted from the standard equation because it was an outlier. The likely reason for the inconsistency between the two standards in the absorbance axis was discussed in the Materials and Methods section.

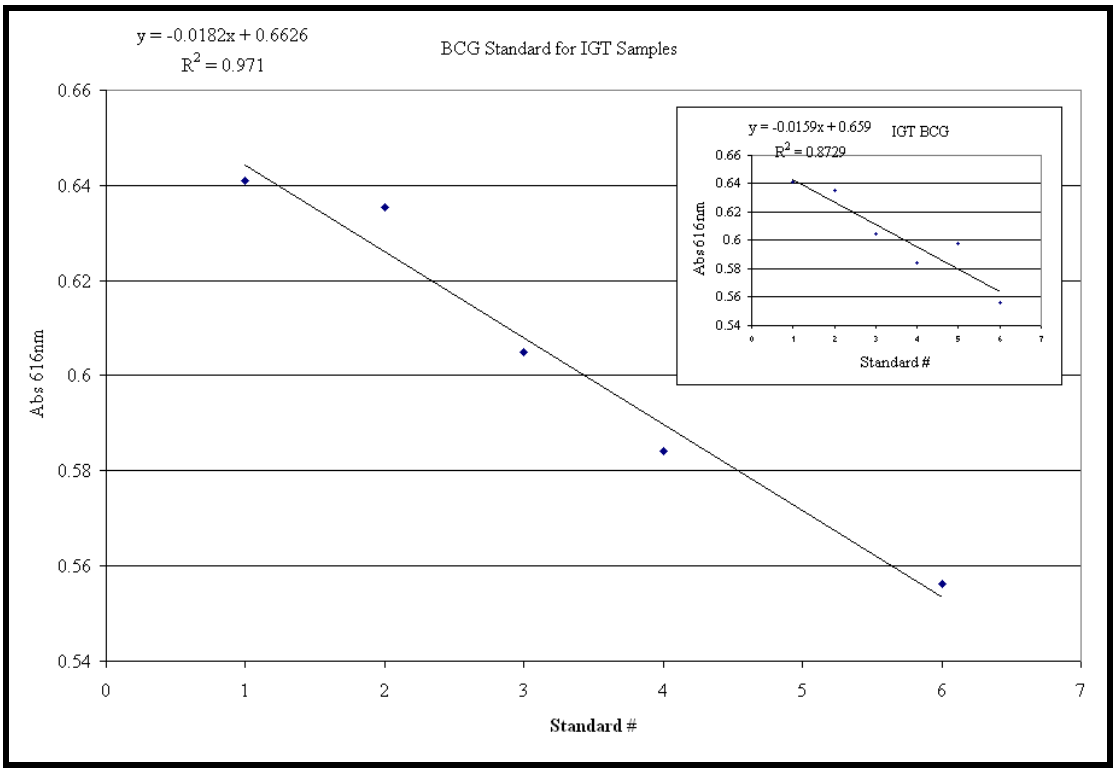

Figure 97 BCG standard curve made from dilutions of the GH plasma and used for the 13 IGT samples. 2 x 2 circular reads of each well.

To calculate the BEPHE equation (Equation 6-**B**CG **E**rror from **P**olyclonal **H**SA **E**LISA), the BCG absorbance values for the experimental samples needed to be converted to the same concentration units as the ELISA result, mg (HSA)/mL. The concentration of the "GH" plasma that was used in the standard curves for the BCG assays was determined by ELISA. The standard dilution units (6,5,4,3,2,1) used in the BCG assays were then converted to units of mg/mL by converting the undiluted "GH" standard point 5 (see Table 18) to the units of mg/mL (37.1 mg/mL, see Figure 94) So, the experimental values of the BCG assays that were converted from absorbance values to the standard units (6,5,4,3,2,1) by the best fit equations, could then be converted to

mg/mL by using the conversion factor, (37.1 mg/mL)/5. By using the same standard plasma for the 2 BCG standard curves from different days, the 2 datasets were appropriately internally related, being matched to the same scale. However, because the BCG measurement of the "GH" standard HSA is also subject to the sample-dependent inhibitions of the binding site, there is an inherent arbitrariness to the BCG standard's value. For this reason the "0" value of the vertical BEPHE axis was set, by arbitrary definition, as the average value of the 13 IGT samples.

The error values of each BEPHE value are expressed as the standard deviation of the nine calculations of Equation 6 that resulted from the unique combinations of 3 technical repetitions of the ELISA HSA concentrations and 3 technical repetitions of the BCG measurements.

● *Statistical Analysis.* Correlations between selected quantitative metabolic variables and the BEPHE assay were evaluated by Pearson correlation analysis assuming normally distributed variables, using an Excel spreadsheet "Pearson( )" function. The independence of the associations was evaluated by Pearson linear regression analysis and the statistical significance was accepted if the computed $P < 0.05$. P-values were computed by GraphPad software online calculator [362] from the calculated Pearson coefficient, r), and degrees of freedom (dF= n-2).

A simple histogram comparison of the BEPHE results of the T2DM samples with the NGT samples found that there was not a significant difference between the 2 groups. Realizing that this could be due to the somewhat arbitrary classifications of "diseased" and "not diseased", the datasets were plotted against metabolic and biometric data that

were provided by NIH. Upon plotting the T2DM and NGT data against Ha1c, a significant correlation coefficient ($P < 0.05$) was found and it was decided to repeat the BEPHE assay to include the 13 IGT samples. Subsequent analyses found that the BEPHE result had the strongest correlation with FPG (Figure 98, Figure 99 and Table 19). The correlation for the entire dataset, n=31, yielded a p-value = 0.0003 for 29 degrees of freedom (dF). This p-value is generally regarded as extremely statistically significant [363]. Significant correlations were found between: the BEPHE result and the FPG of the entire experimental subject group ($p = 0.0003$, n=31, Figure 98); the BEPHE result and the FPG of the entire hyperglycemic (IGT and T2DM) subgroup ($p= 0.001$, n=21, Figure 99); and the BEPHE result and the FPG of just the IGT subgroup ($p = 0.006$, n =13, Figure 99). The relationships between the subgroups and other associations are summarized in Table 19.

As seen in Table 19, the strong correlation between BEPHE and FPG is supported by significant correlations with other measurements of glucose metabolism including; 1 hour glucose (1HG), 2 hour glucose (2HG), and Ha1c, with an apparent trend of weakening correlations. This initially was a surprise, as it was expected that, if the BEPHE assay was found to reflect metabolic status, it would reflect a long term variation in the sugjects, on the order of circulatory protein half-life, such as Ha1c. The closer association of BEPHE with FPG suggests that the binding status of HSA is responsive to short term variations, on the order of 8 hours, which is the approximate time of the time of the fast. This finding is consistent with the changes of binding being due to circulatory

NEFAs, which undergo rapid postprandial fluctuations, are generally elevated in IGT and T2DM, and are bound by HSA, although we don't have direct measurements

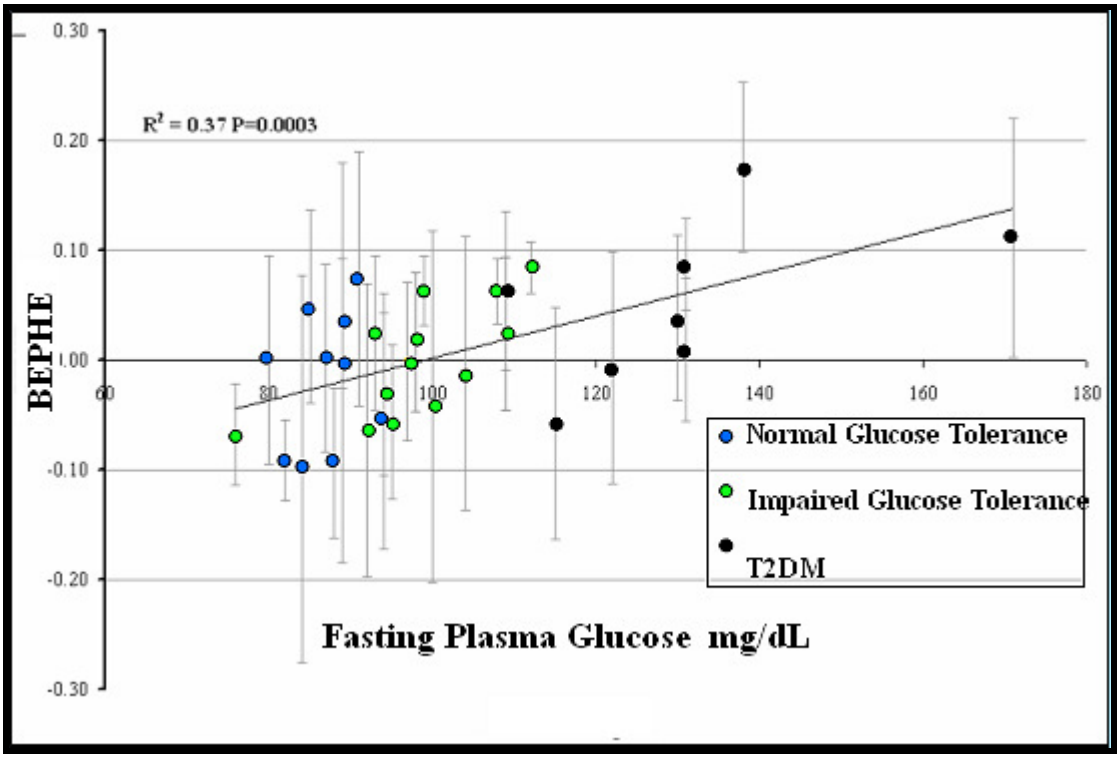

Figure 98 BEPHE assay values for all the experimental subject samples and the correlation with fasting plasma glucose. The blue points are NGT samples. The green points are IGT samples. The black points are T2DM samples. Data are expressed as mean $\pm$ S.D and the data points are fitted by linear regression analysis. The BEPHE scale was shifted so that the mean IGT BEPHE assay value is arbitrarily set to 0. The linear fits to the IGT and T2DM measurements are shown in Figure 99.

of them. However, according to Rodkey, lipids do not interfere with (compete with the binding of BCG) the neutral pH BCG assay [340]. Also, investigating the question of interfering compounds in the case of renal patients, Dromgoole explicitly showed that NEFAs did not interfere with HSA binding by a different anionic, HSA-binding dye,

methyl orange [355]. Nevertheless, in the absence of direct evidence to the contrary, the possibility that HSA-bound NEFAs could play a role in the altered binding property

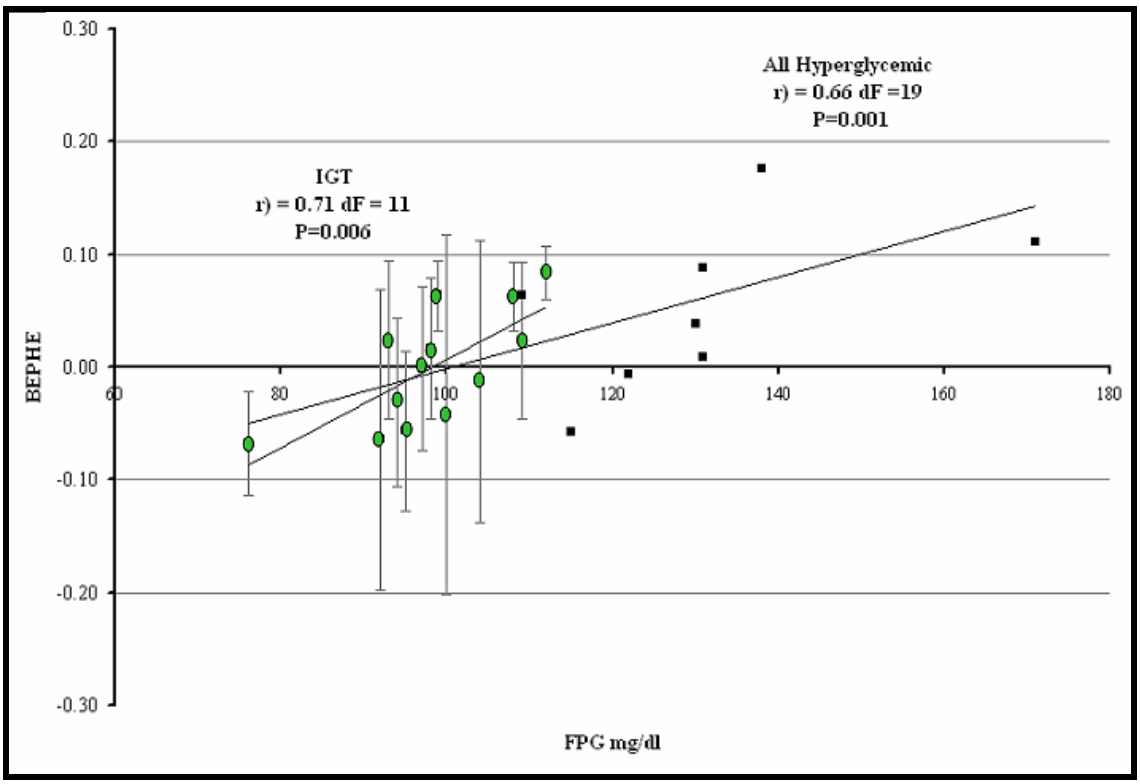

Figure 99 BEPHE assay for hyperglycemic (IGT and T2DM) samples vs. FPG. The IGT data (green spots) are expressed as the mean ± S.D and the data points are fitted by linear regression analysis. The BEPHE scale was shifted so that the mean IGT BEPHE assay value is arbitrarily set to 0. The IGT measurements include the error bars. The error bars for the T2DM samples are shown in Figure 98.

of HSA is acknowledged. The possible HSA ligand correlated with FPG is being investigated by others in our lab by quantitative gas chromatography (GC) /MS of organic extractions from immuno-purified HSA. Glucose itself, which is responsible for the change inherent in FPG, may have also changed BCG binding; therefore this possibility was investigated *in vitro*, as described below.

Table 19 BEPHE assay correlations with metabolic parameters. r) = Pearson correlation coefficient. 1HG = 1 hour glucose. 2HG = 2 hour glucose. Alb/Cr= Albumin creatine ratio. ‡ CRP was ns unless an outlier was removed. This is discussed in the text.

BEPHE corr	All experimental n=31		All Hyperglycemic n=21		IGT n=13	
	r)	p value dF=29	r)	p value dF=19	r)	p value dF=11
FPG	0.61	0.0003	0.66	0.001	0.71	0.006
1HG	0.41	0.022	0.44	0.046	0.56	0.47
2HG	0.44	0.013	0.44	0.046	-0.21	ns
HA1c	0.37	0.04	0.36	ns	-0.21	ns
Triglycer.	0.19	ns	0.03	ns	0.26	ns
Cholesterol	-0.11	ns	-0.19	ns	-0.16	ns
HDL	-0.35	ns	-0.11	ns	-0.42	ns
CRP‡	0.32	ns	0.25	ns	0.01	ns
Alb/Cr	0.09	ns	-0.19	ns	0.05	ns
HSA ELISA	0.31	ns	0.35	ns	0.49	ns

On the other hand, averring that HSA affinity is responsive to short term changes in HSA cargo rests on the assumption that the alteration of HSA binding is an effect and not a cause of hepatic insulin resistance. An agent that was causal of hepatic insulin resistance would appear to be related to FPG, as the BEPHE correlation does. We have seen that several acute-phase proteins, that are known to bind HSA, were found to be changed in the HSA depleted plasma of the T2DM samples in our experiments. The possibility exists that chronic changes in the HSA-bound proteins, or undiscovered T2DM associated compounds that are bound to HSA, chronically alter the trafficking of NEFAs by HSA, and contribute to the ectopic FFA deposition and/or high circulatory NEFAs that are associated with insulin resistance. If this is true, HSA and its binding character would be on the causal chain leading to IR. To resolve this interesting question, a BEPHE experiment could be done, using samples from non-fasting patients with a range of known FPGs. Then, if a close association of the non-fasting BEPHE with FPG was found, this would show that the BEPHE result was not merely a reflection of a

short-term effect of post-prandial metabolism, but a more stable, long-term condition that may; 1) affect HGP and 2) also be developed into a diagnostic marker that does not require fasting.

The literature on the BCG assay suggests several important control experiments. The first control was suggested by experiments which showed that the BCG assay systematically over-estimated HSA at low HSA concentrations. The possibility existed that if the glucometric measurements, such as FPG, were correlated with HSA concentrations, then the observed correlations of BEPHE to the glucometric measurements could be due to this reported systematic error of the BCG assay. To check for this effect in our experiment, a correlation was sought between the BEPHE result and HSA concentration as determined by ELISA. As shown in Table 19, under "HSA ELISA", there is no significant correlation of the BEPHE assay with HSA concentration. This control assures that the relationships seen between the BEPHE assay and glucometric measures is not a result of the reported systematic error of the BCG assay at low concentrations.

The second control was suggested by the literature report that the (low pH=4.2) BCG assay had a slow reaction of the dye with acute-phase globulins, leading to overestimation of HSA in patients with inflammatory infections or low levels of HSA. We have already seen that there is no correlation of BEPHE with the HSA concentration. Table 19 includes the result of the BEPHE correlations with NIH measurements of the inflammatory marker, C-reactive protein (CRP). On the whole, if all the members of the subgroups are included, there is no significant correlation between BEPHE and CRP

levels (Figure 100, “All experimental”). But if the outlier, at BEPHE =-0.015, CRP = 28 mg/L is removed, then a very strong association (r) = 0.58, dF = 28, p = 0.0008) of CRP with BEPHE is found (Figure 100, “Outlier removed”). In light of the known close association of the inflammatory state with IR, and therefore FPG, the plot of the BEPHE vs. CRP would be expected to resemble that of the BEPHE vs. FPG. A comparison of outlier-removed plot of BEPHE vs CRP in Figure 100, with the plot of BEPHE vs FPG in

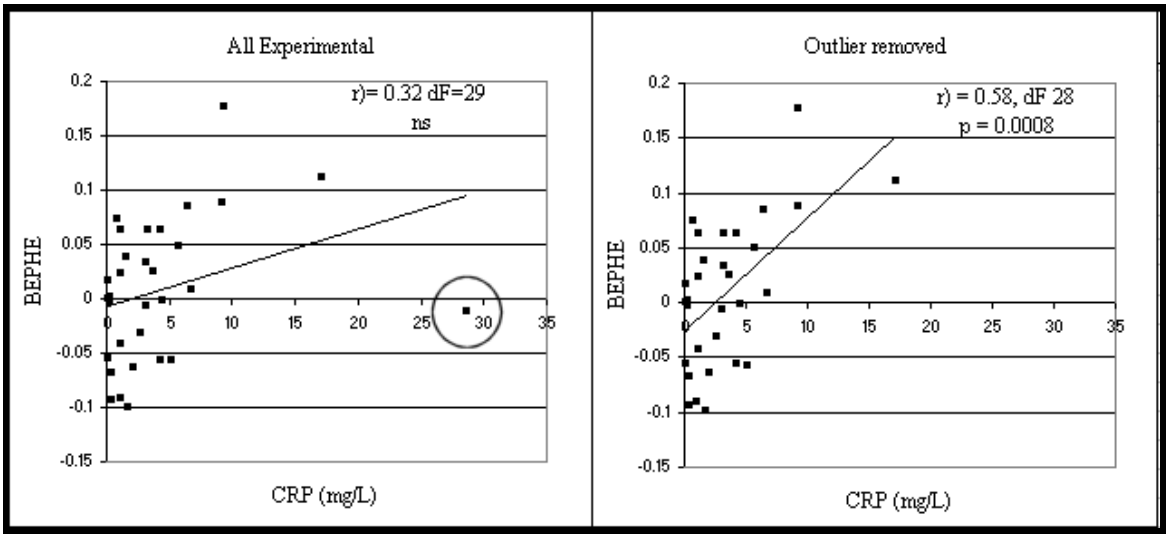

Figure 100 BEPHE vs CRP, with outlier (circled data point, left) and without outlier (right).

Figure 98 reveals that the 2 plots are indeed similar in the general distribution of the data points and measures of correlation. A CRP outlier may have been the result of an undetected acute infection in that person.

The correlation of BEPHE with CRP suggests that there might be a correlation with other acute-phase proteins. The BEPHE error value increases with less BCG binding and the positive correlations we find of BEPHE with FPG and CRP are opposite

from the negative slopes that would be expected from the reported increased BCG binding to acute-phase proteins [348], if the reported slow, acute-phase protein binding of BCG was important in our experiment. This contradiction shows that the observed correlations of the BEPHE assay with FPG and CRP are not consistent with the reported artefactual, non-specific binding of BCG to acute-phase proteins [348].

Although the 250-fold dilution of sample that we used in the BCG assay should effectively dilute lipemic contributors to light scattering, since lipids are an integral part of this experiment, it was prudent to include 3rd a control for these also. Table 19 also shows that there is no significant correlation of triglycerides, cholesterol or HDL with BEPHE. Additionally, direct measurements of light scattering of the NGT and T2DM samples, identically prepared and analyzed as in the original BCG assay, except that they were prepared only with non-chromagenic dilution buffer to replace the chromagenic buffer, showed no significant correlations. The light scattering in this control experiment was so low that a correlation of absorbances of the 6 member plasma standard dilution series with their concentrations could not be made. These measurements were carried out to assure that light scattering was not an important contributor to the observed BEPHE correlations.

Finally, since FPG is inherently associated with the glucose concentration of the plasma samples, we performed a control experiment to determine if BCG binding to HSA is dependent upon glucose concentration, by using exogenously added D-glucose (Mallinckrodt, catalog #4912). To do this, normal chromagenic BCG reagent was made with 5 mM D-glucose and a serial 2-fold dilution series of the glucose concentration was

made with non-glucose BCG buffer. As in the BCG assay, 4 µL of plasma was added to 996 µL of the BCG/glucose buffer and readings were made in triplicate on the microplate reader. The plasma sample used in this control was the NGT standard plasma that was used for the BCG standard curves, to which an average endogenous FPG of 4.9 mM was imputed. The result of the BCG binding assay vs. D-glucose concentration is shown in the supplementary Figure 135. Because of the imputed endogenous glucose concentration in the NGT plasma, the dilution series asymptotically approaches 4.9 mM/250 = 0.0196 mM. The range of FPGs, as measured by NIH for the samples included in this experiment, and diluted 250-fold, is represented at its extremes by the vertical horizontal lines at 0.0177 mM and 0.081 mM. The value representing the 250-fold dilution of the FPG diagnostic cutpoint for T2DM is represented by a vertical dashed line at 7mM/250 = 0.028 mM. The result shows that there was no significant correlation of the BCG-HSA binding to the concentration of exogenously added D-glucose.

Table 19 shows that there is no significant correlation between BEPHE and the urine albumin/creatinine ratio, as measured by NIH. Albumin/creatinine is a measure of urine HSA. The 66 kDa HSA should not normally be detectable in urine, as the normal kidney function is to retain proteins greater than ~40 kDa in the blood stream. Because it is a relatively small and abundant protein it is the most detectable protein in urine when kidney filtration fails. Creatinine is a metabolite of muscle and is normally excreted into the urine consistently. Therefore creatinine corrects for changes in urine concentration when it is measured along with urine HSA [364]. According to NIH [365], urine albumin/creatinine values under 30 µg/mg show healthy kidney function. All of the

subjects in this experiment had a value of the urine albumin/creatinine ratio that was below 30 μg/mgs, indicating normal renal function.

The results presented above indicate that the binding properties of HSA at physiological pH are strongly associated with FPG, a glucometric parameter of primary importance to the diagnosis of insulin resistance and T2DM, as well as CRP, a measure of inflammation. HSA has a fundamentally important function in the trafficking of circulatory NEFAs and altered HSA binding appears to be at the interface of fatty acid metabolism and glucose control. Because HSA is also known to bind abundant proteins such as Hpt and Apo A-I, which are involved in acute-phase responses, as well as remediation of oxidative damage and cholesterol transport, the altered binding may link HSA to innate immunity, complications of T2DM and the metabolic syndrome.

● *Sandwich ELISA for insulin and the calculation of HOMA-IR.* After reading the absorbances, the duplicate readings were averaged and the blank standard absorbance value was subtracted from all the standard and experimental absorbances. A second-order quadratic equation was used to fit the data on the log-log plot of the data. Figure 101 shows the 5 point, insulin concentration (μIU/mL) vs. absorbance (450 nm) standard curve for the insulin ELISA. The R^2 is 0.9996. The quadratic equation was used to calculate the concentration for the provided antigen control and its experimental value was determined to be 6.57 μIU/mL[9]. This was within 5.85 - 11.03 μIU/mL, which the kit's Certificate of Analysis stated as the acceptable range for quality control.

[9] IU- International Units. The conversion of 1 IU of human insulin = 6 nmol = 34.8 μg.

Figure 102 shows the relationship of fasting plasma insulin (FPI) vs FPG for NGT (n =9, closed diamonds) and T2DM (n=7, open squares) subjects. Except for the

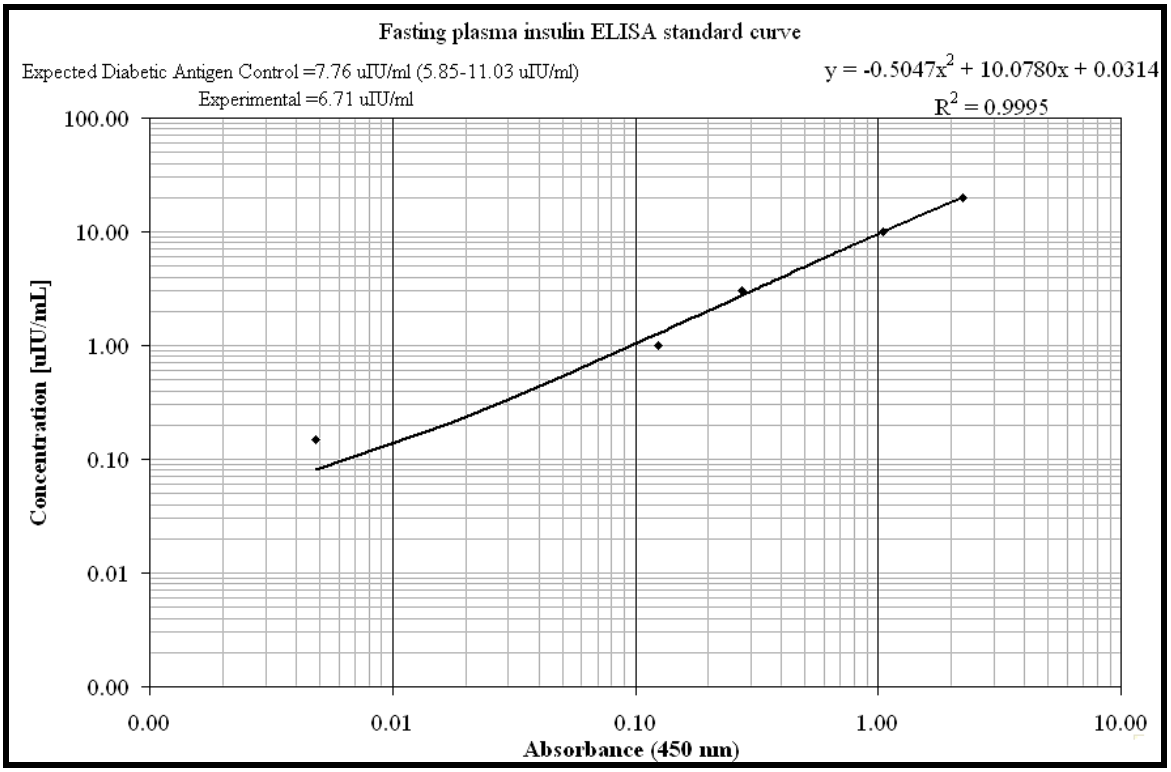

Figure 101 Standard curve for insulin ELISA.

highly insulinemic NGT outlier (FPG=88, FPI=20.4), the trend showing the weakening of the feed-back loop between basal plasma glucose and insulin concentrations is clear with $P = 0.0006$. After the removal of the outlier, the correlation improved to $P < 0.0001$. The rise in both of FPG and FPI is indicative of both insulin resistance and β-cell decompensation. If there was no β-cell decompensation the plot would show an increase in just insulin without increased FPG. The loss of ability to secrete enough insulin to

overcome the loss of insulin potency is seen in the increase FPG. Both insulin resistance and β-cell decompensation are required to explain the rise in both FPI and FPG.

A comparison of the average FPI between the NGT and T2DM groups (7.1 ± 5.2 vs.15.8 ± 5.2 μIU/mL, p = 0.005) is shown in Figure 103A. After the removal of

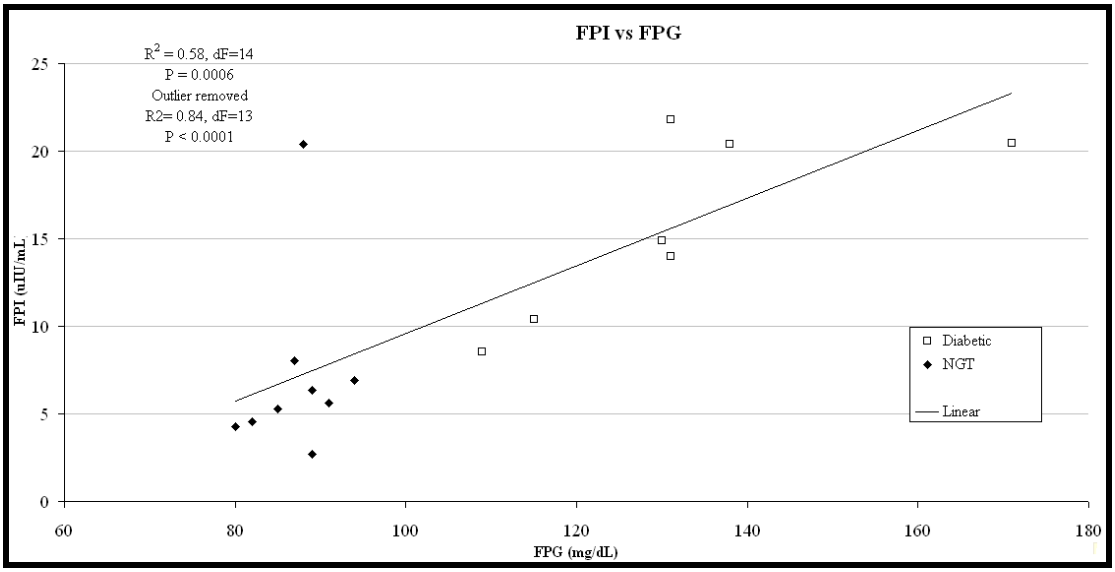

Figure 102 FPI vs FPG. NGT (n=9, closed diamonds), T2DM (n=7, open squares).

the NGT outlier the p < 0.0001 Figure 103B shows the comparison of the calculated average HOMA-IR values for the two groups (5.3 ± 2.3 vs.1.5 ± 1.1 (mmol x μIU)/(L x mL), p = 0.005, unequal variances). Figure 103C further highlights the FPI of the 2 groups in the context of the 2 hour glucose (2HG) test, which was the diagnostic test

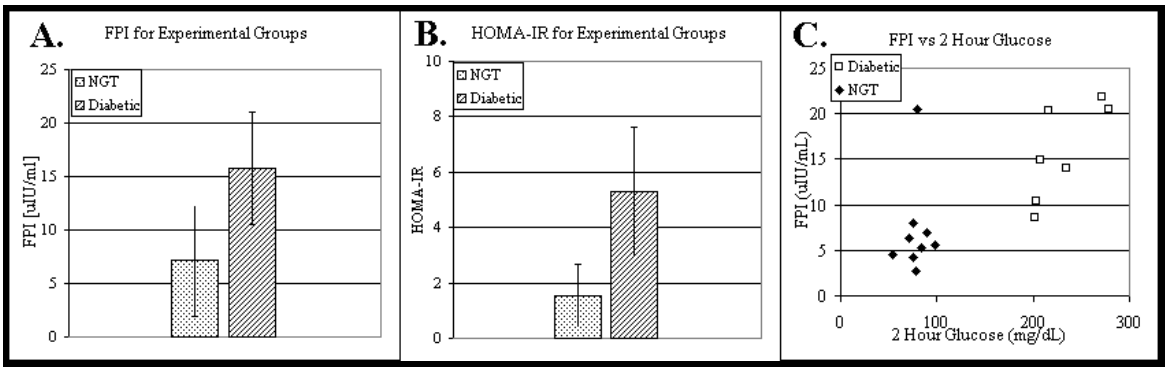

Figure 103 Some additional context of FPI in T2DM.

for assigning the subjects to groups of NGT (2HG < 140 mg/dL) or T2DM (2HG > 200 mg/dL, see page 145).

Figure 104 shows the relationship of the BEPHE assay with HOMA-IR for the NGT and T2DM groups. There is a statistically significant correlation of $P < 0.04$ which, with the outlier removed becomes $P < 0.009$. This is slightly less significant than the

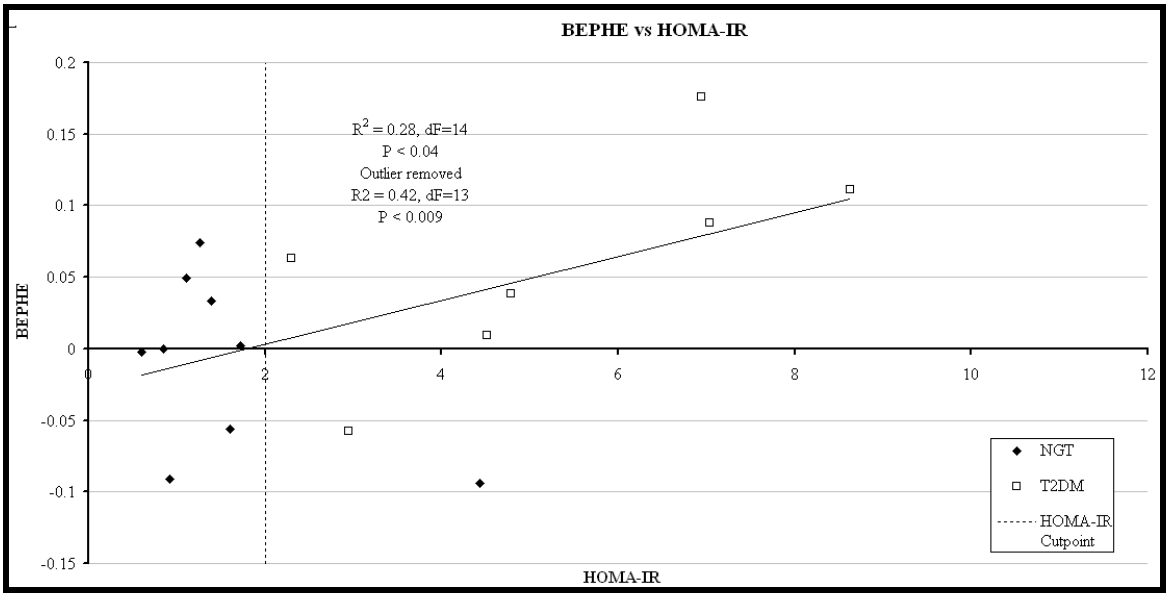

Figure 104 BEPHE vs HOMA-IR.

correlation found between the BEPHE assay and FPG for these subjects ($dF = 14$, $P < 0.02$). The correlation of the BEPHE assay with FPI for the measured subject, with the outlier removed was $P = 0.01$ ($dF = 13$).

We wished to investigate the possibility that hyperglycemia-associated oxidative modifications of HSA might have contributed to alterations of HSA binding. This is plausible since HSA is implicated in anti-oxidant mechanisms in plasma [330] and antioxidants are typically oxidized under stress. The next chapter discusses the rationale and experiments that investigated 2 possible modes of HSA oxidation as possible causes of the altered binding.

ASSESSMENT OF OXIDATIVE MODIFICATIONS OF HUMAN SERUM ALBUMIN

Introduction and Method Development

Oxidative stress has been a focus of attention in many studies on the development of T2DM and oxidative stress is also believed to arise from hyperglycemia per se [284].. As we saw in the earlier discussion, oxidative stress is also thought to contribute to the development of the complications that arise late in both T1DM and T2DM. Several mechanisms have been proposed to explain why DM is associated with oxidative stress. These mechanisms fall into two categories: increased production of reactive oxygen species (ROS) and decreased antioxidant capacity [366]. An antioxidant is defined as *any substance that, when present at low concentrations compared with those of an oxidizable substrate, significantly delays or prevents oxidation of that substrate* [366]. Virtually every type of molecule in the body can be an "oxidizable substrate" and be damaged by oxidative stress [366].

Hyperglycemia can increase ROS production by changes in the redox potential of glutathione [367], and by increasing the production of superoxide in the electron-transport chain [151]. A non-hyperglycemic mechanism for ROS production has also been reported in T1DM, involving increased activity of xanthine oxidase, a superoxide generating enzyme [368]. Decreased antioxidant defenses have also been reported in DM including reduced total antioxidant capacity in human plasma in both T1DM [369], and in T2DM [370].

HSA, which is thought to be an important antioxidant of the blood [320, 336], has also been reported to be more highly oxidized in T1DM [371] and T2DM [330, 372]. 34 of the 35 cysteines in HSA participate in disulfide bonds and are not normally redox active. HSA has one reduced cysteine, Cys-34, which, because of the abundance of HSA, constitutes a millimolar range of thiols, the largest pool of thiols in circulation [336]. Reduced glutathione, by comparison, is only in the μM range in plasma [373]. Reduced Cys-34 HSA is known as mercaptoalbumin (HMA). HSA in which the Cys-34 is oxidatively bound to species, such as glutathione, cysteine [318] or homocysteine [336] is referred to as nonmercaptoalbumin (HNA) [372]. In healthy adults, 70-80% of Cys-34 in HSA is in reduced form., the rest is oxidized to form HNA [336]. A 1992 size-exclusion chromatography study by Suzuki et al. [372] showed that T2 diabetics had HNA/HMA ratios that were weakly dependent on blood glucose levels. Maleimide-containing fluorescent dyes, which selectively label free thiols at pH=7 [374], have also been used to differentially detect redox states of thiol containing proteins [375] in 2D DiGE experiments. This strategy was chosen for the first oxidation detection methods to assess the oxidative status of HSA, as described later in Material and Methods.

Another type of biological oxidative modification is the carbonylation of proteins. Carbonyls, including aldehydes and ketones, are introduced irreversibly and non-enzymatically [376] in proteins by a variety of mechanisms including the direct oxidation of amino acid side chains by ROS, formation of oxidized AGES adducts from reducing sugars, and the formation of adducts with lipid peroxides [376, 377], all of which have been recently found in human plasma proteins [377]. Native, freshly synthesized proteins

do not contain aldehydes or ketones, and thus, the presence of these carbonyl groups in proteins is indicative of oxidative stress.

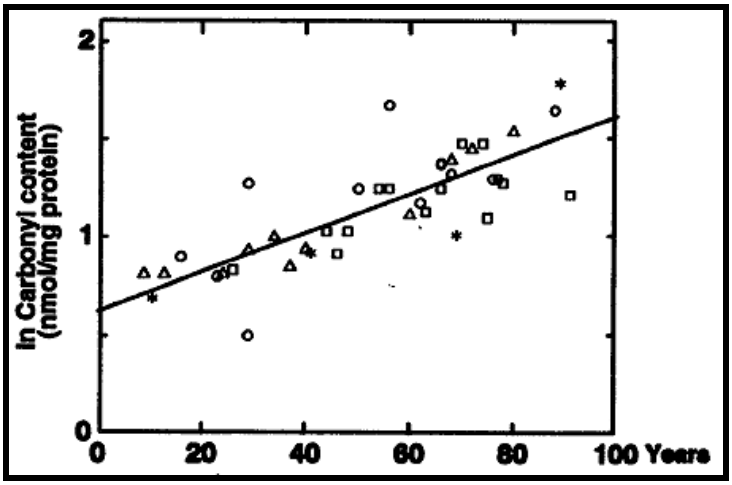

Figure 105 Semilog plot of the total carbonyl content vs age for: ○ human occipital lobe brain tissue, □ human eye lens cortex, Δ cultured dermal fibroblasts [378].

Figure 105 shows the positive correlation of the protein carbonyl content for several different human tissues, as a function of the age of the donor [378]. HSA has also been shown to have an age-related susceptibility to carbonylation in mice and rats [379]. Because T2DM is correlated with oxidative stress, increased circulating NEFA, and hyperglycemia, and because the roles of HSA include the sequestration of oxidizing metals such as iron and copper, and the trafficking of NEFA, the carbonylation of HSA seemed a possible explanation for the BEPHE result noted earlier.

Therefore, the goal for the second method of measuring oxidative damage was to probe for differing levels of carbonyls in HSA between the NGT and T2DM subjects. Hydrazides have been shown to react with carbonyl groups under mild conditions, forming a hydrazone (Figure 106) bond [377]. The following is a brief overview of the

strategy, using hydrazide reactivity, to detect carbonyl oxidative damage. A detailed protocol will be provided in Materials and Methods.

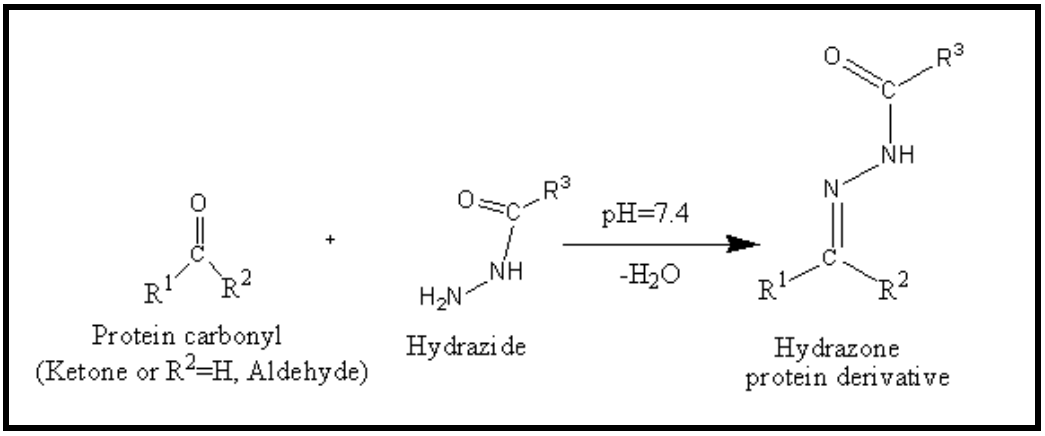

Figure 106 Reaction of hydrazide with carbonyl to produce hydrazone derivative.

be given in Materials and Methods.

A commercial hydrazide-biotin (HB) conjugate (biotin is in the R^3 position in Figure 106) was reacted with plasma to detect protein carbonyl groups [377]. This results in a biotinylated tag at the sites of oxidative damage. Hydrazones are acid-labile [380], but they are stable under the mildly basic conditions of PAGE and the gel blotting process [379]. After biotinylation, the proteins were resolved on 1D gels and subsequently transferred to a PVDF membrane. The PVDF membrane was then incubated with NeutrAvidin-horseradish peroxidase (NHRP) to detect the biotin-derivatized proteins. NeutrAvidin binds to biotin with an affinity, $k_a \approx 10^{15}$, which is unusually high for a protein-ligand complex and is essentially irreversible. At this point in the protocol, the oxidative damage sites were tagged with HRP. Luminol, a chemiluminescent substrate for HRP, and H_2O_2, were added to produce a time-sensitive

release of light (Figure 107, [381]), which was quantified on the Typhoon scanner and the intensity of which is proportional to the amount of oxidative damage.

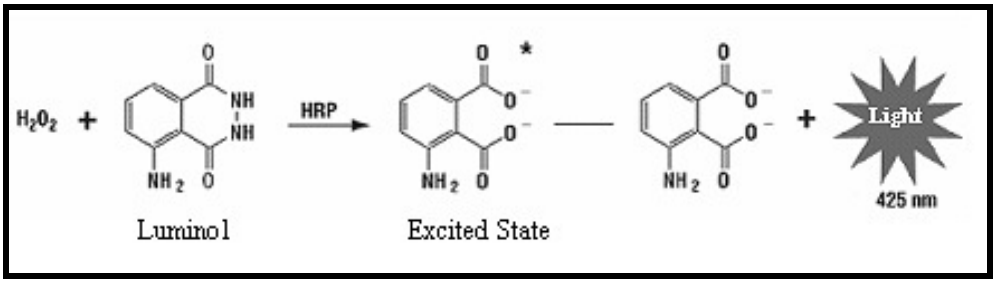

Figure 107 Chemiluminescence reaction of luminol with HRP.

In addition to the chemiluminescent detection of the PVDF membrane bound carbonylated proteins, we wished to develop a means for measuring the relative amounts of total PVDF membrane-bound HSA in order to normalize for: 1) biological differences of HSA concentration between subjects, 2) variations in the transfer of proteins to the membrane, and 3) variations in the initial loading of small aliquots of plasma, which were on the order of 0.5 µL. To provide for the measurement of the measurement of the total amount of HSA, the final step of the protocol uses amido black staining of the PVDF membrane-bound proteins and their spectrophotometric quantification.

In summary, in order to investigate the possibility that oxidative modifications of HSA might be associated with newly diagnosed T2DM of this study, we developed two 1D-PAGE assays. The first experiment used two spectrally resolved fluorescent dyes with different reactive chemistries, maleimide and NHS-ester, in a single labeling reaction, to investigate the oxidative status of Cys-34 of HSA. The second experiment

used the detection of protein carbonyl groups by reaction with a hydrazide reagent coupled to chemiluminescence detection, as described.

Materials and Methods

● *Maleimide labeling test for loss of reactivity due to oxidation of HSA Cys-34.* An NHS-ester lysine reactive blue fluorescent dye (ZB dipropyl, Figure 57) was used label proteins to control for variations in loading and the biological variability of plasma levels of HSA in different subjects. A thiol-reactive maleimide red fluorescent dye (KJS-IX103, Figure 57) was used to label reduced cysteines, which, in native HSA, comprises its only free thiol, Cys-34.

To first investigate the feasibility of using these two dyes in a loading control experiment, an experiment was conducted with control plasma where plasma thiols were blocked from maleimide reactivity with H_20_2 to different extents in a concentration dependent manner. H_20_2 has been shown to oxidize Cys-34 to the non-reactive sulfenic acid derivative [330].

First, 8.9 M H_20_2 (Sigma, catalog # H-1009) was diluted 100-fold into Milli-Q water. The 0.089 M H_20_2 was further diluted 10 times in a 3/2 fold dilution series of 6 µL aliquots in 0.6 mL microfuge tubes. To each dilution, 0.5 µL of citrated human plasma was added and allowed to react on ice, in the dark, for 2 hours. After reacting, the reactions were frozen to -80 °C and lyophilized to dryness overnight to remove the unreacted H_20_2. To label, the dried samples were dissolved in 25 µL of denaturing, non-reducing labeling buffer. The buffer consisted of 30 mM NaH_2PO_4, 8 M urea and 4%

SDS, pH=7.0. After heating the samples in 95 °C water bath for 2 minutes and cooling on ice, 1 µL of the dye mixture containing both 0.66 mM ZB dipropyl and 0.50 mM-KJS IX103 dyes in DMF was added to each. After reacting at room temperature for 25 minutes, in the dark, the samples were diluted with 25 µL of 2x reducing sample buffer, vortexed and heated in 95 °C water bath for 5 minutes. To make 2X reducing sample buffer, 1 mL of 1 M Tris-HCl pH 6.8 was added to 2 mL 10% SDS, 3 mL 50% glycerol, 3.5 mL Milli-Q water and 0.5 mL B-mercaptoethanol (Sigma-Aldrich, catalog # M7154-25mL and a trace of bromophenol blue). 10 µL of labeled protein solution in sample buffer was added to each lane of 1.5mm, 12% polyacrylamide gels.

After running the gels, the images were scanned at 100 µ m resolution: for the NHS-ester dye, using the argon 488 nm laser and 510 nm bandpass 30 nm filter with a PMT voltage of 500 V and for the maleimide dye, using the HeNe 633 nm laser and 655 nm bandpass 30 nm laser with a PMT voltage of 650 V.

Densitometric quantitation of the HSA bands was done using Quantity One 1D image analysis software (Bio-Rad, basic version 4.6.5) of the .gel files from the Typhoon scanner. The rectangular volume tool of constant area was used to quantify the individual band volumes.

To calculate the loading correction factor, an average band volume was calculated from the optical signal for the ten NHS-ester labeled HSA bands of the dilution series. Each individual NHS-ester labeled HSA band volume was then expressed as a fraction of the calculated average HSA band volume to derive the correction factor. This factor,

calculated for the ten individual lanes was then used to divide the densitometric volumes of the maleimide labeled HSA. This mathematical form of this correction is:

Equation 8 $$V_{\text{Corrected Relative Oxidation}} = V_{\text{Indiv. Maleimide}} \times (V_{\text{Average NHS-ester}} / V_{\text{Indiv. NHS-ester}})$$

● *Comparison of oxidized Cys-34 between control and T2DM subjects*. To compare the oxidative state of Cys-34 of HSA between the control and T2DM subjects, plasma from 7 T2DM patients and 8 control subjects was labeled and quantified following the protocol developed in the previous section, without the H_2O_2 treatment. The preliminary protocol was slightly modified to increase the signals of the dyes: instead of 1ul of both 0.66 mM ZB dipropyl and 0.50 mM-KJS IX103 in DMF, 1.5 µL of both 0.66 mM ZB dipropyl and 1 mM KJS IX103 in DMF was used in the 25 µL dye labeling reactions. Relative Cys-34 oxidation was expressed using the calculation of Equation 8, as previously described.

● *Differential carbonyl oxidative stress of HSA in experimental groups*. Preliminary experiments resolved several issues to optimize both the chemiluminescent detection of the protein-bound carbonyls as well as the detection of the relative amounts of HSA in the different samples to be compared. The experimental details for these preliminary experiments are not given, but the methods are described for the final comparison of the control and T2DM samples.

To assess the possible effects of linker lengths between the hydrazide and biotin moieties of the HB conjugates for protein carbonyl labeling, 3 different linkers were tested (Figure 108). Using identical plasma ("GH" standard plasma, as described)

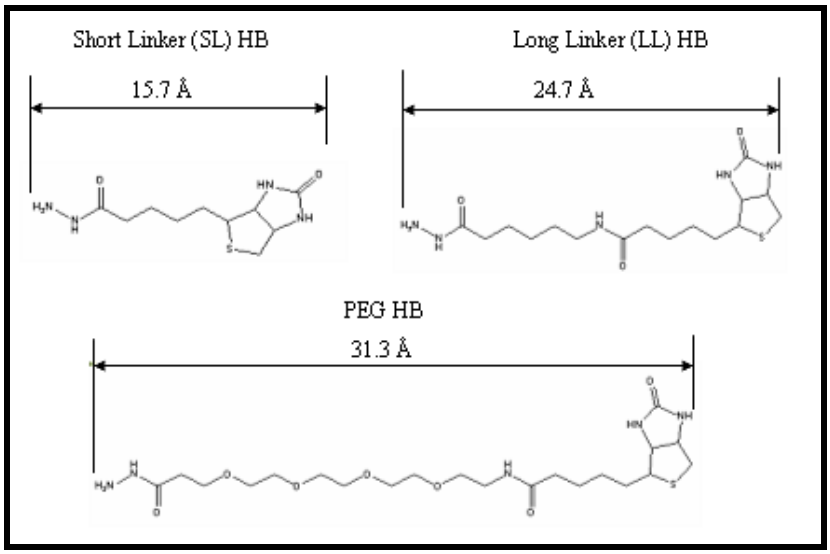

Figure 108 Hydrazide-biotin linkers. Short linker (Thermo, EZ-Link Biotin Hydrazide, catalog# 21339), Long linker (Thermo, EZ-Link Biotin-LC-Hydrazide, catalog# 21340), (Thermo, EZ-Link Biotin- PEG_4-Hydrazide, catalog# 21360), found at [382].

and HB reagent concentrations (5mM), the linkers were tested under native (pH 7.4, 10 mM NaH_2PO_4 buffer) and denaturing (added 2.5% SDS, 2.5% B-mercaptoethanol (BME)) conditions. Figure 109 shows the effects of HB linker length on the chemiluminescence signal. The left image, of the amido black stained membrane, shows that the protein load of the biotinylated standard is low, and the amount of plasma protein in the 6 lanes to the right of the standard is essentially the same in each lane. The right image shows the chemiluminescence signal of the same samples that depends on the reactivity of the hydrazide reagent. Interestingly, while the long linker HB (LL) and the PEG linker showed a significantly higher signal than the short linker HB (SL) in HSA (the large misshapen bands marked with an arrow), the signal did not appear to depend

upon non-denaturation (ND) or denaturation (D) conditions. The HSA chemiluminescent signal did appear to depend upon the linker length between SL HB and the LL/PEG.

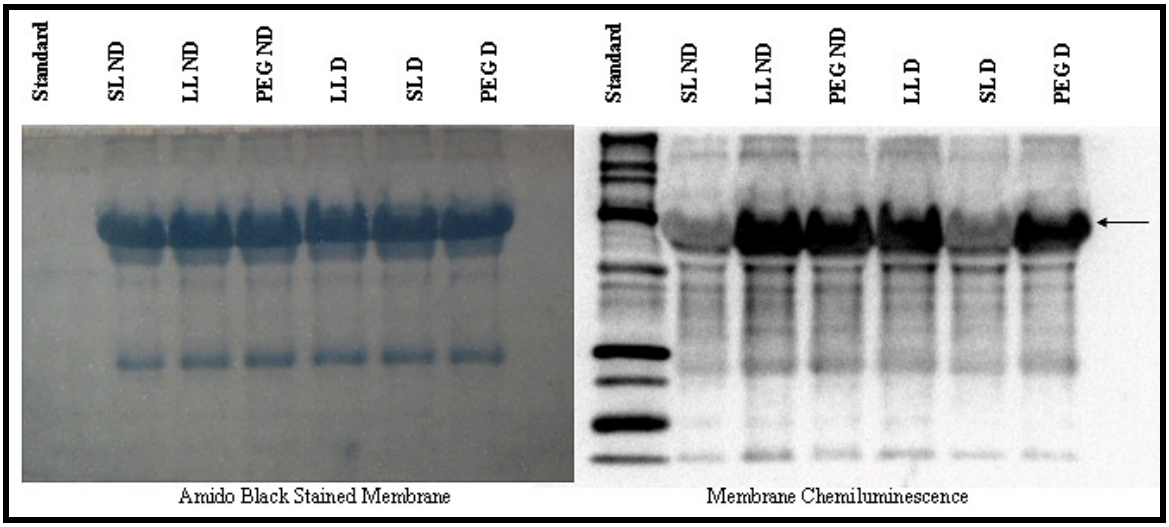

Figure 109 The effect of linker length and conformation of HSA on chemiluminescence signal to detect protein-bound carbonyls in "GH" standard plasma. SL-short linker, LL-long linker, PEG-linker.

Since denaturation showed no distinct difference in the signal from the native case, we chose to utilize the non-denaturing buffer for the main experiment, although the lack of difference may have resulted because the reaction continued through the denaturing conditions of the reduction step, which both methods had in common. Since the LL HB showed better signal than the SL HB and the LL HB signal was as strong as the PEG HB, we chose to use the LL HB reagent for the T2DM comparison experiment.

One issue, important to the quantification of HSA, and made apparent in Figure 109, was the desirability of the formation of well-shaped bands. Subsequent experiments to that shown in Figure 109 indicated that using a 10-tooth comb, and 1.5 mm thick gels, improved band shape and improved transfer of HSA could be obtained by changing from

12% bis-acrylamide to 10% bis-acrylamide separating gels. It was later also found that, because HSA is so abundant, if too much plasma was loaded on the gel, this created a saturation of the amido black staining of the membrane bound HSA. This was resolved by further reducing the amount of loaded plasma to be within a range that produced a good concentration dependent amido black standard curve.

The success of using the NeutrAvidin-HRP (NHRP) bound HSA bands for the quantitation of total HSA was potentially complicated by the fact that NeutrAvidin and HRP are proteins, and could increase the amido black signal from HSA depending on how much carbonyl was present. This question was investigated by labeling standard plasma with a 9-point, 2-fold dilution series of the HB reagent, using the same amount of plasma in each sample and a dilution series of the HB reagent. Figure 110 shows that the

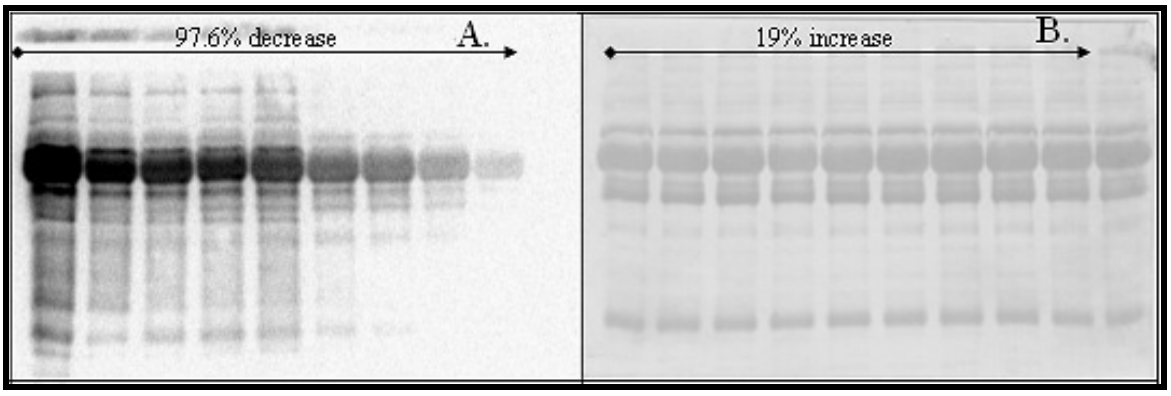

Figure 110 A) Decreased chemiluminescent signal to detect protein-bound carbonyls caused by dilution of the hydrazide-biotin reagent, using the same amount of plasma in each reaction. The dilution of the chemiluminescent signal is concomitant with B) increased amido black signal.

chemiluminescent signal, across the dilution series, decreases 98% with good correlation with the HB concentration ($R^2 = 0.85$, logarithmic fit). Interestingly, there is a

concomitant, significant 19% increase ($R^2 = 0.55$, logarithmic fit) in the amido black assay across the dilution series. This relatively small increase in amido black signal with dilution of the HB reagent is counter to what was expected if the bound NHRP was playing a significant addditive role in the amido black signal. It is unknown why the anti-correlation would occur, but it does imply that the mass of remaining NHRP is negligible compared to the amount of HSA, at the time of the amido black assay. This may be the result of disrupted biotin-neutravidin interaction in the acidic conditions of the amido black assay, causing the removal of the NHRP conjugate from the proteins. Nevertheless, the overall result showed that an amido black assay of the total protein was feasible after the NHRP/chemiluminescence assay, allowing the amido black to act as a control for loading and for biological variation of the HSA levels in the plasma of different subjects.

The previous experiment raised the issue of the number of potential carbonyl reactive sites on HSA, relative to the concentration of the HB reagent. Figure 111 is a plot of the HSA-carbonyl dependent chemiluminescent signal vs the HB reagent concentration made by quantification of HSA chemiluminescent signal of Figure 110A. Shown in Figure 111 are the 8-point and 9- point logarithmic fits for the data. As is the case in the data shown, it was often observed that the 1st lane, with the highest HB reagent concentration (5mM HB), gave aberrantly high readings. So, for the succeeding experiment to seek correlations between protein carbonyls and T2DM, the experimental samples were confined to the inner gel lanes. The outlier 5 mM point is omitted in the 8-point fit, which then shows a significantly higher correlation. The traces show that, for

the amount of HSA in 0.4 µL of plasma (~23 µM HSA in HB reaction), there was a logarithmic relationship throughout the range of HB reagent concentrations, from 0.02 mM to 5 mM, in a 10 µL reaction. This flattening of the signal at high HB reagent

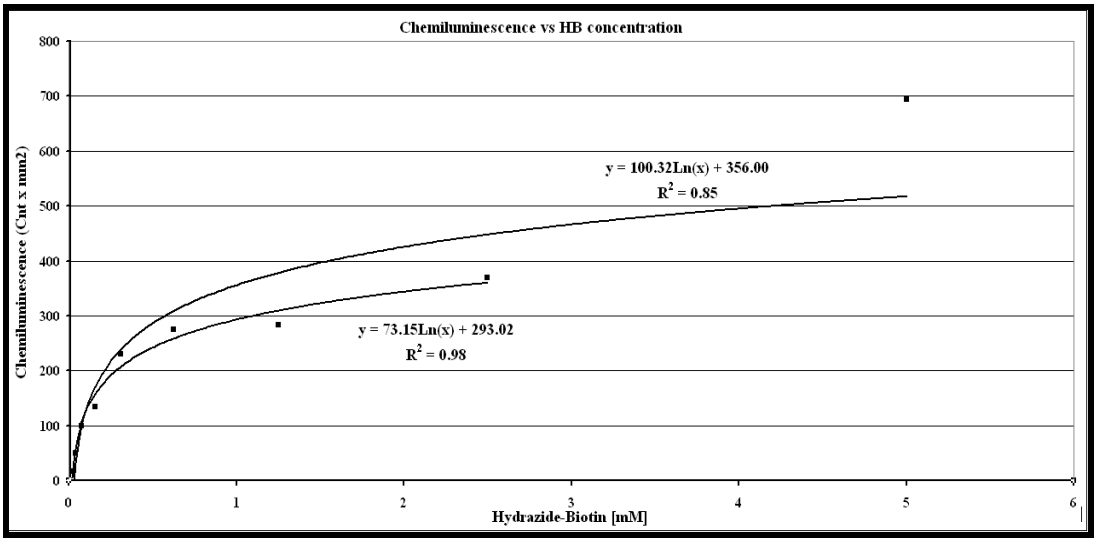

Figure 111 Chemiluminescence to detect HSA-bound carbonyls vs. HB reagent concentration- using ~23 µM HSA in a 10 µL reaction volume.

concentration indicates that the reactive sites of HSA were becoming relatively saturated with the HB reagent at this ~1000-fold excess. At the highest concentration of HB, where the reactive carbonyls are approaching saturation and variation in the HB concentration is no longer an important variable, the measured differences are more exclusively dependent upon the carbonyl content of HSA.

Because of the thick HSA band in Figure 110, it was decided that the amount of plasma could be further reduced to enable quantification that would be better distinguished from similar MW species. Figure 112 shows the result of a similar

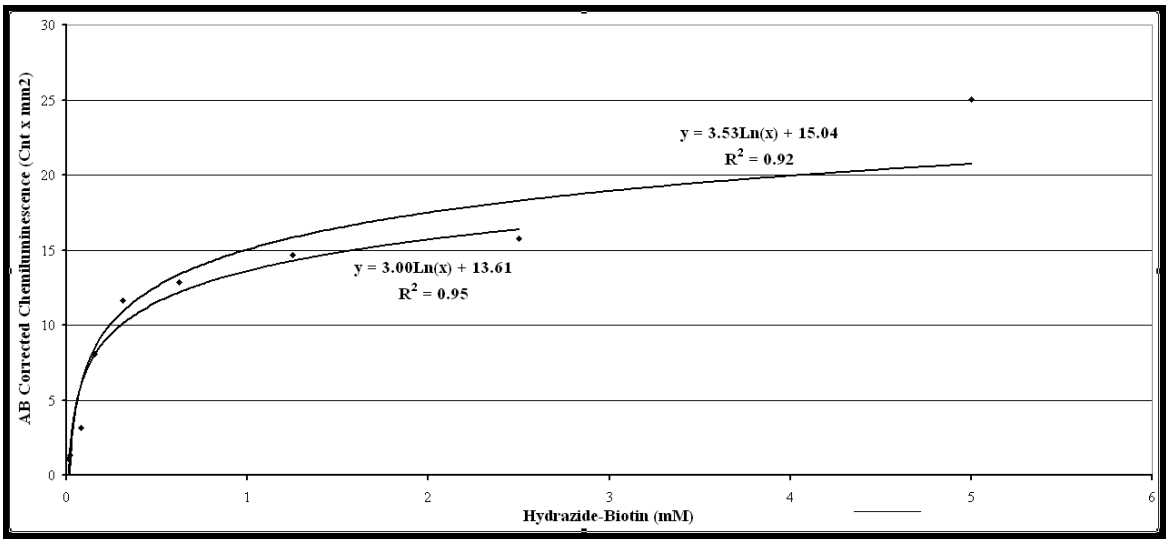

Figure 112 Chemiluminescence to detect HSA-bound carbonyls where the amplitudes of the signal have been corrected for protein loading using the amido black assay vs HB reagent concentration using ~1.1 μM HSA in a 10 μL reaction volume.

experiment to the experiment shown in Figure 111, but using a 20.5-fold less plasma (~1.1 μM HSA), for a ~20,000-fold excess of HB, at the highest HB reagent concentration. In Figure 112 the chemiluminescence values have also been corrected for loading variation, using the amido black assay. An average amido black value from all the data points was calculated. Correction factors for the individual chemiluminescence values were then calculated as the ratio of individual amido black values to the average of all the amido black values as before, by analogy to Equation 8. The range of these correction factors was 0.85-1.31 for levels of HSA. Individual chemiluminescence values were corrected for loading by dividing them by the individual correction factors. As before, the fit lines represent fitting the data with and without the 5 mM HB point, as it again showed aberrantly high signal. As expected, the trace shows saturation of the

signal at high HB reagent concentration. The control and T2DM samples were then measured with the same plasma concentration as used in Figure 112.

Negative controls show that standard plasma, which was processed the same as hydrazide-biotinylated plasma, except without hydrazide-biotin, showed no chemiluminescence (not shown). This negative control showed that there was no detectable endogenous protein-bound biotin in the tested plasma.

Attempts to assert better control over the time of the protein hydrazide-biotinylation reaction, by quenching unreacted hydrazide at 1 hour with formaldehyde, led to excessive loss of resolution of the bands in the 1D gels. This loss of resolution was likely the result of cross-linking of proteins. It is possible that the use of acetaldehyde would effectively quench hydrazide without the undesirable cross-linking, but this was not investigated.

This method below includes a procedure, using a visible pre-stained molecular weight marker ladder that was run on the 3 gels of the experiment, to enable the excision of the HSA regions of the gels. The 3 trimmed gels were reduced in dimension enough so that they could be stacked vertically in the blot and transferred simultaneously onto a single membrane.

Prior to the day of the experiment, 2mg of NHRP (Thermo Scientific, catalog #31001) was dissolved in 0.4 mL dI water and 0.4 mL glycerol (Sigma, SigmaUltra, catalog # G6279-1L). 10 υL aliquots of the dissolved NHRP solution in 0.6 mL microfuge tubes were then stored at -20° C until the time of use. It is important to avoid storage of the reagent at lower than -20° C or the solution will freeze which may affect

protein conformation stability. The recommended concentration range of the NHRP reagent is from 20,000-fold to 100,000-fold dilutions. Preliminary experiments found that a 5000-fold dilution was required for good signal with the high dilution of the plasma samples that was found to be optimum. The relatively high concentration of NHRP that was used did not appear to create higher background chemiluminescent signal on the membrane.

The following solutions were also made prior to the day of the experiment: Transfer Buffer-5.8 gms Tris Base (Bio-Rad, catalog # 161-0719), 2.9 gms glycine, 0.4 gms SDS, 200 mL MeOH, bring to 1 L with dI water pH-8.5. Tris-Buffered Saline (TBS)-Tween- add 6.05 gms Tris base, 8.76 gms NaCl to 800 mL dI water, pH to 7.5, then add 1 mL Tween 20 detergent (Sigma, catalog # P5927-500ML) and bring to 1L with dI water. Blocking Buffer- 5% unfortified nonfat dried milk powder (Bozeman Co-op) in TBS-Tween, 0.02% thimerosal (Sigma, catalog # T-4687). Dilution Buffer- TBS pH=6.8. Wash Buffer-TBS-Tween pH=6.8. HB reaction buffer- 10 mM NaH_2PO_4 pH 7.4.

10-well, 1.5 mm thick, 10% bis-acrylamide separating gels with 5% bis-acrylamide stacking gels were prepared using Bio-Rad Mini Protean 3 system (Bio-Rad glass plates, catalog # 1653312 and1653308) prior to the day before the experiment.

Immediately before the experiment, the previously prepared HB reaction buffer was degassed and approximately 300 µL of the following was made: 5 mM HB (Thermo, EZ-Link Biotin-LC-Hydrazide, catalog# 21340) in degassed HB reaction buffer. The air in the tube was exchanged with Argon, the tube was sealed with Parafilm and the

weighed solid was vortexed in solution until the HB was dissolved. This was kept on ice until adding to the plasma samples.

Sufficient water was heated in a beaker to near boiling, to heat the protein samples for reduction and solubilization after the HB reaction, prior to 1D PAGE.

To react the plasma proteins with HB reagent, previously prepared and frozen (-80 ° C) 0.4 µL aliquots of the plasma samples to be tested were thawed on ice and diluted with 19.2 µL of the degassed HB reaction buffer (10 mM NaH_2PO_4, pH 7.4) and briefly vortexed. 1 µL of the diluted plasma was added to 10 µL of the 5 mM HB solution in 0.6 mL microfuge tubes. The air in the tubes was exchanged with Argon and the tubes were sealed with Parafilm, wrapped in aluminum foil and vortexed for 1 hour at RT.

After 1 hour, the reactions were briefly centrifuged to bring the liquid to the bottom of the tube and 10 µL of 2X reducing, sample buffer (1 mL of 1 M Tris-HCl pH 6.8, 2 mL 10% SDS, 3 mL 50% glycerol, 3.5 mL Milli-Q water and 0.5 mL B-mercaptoethanol (Sigma-Aldrich, catalog # M7154-25mL, and a trace of bromophenol blue) was added to each reaction. 30 µL of the visible standard (Fisher Scientific, EZ-RUN Pre-stained Rec Protein Ladder, catalog #BP3603-500) was mixed with 30 µL of the 2X sample buffer. The vials were placed in a floatation device and incubated in hot water bath (~95 ° C) for 5 minutes.

After reduction of the samples, the ~20 µL reactions were centrifuged and added to the wells of the interior lanes of the 1D gels. The 2 outer lanes were reserved for visible pre-stained protein ladders and into these lanes 10 µL of prepared, reduced standard solutions were added. Gels were run at 120V until the bromophenol blue dye

reached the bottom edge of the gel. The sample and standard layouts for the 3 gels are shown in Figure 114A.

After running proteins on the 1D gels, the visible protein bands representing MW 100 kDa and 40 kDa in the ladders were used to guide cutting identical MW regions from the 3 gels to include HSA (Figure 114B). A small diagonal was cut on the upper right hand corner of the cropped gels for later orientation. The gels were placed in separate, labeled Pipetteman boxes and equilibrated with transfer buffer while gently shaking for 30 minutes. Using gloves for handling the 0.45 µm thick PVDF membrane (Thermo Scientific, catalog # 88585), a piece was cut to the same approximate dimensions as the 3 vertically stacked cropped gels. A small diagonal on the upper right hand corner of the membrane was cut for orientation with the gels. The membrane was wetted with MeOH for 15 seconds and then equilibrated with transfer buffer for 15-20 minutes. 4 pieces of filter paper (Whatman), cut to the approximate dimensions of the gels/PVDF membrane,

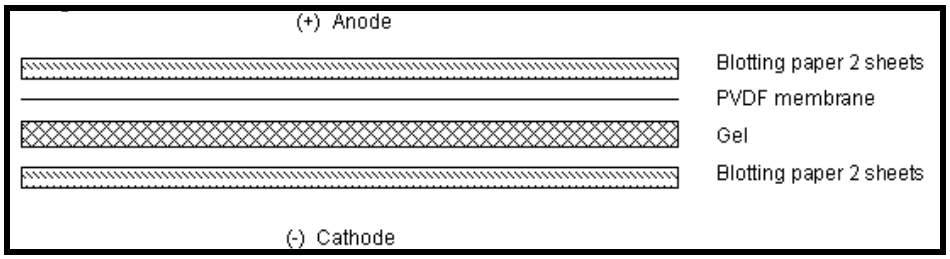

Figure 113 Transfer configuration

were wetted with transfer buffer. The gels, membrane, and blotting papers were assembled in a "blot" under transfer buffer as shown in Figure 113. 5 blotting sponges were soaked in transfer buffer and compressed to remove any air bubbles. Carefully

"sandwiching" the PVDF/gel assemblage between the sponges, and removing air bubbles, the entire assemblage was placed into the blot module and buffer-filled transfer tank (Invitrogen, Novex Mini-Cell and XCell II Blot Module, catalog # EI9051), orienting the polarity with the blot as in Figure 113. The tank was placed on ice and run at 25V for 90 minutes to transfer the protein bands to the membrane.

After the transfer, the membrane was removed from the blot and dried at 37 ° C for 10-15 minutes and then blocked in ~50 mL of blocking buffer in a Pipetteman-tip box, while gently shaking for 30 minutes.

To prepare the NHRP solution for reacting with the membrane-bound biotinylated proteins, two 10 µL aliquots of previously prepared and stored NHRP in 50% glycerol were washed from the tubes with 20 µL of the HB reaction buffer (10mM NaH_2PO_4, pH=7.4) and added to 50 mL of the dilution buffer (~5000-fold final dilution of NHRP). After completion of the blocking step, the membrane was transferred to the ~50 mL solution of diluted NHRP in a Pipetteman-tip box and incubated for 1 hour, while gently shaking. After incubation, the NHRP solution was poured off and the membrane was washed over a period of 30 minutes, while gently shaking between 6 exchanges, ~50 mL each, of wash buffer.

The emission of light from the chemiluminescence is time-sensitive and the procedure should be done with due expedience. In order to avoid variable delays, the Typhoon imager should be warmed up prior to the imaging time.

To image the membrane, after warming up the Typhoon imager, the membrane was placed in a clean Pipetteman-tip box, transfer side up, and a 1:1 mixture (1.5 mL of

each component) of the two-component chemiluminescent substrate (Thermo Scientific, SuperSignal West Pico Chemiluminescent Substrate, catalog # 34077) was added. The substrate solution was uniformly passed over the surface of the membrane for 5 minutes. The membrane was then carefully placed in a plastic sheet-cover and imaged, transfer side down, using the normal sensitivity, 600V chemiluminescence setting of the Typhoon imager. Image scanning took approximately 5 minutes (Figure 114C).

The .gel data file was imported as a TIFF image file into Quantity One (Bio-Rad, v. 4.6.5) gel analysis software for quantitation of the HSA bands. Band volumes were quantified using the summation of pixel intensities within a rectangular area of identical dimensions for each band, using local background subtraction. The background corrected HSA band volumes were imported into an Excel spreadsheet. On examination of the image it was found that there was a signal loss that correlated with the time of the scan (Figure 114C). It was calculated that the average HSA band volume in gel#2 and gel #3 were 74% and 48%, respectively, that of the gel#1. To correct for this time of scanning effect, a normalization factor for gel #2 and gel#3 was calculated to make their average HSA band volumes equal to gel#1. This normalization is similar to the normalization process used in the 2D gel experiments. This factor was then used to correct the individual HSA chemiluminescence band volumes within the gels.

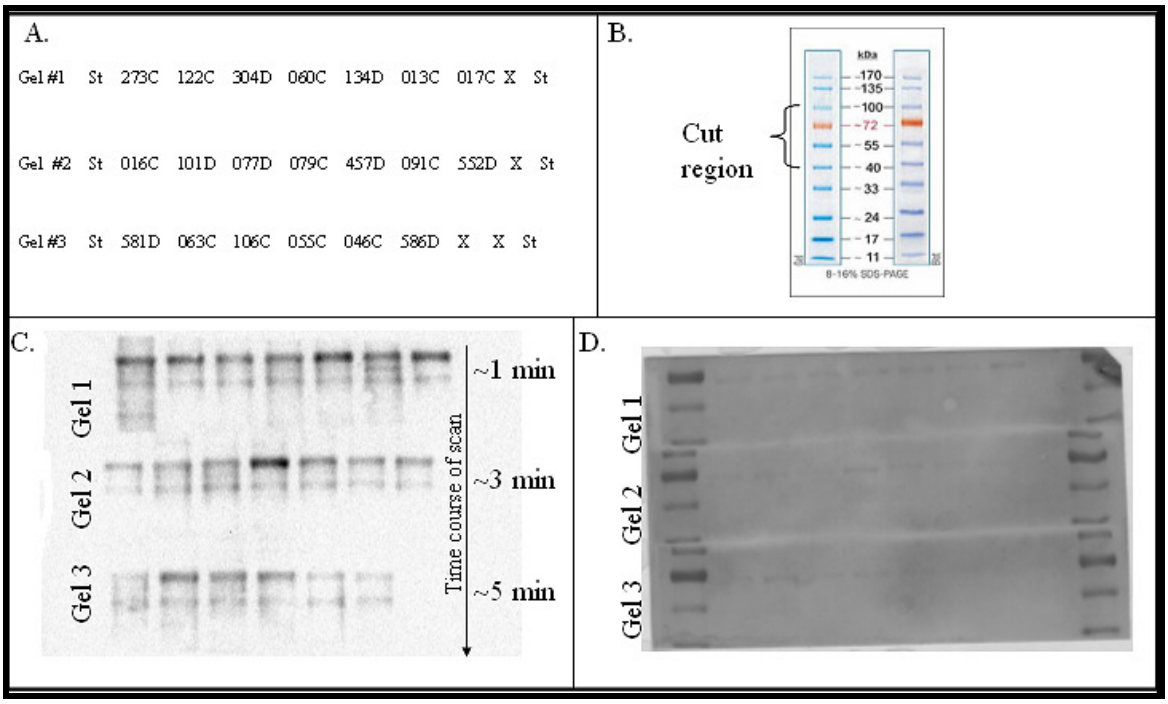

Figure 114 A- Sample assignment for lanes of 3 gels, "C"– normal glucose tolerance, "D"-type-2 diabetic, the numbers are the last digits of the NIH identification numbers. B- MW designations of visible standard and excised region of each gel. C- Chemiluminescent image with apparent scanning-time dependence indicated. D- Amido black stain image showing high and variable background.

To quantify the total HSA bands of the membrane with amido black stain, the following solutions were prepared: Amido black stain- 0.25 gms Naphthol blue black (Fluka- catalog #70492), 225 mL MeOH, 225 dI water, 50 mL glacial acetic acid. Destain solution- 90% MeOH, 2% glacial acetic acid. Elution solution- 25 mL 1N NaOH, 100 µL 0.5 M EDTA pH 8.0, 525 mL 95% EtOH, bring up to 1L with dI water.

After chemiluminescent imaging, the membrane was stained by placing it in 25 mL of amido black stain solution in a Pipetteman-tip box and gently shaking for 1 hour. After staining, the membrane was rinsed in water and destained 2 times with 25 mL destain solution for 3 minutes while gently shaking. The membrane was rinsed with

water until the MeOH was removed. The individual HSA bands were excised and placed in labeled 1.5 mL microfuge tubes. 225 µL of elution solution was added to each tube and the tubes were vortexed until the stain was removed from the membrane pieces. After elution, 200 µL of the each solution was added to the well of a 96-well plate and 3 X 3 circular reads at 630 nM were taken.

Inspection of the amido black stained membrane (Figure 114 D) showed unusually high background and variable regions of light and dark areas. This had not been observed previously to this experiment. It's possible that the source of the high background was the visible pre-stained ladder, which was used for the first time here. Because of high and variable background, the amido black stain to control for loading variation was not used. However, because ELISA assays for HSA had previously been run on the individual samples, these results were used to correct the individual chemiluminescence signals for biological variations of HSA concentration. Unfortunately the ELISA data only controlled for biological variations of HSA concentration and the ability to control for technical variations due to loading and transfer was not possible in this experiment.

Results and Discussion

● *Maleimide labeling test for loss of reactivity due to oxidation of HSA Cys-34.* Figure 115A and Figure 115B show the fluorescent images of the: A, NHS-ester lysine reactive dye labeled polypeptides and B, maleimide cysteine reactive dye labeled polypeptides as a function of H_2O_2 dilutions. The panels at the bottom of A and B show

the densitometric line profile taken along the red horizontal line passing through the HSA bands of the upper panels. In addition to showing that the method is sensitive to oxidative modification of Cys-34, the low density signal of the HSA bands on the left of Figure 115B-top also shows that there is minimal maleimide labeling of the 34 reduced

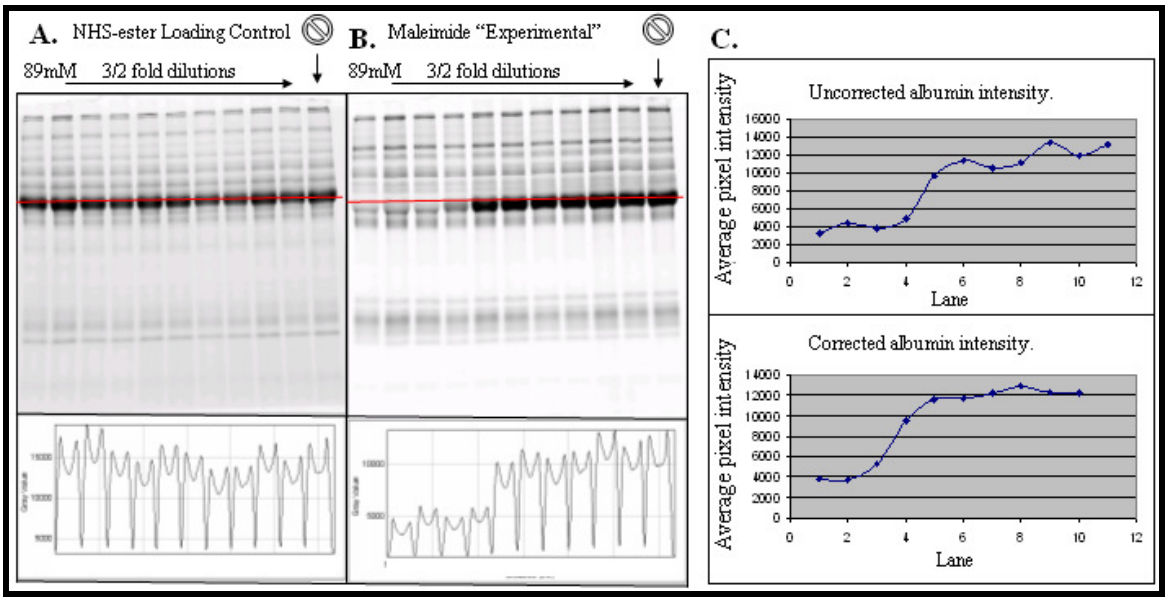

Figure 115 Test "loading control" experiment using H_2O_2 dilution series to "block" maleimide reactive thiol at HSA Cys-34. A) Gel image of the NHS-ester Zdye labeled loading control proteins (top) and profile of the HSA band intensities (bottom). B) Gel image of the maleimide Zdye labeled proteins (top) and profile of the HSA band intensities (bottom). C) The uncorrected intensities (top) and the loading control corrected intensities of the 11 maleimide labeled HSA bands (bottom).

cysteines that had formed the 17 disulfide bridges of HSA prior to reduction, which was performed after the dye-labeling reaction but before adding the samples to the 1D gel. This was likely a result of the overwhelming excess of the thiol, B-mercaptoethanol in the loading buffer. The image indicates that the excess B-mercaptoethanol quenched any unreacted maleimide dye before the dye could react with significant amounts of the

reductively liberate cysteines. Therefore, it was concluded that reducing sample buffer could effectively be used to quench the maleimide dye reaction without causing side labeling reactions with other cysteines in HSA. This is also illustrative of the low cross-reactivity of the maleimide with other residues at the pH employed, (pH= 7.0), most notably lysine. The protonated form of lysine is not nucleophilic and therefore, at pH 7.0 the lysine side chain is predominately not in a form that is reactive with maleimide, as lysine has a pK of approximately 10.5. Also, notice that the trend of thiol oxidation that seen in HSA appears in no other protein across the range of H_20_2 concentrations. This is likely illustrative of the large concentration of HSA's free thiol at Cys-34 and its uniquely important role as modulator of redox state of blood [320, 336] .

Figure 115 C-top shows the uncorrected densitometric quantitation of the maleimide labeled HSA bands. Figure 115 C-bottom shows the densitometric quantitation of the maleimide labeled HSA bands after correction for HSA loading by using the spectrally resolved lysine reactive NHS-ester fluorescent dye. By comparing these two plots, it can be seen that the data points in the corrected plot show much less variation, producing a smoother sigmoidal curve than in the uncorrected plot. From this experiment, it was concluded that the simultaneous two-dye labeling method appeared to be a useful way to more accurately measure the relative differences in amount of native unoxidized Cys-34 of HSA, and to correct for errors introduced from the pipetting of low volumes of viscous plasma and for variations in HSA concentrations in the different samples.

● *Comparison of oxidized Cys-34 between experimental NGT and T2DM subjects*. Figure 116 shows the fluorescence 1D PAGE gel images of the doubly dye-labeled NGT and T2DM plasma samples, one label for the HSA cysteine (maleimide) and the second label to correct for sample loading and biological variation (NHS-ester). The corrected, relative oxidation of HSA was calculated using Equation 8 and a comparison of the average values was made between the experimental groups. The values for the control

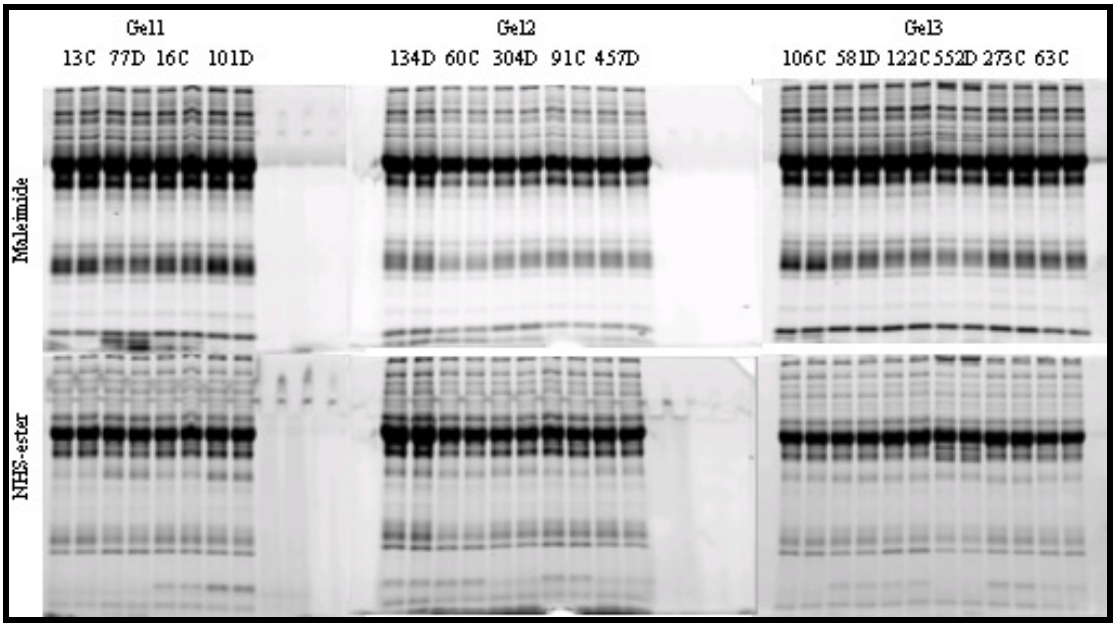

Figure 116 Gel images for experiment detecting oxidized HSA Cys-34 in NGT and T2DM samples. C=Control (NGT). D=T2DM. The numbers are the last digits of the NIH sample identifications.

group (n =8) were 312997 $\pm$ 61215 CNT x mm^2 and for the T2DM group (n=7) were 306736 + 100767 CNT x mm^2, a non-significant difference. Thus, we found no evidence for differences in the levels of reduced Cys-34 in the HSA from NGT and from T2DM samples

● *Differential measurement of oxidative stress of HSA in experimental groups carried out by analysis of carbonyls*. A comparison of the average normalized spot volumes between the experimental groups showed borderline significant difference between them, surprisingly, with less chemiluminescence, indicating less oxidative carbonylation, in the T2DM group. Figure 117 shows the comparison between the groups using the average normalized spot volumes (Figure 117B) and the average normalized, spot volumes per [HSA] (Figure 117B) using the HSA ELISA data. There are 2 more data points in the NGT data set of the average normalized spot volumes (n=12) than in the NGT average normalized spot volumes per [HSA] because there was no HSA ELISA data for these 2 individuals. Two-tailed t-tests with unmatched variances yielded $p = 0.04$ and $p < 0.05$, respectively. The individual background corrected values are shown with the quantified HSA band areas in Supplementary Figure 136.

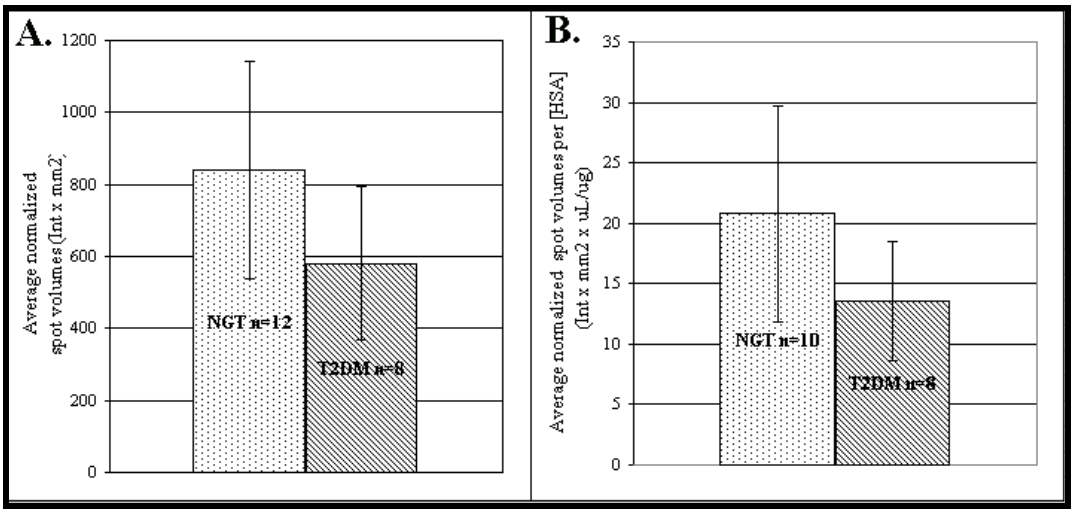

Figure 117 HSA carbonyl assay results. A- Average normalized spot volumes. B- Average normalized spot volumes per [HSA], HSA concentrations in each subject sample determined by ELISA.

The HSA carbonyl data were plotted against several metabolic parameters important to classification T2DM. There was no correlation of the carbonyl assay with the measurements NIH made of total cholesterol, HDL, LDL, CRP, or urine albumin/creatinine level. In contrast, as seen in Figure 118, there were moderate to good correlations of HSA carbonyl content with the FPG (P = 0.03, dF = 16), % Ha1c (P= 0.01, dF =16) and BMI (P = 0.03, dF =16). There was no significant correlation between

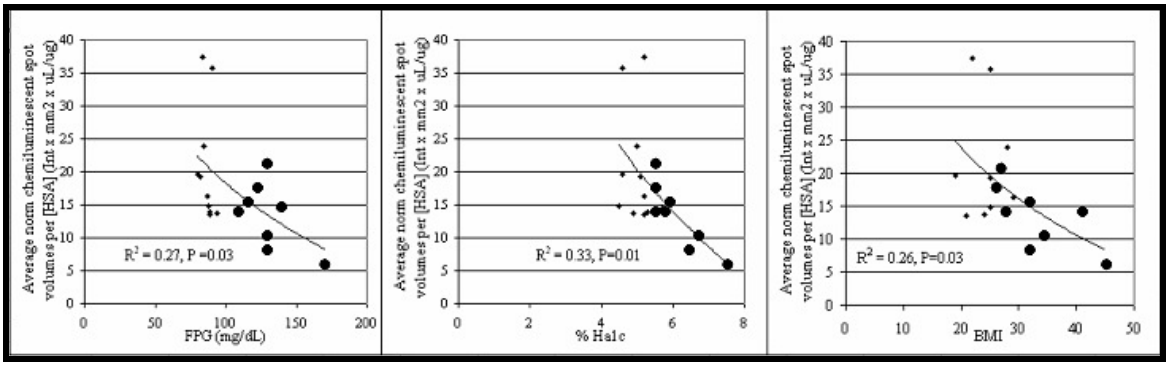

Figure 118 Average normalized protein carbonyl dependent chemiluminescent spot volumes per [HSA] vs. 3 important metabolic parameters and logarithmic fits to the data. T2DM datapoints are the heavy enclosed circles.

FPG, Ha1c or BMI with the total HSA concentration. In view of these correlations of the carbonyl assay with glucometric measurements and BMI, we were surprised to find no correlation between the carbonyl assay and the BEPHE assay (Figure 119).

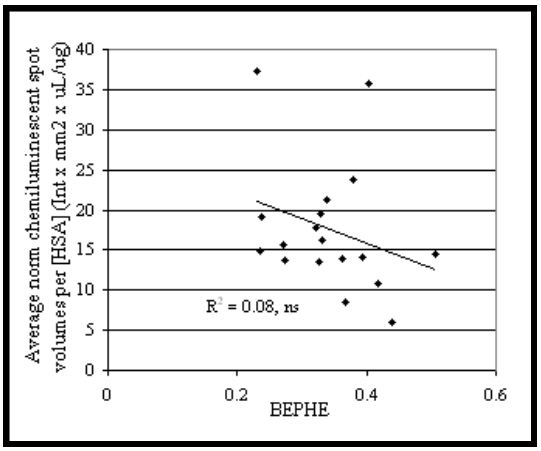

Figure 119 Lack of correlation between carbonyl assay and the BEPHE assay. The BEPHE assay corrects for the HSA concentration in each plasma sample.

It was surprising that the chemiluminescent measure of oxidation would be anti-correlated with the metabolic measures shown in Figure 118, which are of such central importance to classification T2DM. In light of the reported increase of oxidative stress in T2DM, it suggests that HSA might be protected from oxidation or from the hydrazide reaction, perhaps by binding partners. This interpretation would agree with the BEPHE result, which showed that HSA was "protected" from binding the BCG dye in a FPG dependent manner. Unexpectedly the BEPHE and protein carbonyl assays did not correlate with each other, perhaps because of the accumulated errors between them.

While the chemiluminescence measures of HSA carbonyl content correlations are interesting, the assumption that was made to normalize the 3 data sets may not be true for the small sets composed of 7, 7 and 6 subjects. The assumption was that the averaged chemiluminescences of the 3 sets should be equal. Recall that the total signal volumes of the gel #2 and gel #3 data sets were corrected so that their average individual intensities were equal to gel #1, to correct for scanning time. Figure 120 shows the same plot as the

central plot in Figure 118, with data point symbols representing the data points from the 3 gels. It can be seen that none of the data points that were corrected cluster at either extreme of the trend, absolving the multiplication factor that was used for normalization from causing the correlations. Also, the control and T2DM plasma samples were equitably distributed between the gels and over the time course of the scan, so it is unlikely that a systematic bias increased the signal of one group over the other. Nevertheless, the experimental irregularities that occurred, and the relatively small number of data points, prevent this experiment from being taken as strong evidence for the extraordinary conclusion that it suggests. Sample limitations prevented our extension

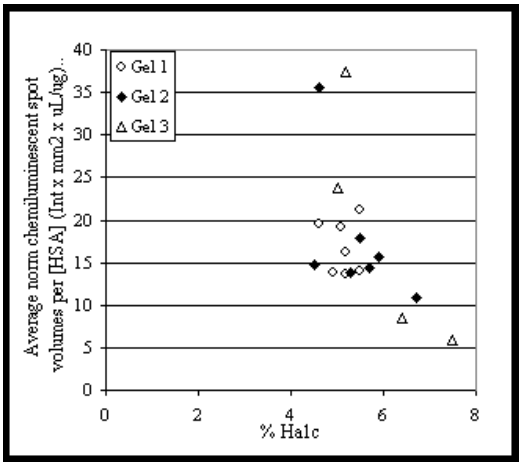

Figure 120 No cluster of constituent samples from the corrected 3 gel data sets form the trend. Two samples from gel 3 are not included because of lacking ELISA data for HSA concentration.

of this experiment to larger data sets, but the preliminary data and the method, especially with the addition of 2 simple modifications, as will be detailed in the CONCLUSION, seem promising.

CONCLUSION

These studies demonstrated several new findings: First, the protocol that was developed for analyzing lower abundance plasma proteins by immunodepletion, RP sub-fractionation, fluorescent dye protein labeling and 2DGE fluorescence quantification is a sensitive means to search for differences in health and disease. A large number of protein species were separated and the method has the advantage that it is able to distinguish many diffenent protein isoforms that may vary with health and disease. Previous examples of this combination of technologies are surprisingly absent in the literature. The validation of our method was borne out by the detection of decreased levels of ZAG and Apo AI, and increased levels of SAA-1 preprotein in T2DM. Each of these changes has previously been shown to occur in the T2DM milieu.

One reason why there are few examples of immunodepletion and sub-fractionation prior to 2DGE in the search for disease associated proteins may be the potential that these technologies have for introducing technical variation, which isthe bane of expression proteomics, to the levels of analyte proteins. We believe that the variations that were caused by individual runs were largely overcome in our protocol by the incorporation of multiple runs of the biological replicates that were pooled prior to 2DGE, as means of averaging out technical variability. The pooling of technical replicates was done in combination with the pooling of samples from 2 or 3 individuals to "smooth" out biological variations within each biological replicate.

The second contribution of this study was the identification of 2 new and potentially important protein players in the pathology of T2DM, namely CRISP-3 and

CFHR-5. CRISP-3 has a "profile" of a protein poised at the edge of pathogenesis. The CRISP family is found in a variety of animal venoms and its family members are believed to derive their toxic effects from various channel blocking abilities. Udby showed that CRISP-3 circulates in 1:1 stoichiometry with α1BG and believed that the reason for this complex was to safely escort the neutrophil-secreted CRISP-3, as a means of protection for tissues from the pathological effects of freely circulating CRISP-3. CRISP-3 is believed to be an L-type Ca^{2+} channel blocker and it has been shown that the β-cell's insulin secretion response to blood glucose, which is the site of the central impairment that turns insulin resistant people into T2 diabetics, is dependent upon L-type Ca^{2+} channels. Our detection of significantly lower levels of an isoform of glycosylated CRISP-3 in T2DM suggests that it may have escaped the bonds of its circulating escort and potentially entered tissues. One must wonder what would be the cytotoxic effects in mammals from chronic exposure to increased levels of free CRISP-3. How could such a modulator of B-cell function lead to the T2DM associated morphological changes of the islets of Langerhans? A similar question was asked in a 2005 review about how hyperglycemia, possibly in concert with FFAs and mediated by oxidative stress could cause the morphological changes in the islets. The reviewer's answer was that the "mechanisms regulating β-cell proliferation, apoptosis and function are inseparable processes" [145], suggesting that an "outside" agent that affects B-cell function could ultimately lead to the observed aberrations in proliferation and apoptosis. Because circulating CRISP-3 originates from neutrophils, this finding strengthens the already strong connection of T2DM with innate immunity.

A similar argument can be made for the significantly lower levels of circulating CFHR-5 in T2DM; that the net loss in the circulation may be made up by that found in tissue. Renal deposits of CFHR-5 have almost invariably been found in a variety of kidney pathologies. Our cohort of newly diagnosed T2 diabetics shows no impairment of kidney function, as demonstrated by normal urine albumin/creatinine levels, but renal disease is often a complication that accompanies advanced T2DM. The diminished amount of CFHR-5 that accompanies the pathological state of T2DM suggests that it may already be depositing in tissues.

The power of the 2D gel strategy was demonstrated in CRISP-3, as it detected a significant change in a single isoform of that polypeptide, which has 2 M_rs (glycosylated and non-glycosylated) and at least 3 detectable pIs. This has implications for standard immunological techniques, specifically ELISAs, as well as bottom-up proteomics, which are not sensitive to MW or pI differences, and 1D western blots, which are not sensitive to pI differences. The changes that were detected in ZAG and SAA-1 preprotein were also limited to 2 and 1 isoforms, respectively.

Third, the investigation of HSA-BCG dye binding showed that HSA binding property was significantly associated with important metabolic parameters of glycemic control, primarily FPG, throughout the range of fasting glucose of this study; including NGT, IGT and T2DM subjects. This association appears to be independent of *in vitro* addition of D-glucose, leaving open the possibility of a role for HSA that is not merely epiphenomenal to the hyperglycemic state and might be on or indicative of a causal

pathway. The specific issue of disease specific differences of lipid cargo of HSA is currently under investigation by others in the Dratz laboratory.

Fourth, regarding oxidative modifications of HSA, the novel use of multiplex, mixed reactive chemistry, dye-labeling demonstrated that the change in binding does not appear to be related to oxidative alterations to Cys-34 of HSA. However, our results did show an unexpected significant anti-correlation of HSA's carbonyl content with FPG, Ha1c, and BMI. The strong anti-correlation with Ha1c suggests that HSA may be bound *in vivo* by species in T2DM that protect HSA from oxidative carbonylation. One would well wonder what is being oxidized in HSA's stead, in the known increased oxidative environment of T2DM.

As we have discussed, HSA is the primary carrier of NEFAs and –SNO in the blood. It also carries peptides, proteins, metals, small molecules and drugs. HSA is the most important osmolyte and antioxidant in the blood. Paradoxically, studying HSA may have been relatively convenient, historically, because of it abundance and the relative ease of purification, but because of its abundance, studying HSA's fine interplay with other factors may make HSA's interactions the hardest of all the blood proteins to fully understand. Because of its abundance HSA may have profoundly important interactions *in vivo* that tend to evanesce *in vitro* because of changes in the mass action environment that are necessary to study it. HSA is very abundant; ½ of the blood plasma protein mass, far more than the next most abundant protein and at least 10 orders of magnitude more than the rarest detected blood proteins. This is on the order of ½ pound of HSA circulating in the average size person, a mass similar to that of a small organ such as the

spleen, flowing through the blood. Important interactions of HSA may hide beneath its abundance. Our results suggest that the binding of HSA reflects glycemic control and this may be related to innate immunity and lipid metabolism.

Since we have analyzed protein level differences on the order of μg/mL, we might expect to detect changed levels of the important 30 kDa adipocytokine, adiponectin (Acrp30 or AdipoQ). Acrp30 is present in average plasma concentrations of 5-10 μg/mL [383] and has been shown to be down in T2DM [311]. It may not have been detected because our criteria of accepting only measured changes greater than 1.4 fold. Acrp30 has been found down in T2 diabetic women (1.5-fold) but in men it was only down 1.2-fold [311]. Because of our mixed sex cohort it is possible that the changes of Acrp30 did not reach the needed 1.4-fold change between our groups. Alternatively, it is certainly possible that a 30 kDa protein was obscured by other proteins in the gels, even after sub-fractionation.

Some changes in the future use of the aforementioned protocols should be suggested here. Briefly, they are:

1) In our protocol for the RP sub-fractionation in the 2DGE experiment, the cutoff time between F2 and F3 occurs at a peak (Figure 60). This was done to maintain a similar amount of protein in F2 as in the other fractions. In hindsight I would suggest that all cutoffs be made at minima, not because minima are more dependable than the peaks but for the simple reason that fewer proteins are likely to be disrupted by the cuts at the minima.

2) In hindsight I would recommend that uniform gels be given consideration over gradient gels whenever possible. Our preliminary experiments showed that gradient gels spread out the congested regions of high MW proteins, but I suspect that an unforeseen price was paid by using gradient gels because they are susceptible to distortions in their gradients that sometimes make spot matching more difficult. On these same lines I would recommend that samples within a fraction should be run on as few different batches of acrylamide gels as possible. Of course it isn't always possible to run all the samples within a fraction on a single batch of gels in large experiments, since gels are usually poured in batches no greater than 12.
3) A final wash of the lyophilized proteins from the 15 mL conical vials with a small amount of organic solvent may be of benefit, particularly for the more hydrophobic RP fractions, such as F5 and F6. These 2 fractions did not yield any changed proteins in our experiment and with the decreasing amounts of changes that were detected, apparently in anti-correlation with hydrophobicity (4 POIs in F1, 2 POIs in F2 [1 unidentified], none in F3, 1 POI in F4, none in F5 or F6), one wonders if this anti-correlation was caused by technical variability that was higher in more hydrophobic proteins.
4) The scanning of chemiluminescence by the Typhoon is a painfully time dependent method relative to the lifetime of the chemiluminescent signal. The Typhoon scanner was chosen for our method because it appeared to have the advantage of greater linear dynamic range than X-ray film and could therefore

measure smaller differences between the samples. In order to avoid the time dependence and the necessity for normalization of the blot intensities I would suggest the simple step of cutting the blotted membrane into the dimensions of the original gels and aligning them side-by-side along the Y-axis of the scanner. Having done this, the bands of like proteins on the membrane pieces will be scanned at the same approximate times. High background of the membrane may also be avoided by cutting the visible protein standards from the gels before performing the transfer.

S.B.L.

BIBLIOGRAPHY

1. Gabay, C. and I. Kushner, *Acute-Phase Proteins and Other Systemic Responses to Inflammation.* N Engl J Med, 1999. **340**(6): p. 448-454.

2. *Definition and Diagnosis of Diabetes Mellitus and Intermediate Hyperglycemia: Report of a WHO/IDF Consultation*. 2006, World Health Organization/ International Diabetes Federation. p. 1-50.

3. Evans, J.L., et al., *Oxidative Stress and Stress-Activated Signaling Pathways: A Unifying Hypothesis of Type 2 Diabetes.* Endocr Rev, 2002. **23**(5): p. 599-622.

4. *National Diabetes Fact Sheet: General Information and National Estimates on Diabetes in the United States, 2007.* 2010, Atlanta, GA: US Dept of Health and Human Serices, Centers for Disease Control and Prevention.

5. *American Diabetes Association: Diagnosis and Classification of Diabetes Mellitus.* Diabetes Care, 2007. **30**(Supplement 1): p. S42-S47.

6. *Program Announcement: Proteomic and Metabolic Approaches to Diagnose Diabetes and Pre-Diabetes PAR-04-076*. 2004: US Department of Health and Human Services (DHHS) and National Institutes of Health (NIH).

7. *Merriam-Webster's Collegiate Dictionary*. 10th ed. 1993.

8. Clendening, L., ed. *Source Book of Medical History*. 2nd ed. 1960, Dover Publications, Inc.

9. *Encyclopaedia Britannica.* 1878(9th Edition): p. 147-8.

10. http://embryology.med.unsw.edu.au/notes/images/git/historic-pancreas1.jpg.

11. Howard, J.M., Hess, W., *History of the Pancreas: Mysteries of a Hidden Organ*. Illustrated ed. 2002: Springer. p.4.

12. Langerhans, P., *Beitrage zur mikrskopischen Anatoomie der Bauchspeicheidruse [Contributions to the microscopic anatomy of the pancreas]*, in *Medicine and Surgery*. 1869, Berlin Pathological Institute: Berlin.

13. Bliss, M., *The Discovery of Insulin*. 1982: The University of Chicago Press. p. 25.

14. Von Mering, J., Minkowski, O., *Diabetes mellitus nach Pankeasextirpation.* Centralblatt fur klinische Medicin, 1889. **10**(23): p. 393-394.

15. Opie, E.L., *THE RELATION OE DIABETES MELLITUS TO LESIONS OF THE PANCREAS. HYALINE DEGENERATION OF THE ISLANDS OE LANGERHANS.* J. Exp. Med., 1901. **5**(5): p. 527-540.

16. Opie, E.L., *ON THE RELATION OF CHRONIC INTERSTITIAL PANCREATITIS TO THE ISLANDS OF LANGERHANS AND TO DIABETES MELLITUS.* J. Exp. Med., 1901. **5**(4): p. 397-428.

17. Hull, R.L., et al., *Islet Amyloid: A Critical Entity in the Pathogenesis of Type 2 Diabetes.* J Clin Endocrinol Metab, 2004. **89**(8): p. 3629-3643.

18. Ahronheim, J.H., *Nature of hyaline material in pancreatic islets in diabetes mellitus.* American Journal of Pathology, 1943. **19**: p. 873-82.

19. Ehrlich J.C., R.I.M., *Amyloidosis of the islets of Langerhans. A restudy of islet hyaline in diabetic and non diabetic individuals.* American Journal of Pathology, 1961. **38**: p. 49-59.

20. Westermark, P., *Amyloid and Polypeptide Hormones - What Is Their Interrelationship.* Amyloid-International Journal of Experimental and Clinical Investigation, 1994. **1**(1): p. 47-60.

21. Hoppener, J.W.M., B. Ahren, and C.J.M. Lips, *Islet Amyloid and Type 2 Diabetes Mellitus.* N Engl J Med, 2000. **343**(6): p. 411-419.

22. Banting, F.G., Best, C.H., *Pancreatic Extracts.* The Journal of Laboratory and Clinical Medicine, 1922. **VII**: p. 464-72.

23. Banting, F.G., Best, C.H., *The Internal Secretion of the Pancreas.* The Journal of Laboratory and Clinical Medicine, 1922. **VII**(5): p. 251-66.

24. Banting, F.G., Best, C.H., Collip, J.B., Campbell, W.R., Fletcher, A.A., *Pancreatic Extracts in the Treatments of Diabetes Mellitus.* Canadian Medical Association Journal, 1922. **12**(3): p. 141-146.

25. Kirkbride, M.B., *THE ISLANDS OF LANGERHANS AFTER LIGATION OF THE PANCREATIC DUCTS.* J. Exp. Med., 1912. **15**(1): p. 101-105.

26. Bliss, M., *The Discovery of Insulin*. 1982, The University of Chicago Press.

27. Davidson, J.K., *Clinical Diabetes Mellitus*. Third ed. 2000: Thieme.

28. Bliss, M., *The Discovery of Insulin*. 1982: The University of Chicago Press. p. 49.

29. Dewitt, L.M., *MORPHOLOGY AND PHYSIOLOGY OF AREAS OF LANGERHANS IN SOME VERTEBRATES.* J. Exp. Med., 1906. **8**(2): p. 193-239.

30. Hagedorn, H.C., Jensen, B. N., Krarup, N. B., Wodstrup, I., *Protamine Insulinate.* Journal of the American Medical Association, 1936. **106**(3): p. 177-80.

31. Root, H.F., White, P., Marble, A., Stotz, E. H., *CLINICAL EXPERIENCE WITH PROTAMINE INSULINATE.* 1936. **106**(3): p. 180-3.

32. Bliss, M., *The History of Insulin.* Diabetes Care, 1993. **16**(Supplement 3): p. 4-7.

33. Scott, D.A. and A.M. Fisher, *The effect of zinc salts on the action of insulin.* Journal of Pharmacology and Experimental Therapeutics, 1935. **55**(2): p. 206-221.

34. *Medical Management of Type 1 Diabetes*. 5th ed, ed. F.R. Kaufman. 2008: American Diabetes Association. 58-59.

35. Himsworth, H.P., *DIABETES MELLITUS: ITS DIFFERENTIATION INTO INSULIN-SENSITIVE AND INSULIN INSENSITIVE TYPES.* The Lancet, 1936. **1**: p. 127-130.

36. Bach, J.F., *Insulin-Dependent Diabetes-Mellitus as an Autoimmune-Disease.* Endocrine Reviews, 1994. **15**(4): p. 516-542.

37. Tisch, R., et al., *Immune-Response to Glutamic-Acid Decarboxylase Correlates with Insulitis in Nonobese Diabetic Mice.* Nature, 1993. **366**(6450): p. 72-75.

38. DeFronzo, R.A., Hendler, R., Simonson, D., *Insulin Resistance is a Prominent Feature of Insulin-dependent Diabetes.* Diabetes, 1982. **31**(September): p. 795-82.

39. Warram, J.H., et al., *Slow Glucose Removal Rate and Hyperinsulinemia Precede the Development of Type II Diabetes in the Offspring of Diabetic Parents.* Annals of Internal Medicine, 1990. **113**(12): p. 909.

40. *Medical Management of Type 2 Diabetes*. 6th ed, ed. C.F. Burant. 2008: American Diabetes Association.

41. Besser, G.M., Thorner, M.O., *Comprehensive Clinical Endocrinology*. Third ed. 2002: Mosby.

42. Ridderstrale, M., Groop, L., *Genetic dissection of type 2 diabetes.* Molecular and Cellular Endocrinology, 2009. **297**: p. 10-17.

43. Björntorp, P. and L. Sjöström, *Carbohydrate storage in man: Speculations and some quantitative considerations.* Metabolism: Insulin Insensitivity, 1978. **27**(12, Supplement 2): p. 1853-1865.

44. Rosenbloom, A.L., et al., *Emerging Epidemic of type 2 diabetes in youth.* Diabetes Care, 1999. **22**(2): p. 345-354.

45. Neel, J.V., *Diabetes Mellitus: A "Thrifty" Genotype Rendered Detrimental by "Progress".* American Journal of Human Genetics, 1962. **14**: p. 352-61.

46. Mokdad, A.H., et al., *Prevalence of Obesity, Diabetes, and Obesity-Related Health Risk Factors, 2001.* JAMA, 2003. **289**(1): p. 76-79.

47. Kahn, C.R., D. Vicent, and P.D. Doria, Alessandro, *GENETICS OF NON-INSULIN-DEPENDENT (TYPE-II) DIABETES MELLITUS.* Annual Review of Medicine, 1996. **47**(1): p. 509.

48. Kaprio, J., Tuomilehto, J., Koskenvuo, M., Romanov, K., Reunanen, A., Eriksson, J., Stengard, J., Kesaniemi, Y.A., *Concordance for type 1 (insulin-dependent) and type 2 (non-insulin-dependent) diabetes mellitus in a population-based cohort of twins in Finland.* Diabetologia, 1992. **35**: p. 1060-1067.

49. Newman, B., Selby, J.V., King, M.C., Slemenda, C., Fabsitz, R., Friedman, G.D., *Concordance for Type 2 (non-insulin-dependent) diabetes mellitus in male twins.* Diabetologia, 1987. **30**: p. 763-768.

50. Nelson, W.J. and R. Nusse, *Convergence of Wnt, beta-catenin, and cadherin pathways.* Science, 2004. **303**(5663): p. 1483-1487.

51. Zhou, L., et al., *Regulation of lactate production at the onset of ischaemia is independent of mitochondrial NADH/NAD+: insights from in silico studies.* The Journal of Physiology, 2005. **569**(3): p. 925-937.

52. Zhao, F.-Q. and A.F. Keating, *Functional Properties and Genomics of Glucose Transporters.* Current Genomics, 2007. **8**(2): p. 113-128.

53. Seidner, G., et al., *GLUT-1 deficiency syndrome caused by haploinsufficiency of the blood-brain barrier hexose carrier.* Nature Genetics, 1998. **18**(2): p. 188-191.

54. Guillam, M.T., et al., *Early diabetes and abnormal postnatal pancreatic islet development in mice lacking Glut-2.* Nature Genetics, 1997. **17**(3): p. 327-330.

55. Mueckler, M., *Facilitative glucose transporters.* European Journal of Biochemistry, 1994. **219**(3): p. 713.

56. Stenbit, A.E., et al., *GLUT4 heterozygous knockout mice develop muscle insulin resistance and diabetes.* Nature Medicine, 1997. **3**(10): p. 1096-1101.

57. Reaven, G.M., *Role of Insulin Resistance in Human Disease: Banting Lecture.* Diabetes, 1988. **37**: p. 1595-1607.

58. Lillioja, S., et al., *Impaired Glucose-Tolerance as a Disorder of Insulin Action - Longitudinal and Cross-Sectional Studies in Pima-Indians.* New England Journal of Medicine, 1988. **318**(19): p. 1217-1225.

59. Warram, J.H., et al., *Slow Glucose Removal Rate and Hyperinsulinemia Precede the Development of Type II Diabetes in the Offspring of Diabetic Parents..* Annals of Internal Medicine, 1990. **113**(12): p. 909.

60. Lillioja, S., et al., *Insulin Resistance and Insulin Secretory Dysfunction as Precursors of Non-Insulin-Dependent Diabetes Mellitus: Prospective Studies of Pima Indians.* N Engl J Med, 1993. **329**(27): p. 1988-1992.

61. Defronzo, R.A., Bonadonna, R.C., Ferrannini, E., *Pathogenesis of NIDDM: A Balanced Overview.* Diabetes Care, 1992. **15**(3): p. 318-368.

62. Kahn, S.E., *The Importance of B-Cell Failure in the Development and Progression of Type 2 Diabetes.* J. Clin. Endocrinol. Metab., 2001. **86**(9): p. 4047-4058.

63. Warram, J.H., et al., *Slow Glucose Removal Rate and Hyperinsulinemia Precedes the Development of Type II Diabetes in the Offspring of Diabetic Parents.* Annals of Internal Medicine, 1990. **113**(12): p. 909.

64. Wolf, G., *Role of fatty acids in the development of insulin resistance and type 2 diabetes mellitus.* Nutrition Reviews, 2008. **66**(10): p. 597-600.

65. Shulman, G.I., Rothman, D. L., Jue, T., Stein, P., DeFronzo, R. A., Shulman, R. G., *Quantitation of muscle glycogen synthesis in normal subjects and subjects with non-insulin-dependent diabetes by ^{13}C nuclear magnetic resonance spectroscopy.* New England Journal of Medicine, 1990. **322**: p. 223-228.

66. Rothman, D.L., Shulman, R. G., Shulman, G. I., *31P nuclear magnetic resonance measurements of muscle glucose-6-phosphate. Evidence for reduced insulin-dependent muscle glucose transport or phosphorylation activity in non-insulin-dependent diabetes mellitus.* J Clin Inv, 1992. **89**(4): p. 1069-1075.

67. Cline, G.W., et al., *Impaired Glucose Transport as a Cause of Decreased Insulin-Stimulated Muscle Glycogen Synthesis in Type 2 Diabetes.* N Engl J Med, 1999. **341**(4): p. 240-246.

68. Shepherd, P.R. and B.B. Kahn, *Glucose Transporters and Insulin Action -- Implications for Insulin Resistance and Diabetes Mellitus.* N Engl J Med, 1999. **341**(4): p. 248-257.

69. Eckel, R.H., Grundy, S.M., Zimmet, P.Z., *The metabolic syndrome.* The Lancet, 2005. **365**: p. 1415-28.

70. Randle, P.J., et al., *Glucose Fatty-Acid Cycle - Its Role in Insulin Sensitivity and Metabolic Disturbances of Diabetes Mellitus.* Lancet, 1963. **1**(728): p. 785-&.

71. Groop, L., Bonadonna, R.C., DelPrato, S., Ratheiser, K., Zyck, K., Ferrannini, E., DeFronzo, R.A., *Glucose and Free Fatty Acid Metabolism in Non-insulin-dependent Diabetes Mellitus.* Journal of Clinical Investigation, 1989. **84**: p. 205-213.

72. Savage, D.B., K.F. Petersen, and G.I. Shulman, *Disordered Lipid Metabolism and the Pathogenesis of Insulin Resistance.* Physiol. Rev., 2007. **87**(2): p. 507-520.

73. Perseghin, G., et al., *Metabolic defects in lean nondiabetic offspring of NIDDM parents: a cross-sectional study. (non-insulin-dependent diabetes mellitus).* Diabetes, 1997. **46**: p. 1001-9.

74. Roden, M., Price, T.B., Perseghin, G., Petersen, K.F., Rothman, D.L., Cline, G.W., Shulman, G.I., *Mechanism of free fatty acid-induced insulin resistance in humans.* Journal of Clinical Investigation, 1996. **97**(12): p. 2859-2865.

75. Dresner, A., Laurent, D., Marcucci, M., Griffin, M.E., Dufour, S., Cline, G.W., Slezak, L.A., Andersen, D.K., Hundal, R.S., Rothman, D.L. Petersen, K.F., Shulman, G.I., *Effects of free fatty acids on glucose transport and IRS-1-associated phosphatidylinositol 3-kinase activity.* Journal of Clinical Investigation, 1999. **103**(2): p. 253-259.

76. Saltiel, A.R., Kahn, C.R., *Insulin signalling and the regulation of glucose and lipid metabolism.* Nature, 2001. **414**: p. 799-806.

77. Frojdo, S., H. Vidal, and L. Pirola, *Alterations of insulin signaling in type 2 diabetes: A review of the current evidence from humans.* Biochimica Et Biophysica Acta-Molecular Basis of Disease, 2009. **1792**(2): p. 83-92.

78. Withers, D.J., et al., *Disruption of IRS-2 causes type 2 diabetes in mice.* Nature, 1998. **391**(6670): p. 900-904.

79. Storlein, L.H., Jenkins, A.B., Chisholm, D. J., Pascoe, W.S., Khouri,S., Kraegen, E.W., *Influence of Dietary Fat Composition on Development of Insulin Resistance in Rats: Relationship to Muscle Triglyceride and ω-3 Fatty Acids in Muscle Phospholipid.* Diabetes, 1991. **40**: p. 280-289.

80. Borkman, M., Chisholm, D., Storlein, L., Kraegen, F., Simons, L., *Effects of fish oil supplementation on glucose and lipid metabolism in NIDDM.* Diabetes, 1989. **38**: p. 1314-19.

81. Griffin, M., et al., *Free fatty acid-induced insulin resistance is associated with activation of protein kinase C theta and alterations in the insulin signaling cascade.* Diabetes, 1999. **48**(6): p. 1270-1274.

82. Mellor, H. and P.J. Parker, *The extended protein kinase C superfamily.* Biochem. J., 1998. **332**(2): p. 281-292.

83. Chalkley, S.M., Hettiarachchi, M., Chisholm, D.J., Kraegen, E.W., *Five-Hour Fatty Acid Elevation Increases Muscle Lipids and Impairs Glycogen Synthesis in the Rat.* Metabolism, 1998. **47**(9): p. 1121-1126.

84. Yu, C., et al., *Mechanism by Which Fatty Acids Inhibit Insulin Activation of Insulin Receptor Substrate-1 (IRS-1)-associated Phosphatidylinositol 3-Kinase Activity in Muscle.* J. Biol. Chem., 2002. **277**(52): p. 50230-50236.

85. Kim, J.K., et al., *PKC-θ knockout mice are protected from fat-induced insulin resistance.* Journal of Clinical Investigation, 2004. **114**(6): p. 823-827.

86. Gavrilova, O., Marcus-Samuels, B., Graham, D., Kim, J.K., Shulman, G.I., Castle,A.L., Vinson, C., Eckhaus, M., Reitman, M.L., *Surgical implantation of adipose tissue reverses diabetes in lipoatrophic mice.* Journal of Clinical Investigation, 2000. **105**: p. 271-278.

87. Shimomura, I., et al., *Leptin reverses insulin resistance and diabetes mellitus in mice with congenital lipodystrophy.* Nature, 1999. **401**(6748): p. 73-76.

88. Silveira, L.R., et al., *Updating the effects of fatty acids on skeletal muscle.* Journal of Cellular Physiology, 2008. **217**(1): p. 1-12.

89. Kim, J.K., et al., *Inactivation of fatty acid transport protein 1 prevents fat-induced insulin resistance in skeletal muscle.* Journal of Clinical Investigation, 2004. **113**(5): p. 756-763.

90. Choi, C.S., et al., *Continuous fat oxidation in acetyl-CoA carboxylase 2 knockout mice increases total energy expenditure, reduces fat mass, and improves insulin sensitivity.* Proceedings of the National Academy of Sciences of the United States of America, 2007. **104**(42): p. 16480-16485.

91. Consitt, L.A., J.A. Bell, and J.A. Houmard, *Intramuscular lipid metabolism, insulin action, and obesity.* IUBMB Life, 2009. **61**(1): p. 47-55.

92. Petersen, K.F., et al., *Impaired Mitochondrial Activity in the Insulin-Resistant Offspring of Patients with Type 2 Diabetes.* N Engl J Med, 2004. **350**(7): p. 664-671.

93. Hotamisligil, G.S., Shargill, N.S., Spiegelman, B.M., *Adipose Expression of Tumor Necrosis Factor-α: Direct Role in Obesity-Linked Insulin Resistance.* Science, 1993. **259**: p. 87-91.

94. Kern, P.A., et al., *Adipose tissue tumor necrosis factor and interleukin-6 expression in human obesity and insulin resistance.* Am J Physiol Endocrinol Metab, 2001. **280**(5): p. E745-751.

95. Tsao, T.-S., H.F. Lodish, and J. Fruebis, *ACRP30, a new hormone controlling fat and glucose metabolism.* European Journal of Pharmacology, 2002. **440**(2-3): p. 213-221.

96. Steppan, C.M. and M.A. Lazar, *Resistin and obesity-associated insulin resistance.* Trends in Endocrinology and Metabolism, 2002. **13**(1): p. 18-23.

97. Qi, Y., et al., *Adiponectin acts in the brain to decrease body weight.* Nature Medicine, 2004. **10**(5): p. 524-529.

98. Morino, K., et al., *Reduced mitochondrial density and increased IRS-1 serine phosphorylation in muscle of insulin-resistant offspring of type 2 diabetic parents.* Journal of Clinical Investigation, 2005. **115**(12): p. 3587.

99. Lowell, B.B. and G.I. Shulman, *Mitochondrial dysfunction and type 2 diabetes.* Science, 2005. **307**(5708): p. 384-387.

100. Samuel, V.T., K.F. Petersen, and G.I. Shulman, *Lipid-induced insulin resistance: unravelling the mechanism.* Lancet. **375**(9733): p. 2267-2277.

101. Defronzo, R.A., *The Triumvirate: B-Cell, Muscle, Liver A Collusion Responsible for NIDDM.* Diabetes, 1988. **37**: p. 667-693.

102. Consoli, A., Nurjhan, N., Capani, F., Gerich, J., *Predominant Role of Gluconeogenesis in Increased Hapatic Glucose Production in NIDDM.* Diabetes, 1989. **38**: p. 550-557.

103. Magnusson, I., Rothman, D.L., Katz, L.D., Shulman, R.G., Shulman, G.I., *Increased Rate of Gluconeogenesis in Type II Diabetes Mellitus.* Jounal of Clinical Investigation, 1992. **90**: p. 1323-1327.

104. Ferrannini, E., et al., *The disposal of an oral glucose load in patients with non-insulin-dependent diabetes.* Metabolism, 1988. **37**(1): p. 79-85.

105. Considine, R.V., Nyce, M.R., Allen, L.E., Morales, L.M., Triester, S., Serrano, J., Colberg, J., Lanza-Jacoby, S., Caro, J.F., *Protein Kinase C is Increased in the Liver of Humans and Rats with Non-insulin Dependent Diabetes Mellitus: an*

Alteration not due to Hyperglycemia. Journal of Clinical Investigation, 1995. **95**: p. 2938-2944.

106. Samuel, V.T., Liu, Z.X., Qu, X., Elder, B.D., Bilz, S., Befroy, D., Romanelli, A.J., Shulman, G.I., *Mechanism of Hepatic Insulin Resistance in Non-alcoholic Fatty Liver Disease.* The Journal Of Biological Chemistry, 2004. **279**(July 30): p. 32345-32353.

107. Zimmet, P., Alberti, K.G., Shaw, J., *Global and societal implications of the diabetes epidemic.* Nature, 2001. **414**: p. 782-787.

108. Moller, D.E. and J.S. Flier, *Insulin Resistance - Reply.* New England Journal of Medicine, 1992. **326**(9): p. 647-647.

109. Hotamisligil, G.S., Peraldi, P., Budavari, A., Ellis, R., White, M. F., Speigelman, B. M., *IRS-1 Mediated Inhibition of Insulin Receptor Tyrosine Kinase Activity in TNF-α-and Obesity-Induced Insulin Resistance.* Science, 1996. **271**: p. 665-668.

110. Kopelman, P.G., *Obesity as a medical problem.* Nature, 2000. **404**: p. 635-643.

111. Knowler, W.C., et al., *Reduction in the incidence of type 2 diabetes with lifestyle intervention or metformin.* New England Journal of Medicine, 2002. **346**(6): p. 393-403.

112. Willett, W.C., W.H. Dietz, and G.A. Colditz, *Guidelines for Healthy Weight.* N Engl J Med, 1999. **341**(6): p. 427-434.

113. Reaven, G.M., *Role of Insulin Resistance in Human-Disease.* Diabetes, 1988. **37**(12): p. 1595-1607.

114. Haiyan Xu, G.T., et al., *Chronic inflammation in fat plays a crucial role in the development of obesity-related insulin resistance.* Journal of Clinical Investigation, 2003. **112**(12): p. 1821-1830.

115. Reaven, G.M., *Insulin resistance, the insulin resistance syndrome.* Panminerva Medica, 2005. **47**(4): p. 201-10.

116. *http://www.nhlbi.nih.gov/health/dci/Diseases/ms/ms_whatis.html.*

117. Hotamisligil, G.S., *Inflammation and Metabolic Disorders.* Nature, 2006. **444**: p. 860-867.

118. Uhlar, C.M. and A.S. Whitehead, *Serum amyloid A, the major vertebrate acute-phase reactant.* European Journal of Biochemistry, 1999. **265**(2): p. 501.

119. Pickup, J.C., et al., *NIDDM as a disease of the innate immune system: association of acute-phase reactants and interleukin-6 with metabolic syndrome X.* Diabetologia, 1997. **40**(11): p. 1286-1292.

120. Pickup, J.C. and M.A. Crook, *Is Type II diabetes mellitus a disease of the innate immune system?* Diabetologia, 1998. **41**(10): p. 1241-1248.

121. Pittas, A.G., N.A. Joseph, and A.S. Greenberg, *Adipocytokines and Insulin Resistance.* J Clin Endocrinol Metab, 2004. **89**(2): p. 447-452.

122. Rajala, M.W. and P.E. Scherer, *Minireview: The adipocyte - At the crossroads of energy homeostasis, inflammation, and atherosclerosis.* Endocrinology, 2003. **144**(9): p. 3765-3773.

123. Old, L.J., *Tumor Necrosis Factor.* Science, 1985. **230**(4726): p. 630-632.

124. Weisberg, S.P., McCann, D., Desai, M., Rosenbaum, M., Leibel, R.L., Ferrante, A.W., *Obesity is associated with macrophage accumulation in adipose tissue.* Journal of Clinical Investigation, 2003. **112**: p. 1796-1808.

125. Xu, H., Barnes, G.T., Yang, Q., Tan, G., Yang, D., Chou, C., Sole, J., Nichols, A., Ross, J.S., Tartaglia, L.A., Chen, H., *Chronic inflammation in fat plays a crucial role in the development of obesity-related insulin resistance.* Journal of Clinical Investigation, 2003. **112**: p. 1821-1830.

126. Greene, M.W., et al., *TNF[alpha] activation of PKC[delta], mediated by NF[kappa]B and ER stress, cross-talks with the insulin signaling cascade.* Cellular Signalling, 2010. **22**(2): p. 274-284.

127. Wellen, K.E. and G.S. Hotamisligil, *Inflammation, stress, and diabetes.* Journal of Clinical Investigation, 2005. **115**(5): p. 1111-1119.

128. Shoelson, S.E., J. Lee, and A.B. Goldfine, *Inflammation and insulin resistance.* Journal of Clinical Investigation, 2006. **116**(7): p. 1793-1801.

129. Dominguez, H., et al., *Metabolic and vascular effects of tumor necrosis factor-alpha blockade with etanercept in obese patients with type 2 diabetes.* Journal of Vascular Research, 2005. **42**(6): p. 517-525.

130. Chawla, A., et al., *Nuclear receptors and lipid physiology: Opening the X-files.* Science, 2001. **294**(5548): p. 1866-1870.

131. Dubois, M., et al., *Expression of peroxisome proliferator-activated receptor gamma (PPAR gamma) in normal human pancreatic islet cells.* Diabetologia, 2000. **43**(9): p. 1165-1169.

132. Yki-Jarvinen, H., *Thiazolidinediones.* N Engl J Med, 2004. **351**(11): p. 1106-1118.

133. Mogi, M., M. Iwai, and M. Horiuchi, *Emerging Concept of Adipogenesis Regulation by the Renin-Angiotensin System.* Hypertension, 2006. **48**(6): p. 1020-1022.

134. Miyazaki, Y., et al., *Effect of rosiglitazone on glucose and non-esterified fatty acid metabolism in Type II diabetic patients.* Diabetologia, 2001. **44**(12): p. 2210-2219.

135. Burant, C.F., ed. *MEDICAL MANAGEMENT OF TYPE 2 DIABETES*. SIXTH ed. 2008, AMERICAN DIABETES ASSOCIATION.

136. Saito, K., N. Yaginuma, and T. Takahashi, *Differential Volumetry of a-Cells, B-Cells and D-Cells in the Pancreatic-Islets of Diabetic and Non-Diabetic Subjects.* Tohoku Journal of Experimental Medicine, 1979. **129**(3): p. 273-283.

137. Ward, W.K., et al., *Diminished B cell secretory capacity in patients with noninsulin-dependent diabetes mellitus.* The Journal of Clinical Investigation, 1984. **74**(4): p. 1318-1328.

138. Gepts, W. and P.M. Lecompte, *The Pancreatic-Islets in Diabetes.* American Journal of Medicine, 1981. **70**(1): p. 105-115.

139. Bagdade, J.D., E.L. Bierman, and D. Porte, *Significance of Basal Insulin Levels in Evaluation of Insulin Response to Glucose in Diabetic and Nondiabetic Subjects.* Journal of Clinical Investigation, 1967. **46**(10): p. 1549-&.

140. Polonsky, K.S., et al., *Abnormal Patterns of Insulin-Secretion in Non-Insulin-Dependent Diabetes-Mellitus.* New England Journal of Medicine, 1988. **318**(19): p. 1231-1239.

141. Orahilly, S., R.C. Turner, and D.R. Matthews, *Impaired Pulsatile Secretion of Insulin in Relatives of Patients with Non-Insulin-Dependent Diabetes.* New England Journal of Medicine, 1988. **318**(19): p. 1225-1230.

142. Matthews, D.R., et al., *Pulsatile Insulin Has Greater Hypoglycemic Effect Than Continuous Delivery.* Diabetes, 1983. **32**(7): p. 617-621.

143. Kahn, S.E. and P.A. Halban, *Release of incompletely processed proinsulin is the cause of the disproportionate proinsulinemia of NIDDM.* Diabetes, 1997. **46**(11): p. 1725-1732.

144. Rossetti, L., A. Giaccari, and R.A. Defronzo, *Glucose Toxicity.* Diabetes Care, 1990. **13**(6): p. 610-630.

145. Donath, M.Y., et al., *Mechanisms of beta-cell death in type 2 diabetes.* Diabetes, 2005. **54**: p. S108-S113.

146. Klein, R., et al., *Glycosylated Hemoglobin Predicts the Incidence and Progression of Diabetic Retinopathy.* JAMA, 1988. **260**(19): p. 2864-2871.

147. The Diabetes Control and Complications Trial Research Group, *The Effect of Intensive Treatment of Diabetes on the Development and Progression of Long-Term Complications in Insulin-Dependent Diabetes Mellitus.* N Engl J Med, 1993. **329**(14): p. 977-986.

148. *The UK Prospective Diabetes Study Group: Intensive blood-glucose control with sulphonylureas or insulin compared with conventional treatment and risk of complications in patients with type 2 diabetes (UKPDS 33).* Lancet, 1998. **352**(9131): p. 837-853.

149. Makita, Z., et al., *Hemoglobin-AGE: A Circulating Marker of Advanced Glycosylation.* Science, 1992. **258**(5082): p. 651-653.

150. Stratton, I.M., et al., *Association Of Glycaemia With Macrovascular And Microvascular Complications Of Type 2 Diabetes (UKPDS 35): Prospective Observational Study.* BMJ: British Medical Journal, 2000. **321**(7258): p. 405-412.

151. Brownlee, M., *The pathobiology of diabetic complications - A unifying mechanism.* Diabetes, 2005. **54**(6): p. 1615-1625.

152. Brownlee, M., *Biochemistry and molecular cell biology of diabetic complications.* Nature, 2001. **414**(6865): p. 813-820.

153. Carr, M.E., *Diabetes mellitus: A hypercoagulable state.* Journal of Diabetes and its Complications, 2001. **15**(1): p. 44-54.

154. Lee, A.Y.W. and S.S.M. Chung, *Contributions of polyol pathway to oxidative stress in diabetic cataract.* FASEB J., 1999. **13**(1): p. 23-30.

155. Ramirez, M.A. and N.L. Borja, *Epalrestat: An aldose reductase inhibitor for the treatment of diabetic neuropathy.* Pharmacotherapy, 2008. **28**(5): p. 646-655.

156. Hotta, N., et al., *Clinical Efficacy of Fidarestat, a Novel Aldose Reductase Inhibitor, for Diabetic Peripheral Neuropathy.* Diabetes Care, 2001. **24**(10): p. 1776-1782.

157. Furth, A.J., *Glycated proteins in diabetes.* British Journal of Biomedical Science, 1997. **54**(3): p. 192-200.

158. Bunn, H.F., K.H. Gabbay, and P.M. Gallop, *The Glycosylation of Hemoglobin: Relevance to Diabetes Mellitus.* Science, 1978. **200**(4337): p. 21-27.

159. Iberg, N. and R. Fluckiger, *Nonenzymatic glycosylation of albumin in vivo. Identification of multiple glycosylated sites.* J. Biol. Chem., 1986. **261**(29): p. 13542-13545.

160. Cohen, M.P., E. Hud, and V.Y. Wu, *Amelioration of Diabetic Nephropathy by Treatment with Monoclonal-Antibodies against Glycated Albumin.* Kidney International, 1994. **45**(6): p. 1673-1679.

161. Cohen, M.P., et al., *Prevention of Diabetic Nephropathy in Db/Db Mice with Glycated Albumin Antagonists - a Novel Treatment Strategy.* Journal of Clinical Investigation, 1995. **95**(5): p. 2338-2345.

162. Kisugi, R., et al., *Structural and glycation site changes of albumin in diabetic patient with very high glycated albumin.* Clinica Chimica Acta, 2007. **382**(1-2): p. 59-64.

163. Hammes, H.-P., et al., *Aminoguanidine Treatment Inhibits the Development of Experimental Diabetic Retinopathy.* Proceedings of the National Academy of Sciences of the United States of America, 1991. **88**(24): p. 11555-11558.

164. Bolton, W.K., et al., *Randomized trial of an inhibitor of formation of advanced glycation end products in diabetic nephropathy.* American Journal of Nephrology, 2004. **24**(1): p. 32-40.

165. Ishii, H., et al., *Amelioration of vascular dysfunctions in diabetic rats by an oral PKC beta inhibitor.* Science, 1996. **272**(5262): p. 728-731.

166. Du, X.-L., et al., *Hyperglycemia-Induced Mitochondrial Superoxide Overproduction Activates the Hexosamine Pathway and Induces Plasminogen Activator Inhibitor-1 Expression by Increasing Sp1 Glycosylation.* Proceedings of the National Academy of Sciences of the United States of America, 2000. **97**(22): p. 12222-12226.

167. Nishikawa, T., et al., *Normalizing mitochondrial superoxide production blocks three pathways of hyperglycaemic damage.* Nature, 2000. **404**(6779): p. 787-790.

168. Nugent, D.A., D.M. Smith, and H.B. Jones, *A Review of Islet of Langerhans Degeneration in Rodent Models of Type 2 Diabetes.* Toxicologic Pathology, 2008. **36**(4): p. 529-551.

169. Allgot, B., Gan, D., King, H., Lefebvre, P., Mbanya, J., Silink, M., Siminerio, L., Williams, R., Zimmet, P., *Diabetes Atlas, 2nd Edition*, D. Gan, Editor. 2003, International Diabetes Federation. p. 1-58.

170. Stumvoll, M., Goldstein, B.J., van Haeften, T.W., *Type 2 diabetes: principles of pathogenesis and therapy.* Lancet, 2005. **365**: p. 1333-46.

171. Elliott, S.S., et al., *Fructose, weight gain, and the insulin resistance syndrome.* Am J Clin Nutr, 2002. **76**(5): p. 911-922.

172. Issaq, H.J., Z. Xiao, and T.D. Veenstra, *Serum and plasma proteomics.* Chemical Reviews, 2007. **107**(8): p. 3601-3620.

173. Rai, A.J., Gelfand, C.A., Haywood, B.C., Warunek, D.J., Yi, J., Schuchard, M.D., Mehigh, R.J., Cockrill,S.L., Scott, G.B.I., Tammen, H., Schulz-Knappe, P., Speicher, D.W., Vitzthum, F., Haab, B.B., Siest, G., Chan, D.W., *HUPO Plasma Proteome Project specimen collection and handling: Towards the standardization of parameters for plasma proteome samples.* Proteomics, 2005. **5**: p. 3262-3277.

174. Di Nisio, M., S. Middeldorp, and H.R. Buller, *Drug therapy - Direct thrombin inhibitors.* New England Journal of Medicine, 2005. **353**(10): p. 1028-1040.

175. Kim, M.R., Kim, C.W., *Human blood plasma preparation for two-dimensional gel electrophoresis.* Journal of Chromatography B-Analytical Technologies in the Biomedical and Life Sciences, 2007. **849**(1-2): p. 203-210.

176. Anderson, N.L., Anderson, N.G., *The Human Plasma Proteome: History, Character, and Diagnostic Prospects.* Molecular and Cellular Proteomics, 2002. **1**(11): p. 845-867.

177. Good, D.M., et al., *Body Fluid Proteomics for Biomarker Discovery: Lessons from the Past Hold the Key to Success in the Future.* Journal of Proteome Research, 2007. **6**(12): p. 4549-4555.

178. Yocum, A.K., et al., *Effect of Immunoaffinity Depletion of Human Serum during Proteomic Investigations.* Journal of Proteome Research, 2005. **4**(5): p. 1722-1731.

179. Pieper, R., Gatlin, C.L., Makusky, A.J., Russo, P.S., Schatz, C.R., Miller, S.S., Su, Q., McGrath, A.M., Estock, M.A., Parmar, P.P., Zhao, M., Huang, S., Zhou, J., Wang, F., Esquer-Blasco, R., Anderson N.L., Taylor, J., Steiner, S., *The Human Serum Proteome: Display of nearly 3700 chromatographically separated protein spots on two-dimensional elecrophoresis gels and identification of 325 distinct proteins.* Proteomics, 2003. **3**: p. 1345-1364.

180. Zhou, M., et al., *An investigation into the human serum interactome.* ELECTROPHORESIS, 2004. **25**(9): p. 1289-1298.

181. Anderson, N.L., Polanski, M., Pieper, R., Gatlin, T., Tirumalai, R.S., Conrads, T.P., Veenstra, T.D., Adkins, J.N., Pounds, J.G. Fagan, R., Lobley, A., *The*

Human Plasma Proteome: A Nonredundant List Developed by Combination of Four Separate Sources. Molecular and Cellular Proteomics, 2004. **3**(4): p. 311-326.

182. Patton, W.F., *A thousand points of light: The application of fluorescence detection technologies to two-dimensional gel electrophoresis and proteomics.* Electrophoresis, 2000. **21**(6): p. 1123-1144.

183. Rai, A.J., Vitzthum, F., *Effects of preanalytical variables on peptide and protein measurements in human serum and plasma: implications for clinical proteomics.* Expert Review of Proteomics, 2006. **3**(4): p. 409-426.

184. Adkins, J.N., Varnum, S.M., Auberry, K.J., Moore, R.J., Angell, N.H., Smith, R.D., Springer, D.L., Pounds. J.G., *Toward a Human Blood Serum Proteome: Analysis by Multidimensional Separation Coupled with Mass Spectrometry.* Molecular and Cellular Proteomics, 2002. **1**(12): p. 947-955.

185. Musselman, I., Speicher, D.W., *Human Serum and Plasma Proteomics.* Current Protocols in Protein Science, 2005. **24.1**(Supplement 42): p. 1-17.

186. Rabilloud, T., *Solubilization of proteins for electrophoretic analyses.* Electrophoresis, 1996. **17**(5): p. 813-829.

187. Means, G.E., Feeney, R. E., *Chemical Modification of Proteins*. 1971: Holden-Day, Inc.

188. Granger, J., et al., *Albumin depletion of human plasma also removes low abundance proteins including the cytokines.* PROTEOMICS, 2005. **5**(18): p. 4713-4718.

189. Mrozinski, P., Zolotarjova, N., Chen, H., *Human Serum and Plasma Protein Depletion - Novel High-Capacity Affinity Column for the Removal of the "Top 14" Abundant Proteins.* Application Note, 2008: p. 1-6.

190. Zolotarjova, N., et al., *Combination of affinity depletion of abundant proteins and reversed-phase fractionation in proteomic analysis of human plasma/serum.* Journal of Chromatography A, 2008. **1189**(1-2): p. 332-338.

191. Sahab, Z., Semaan, S., Sang, Q.X., *Methodology and Applications of Disease Biomarker Identification in Human Serum.* Biomarker Insights, 2007. **2**: p. 21-43.

192. Issaq, H.J., Xiao, Z., Veenstra, T.D., *Serum and Plasma Proteomics.* Chemical Reviews, 2007. **107**(8): p. 3601-3620.

193. Tirumalai, R.S., et al., *Characterization of the Low Molecular Weight Human Serum Proteome.* Molecular and Cellular Proteomics, 2003. **2**(10): p. 1096-1103.

194. Liu, T., et al., *High dynamic range characterization of the trauma patient plasma proteome.* Molecular & Cellular Proteomics, 2006. **5**(10): p. 1899-1913.

195. Pieper, R., et al., *Multi-component immunoaffinity subtraction chromatography: An innovative step towards a comprehensive survey of the human plasma proteome.* Proteomics, 2003. **3**(4): p. 422-432.

196. Chromy, B.A., et al., *Proteomic Analysis of Human Serum by Two-Dimensional Differential Gel Electrophoresis after Depletion of High-Abundant Proteins.* Journal of Proteome Research, 2004. **3**(6): p. 1120-1127.

197. Gundry, R.L., Fu, Q., Jelinek, C.A., Van Eyk, J.E. Cotter, R.J., *Investigation of an Albumin-Enriched Fraction of Human Serum and its Albuminome.* Proteomics. Clinical Applications, 2007. **1**: p. 73-88.

198. Echan, L.A., et al., *Depletion of multiple high-abundance proteins improves protein profiling capacities of human serum and plasma.* PROTEOMICS, 2005. **5**(13): p. 3292-3303.

199. Whiteaker, J.R., et al., *Head-to-head comparison of serum fractionation techniques.* Journal of Proteome Research, 2007. **6**(2): p. 828-836.

200. Barrett, W., Martosella, J., Boyes, B., Szafranski, C., Nicol, *A Rapid Method to Desalt and Concentrat Proteomic Samples Using the Agilent mRP-C18 Column: Application Sheet*. 2005.

201. Martosella, J., et al., *Reversed-Phase High-Performance Liquid Chromatographic Prefractionation of Immunodepleted Human Serum Proteins to Enhance Mass Spectrometry Identification of Lower-Abundant Proteins.* Journal of Proteome Research, 2005. **4**(5): p. 1522-1537.

202. Görg, A., W. Weiss, and M.J. Dunn, *Current two-dimensional electrophoresis technology for proteomics.* PROTEOMICS, 2004. **4**(12): p. 3665-3685.

203. Santoni, V., M. Molloy, and T. Rabilloud, *Membrane proteins and proteomics: Un amour impossible?* Electrophoresis, 2000. **21**(6): p. 1054-1070.

204. Herbert, B., *Advances in protein solubilisation for two-dimensional electrophoresis.* Electrophoresis, 1999. **20**(4-5): p. 660-663.

205. O'Farrell, P.H., *High Resolution Two-Dimensional Electrophoresis of Proteins.* Jounal of Biological Chemistry, 1975. **250**(10): p. 4007-4021.

206. Bjellqvist, B., et al., *Isoelectric-Focusing in Immobilized Ph Gradients - Principle, Methodology and Some Applications.* Journal of Biochemical and Biophysical Methods, 1982. **6**(4): p. 317-339.

207. Gorg, A., W. Postel, and S. Gunther, *The Current State of Two-Dimensional Electrophoresis with Immobilized Ph Gradients.* Electrophoresis, 1988. **9**(9): p. 531-546.

208. Sarioglu, H., Lottspeich, F., Walk, T., Jung, G., Eckerskorn, C., *Deamidation as a Widespread Phenomenon in Two-dimensional Polyacrylamide Gel Electrophoresis of Human Blood Plasma Proteins.* Electrophoresis, 2000. **21**: p. 2209-2218.

209. Halligan, B.D., et al., *ProMoST (Protein Modification Screening Tool): a web-based tool for mapping protein modifications on two-dimensional gels.* Nucleic Acids Research, 2004. **32**: p. W638-W644.

210. Righetti, P.G., Castagna, A. Antonioli, P., Boschetti, E., *Prefractionatation techniques in proteome analysis: The mining tools of the third millennium.* Electrophoresis, 2005. **26**: p. 297-319.

211. Görg, A., et al., *The current state of two-dimensional electrophoresis with immobilized pH gradients.* Electrophoresis, 2000. **21**(6): p. 1037-1053.

212. Galvani, M., et al., *Protein alkylation in the presence/absence of thiourea in proteome analysis: A matrix assisted laser desorption/ionization-time of flight-mass spectrometry investigation.* ELECTROPHORESIS, 2001. **22**(10): p. 2066-2074.

213. Rabilloud, T., et al., *Improvement of the solubilization of proteins in two-dimensional electrophoresis with immobilized pH gradients.* Electrophoresis, 1997. **18**(3-4): p. 307-316.

214. Herbert, B., et al., *Reduction and alkylation of proteins in preparation of two-dimensional map analysis: Why, when, and how?* Electrophoresis, 2001. **22**(10): p. 2046-2057.

215. Olsson, I., et al., *Organic disulfides as a means to generate streak-free two-dimensional maps with narrow range basic immobilized pH gradient strips as first Product dimension.* Proteomics, 2002. **2**(11): p. 1630-1632.

216. Gorg, A., et al., *The current state of two-dimensional electrophoresis with immobilized pH gradients.* Electrophoresis, 2000. **21**(6): p. 1037-1053.

217. Pan, C.S., et al., *Recent developments in methods and technology for analysis of biological samples by MALDI-TOF-MS.* Analytical and Bioanalytical Chemistry, 2007. **387**(1): p. 193-204.

218. De Hoffman, E., Stroobant, V., *Mass Spectrometry: Principles and Applications*. 3rd ed. 2007: John Wiley and Sons.

219. Knochenmuss, R. and R. Zenobi, *MALDI ionization: The role of in-plume processes.* Chemical Reviews, 2003. **103**(2): p. 441-452.

220. Gross, J., *Mass Spectrometry : A Textbook*. 2004, Berlin Heidelberg: Springer-Verlag.

221. Harris, W.A., D.J. Janecki, and J.P. Reilly, *Use of matrix clusters and trypsin autolysis fragments as mass calibrants in matrix-assisted laser desorption/ionization time-of-flight mass spectrometry.* Rapid Communications in Mass Spectrometry, 2002. **16**(18): p. 1714-1722.

222. Agilent, *Agilent Nanospray and HPLC-Chip/MS Protein Identification Solutions:LC/MS Application Guide* *http://www.chem.agilent.com/Library/usermanuals/Public/G2458-90002_LC-MSAppGuide_online.pdf*. 2005.

223. Poon, F., Mathura, V., *Bioinformatics: A Concept-Based Introduction*, ed. V. Mathura, Kangueane, P. 2009: Springer US.

224. Agilent, *Electron Transfer Dissociation (ETD) User Guide.* *http://www.chem.agilent.com/Library/usermanuals/Public/G2474-90003_ETD_v.2.pdf*. 2007.

225. Unlu, M., M.E. Morgan, and J.S. Minden, *Difference gel electrophoresis: A single gel method for detecting changes in protein extracts.* Electrophoresis, 1997. **18**(11): p. 2071-2077.

226. Alban, A., et al., *A novel experimental design for comparative two-dimensional gel analysis: Two-dimensional difference gel electrophoresis incorporating a pooled internal standard.* Proteomics, 2003. **3**(1): p. 36-44.

227. Quero, C., et al., *Determination of protein markers in human serum: Analysis of protein expression in toxic oil syndrome studies.* Proteomics, 2004. **4**(2): p. 303-315.

228. Brand, J., et al., *Depletion efficiency and recovery of trace markers from a multiparameter immunodepletion column.* Proteomics, 2006. **6**(11): p. 3236-3242.

229. *Typhoon User's Guide*. 2002, Amersham Biosciences. p. 9-11.

230. . This staining protocol was acquired on-line from the European molecular biology laboratory (EMBL) proteomic core facility at http://proteomics.embl.de/colloidal_coomassie.html. It is a modification of the protocol given in Neuhoff et al., Electrophoresis 6, 427-448, 1985.

231. . This University of California at San Francisco in-gel digestion protocol was acquired on-line at http://donatello.ucsf.edu/ingel.html.

232. *Matrix Science Website, http://www.matrixscience.com/help/scoring_help.html.*

233. Agilent, *Agilent G2721AA Spectrum Mill MS Proteomics Workbench: Application Guide, 3rd Edition*. 2004.

234. Klarskov, K., et al., *Analysis of Recombinant Schistosoma-Mansoni Antigen Rsmp28 by Online Liquid-Chromatography Mass-Spectrometry Combined with Sodium Dodecyl-Sulfate Polyacrylamide-Gel Electrophoresis.* Analytical Biochemistry, 1994. **216**(1): p. 127-134.

235. Sun, G. and V.E. Anderson, *Prevention of artifactual protein oxidation generated during sodium dodecyl sulfate-gel electrophoresis.* ELECTROPHORESIS, 2004. **25**(7-8): p. 959-965.

236. *Agilent G2721AA Spectrum Mill MS Proteomics Workbench: Application Guide 3rd Edition*. 2004. p. 19.

237. Flik, G., *ZigZAGging through Fat Stores.* Journal of Clinical Endocrinology & Metabolism, 2009. **94**(12): p. 4668-4670.

238. Yeung, D.C.Y., et al., *Serum Zinc-{alpha}2-Glycoprotein Correlates with Adiposity, Triglycerides, and the Key Components of the Metabolic Syndrome in Chinese Subjects.* J Clin Endocrinol Metab, 2009. **94**(7): p. 2531-2536.

239. Selva, D.M., et al., *Lower Zinc-{alpha}2-Glycoprotein Production by Adipose Tissue and Liver in Obese Patients Unrelated to Insulin Resistance.* J Clin Endocrinol Metab, 2009. **94**(11): p. 4499-4507.

240. Hassan, M., Waheed, A., Yadav, S., Singh, T., Ahmad, F., *Zinc α2-Glycoprotein: A Multidisciplinary Protein.* Molecular Cancer Research, 2008. **6**(6): p. 892-906.

241. Buergi, W. and K. Schmid, *Preparation and Properties of Zn-Alpha2-Glycoprotein of Normal Human Plasma.* Journal of Biological Chemistry, 1961. **236**(4): p. 1066-&.

242. Rolli, V., et al., *Lipolysis is altered in MHC class I zinc-[alpha]2-glycoprotein deficient mice.* FEBS Letters, 2007. **581**(3): p. 394-400.

243. Sanchez, L.M., C. Lopez-Otin, and P.J. Bjorkman, *Biochemical Characterization and Crystalization of Human Zn-α2-Glycoprotein, a Soluble Class I Major Histocompatibility Complex Homolog.* Proceedings of the National Academy of Sciences of the United States of America, 1997. **94**(9): p. 4626-4630.

244. Sanchez, L.M., A.J. Chirino, and P.J. Bjorkman, *Crystal structure of human ZAG, a fat-depleting factor related to MHC molecules.* Science, 1999. **283**(5409): p. 1914-1919.

245. Delker, S.L., et al., *Crystallographic studies of ligand binding by Zn-[alpha]2-glycoprotein.* Journal of Structural Biology, 2004. **148**(2): p. 205-213.

246. Todorov, P.T., et al., *Purification and Characterization of a Tumor Lipid-mobilizing Factor.* Cancer Res, 1998. **58**(11): p. 2353-2358.

247. Stejskal, D., Karpisek, M., Reutova, H., Stejskal, P., Kotolova, H., Kollar, P., *Determination of Serum Zinc-alpha-2-glycoprotein in patients with metabolic syndrome by new ELISA.* Clinical Biochemistry, 2008. **41**: p. 313-316.

248. Ceperuelo-Mallafre, V., et al., *Circulating and Adipose Tissue Gene Expression of Zinc-{alpha}2-Glycoprotein in Obesity: Its Relationship with Adipokine and Lipolytic Gene Markers in Subcutaneous and Visceral Fat.* J Clin Endocrinol Metab, 2009. **94**(12): p. 5062-5069.

249. Gao, D., P. Trayhurn, and C. Bing, *Macrophage-secreted factors inhibit ZAG expression and secretion by human adipocytes.* Molecular and Cellular Endocrinology, 2010. **325**(1-2): p. 135-142.

250. Metz, T.O., et al., *Application of Proteomics in the Discovery of Candidate Protein Biomarkers in a Diabetes Autoantibody Standardization Program Sample Subset.* Journal of Proteome Research, 2007. **7**(2): p. 698-707.

251. Wijesekara, N., F. Chimienti, and M.B. Wheeler, *Zinc, a regulator of islet function and glucose homeostasis.* Diabetes Obesity & Metabolism, 2009. **11**: p. 202-214.

252. Westermark, G.T. and P. Westermark, *Serum amyloid A and protein AA: Molecular mechanisms of a transmissible amyloidosis.* Febs Letters, 2009. **583**(16): p. 2685-2690.

253. Migita, K., et al., *Serum amyloid A protein induces production of matrix metalloproteinases by human synovial fibroblasts.* Laboratory Investigation, 1998. **78**(5): p. 535-539.

254. Tillett, W.S. and T. Francis, Jr., *SEROLOGICAL REACTIONS IN PNEUMONIA WITH A NON-PROTEIN SOMATIC FRACTION OF PNEUMOCOCCUS.* J. Exp. Med., 1930. **52**(4): p. 561-571.

255. Badolato, R., et al., *Serum Amyloid-a Is a Chemoattractant - Induction of Migration, Adhesion, and Tissue Infiltration of Monocytes and*

Polymorphonuclear Leukocytes. Journal of Experimental Medicine, 1994. **180**(1): p. 203-209.

256. Volanakis, J., *Human C-reactive protein: expression, structure, and function.* Molecular Immunology, 2001. **38**: p. 189-197.

257. Ridker, P.M., et al., *C-Reactive Protein and Other Markers of Inflammation in the Prediction of Cardiovascular Disease in Women.* N Engl J Med, 2000. **342**(12): p. 836-843.

258. Kisilevsky, R., *Serum Amyloid-a (Saa), a Protein without a Function - Some Suggestions with Reference to Cholesterol-Metabolism.* Medical Hypotheses, 1991. **35**(4): p. 337-341.

259. Clark, A., Moffitt, J., *Protein Misfolding, Aggregation, and Conformational Diseases*, in *Protein Reviews*. 2007, Springer US. p. 199-216.

260. Hatanaka, E., et al., *Interaction between serum amyloid A and leukocytes - A possible role in the progression of vascular complications in diabetes.* Immunology Letters, 2007. **108**(2): p. 160-166.

261. Kumon, Y., et al., *Serum Amyloid-a Protein in Patients with Non-Insulin-Dependent Diabetes-Mellitus.* Clinical Biochemistry, 1994. **27**(6): p. 469-473.

262. Boos, C.J. and G.Y.H. Lip, *Is Hypertension an Inflammatory Process?* Current Pharmaceutical Design, 2006. **12**(13): p. 1623-1635.

263. Dinarello, C.A., *The IL-1 family and inflammatory diseases.* Clinical and Experimental Rheumatology, 2002. **20**(5): p. S1-S13.

264. Banka, C., et al., *Serum amyloid A (SAA): influence on HDL-mediated cellular cholesterol efflux.* J. Lipid Res., 1995. **36**(5): p. 1058-1065.

265. VanLenten, B.J., et al., *Anti-inflammatory HDL becomes pro-inflammatory during the acute phase response - Loss of protective effect of HDL against LDL oxidation in aortic wall cell cocultures.* Journal of Clinical Investigation, 1995. **96**(6): p. 2758-2767.

266. Castelli, W.P., et al., *Incidence of Coronary Heart-Disease and Lipoprotein Cholesterol Levels - the Framingham-Study.* Jama-Journal of the American Medical Association, 1986. **256**(20): p. 2835-2838.

267. Buring, J., et al., *Decreased HDL2 and HDL3 cholesterol, Apo A-I and Apo A-II, and increased risk of myocardial infarction.* Circulation, 1992. **85**(1): p. 22-29.

268. Kjeldsen, L., et al., *SGP28, a novel matrix glycoprotein in specific granules of human neutrophils with similarity to a human testis-specific gene product and to a rodent sperm-coating glycoprotein.* Febs Letters, 1996. **380**(3): p. 246-250.

269. Udby, L., et al., *An ELISA for SGP28/CRISP-3, a cysteine-rich secretory protein in human neutrophils, plasma, and exocrine secretions.* Journal of Immunological Methods, 2002. **263**(1-2): p. 43-55.

270. Gibbs, G.M., K. Roelants, and M.K. O'Bryan, *The CAP Superfamily: Cysteine-Rich Secretory Proteins, Antigen 5, and Pathogenesis-Related 1 Proteins--Roles in Reproduction, Cancer, and Immune Defense.* Endocr Rev, 2008. **29**(7): p. 865-897.

271. Kratzschmar, J., et al., *The human cysteine-rich secretory protein (CRISP) family primary structure and tissue distribution of CRISP-1, CRISP-2 and CRISP-3.* European Journal of Biochemistry, 1996. **236**(3): p. 827-836.

272. Fry, B.G., et al., *Evolution of an arsenal.* Molecular & Cellular Proteomics, 2008. **7**(2): p. 215-246.

273. Liao, Q., et al., *Preferential expression of cystein-rich secretory protein-3 (CRISP-3) in chronic pancreatitis.* Histology and Histopathology, 2003. **18**(2): p. 425-433.

274. Udby, L., et al., *Cysteine-rich secretory protein 3 is a ligand of alpha B-1-glycoprotein in human plasmas.* Biochemistry, 2004. **43**(40): p. 12877-12886.

275. Yamazaki, Y. and T. Morita, *Structure and function of snake venom cysteine-rich secretory proteins.* Toxicon, 2004. **44**(3): p. 227-231.

276. Shikamoto, Y., et al., *Crystal structure of a CRISP family Ca2+-channel blocker derived from snake venom.* Journal of Molecular Biology, 2005. **350**(4): p. 735-743.

277. Catterall, W.A., *Structure and regulation of voltage-gated Ca2+ channels.* Annual Review of Cell and Developmental Biology, 2000. **16**: p. 521-555.

278. Ashcroft, F.M., et al., *Stimulus-Secretion Coupling in Pancreatic Beta-Cells.* Journal of Cellular Biochemistry, 1994. **55**: p. 54-65.

279. Trus, M., et al., *The L-type voltage-gated Ca2+ channel is the Ca2+ sensor protein of stimulus-secretion coupling in pancreatic beta cells.* Biochemistry, 2007. **46**(50): p. 14461-14467.

280. Proks, P., et al., *Sulfonylurea stimulation of insulin secretion.* Diabetes, 2002. **51**: p. S368-S376.

281. Torchilin, V.P. and A.N. Lukyanov, *Peptide and protein drug delivery to and into tumors: challenges and solutions.* Drug Discovery Today, 2003. **8**(6): p. 259-266.

282. Rabbani, N., et al., *Increased Glycation and Oxidative Damage to Apolipoprotein B100 of LDL Cholesterol in Patients With Type 2 Diabetes and Effect of Metformin.* Diabetes, 2010. **59**(4): p. 1038-1045.

283. Januszewski, A.S., et al., *Lipid-derived modifications of plasma proteins in experimental and human diabetes. Maillard Reaction: Chemistry at the Interface of Nutrition, Aging, and Disease.* Annals of the New York Academy of Sciences, 2005. **1043**: p. 404-412.

284. Rösen, P., et al., *The role of oxidative stress in the onset and progression of diabetes and its complications: asummary of a Congress Series sponsored byUNESCO-MCBN, the American Diabetes Association and the German Diabetes Society.* Diabetes/Metabolism Research and Reviews, 2001. **17**(3): p. 189-212.

285. Blank, M. and Y. Shoenfeld, *Histidine-rich glycoprotein modulation of immune/autoimmune, vascular, and coagulation systems.* Clinical Reviews in Allergy & Immunology, 2008. **34**(3): p. 307-312.

286. Gorgani, N.N., et al., *Histidine-rich glycoprotein binds to human IgG and C1q and inhibits the formation of insoluble immune complexes.* Biochemistry, 1997. **36**(22): p. 6653-6662.

287. Jones, A.L., M.D. Hulett, and C.R. Parish, *Histidine-rich glycoprotein: A novel adaptor protein in plasma that modulates the immune, vascular and coagulation systems.* Immunology and Cell Biology, 2005. **83**(2): p. 106-118.

288. Stewart, A.J., C.A. Blindauer, and P.J. Sadler, *Plasma fatty acid levels may regulate the Zn2+-dependent activities of histidine-rich glycoprotein.* Biochimie, 2009. **91**(11-12): p. 1518-1522.

289. McRae, J.L., et al., *Human factor H-related protein 5 has cofactor activity, inhibits C3 convertase activity, binds heparin and C-reactive protein, and associates with lipoprotein.* Journal of Immunology, 2005. **174**(10): p. 6250-6256.

290. *ExPASy Proteomics Server pI calculator for NCBI Human CFHR-5 sequence, accession #AAI11774.*

291. Murphy, B., et al., *Factor H-related protein-5: A novel component of human glomerular immune deposits.* American Journal of Kidney Diseases, 2002. **39**(1): p. 24-27.

292. Skerka, C. and P.F. Zipfel, *Complement factor H related proteins in immune diseases.* Vaccine, 2008. **26**: p. I9-I14.

293. Zipfel, P.F., *Complement and immune defense: From innate immunity to human diseases.* Immunology Letters, 2009. **126**(1-2): p. 1-7.

294. Zipfel, P.F. and C. Skerka, *Complement regulators and inhibitory proteins.* Nature Reviews Immunology, 2009. **9**(10): p. 729-740.

295. Park, C.T. and S.D. Wright, *Plasma lipopolysaccharide-binding protein is found associated with a particle containing apolipoprotein A-I, phospholipid, and factor H-related proteins.* Journal of Biological Chemistry, 1996. **271**(30): p. 18054-18060.

296. McRae, J.L., et al., *Human factor H-related protein 5 (FHR-5) - A new complement-associated protein.* Journal of Biological Chemistry, 2001. **276**(9): p. 6747-6754.

297. *http://www.framinghamheartstudy.org/.*

298. Després, J.-P., et al., *HDL-cholesterol as a marker of coronary heart disease risk: the Québec cardiovascular study.* Atherosclerosis, 2000. **153**(2): p. 263-272.

299. Lewis, G.F. and D.J. Rader, *New insights into the regulation of HDL metabolism and reverse cholesterol transport.* Circulation Research, 2005. **96**(12): p. 1221-1232.

300. Garrett, R., Grisham, C., *Biochemistry*. 2nd ed. 1999: Harcourt College Publishers.

301. Davidson, W.S., et al., *The role of apolipoprotein AI domains in lipid binding.* Proceedings of the National Academy of Sciences of the United States of America, 1996. **93**(24): p. 13605-13610.

302. Barter, P.J., et al., *Antiinflammatory Properties of HDL.* Circ Res, 2004. **95**(8): p. 764-772.

303. Levy, A.P., et al., *Haptoglobin: Basic and Clinical Aspects.* Antioxidants & Redox Signaling, 2010. **12**(2): p. 293-304.

304. Watanabe, J., et al., *Hemoglobin and Its Scavenger Protein Haptoglobin Associate with ApoA-1-containing Particles and Influence the Inflammatory Properties and Function of High Density Lipoprotein.* Journal of Biological Chemistry, 2009. **284**(27): p. 18292-18301.

305. Langlois, M.R. and J.R. Delanghe, *Biological and clinical significance of haptoglobin polymorphism in humans.* Clinical Chemistry, 1996. **42**(10): p. 1589-1600.

306. Kristiansen, M., et al., *Identification of the haemoglobin scavenger receptor.* Nature, 2001. **409**(6817): p. 198-201.

307. Levy, A.P., et al., *Haptoglobin Phenotype and Vascular Complications in Patients with Diabetes.* N Engl J Med, 2000. **343**(13): p. 969-970.

308. Nakhoul, F.M., et al., *Haptoglobin phenotype and diabetic nephropathy.* Diabetologia, 2001. **44**(5): p. 602-604.

309. Engstrom, G., et al., *Complement C3 is a risk factor for the development of diabetes - A population-based cohort study.* Diabetes, 2005. **54**(2): p. 570-575.

310. Spagnuolo, M.S., et al., *Assignment of the binding site for haptoglobin on apolipoprotein A-I.* Journal of Biological Chemistry, 2005. **280**(2): p. 1193-1198.

311. Hotta, K., et al., *Plasma Concentrations of a Novel, Adipose-Specific Protein, Adiponectin, in Type 2 Diabetic Patients.* Arterioscler Thromb Vasc Biol, 2000. **20**(6): p. 1595-1599.

312. *ExPASy Proteomics Server pI calculator for human adiponectin sequence, http://www.expasy.org/cgi-bin/pi_tool?Q15848-ADIPO_HUMAN (Q15848)..*

313. Walpole, R., Myers, R., *Probability and Statistics for Engineers and Scientist*. 4th ed. 1989, New York: Macmillan Publishing Company.

314. *From the Hypergeometric Calculator: Online Statistical Table- http://stattrek.com/Tables/Hypergeometric.aspx.*

315. Garbett, N.C., et al., *Calorimetry outside the box: A new window into the plasma proteome.* Biophysical Journal, 2008. **94**(4): p. 1377-1383.

316. Arroyo, V., *Human Serum Albumin: Not Just a Plasma Volume Expander.* Hepatology, 2009. **50**(2): p. 355-357.

317. Peters, T., *All About Albumin: Biochemistry, Genetics and Medical Applications.* 1996: Academic Press.

318. He, X.M. and D.C. Carter, *Atomic-Structure and Chemistry of Human Serum-Albumin.* Nature, 1992. **358**(6383): p. 209-215.

319. Peters, T., *Serum Albumin.* Advances in Protein Chemistry, 1985. **37**: p. 161-245.

320. Oettl, K. and R.E. Stauber, *Physiological and pathological changes in the redox state of human serum albumin critically influence its binding properties.* British Journal of Pharmacology, 2007. **151**(5): p. 580-590.

321. Stamler, J.S., et al., *Nitric-Oxide Circulates in Mammalian Plasma Primarily as an S-Nitroso Adduct of Serum-Albumin.* Proceedings of the National Academy of Sciences of the United States of America, 1992. **89**(16): p. 7674-7677.

322. Curry, S., P. Brick, and N.P. Franks, *Fatty acid binding to human serum albumin: new insights from crystallographic studies.* Biochimica Et Biophysica Acta-Molecular and Cell Biology of Lipids, 1999. **1441**(2-3): p. 131-140.

323. Hamilton, J.A., *Fatty acid transport: difficult or easy?* Journal of Lipid Research, 1998. **39**(3): p. 467-481.

324. Hamilton, J.A. and F. Kamp, *How are free fatty acids transported in membranes? Is it by proteins or by free diffusion through the lipids?* Diabetes, 1999. **48**(12): p. 2255-2269.

325. Kantor, H.L. and J.H. Prestegard, *Fusion of Phosphatidylcholine Bilayer Vesicles - Role of Free Fatty-Acid.* Biochemistry, 1978. **17**(17): p. 3592-3597.

326. Kampf, J.P., *Is membrane transport of FFA mediated by lipid, protein, or both? An unknown protein mediates free fatty acid transport across the adipocyte plasma membrane.* Physiology, 2007. **22**: p. 7-14.

327. Vorum, H. and B. Honore, *Influence of fatty acids on the binding of warfarin and phenprocoumon to human serum albumin with relation to anticoagulant therapy.* Journal of Pharmacy and Pharmacology, 1996. **48**(8): p. 870-875.

328. Havelund, S., et al., *The mechanism of protraction of insulin detemir, a long-acting, acylated analog of human insulin.* Pharmaceutical Research, 2004. **21**(8): p. 1498-1504.

329. Shaklai, N., R.L. Garlick, and H.F. Bunn, *Nonenzymatic Glycosylation of Human-Serum Albumin Alters Its Conformation and Function.* Journal of Biological Chemistry, 1984. **259**(6): p. 3812-3817.

330. Faure, P., Wiernsperger, N., Polge, C., Faviers, A., Halimi, S., *Impairment of the antioxidant properties of serum albumin in patients with diabetes: protective effects of metformin.* Clinical Science, 2008. **114**: p. 251-256.

331. Kirpichnikov, D., S.I. McFarlene, and J.R. Sowers, *Metformin: An Update.* Annals of Internal Medicine, 2002. **137**(1): p. 25-33.

332. Hundal, R.S. and S.E. Inzucchi, *Metformin - New understandings, new uses.* Drugs, 2003. **63**(18): p. 1879-1894.

333. Curry, S., et al., *Crystal structure of human serum albumin complexed with fatty acid reveals an asymmetric distribution of binding sites.* Nature Structural Biology, 1998. **5**(9): p. 827-835.

334. *http://www.pdb.org/pdb/explore/explore.do?structureId=1BKE.*

335. Valko, M., H. Morris, and M.T.D. Cronin, *Metals, toxicity and oxidative stress.* Current Medicinal Chemistry, 2005. **12**(10): p. 1161-1208.

336. Roche, M., et al., *The antioxidant properties of serum albumin.* FEBS Letters, 2008. **582**(13): p. 1783-1787.

337. Halliwell, B., *Albumin - an Important Extracellular Antioxidant.* Biochemical Pharmacology, 1988. **37**(4): p. 569-571.

338. Schumann, K., et al., *Hohenheim Consensus Workshop: Copper.* European Journal of Clinical Nutrition, 2002. **56**(6): p. 469.

339. Halliwell, B., Gutteridge, J.M., *The Antioxidants of Human Extracellular Fluids.* Archives of Biochemistry and Biophysics, 1990. **280**(1): p. 1-8.

340. Rodkey, F.L., *The Direct Spectrophotometric Determination of Albumin in Human Serum.* Clinical Chemistry, 1965. **11**(4): p. 478-487.

341. Hill, P.G., *The Measurement of Albumin in Serum and Plasma.* Annals of Clinical Biochemistry, 1985. **22**(NOV): p. 565-578.

342. Diamond, D., et al., *Integration of analytical measurements and wireless communications--Current issues and future strategies.* Talanta, 2008. **75**(3): p. 606-612.

343. Doumas, B., Watson, W., Biggs, H., *Albumin Standards and the Measurement of Serum Albumin with Bromcresol Green.* Clinica Chimica Acta, 1970. **31**: p. 87-96.

344. WAKO Pure Chemical Industries, L., *LabAssay A/G BCG method, Biuret method whitesheet*. p. 1-10.

345. Langhoff, E. and J. Ladefoged, *Sodium activity, sodium concentration, and osmolality in plasma in acute and chronic renal failure.* Clin Chem, 1985. **31**(11): p. 1811-1814.

346. Webster, D., Bignell, A.H.C., Attwood, E.C., *An Assessment of the Suitability of Bromocresol Green for the Determination of Serum Albumin.* Clinica Chimica Acta, 1974. **53**: p. 101-108.

347. Webster, D., *A Study of the Interaction of Bromocresol Green with Isolated Serum Globulin Fractions.* Clinica Chimica Acta, 1974. **53**: p. 109-115.

348. Gustafsson, J., *Improved specificity of serum albumin determination and estimation of "acute phase reactants" by use of the bromcresol green reaction.* Clin Chem, 1976. **22**(5): p. 616-622.

349. Louderba.A, E.H. Mealey, and N.A. Taylor, *A New Dye-Binding Technic Using Bromcresol Purple for Determination of Albumin in Serum.* Clinical Chemistry, 1968. **14**(8): p. 793-&.

350. Pinnell, A. and B. Northam, *New automated dye-binding method for serum albumin determination with bromcresol purple.* Clin Chem, 1978. **24**(1): p. 80-86.

351. Pradhan, A.D., et al., *C-Reactive Protein, Interleukin 6, and Risk of Developing Type 2 Diabetes Mellitus.* JAMA, 2001. **286**(3): p. 327-334.

352. Rodkey, F.L., *Binding of Bromocresol Green by Human Serum Albumin.* Archives of Biochemistry and Biophysics, 1964. **108**(3): p. 510-&.

353. Reed, R.G., et al., *Fragments of bovine serum albumin produced by limited proteolysis. Conformation and ligand binding.* Biochemistry, 1975. **14**(21): p. 4578-4583.

354. Dromgoole, S.H., *The effect of haemodialysis on the binding capacity of albumin.* Clinica Chimica Acta, 1973. **46**(4): p. 469-472.

355. Dromgoole, S.H., *The effect of uremia and kidney transplantation on the binding capacity of albumin.* Clinica Chimica Acta, 1974. **52**(3): p. 301-303.

356. Maguire, G.A., Price, C.P., *Bromocresol purple method for serum albumin give falsely low values in patients with renal insufficiency.* Clinica Chimica Acta, 1986. **155**: p. 83-88.

357. Sarafidis, P.A., et al., *Validity and reproducibility of HOMA-IR, 1/HOMA-IR, QUICKI and McAuley's indices in patients with hypertension and type II diabetes.* Journal of Human Hypertension, 2007. **21**(9): p. 709-716.

358. Hui, J.M., et al., *Beyond insulin resistance in NASH: TNF-alpha or adiponectin?* Hepatology, 2004. **40**(1): p. 46-54.

359. BONORA, E., et al., *Homeostasis Model Assessment Closely Mirrors the Glucose Clamp Technique in the Assessment of Insulin Sensitivity.*, in *Diabetes Care*. 2000. p. 57.

360. Shalitin, S., et al., *Insulin resistance and impaired glucose tolerance in obese children and adolescents referred to a tertiary-care center in Israel.* 2005. **29**(6): p. 571-578.

361. Quinlan, G.J., G.S. Martin, and T.W. Evans, *Albumin: Biochemical properties and therapeutic potential.* Hepatology, 2005. **41**(6): p. 1211-1219.

362. *http://www.graphpad.com/quickcalcs/pvalue1.cfm.*

363. Motulsky, H., *Intuitive Biostatistics*. 1995, Oxford University Press. p. 113.

364. *American Association for Clinical Chemistry* *http://www.labtestsonline.org/understanding/analytes/microalbumin/sample.html.*

365. NKDEP, *Urine Albumin-to-Creatinine Ratio (UACR) NIH Publication No. 08-6286.* *http://www.nkdep.nih.gov/resources/UACR_GFR_QuickReference_508.pdf*. 2008, National Kidney Disease Education Program.

366. Halliwell, B. and M. Whiteman, *Measuring reactive species and oxidative damage in vivo and in cell culture: how should you do it and what do the results mean?* British Journal of Pharmacology, 2004. **142**(2): p. 231-255.

367. West, I.C., *Radicals and oxidative stress in diabetes.* Diabetic Medicine, 2000. **17**(3): p. 171-180.

368. Yorek, M.A., *The Role of Oxidative Stress in Diabetic Vascular and Neural Disease.* Free Radical Research, 2003. **37**(5): p. 471.

369. Vessby, J., et al., *Oxidative stress and antioxidant status in type 1 diabetes mellitus.* Journal of Internal Medicine, 2002. **251**(1): p. 69-76.

370. Medina, L.O., et al., *Determination of the antioxidant status of plasma from type 2 diabetic patients.* Diabetes Research and Clinical Practice, 2007. **77**(2): p. 193-197.

371. Rasheed, Z., Ali, R., *Reactive oxygen species damaged human serum albumin in patients with type 1 diabetes mellitus: Biochemical and immunological studies.* Life Sciences, 2006. **79**: p. 2320-2328.

372. Suzuki, E., et al., *Increased Oxidized Form of Human Serum-Albumin in Patients with Diabetes-Mellitus.* Diabetes Research and Clinical Practice, 1992. **18**(3): p. 153-158.

373. Pastore, A., et al., *Analysis of glutathione: implication in redox and detoxification.* Clinica Chimica Acta, 2003. **333**(1): p. 19-39.

374. Shaw, J., et al., *Evaluation of saturation labelling two-dimensional difference gel electrophoresis fluorescent dyes.* Proteomics, 2003. **3**(7): p. 1181-1195.

375. Hurd, T.R., et al., *Detection of reactive oxygen species-sensitive thiol proteins by redox difference gel electrophoresis - Implications for mitochondrial redox signaling.* Journal of Biological Chemistry, 2007. **282**(30): p. 22040-22051.

376. Dalle-Donne, I., et al., *Protein carbonylation, cellular dysfunction, and disease progression.* Journal of Cellular and Molecular Medicine, 2006. **10**(2): p. 389-406.

377. Madian, A.G. and F.E. Regnier, *Profiling Carbonylated Proteins in Human Plasma.* Journal of Proteome Research, 2010. **9**(3): p. 1330-1343.

378. Stadtman, E.R., *Protein Oxidation and Aging.* Science, 1992. **257**(5074): p. 1220-1224.

379. Jana, C.K., N. Das, and R.S. Sohal, *Specificity of Age-Related Carbonylation of Plasma Proteins in the Mouse and Rat.* Archives of Biochemistry and Biophysics, 2002. **397**(2): p. 433-439.

380. Sayre, L.M., et al., *Protein adducts generated from products of lipid oxidation: Focus on HNE and ONE.* Drug Metabolism Reviews, 2006. **38**(4): p. 651-675.

381. *http://www.piercenet.com/browse.cfm?fldID=5A3F09D2-5056-8A76-4E96-30DFE2E1B731*.

382. *http://www.piercenet.com/products/browse.cfm?fldID=010311*.

383. Matsuzawa, Y., et al., *Adiponectin and metabolic syndrome.* Arteriosclerosis Thrombosis and Vascular Biology, 2004. **24**(1): p. 29-33.

384. Fielding, C.J. and P.E. Fielding, *Molecular Physiology of Reverse Cholesterol Transport.* Journal of Lipid Research, 1995. **36**(2): p. 211-228.

APPENDIX A

SUPPLEMENTARY FIGURES

The following MS data for the POIs include only peptides with ion scores that are greater than 13 and %SPI of 70 or greater.

#	Filename	z	Frag Mode	Score	Fwd-Rev Score	SPI (%)	Spectrum Intensity	Sequence	MH+ Matched (Da)
1	011009_F1_A.0446.0446.0	3	CID	21.18	12.26	88.2	2.32e+008	(K) NILDRQDPPSVVVTSHQAPGEK (K)	2387.231
2	011009_F1_A.0445.0459.4	4	ETD	20.07	14.25	94.8	4.38e+008	(K) NILDRQDPPSVVVTSHQAPGEK (K)	2387.231
3	011009_F1_A.0480.0480.0	3	ETD	19.23	14.28	94.6	3.58e+007	(K) YYYDGKDYIEFNK (E)	1717.774
4	011009_F1_A.0417.0417.3	3	ETD	18.86	10.77	98.2	2.89e+008	(R) QVEGMEDWKQDSQLQK (A)	1948.907
5	011009_F1_A.0367.0367.2	2	CID	17.67	7.68	90.8	5.89e+007	(R) AGEVQEPELR (G)	1127.569
6	011009_F1_A.0410.0410.0	3	ETD	17.06	13.05	84.0	9.42e+007	(R) AKAYLEEECPATLR (K)	1650.816
7	011009_F1_A.0428.0428.4	4	ETD	15.94	6.72	95.9	5.13e+007	(K) NILDRQDPPSVVVTSHQAPGEKK (K)	2515.326
8	011009_F1_A.0606.0606.4	4	ETD	15.82	11.23	85.6	6.94e+006	(K) CLAYDFYPGKIDVHWTR (A)	2141.027
9	011009_F1_A.0418.0418.2	2	CID	15.39	8.74	88.0	8.37e+007	(R) QVEGMEDWKQDSQLQK (A)	1948.907
10	011009_F1_A.0579.0579.2	2	CID	15.31	12.20	90.4	1.74e+007	(R) YSLTYIYTGLSK (H)	1408.736
11	011009_F1_A.0431.0431.5	5	ETD	14.65	10.03	84.7	8.65e+007	(K) YSKNILDRQDPPSVVVTSHQAPGEK (K)	2765.422
12	011009_F1_A.0416.0416.3	3	CID	14.35	8.20	91.0	2.89e+008	(R) QVEGMEDWKQDSQLQK (A)	1948.907
13	011009_F1_A.0376.0376.0	3	CID	13.90	4.38	90.2	2.10e+007	(R) QVEGmEDWKQDSQLQK (A)	1948.907
14	011009_F1_A.0377.0386.3	3	ETD	13.65	10.28	88.7	2.45e+007	(R) QVEGmEDWKQDSQLQK (A)	1948.907
15	011009_F1_A.0479.0479.0	3	CID	13.22	6.18	100.0	3.55e+007	(K) YYYDGKDYIEFNK (E)	1717.774
16	011009_F1_A.0507.0507.0	2	CID	12.98	8.11	94.3	5.67e+007	(K) CLAYDFYPGK (I)	1233.561
17	011009_F1_A.0419.0419.2	2	ETD	12.27	6.94	88.1	8.37e+007	(R) QVEGMEDWKQDSQLQK (A)	1948.907
18	011009_F1_A.0580.0580.2	2	ETD	11.86	6.66	88.6	1.84e+007	(R) YSLTYIYTGLSK (H)	1408.736
19	011009_F1_A.0675.0675.2	2	CID	11.81	4.47	86.5	3.21e+007	(K) EIPAWVPFDPAAQITK (Q)	1782.943
20	011009_F1_A.0389.0389.3	3	ETD	11.68	5.43	81.4	3.48e+007	(R) AKAYLEEECPATLRK (Y)	1778.911
21	011009_F1_A.0679.0679.3	3	CID	10.28	5.28	74.0	7.33e+006	(K) EIPAWVPFDPAAQITK (Q)	1782.943
22	011009_F1_A.0465.0472.2	2	CID	9.26	1.71	97.5	7.38e+007	(K) SQPMGLWR (Q)	974.488

Figure 121 Combined ZAG A and B isoform MS/MS spectral features.

```
1   MVRMVPVLLS LLLLLGPAVP QENQDGRYSL TYVYTGLSKH VEDVPAFQAL GSLNDLQFFR YNSKDRKSQP MGLWRQVEGM  80
81  EDWKQDSQLQ KAREDIFMET LKDIVEYYND SNGSHVLQGR FGCEIENNRS SGAFWKYYYD GKDYIEFNKE IPAWVPFDPA 160
161 AQITKQKWEA EPVYVQRAKA YLEEECPATL RKYLKYSKNI LDRQDPPSVV VTSHQAPGEK KKLKCLAYDF YPGKIDVHWT 240
241 RAGEVQEPEL RGDVLHNGNG TYQSWVVVAV PPQDTAPYSC HVQHSSLAQP LVVPWEAS                        298
```

Figure 122 Combined ZAG A and B isoform sequence coverage map.

Group (#)	Spectra (#)	Distinct Peptides (#)	Distinct Summed MS/MS Search Score	% AA Coverage	Mean Peptide Spectral Intensity	Protein MW (Da)	Protein pI	Database Accession #	Protein Name
1	8	4	85.68	40	1.25e+008	13532.1	6.28	40316910	serum amyloid A1 preproprotein

#	Filename	z	Frag Mode	Score	SPI (%)	Spectrum Intensity	Sequence	MH+ Matched (Da)
1	050508-3.0120.0120.2	2	CID	24.67	96.3	1.74e+007	(R) FFGHGAEDSLADQAANEWGR (S)	2177.963
2	050508-3.0113.0122.0	3	CID	23.01	98.6	4.47e+008	(R) FFGHGAEDSLADQAANEWGR (S)	2177.963
3	050508-3.0277.0279.2	2	CID	20.72	91.1	2.61e+008	(R) SFFSFLGEAFDGAR (D)	1550.727
4	050508-3.0085.0087.3	3	CID	20.63	94.2	1.22e+008	(K) RGPGGAWAAEVISDAR (E)	1612.819
5	050508-3.0280.0282.3	3	CID	20.03	91.6	1.60e+007	(R) SFFSFLGEAFDGAR (D)	1550.727
6	050508-3.0131.0138.0	2	CID	19.66	87.8	1.12e+008	(R) GPGGAWAAEVISDAR (E)	1456.718
7	050508-3.0080.0083.2	2	CID	18.92	94.5	1.76e+007	(K) RGPGGAWAAEVISDAR (E)	1612.819
8	050508-3.0136.0136.0	3	CID	15.79	79.1	9.19e+006	(R) GPGGAWAAEVISDAR (E)	1456.718

Figure 123 SAA1 POI isoform MS/MS spectral features.

```
1   MKLLTGLVFC SLVLGVSSRS FFSFLGEAFD GARDMWRAYS DMREANYIGS DKYFHARGNY DAAKRGPGGA WAAEVISDAR 80
81  ENIQRFFGHG AEDSLADQAA NEWGRSGKDP NHFRPAGLPE KY                                      122
```

Figure 124 SAA1 POI isoform sequence coverage map.

Group (#)	Spectra (#)	Distinct Peptides (#)	Distinct Summed MS/MS Search Score	% AA Coverage	Mean Peptide Spectral Intensity	Database Accession #	Protein Name
1	8	4	73.84	19	4.18e+007	5174675	cysteine-rich secretory protein 3

#	Filename	z	Frag Mode	Score	Fwd-Rev Score	SPI (%)	Spectrum Intensity	Sequence	MH+ Matched (Da)
1	011009_F1_D.0509.0509.3	3	CID	20.14	16.70	87.4	2.16e+007	(K) YYYVCQYCPAGNWANR (L)	2084.874
2	011009_F1_D.0349.0349.0	3	ETD	20.02	14.94	95.3	7.28e+007	(K) MEWNKEAAANAQK (W)	1490.706
3	011009_F1_D.0341.0341.2	2	CID	17.33	11.67	95.3	1.69e+007	(K) YEDLYSNCK (S)	1191.499
4	011009_F1_D.0308.0308.0	3	ETD	16.56	12.39	92.6	6.53e+006	(K) mEWNKEAAANAQK (W)	1490.706
5	011009_F1_D.0348.0348.0	3	CID	16.47	6.80	87.4	7.23e+007	(K) MEWNKEAAANAQK (W)	1490.706
6	011009_F1_D.0432.0432.2	2	CID	16.35	6.17	93.7	1.14e+008	(K) SLKLTLTCK (H)	1063.618
7	011009_F1_D.0307.0307.0	3	CID	15.93	8.68	87.6	6.53e+006	(K) mEWNKEAAANAQK (W)	1490.706
8	011009_F1_D.0511.0511.2	2	CID	15.42	9.74	88.8	2.40e+007	(K) YYYVCQYCPAGNWANR (L)	2084.874

Figure 125 CRISP-3 POI isoform MS/MS spectral features.

```
1   MTLFPVLLFL VAGLLPSFPA NEDKDPAFTA LLTTQTQVQR EIVNKHNELR RAVSPPARNM LKMEWNKEAA ANAQKWANQC 80
81  NYRHSNPKDR MTSLKCGENL YMSSASSSWS QAIQSWFDEY NDFDFGVGPK TPNAVVGHYT QVVWYSSYLV GCGNAYCPNQ 160
161 KVLKYYYVCQ YCPAGNWANR LYVPYEQGAP CASCPDNCDD GLCTNGCKYE DLYSNCKSLK LTLTCKHQLV RDSCKASCNC 240
241 SNSIY                                                                               245
```

Figure 126 CRISP-3 POI isoform sequence coverage map.

Group (#)	Spectra (#)	Distinct Peptides (#)	Distinct Summed MS/MS Search Score	% AA Coverage	Mean Peptide Spectral Intensity	Protein MW (Da)	Protein pI	Database Accession #	Protein Name
1	9	8	106.41	18	5.35e+006	64419.8	6.81	13540563	complement factor H-related 5

#	Filename	z	Frag Mode	Score	SPI (%)	Spectrum Intensity	Sequence	MH+ Matched (Da)
1	121208_120308A.0401.0401.2	2	CID	18.80	92.1	5.87e+006	(R)ITCTEEGWSPTPK(C)	1505.694
2	121208_120308A.0478.0478.0	3	CID	17.61	83.2	8.03e+006	(K)GECHVPILEANVDAQPK(K)	1876.922
3	121208_120308A.0338.0345.0	2	CID	13.85	89.5	3.77e+006	(K)TGDAVEFQCK(F)	1154.515
4	121208_120308A.0479.0479.0	3	ETD	13.80	86.2	8.03e+006	(K)GECHVPILEANVDAQPK(K)	1876.922
5	121208_120308A.0331.0331.0	2	CID	13.78	81.8	4.05e+006	(K)LQGSVTVTCR(N)	1120.578
6	121208_120308A.0450.0450.2	2	CID	12.97	97.2	4.61e+006	(K)ENYLLPEAK(E)	1076.562
7	121208_120308A.0508.0513.2	2	CID	10.18	71.8	7.11e+006	(R)mCSFPFVK(N)	1015.474
8	121208_120308A.0396.0396.0	2	CID	9.84	92.4	3.27e+006	(R)CLDPCVVSEENmNK(N)	1694.718
9	121208_120308A.0516.0516.4	4	ETD	9.38	84.7	3.42e+006	(R)KEEYGHNEVVEYDCNPNFIINGPK(K)	2865.315

Figure 127 CFHR-5 MS/MS spectral features.

```
1   MLLLFSVILI SWVSTVGGEG TLCDFPKIHH GFLYDEEDYN PFSQVPTGEV FYYSCEYNFV SPSKSFWTRI TCTEEGWSPT 80
81  PKCLRMCSFP FVKNGHSESS GLIHLEGDTV QIICNTGYSL QNNEKNISCV ERGWSTPPIC SFTKGECHVP ILEANVDAQP 160
161 KKESYKVGDV LKFSCRKNLI RVGSDSVQCY QFGWSPNFPT CKGQVRSCGP PPQLSNGEVK EIRKEEYGHN EVVEYDCNPN 240
241 FIINGPKKIQ CVDGEWTTLP TCVEQVKTCG YIPELEYGYV QPSVPPYQHG VSVEVNCRNE YAMIGNNMIT CINGIWTELP 320
321 MCVATHQLKR CKIAGVNIKT LLKLSGKEFN HNSRIRYRCS DIFRYRHSVC INGKWNPEVD CTEKREQFCP PPPQIPNAQN 400
401 MTTTVNYQDG EKVAVLCKEN YLLPEAKEIV CKDGRWQSLP RCVESTAYCG PPPSINNGDT TSFPLSVYPP GSTVTYRCQS 480
481 FYKLQGSVTV TCRNKQWSEP PRCLDPCVVS EENMNKNNIQ LKWRNDGKLY AKTGDAVEFQ CKFPHKAMIS SPPFRAICQE 560
561 GKFEYPICE                                                                           569
```

Figure 128 CFHR-5 sequence coverage map.

Group (#)	Spectra (#)	Distinct Peptides (#)	Distinct Summed MS/MS Search Score	% AA Coverage	Mean Peptide Spectral Intensity	Protein MW (Da)	Protein pI	Database Accession #	Protein Name
2	3	3	37.04	8	2.24e+006	59578.6	7.09	4504489	histidine-rich glycoprotein precursor

#	Filename	z	Frag Mode	Score	SPI (%)	Spectrum Intensity	Sequence	MH+ Matched (Da)
1	121208_120308A.0676.0676.2	2	CID	13.87	97.4	2.87e+006	(R)ADLFYDVEALDLESPK(N)	1824.890
2	121208_120308A.0708.0708.2	2	CID	12.75	84.2	8.95e+005	(K)DSPVLIDFFEDTER(Y)	1682.791
3	121208_120308A.0571.0571.0	2	CID	10.42	97.2	2.95e+006	(R)GGEGTGYFVDFSVR(N)	1490.691

Figure 129 HRG precursor fragment spectral features.

```
1   MKALIAALLL ITLQYSCAVS PTDCSAVEPE AEKALDLINK RRRDGYLFQL LRIADAHLDR VENTTVYYLV LDVQESDCSV  80
81  LSRKYWNDCE PPDSRRPSEI VIGQCKVIAT RHSHESQDLR VIDFNCTTSS VSSALANTKD SPVLIDFFED TERYRKQANK 160
161 ALEKYKEEND DFASFRVDRI ERVARVRGGE GTGYFVDFSV RNCPRHHFPR HPNVFGFCRA DLFYDVEALD LESPKNLVIN 240
241 CEVFDPQEHE NINGVPPHLG HPFHWGGHER SSTTKPPFKP HGSRDHHHPH KPHEHGPPPP PDERDHSHGP PLPQGPPPLL 320
321 PMSCSSCQHA TFGTNGAQRH SHNNNSSDLH PHKHHSHEQH PHGHHPHAHH PHEHDTHRQH PHGHHPHGHH PHGHHPHGHH 400
401 PHGHHPHCHD FQDYGPCDPP PHNQGHCCHG HGPPPGHLRR RGPGKGPRPF HCRQIGSVYR LPPLRKGEVL PLPEANFPSF 480
481 PLPHHKHPLK PDNQPFPQSV SESCPGKFKS GFPQVSMFFT HTFPK                                      525
```

Figure 130 HRG precursor fragment sequence coverage map.

Group (#)	Spectra (#)	Distinct Peptides (#)	Distinct Summed MS/MS Search Score	% AA Coverage	Mean Peptide Spectral Intensity	Protein MW (Da)	Protein pI	Database Accession #	Protein Name
1	18	13	238.79	43	1.14e+008	38233.7	6.14	3337390	haptoglobin

#	Filename	z	Frag Mode	Score	SPI (%)	Spectrum Intensity	Sequence	MH+ Matched (Da)
1	092208A.0203.0208.2	2	CID	23.94	97.9	2.83e+007	(K) YVmLPVADQDQCIR (H)	1707.819
2	092208A.0228.0232.2	2	CID	23.74	94.6	3.73e+008	(K) YVMLPVADQDQCIR (H)	1707.819
3	092208A.0166.0169.0	2	CID	23.58	97.4	3.65e+008	(K) SCAVAEYGVYVK (V)	1345.646
4	092208A.0255.0258.2	2	CID	22.78	96.6	1.13e+008	(K) DIAPTLTLYVGK (K)	1290.730
5	092208A.0043.0046.0	3	CID	20.65	92.2	1.21e+007	(K) AVGDKLPECEAVCGKPK (N)	1857.920
6	092208A.0220.0233.3	3	CID	19.57	88.1	1.82e+008	(K) YVMLPVADQDQCIR (H)	1707.819
7	092208A.0189.0194.0	2	CID	19.11	92.9	3.56e+008	(K) VTSIQDWVQK (T)	1203.637
8	092208A.0059.0063.0	3	CID	18.15	92.9	1.13e+007	(K) LRTEGDGVYTLNNEK (Q)	1708.850
9	092208A.0239.0244.0	3	CID	17.99	86.8	7.26e+007	(K) SPVGVQPILnEHTFCAGmSK (Y)	2172.058
10	092208A.0266.0272.2	2	CID	17.31	89.1	4.27e+007	(K) DIAPTLTLYVGKK (Q)	1418.825
11	092208A.0271.0274.2	2	CID	16.47	86.9	3.81e+007	(R) VMPICLPSKDYAEVGR (V)	1834.919
12	092208A.0315.0315.0	3	CID	16.23	86.4	1.02e+007	(K) VVLHPNYSQVDIGLIK (L)	1795.011
13	092208A.0112.0131.2	2	CID	14.59	91.5	2.35e+008	(R) VGYVSGWGR (N)	980.495
14	092208A.0199.0202.0	3	CID	14.53	84.8	2.29e+007	(K) YVmLPVADQDQCIR (H)	1707.819
15	092208A.0144.0146.2	2	CID	14.14	91.2	1.24e+007	(R) VmPICLPSK (D)	1044.558
16	092208A.0173.0196.2	2	CID	13.85	96.9	1.26e+008	(K) GSFPWQAK (M)	920.462
17	092208A.0160.0160.2	2	CID	12.26	88.3	1.71e+007	(R) VGYVSGWGR (N)	980.495
18	092208A.0198.0201.0	2	CID	10.76	96.4	3.94e+007	(R) VMPICLPSK (D)	1044.558

Figure 131 Unreduced haptoglobin MS/MS spectral features.

```
1   ALGAVIALLL WGQLFAVDSG NDVTDIADDG CPKPPEIAHG YVEHSVRYQC KNYYKLRTEG DGVYTLNNEK QWINKAVGDK  80
81  LPECEAVCGK PKNPANPVQR ILGGHLDAKG SFPWQAKMVS HHNLTTGATL INEQWLLTTA KNLFLNHSEN ATAKDIAPTL 160
161 TLYVGKKQLV EIEKVVLHPN YSQVDIGLIK LKQKVSVNER VMPICLPSKD YAEVGRVGYV SGWGRNANFK FTDHLKYVML 240
241 PVADQDQCIR HYEGSTVPEK KTPKSPVGVQ PILNEHTFCA GMSKYQEDTC YGDAGSAFAV HDLEEDTWYA TGILSFDKSC 320
321 AVAEYGVYVK VTSIQDWVQK TIAEN                                                            345
```

Figure 132 Unreduced haptoglobin sequence coverage map.

Group (#)	Spectra (#)	Distinct Peptides (#)	Distinct Summed MS/MS Search Score	% AA Coverage	Mean Peptide Spectral Intensity	Protein MW (Da)	Protein pI	Database Accession #	Protein Name
1	6	5	74.92	20	2.11e+007	30778.0	5.56	4557321	apolipoprotein A-I preproprotein

#	Filename	z	Frag Mode	Score	SPI (%)	Spectrum Intensity	Sequence	MH+ Matched (Da)
1	010909_F4_SPOT.0412.0412.3	3	ETD	18.55	97.8	3.51e+007	(R) QKVEPLRAELQEGAR (Q)	1723.945
2	010909_F4_SPOT.0621.0621.0	2	CID	17.65	86.7	1.16e+007	(K) DLATVYVDVLK (D)	1235.688
3	010909_F4_SPOT.0411.0411.0	3	CID	14.87	84.1	3.51e+007	(R) QKVEPLRAELQEGAR (Q)	1723.945
4	010909_F4_SPOT.0369.0369.2	2	CID	14.76	97.0	1.69e+007	(K) LSPLGEEmR (D)	1031.519
5	010909_F4_SPOT.0398.0398.3	3	ETD	13.13	83.2	8.59e+006	(R) THLAPYSDELRQR (L)	1585.808
6	010909_F4_SPOT.0461.0461.5	5	ETD	10.83	83.0	1.96e+007	(R) AHVDALRTHLAPYSDELRQR (L)	2348.222

Figure 133 Apolipoprotein A-I POI fragment MS/MS spectral features.

```
1   MKAAVLTLAV LFLTGSQARH FWQQDEPPQS PWDRVKDLAT VYVDVLKDSG RDYVSQFEGS ALGKQLNLKL LDNWDSVTST  80
81  FSKLREQLGP VTQEFWDNLE KETEGLRQEM SKDLEEVKAK VQPYLDDFQK KWQEEMELYR QKVEPLRAEL QEGARQKLHE 160
161 LQEKLSPLGE EMRDRARAHV DALRTHLAPY SDELRQRLAA RLEALKENGG ARLAEYHAKA TEHLSTLSEK AKPALEDLRQ 240
241 GLLPVLESFK VSFLSALEEY TKKLNTQ                                                         267
```

Figure 134 Apolipoprotein A-I POI sequence coverage map. The preproapolipoprotein (267 amino acids) is secreted as a 249 amino acid preprotein and is rapidly cleaved by a plasma protease to generate the mature 243 amino acid polypeptide [384].

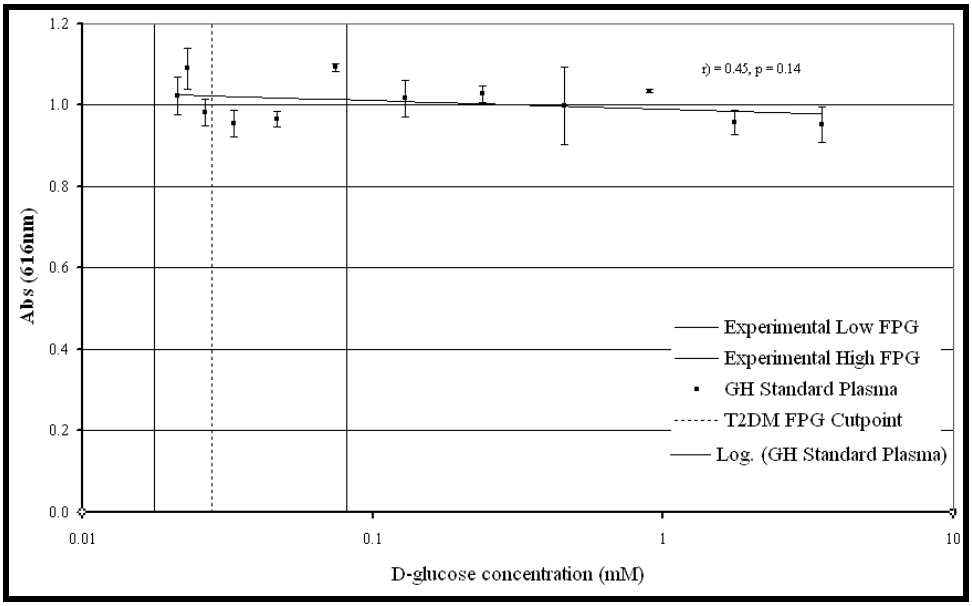

Figure 135 D-glucose control for BCG-HSA binding.

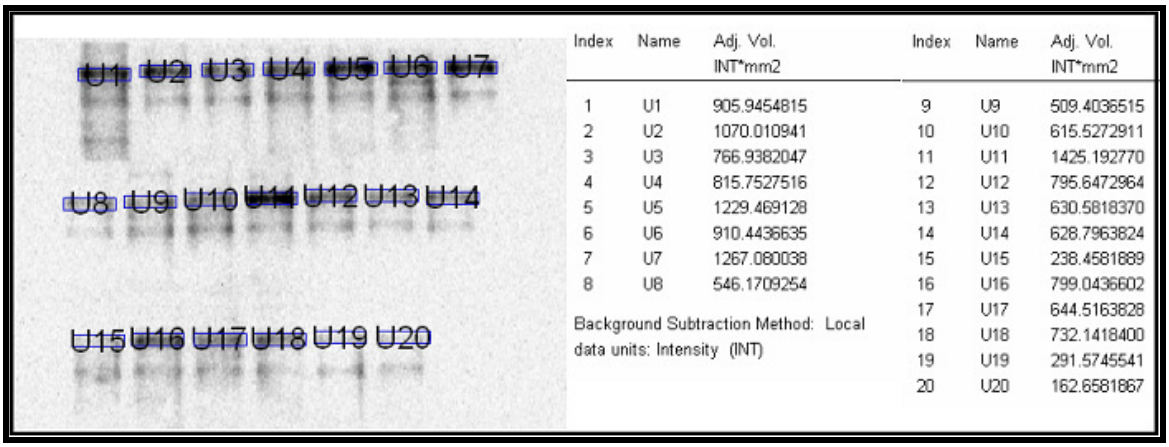

Index	Name	Adj. Vol. INT*mm2	Index	Name	Adj. Vol. INT*mm2
1	U1	905.9454815	9	U9	509.4036515
2	U2	1070.010941	10	U10	615.5272911
3	U3	766.9382047	11	U11	1425.192770
4	U4	815.7527516	12	U12	795.6472964
5	U5	1229.469128	13	U13	630.5818370
6	U6	910.4436635	14	U14	628.7963824
7	U7	1267.080038	15	U15	238.4581889
8	U8	546.1709254	16	U16	799.0436602
			17	U17	644.5163828
			18	U18	732.1418400
			19	U19	291.5745541
			20	U20	162.6581867

Background Subtraction Method: Local
data units: Intensity (INT)

Figure 136 Chemiluminescence quantification data.